A probabilistic assessment of in-season climate drivers of agricultural losses in Europe

Zur Erlangung des akademischen Grades eines
DOKTORS DER NATURWISSENSCHAFTEN (Dr. rer. nat.)
von der KIT-Fakultät für Physik des
Karlsruher Instituts für Technologie (KIT)

genehmigte

DISSERTATION

von

M.Sc. Federico A. Stainoh
aus Buenos Aires, Argentina

Tag der mündlichen Prüfung:	07.11.2025
Referent:	Prof. Dr. Joaquim G. Pinto
Korreferent:	Prof. Dr. Michael Kunz

Abstract

Extreme weather conditions have caused significant losses in the agricultural sector. This has been evident in several countries across Europe, where previously unseen weather and climate extremes have led to record declines in crop yields. In this context, stakeholders and policy makers require a deeper understanding of how weather and climate influence crop production in order to design effective, crop- and location-specific adaptation strategies. Statistical models offer valuable insights in this regard, as they can uncover previously unknown interactions and identify the most influential weather and climate drivers behind substantial yield reductions (factors closely linked to food insecurity and economic instability). However, the interpretation, performance, and robustness of such models can vary significantly depending on the selection of weather and climate predictors, as well as data availability. This thesis employs statistical models that addresses the spatial variability of in-season climate drivers in Europe in the context of abrupt yield losses. The resulting insights are then used to identify the most frequent drivers in present and future climate scenarios.

First, this thesis investigates to what extent variable definition enhance predictability in statistical modeling. The first analysis focuses on abrupt drops in silage maize yield, referred to throughout this thesis as "yield shock", in Germany, and employs two statistical modelling approaches: the Least Absolute Shrinkage and Selection Operator (LASSO), a parametric-based method, and Random Forest, a non-parametric, machine learning-based method. Results show that when using LASSO, models that integrate both simple and complex variables demonstrate superior predictive skill. In contrast, Random Forest does not exhibit a clear advantage when pre-selecting between simple and complex variables. Random Forest can capture non-linear interactions between predictors and the target variable, reducing the necessity for complex variable formulations. Furthermore, the findings indicate that a combination of cold temperatures in April and hot, dry conditions in July significantly increases the likelihood of silage maize yield shock in Germany. These insights support the development of adaptation strategies such as improved irrigation practices and adjustments to planting dates.

In addition to this, an ensemble of Random Forest models is implemented to identify the most important in-season weather and climate drivers of maize and wheat yield shocks across European countries. The further analyses centers on key European maize and wheat producers: France, Romania, and Spain for maize, and France, Germany, Poland, Romania, Spain, and the UK for winter wheat. The Global Data of Historical Yields (GDHY), a global gridded crop data, is used, which provides a larger sample size per country and enhancing the robustness of the developed models. An ensemble of Ran-

dom Forest is employed to individual crop-country domain to identify key drivers under highly variable climatic conditions for each case. The findings reveal pronounced spatial variability in the in-season climate drivers of maize and winter wheat yield shocks. For maize, high temperatures and dry conditions are the main triggers in France and Romania, while in Spain, a lack of precipitation in March emerges as the most critical factor. In the case of winter wheat, yield shocks are driven by a range of in-season conditions, including high and low temperatures as well as extremes in precipitation, depending on the country. In France, warm conditions in December and April are key triggers, whereas in Germany, both cold and warm temperatures in December, along with elevated temperatures in June, increase the likelihood of yield shocks. In Romania and Spain, dry and hot spring conditions are particularly influential, while in the UK, elevated precipitation events in June significantly raise the risk of losses.

Finally, the influence of global warming on yield shock is investigated. The study examines how future climate change scenarios influence yield shocks by using a suite of EUROCORDEX regional climate models, followed by bias correction through various adjustment techniques. By applying present-climate crop yield shock models, the analysis identifies key drivers of future yield losses. For maize, weak trends and higher uncertainty in projected losses stem from low model agreement on future precipitation patterns. Nonetheless, under 2°C and 3°C warmer climate scenarios, drier conditions persist as the dominant driver of yield shock. In contrast, winter wheat exhibits a clearer signal, with rising shock probabilities in countries such as France, Germany, Romania, and Spain, while Poland and the UK see stable or declining risks. Warming trends, projected with high confidence, are likely to reduce cold-related yield shocks, particularly in Germany, Poland, and Romania. However, this warming may increase winter losses in France and Germany, especially in December, and elevate spring and early summer risks across much of Europe. In Spain and the UK, uncertain precipitation projections lead to little change in average loss probabilities.

This thesis shows that the added value of using simple and complex variables is entangled with the statistical method chosen. While parametric methods like LASSO and complex variables can enhance the predictability skill of the model, they may not be necessary when considering more flexible approaches like Random Forest. The strong spatial variability of climate drivers in present and future reveals the necessity to implement adaptation strategies specifically for each crop and country.

Zusammenfassung

Extreme Wetterbedingungen haben zu erheblichen Verlusten im Agrarsektor geführt. Dies ist in mehreren Ländern Europas deutlich geworden, in dem zuvor unbekannte Wetter- und Klimaextreme zu rekordverdächtigen Rückgängen der Ernteerträge geführt haben. In diesem Zusammenhang benötigen Entscheidungsträger:innen und politische Akteur:innen ein tieferes Verständnis darüber, wie Wetter und Klima die landwirtschaftliche Produktion beeinflussen, um wirksame, auf bestimmte Kulturen und Standorte zugeschnittene Anpassungsstrategien zu entwickeln. Statistische Modelle bieten in dieser Hinsicht wertvolle Einblicke, da sie bislang unbekannte Zusammenhänge aufdecken und die einflussreichsten Wetter- und Klilmafaktoren identifizieren können. Diese Faktoren stehen mit erheblichen Etragsverlusten in Verbindung und sind eng mit Enährungssicherheit sowie wirtschaftlicher Instabilität verknüpft. Die Interpretation, Leistungsfähigkeit und Belastbarkeit solcher Modelle können jedoch stark von der Definition der Wetter- und Klimaparameter sowie der Datenverfügbarkeit abhängen. In dieser Arbeit werden statistische Modelle verwendet, um die räumliche Variabilität von klimatischen Einflussfaktoren während der Vegetationsperiode in Europa im Zusammenhang mit abrupten Ertragsverlusten zu untersuchen. Die daraus gewonnenen Erkenntnisse dienen dazu, die häufigsten Einflussfaktoren in aktuellen und zukünftigen Klimaszenarien zu identifizieren.

Zunächst untersucht diese Arbeit, inwieweit die Definition von Variablen die Vorhersagegenauigkeit in der statistischen Modellierung verbessert. Die Analyse konzentriert sich ausschließlich auf abrupte Rückgänge der Silomaiserträge in Deutschland, die im weiteren Verlauf dieser Arbeit als „Ertragsschocks“ bezeichnet werden. Die Arbeit verwendet zwei statistische Modellierungsansätze: den Least Absolute Shrinkage and Selection Operator (LASSO), eine parametrische Methode, sowie Random Forest, eine nichtparametrische, auf maschinellem Lernen basierende Methode. Die Ergebnisse zeigen, dass bei der Anwendung von LASSO Modelle mit einer Kombination aus einfachen und komplexen Variablen eine bessere Vorhersagegenauigkeit aufweisen. Im Gegensatz dazu zeigt Random Forest keinen klaren Vorteil bei der Vorauswahl zwischen einfachen und komplexen Variablen. Random Forest ist in der Lage, nichtlineare Wechselwirkungen zwischen Prädiktoren und der Zielvariablen zu erfassen, was die Notwendigkeit komplexer Variablenformulierungen reduziert. Darüber hinaus deuten die Ergebnisse darauf hin, dass eine Kombination aus kalten Temperaturen im April sowie heißen und trockenen Bedingungen im Juli die Wahrscheinlichkeit eines Silomais-Ertragsschocks in Deutschland deutlich erhöht. Diese Erkenntnisse unterstützen die Entwicklung von Anpassungsstrategien wie verbesserte Bewässerungspraktiken und Anpassungen der Aussaattermine.

Darüber hinaus wird ein Ensemble von Random-Forest-Modellen implementiert, um die wichtigsten witterungs- und klimabedingten Einflussfaktoren während der Vegetationsperiode auf Ertragsschocks bei Mais und Winterweizen in verschiedenen europäischen Ländern zu identifizieren. Die Analyse konzentriert sich auf zentrale europäische Produktionsländer: Frankreich, Rumänien und Spanien für Mais sowie Frankreich, Deutschland, Polen, Rumänien, Spanien und das Vereinigte Königreich für Winterweizen. Verwendet wird der „Global Data of Historical Yields“ (GDHY)-Datensatz, ein globales, rasterbasiertes Ertragsdatensatz, das eine größere Stichprobengröße pro Land aufweist und so die Robustheit der entwickelten Modelle erhöht. Für jede Kombination aus Kulturpflanze und Land wird ein Ensemble von Random-Forest-Modellen angewendet, um unter stark variierenden klimatischen Bedingungen die wichtigsten Einflussfaktoren zu ermitteln. Die Ergebnisse zeigen eine ausgeprägte räumliche Variabilität der klimatischen Einflussfaktoren während der Vegetationsperiode auf Ertragsschocks bei Mais und Winterweizen. Bei Mais sind hohe Temperaturen und Trockenheit die Hauptauslöser in Frankreich und Rumänien, während in Spanien ein Mangel an Niederschlag im März als kritischster Faktor hervorgeht. Im Fall von Winterweizen werden, je nach Land, Ertragsschocks durch eine Vielzahl von Bedingungen während der Vegetationsperiode verursacht, darunter sowohl hohe als auch niedrige Temperaturen sowie extreme Niederschlagsereignisse. In Frankreich sind warme Wetterbedingungen im Dezember und April entscheidende Auslöser, während in Deutschland sowohl kalte als auch warme Temperaturanomalien im Dezember sowie erhöhte Temperaturen im Juni die Wahrscheinlichkeit von Ertragsschocks erhöhen. In Rumänien und Spanien wirken sich insbesondere trockene und heiße Frühjahrsbedingungen stark aus, während im Vereinigten Königreich starke Niederschlagsereignisse im Juni das Risiko von Winterweizen-Ertragsschocks deutlich erhöhen.

Abschließend wird der Einfluss der globalen Erwärmung auf Ertragsschocks untersucht. Die Thesis analysiert, wie zukünftige Klimawandelszenarien Ertragsschocks beeinflussen, basierend auf einer Reihe regionaler Klimamodelle des EURO-CORDEX-Projekts, gefolgt von einer Bias-Korrektur. Durch die Anwendung von Ertragsschock-Modellen auf Basis des heutigen Klimas werden die wichtigsten Einflussfaktoren zukünftiger Ertragsverluste identifiziert. Bei Mais zeigen sich nur schwache Trends und eine hohe Unsicherheit in den Projektionen, was auf geringe Übereinstimmung der Modelle hinsichtlich zukünftiger Niederschlagsmuster zurückzuführen ist. Dennoch bleiben unter Szenarien mit 2°C und 3°C Erwärmung trockenere Bedingungen der dominierende Treiber von Ertragsschocks. Im Gegensatz dazu zeigt Winterweizen ein klareres Signal, mit steigender Wahrscheinlichkeit von Ertragsschocks in Ländern wie Frankreich, Deutschland, Rumänien und Spanien, während in Polen und dem Vereinigten Königreich stabile oder rückläufige Risiken zu beobachten sind. Erwärmungstrends, die mit hoher Sicherheit prognostiziert werden, dürften insbesondere in Deutschland, Polen und Rumänien zu einer Abnahme kältebedingter Ertragsschocks führen. Gleichzeitig könnte diese Erwärmung jedoch die Winterverluste in Frankreich und Deutschland, insbesondere im Dezember, erhöhen und das Risiko im Frühjahr und Frühsommer in weiten Teilen Europas steigern. In Spanien und dem Vereinigten Königreich führen unsichere Niederschlagsprognosen zu nur geringen Veränderungen der durchschnittlichen Verlustwahrscheinlichkeiten.

Diese Arbeit zeigt, dass der Mehrwert durch die Verwendung einfacher und komplexer Variablen stark mit der Wahl der statistischen Methode verknüpft ist. Während parametrische

Methoden wie LASSO und komplexe Variablen die Vorhersagefähigkeit des Modells verbessern können, sind sie bei flexibleren Ansätzen wie Random Forest möglicherweise nicht erforderlich. Die starke räumliche Variabilität klimatischer Einflussfaktoren im heutigen und zukünftigen Klima verdeutlicht die Notwendigkeit, Anpassungsstrategien spezifisch für jede Kulturpflanze und jedes Land zu entwickeln.

Preface

The PhD candidate confirms that the research presented in this thesis contains significant scientific contributions by himself. This thesis reuses material from the following publication

Stainoh, F., Moemken, J., Gouveia, C.M. and Pinto, J.G., 2024 (a). A comparison of climate drivers' impacts on silage maize yield shock in Germany. Theoretical and Applied Climatology, pp.1-13. https://doi.org/10.1007/s00704-024-05179-z

Formal analysis in Stainoh et al. (2024) was solely done by the candidate. The original draft was written by the candidate, with advice from Julia Mömken, Celia M. Gouveia and Joaquim G. Pinto. Parts of Chapter 4 and Chapter 6 reuses material from Stainoh et al. (2024).

Parts of Section 2.1 are based on Watson et al. (1997), Ahrens (2009) and Spiridonov and Ćurić (2021). Section 2.2 is partially based on Andrade and Sadras (2002), Taiz and Zeiger (2002) and Murphy and Hurtado (2020). Finally, parts of section 2.4 and Chapter 5 are based on James et al. (2021).

The candidate wrote the text of this manuscript with advice from Dr. Julia Mömken, Dr. Alexandre M. Ramos and Prof. Dr. Joaquim Pinto.

We acknowledge the German Climate Computing Centre (DKRZ, Hamburg) for providing computational and storage resources.

This project was funded by the European Union's Horizon 2020 research and innovation programme under Marie SkłodowskaCurie grant no. 956396, EDIPI (European weather extremes: drivers, predictability and impacts).

Contents

Abstract **i**

Zusammenfassung **iii**

Preface **vi**

1 Introduction **1**

2 Theoretical Background **5**
2.1 General meteorological background and the European climate 5
2.1.1 Climate in Europe 7
2.1.2 Agriculture in Europe 9
2.2 Environmental factors influencing crop growth and development 11
2.2.1 Temperature 13
2.2.2 Water, transpiration and evapotranspiration 14
2.2.3 Radiation, photosynthesis and photosynthesis pathways 14
2.2.4 Weather hazards and stressors 15
2.3 The importance, the growth and the development of maize and wheat . . . 17
2.3.1 Maize 18
2.3.2 Wheat 20
2.4 Common approaches in agricultural meteorology 22
2.4.1 Statistical learning and machine learning 23
2.4.2 Definition of statistical models 23
2.4.3 Binary classification models 24
2.4.4 The bias-variance tradeoff and cross validation 27
2.5 Climate models 28
2.5.1 Global climate models 28
2.5.2 Regional climate models 31
2.5.3 Systematic biases and adjustment methods 31

3 Research Questions **35**

4 Datasets and Data Transformation **38**
4.1 Crop data 38
4.1.1 Silage maize in Germany 38
4.1.2 Global Dataset of Historical Yields 39
4.1.3 The definition of yield shock 42

4.2 Meteorological data . . . 44
4.2.1 Climate indices for silage maize yield shock in Germany . . . 44
4.2.2 Climate indicators for the GDHY . . . 46
4.3 Future climate model data . . . 47
4.3.1 GCM-RCM model chains . . . 47
4.3.2 Data transformation and bias correction . . . 48

5 Statistical Modelling 50
5.1 Composite analysis . . . 50
5.2 Statistical modelling with LASSO . . . 50
5.2.1 Description of LASSO . . . 51
5.2.2 Model performance with Mathews Correlation Coefficient . . . 52
5.2.3 Variable importance in LASSO . . . 53
5.2.4 Predictor's contribution to low and high probabilities . . . 53
5.3 Statistical modelling with Random Forest . . . 53
5.3.1 Description of Random Forest . . . 53
5.3.2 Variable importance in Random Forest . . . 54
5.3.3 Partial dependence plots . . . 55
5.3.4 Shapley values . . . 56
5.4 Models' setup . . . 56
5.4.1 LASSO for maize yield shock in Germany . . . 56
5.4.2 Random Forest for maize yield shock in Germany . . . 58
5.4.3 Random Forest for crop yield losses across Europe . . . 58
5.4.4 Random Forest for crop loss in warmer climates . . . 60

6 Model Comparison of Climate Drivers of Silage Maize Yield Shock in Germany 62
6.1 Overview of yield shock series and composite analysis . . . 62
6.2 Comparison of variable importance between groups . . . 65
6.3 Comparison of predictive skill between set of variables . . . 68
6.4 Year-to-year prediction and variable contribution during historical losses . . . 69
6.5 Physiological response of silage maize yield shock to key climate drivers . . . 73
6.6 Discussion and summary . . . 74

7 Spatial Heterogeneity of Agricultural Losses Across Europe 77
7.1 Overview yield shock series . . . 77
7.2 Climatology and composite analysis of climate indicators . . . 79
7.3 Determination of variable importance and impact . . . 84
7.4 Performance of Random Forest ensemble . . . 88
7.5 Physiological response and spatial heterogeneity of the impacts . . . 92
7.6 Discussion and summary . . . 95

8 Future Climate Change Influence on Crop Yield Shock 97
8.1 Evaluation of historical simulations . . . 97
8.1.1 Comparison of climate drivers . . . 98
8.1.2 Analysis in predicted yield shock probabilities . . . 100
8.2 Changes in the climate drivers under global warming . . . 101

8.3 Drivers and yield shock risk under warmer climate . . . 105
8.3.1 Maize . . . 105
8.3.2 Winter wheat . . . 110
8.4 Physiological response to future climate warming . . . 116
8.5 Discussion and summary . . . 119

9 Conclusions **122**
9.1 Summary and key findings . . . 122
9.2 Discussion, implications and outlook . . . 125

Acknowledgment **130**

Appendices **132**

A Appendix to Chapter 4 **133**

B Appendix to Chapter 6 **136**

C Appendix to Chapter 7 **142**

D Appendix to Chapter 8 **147**

Bibliography **159**

1 Introduction

Agriculture is the primary source of food security. Originating around 20,000 B.C. in the first sedentary civilizations of the Near East (Flannery, 1973), it served as one of the main drivers of urban civilization development (Kluyver, 2013). Today, agriculture plays a crucial role on both local and global economic development (Food and Agriculture Organization of the United Nations, FAO et al., 2023). In 2014, approximately 14% of the world's ice-free land area was dedicated to crop production (Figure 1.1) with almost 10% of expansion in the last two decades (Potapov et al., 2022). Climate variability represents a major factor influencing crop production (Ray et al., 2015) and has historically acted as a key driver of both societal prosperity and collapse (Butzer and Endfield, 2012).

In recent decades, there has been a substantial increase in production in the agricultural sector (Figure 1.2a, FAO, 2024a). Technological developments (e.g. plant breeding, machinery, fertilization among others) have contributed to the outstanding growth in crop production per area, also referred as yield (Figure 1.2b). On the other hand, climate change has altered expected agricultural trends, primarily by augmenting variability and the frequency of abrupt losses (Lobell et al., 2011). Due to growing frequency and magnitude of extreme weather events (Intergovernmental Panel on Climate Change, IPCC, 2023), global warming has caused food insecurity increase, price volatility, malnutrition and, ultimately, a decline in quality of life (Kalkuhl et al., 2016).

The impact of extreme weather on the agricultural sector are also evident in Europe (Ben-Ari et al., 2018; Webber et al., 2020; Brás et al., 2021; van Oort et al., 2023). The European heatwave of 2003, for instance, caused losses of around 10% in agriculture and in some cases reached 50% (Posthumus et al., 2009). In this context, stakeholders have started implementing adaptation measurements to overcome and leverage the current and projected state of the climate. The Common Agricultural Policies (CAP), for example, aims to help farmers to adapt and mitigate climate change and support them financially (European Commission, 2024). Farmers themselves also adapt to the observed changes, for example by modifying planting date (Olesen et al., 2012) or incorporating more resilient varieties (Olesen et al., 2011). To develop effective adaptation strategies and sustain financial stability, it is necessary to understand the relationship between weather and climate variables and agricultural productivity (Reidsma et al., 2010; Olesen et al., 2012).

Recent literature on climate-related agricultural impacts focus on crop yield as a function of several factors (Figure 1.3). These ones can be grouped in climate (e.g. temperature and precipitation conditions among others), management (e.g. irrigation), soil (soil type and nutrients), technology (plant breeding) and other factors (e.g. carbon dioxide fer-

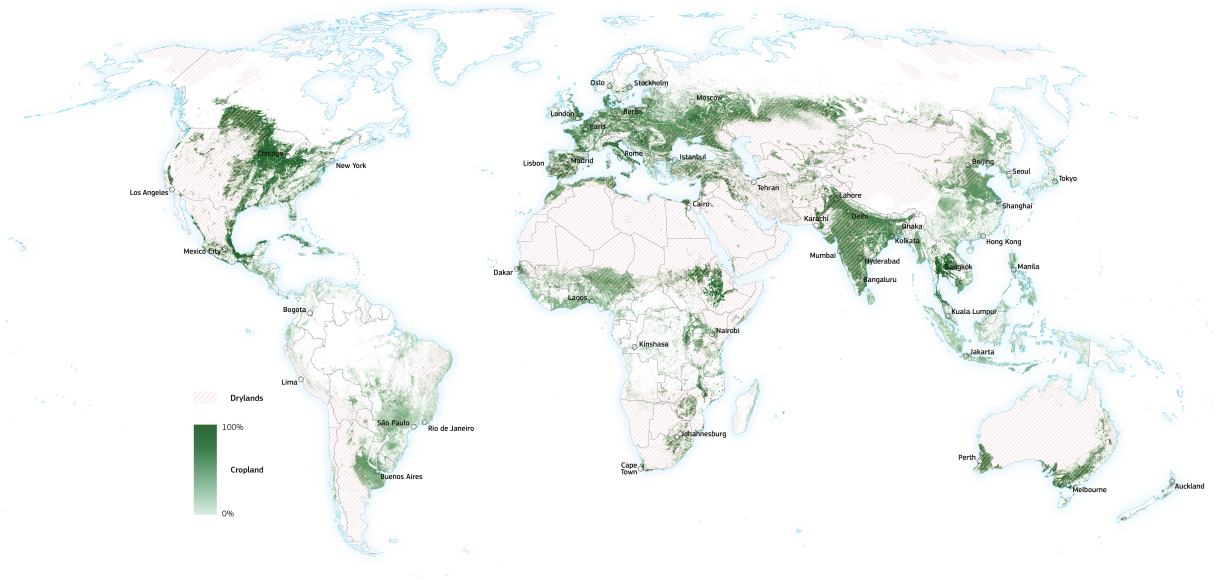

Figure 1.1: Global cropland (green shaded area). Reprinted from (European Commission Joint Research Centre, 2025), *Joint Research Centre*.

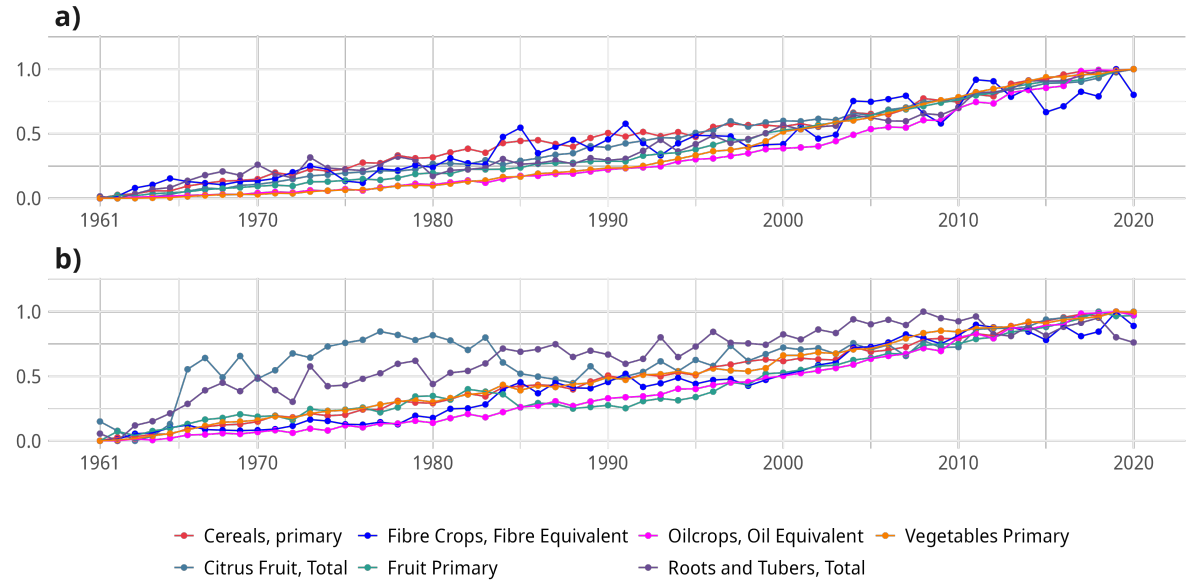

Figure 1.2: Series of (a) worldwide total production and (b) worldwide average yield for the main crop groups (colors). Data is extracted from the Food and Agriculture Organization of the United Nations (FAO, 2024a). To make the groups comparable between them, the individual series are normalized from 0 to 1. For the definition of each group, see FAO (2022).

tilization). The three implemented approaches encompasses experiment-based studies, process-based crop modeling, also called crop simulation models (CSM), and statistical modeling. Field experiments consist of direct measurements that, with proper isolation, provide the most reliable insight into the influence of studied variable. However, the implementation is cost-expensive and geographically constrained, producing limiting in-

Figure 1.3: Crop yield as a function of multiple drivers. Adapted with permission from Figure 1 in Hu et al. (2024), *Elsevier*.

sight. CSMs simulate crop growth by integrating weather, soil, and management factors. They are widely used to explore how crops respond to environmental stressors, evaluate farming strategies, and provide seasonal yield forecasts. Despite their strengths, CSMs often fall short in capturing the effects of extreme weather, require regional calibration, and depend on detailed input data that may not be available (van der Velde et al., 2012; Zampieri et al., 2018; Barlow et al., 2015).

The limitations of CSMs are bridged by statistical models. These are mathematical approaches to predict certain variable (in this case, crop yield) as a function of others (i.e. climate predictors). Statistical models can be used for exploring unknown relations between a set of predictors and a target variable, for evaluating previous evidence on new data or for establishing forecasts tools (Tredennick et al., 2021). With an adequate sample size, statistical models can be easily implemented at any spatial scale. In agriculture, they allow establishing previously unseen relations between a set of predictors and a target variable, and can serve as complementary tools for forecasting and CSM development (Ben-Ari et al., 2018; Zampieri et al., 2018; Webber et al., 2020).

Statistical models have been traditionally implemented to predict crop yield as a continuous variables. This means, they attempt to model the general variability of crop yield rather than targeting a specific segment (i.e. low yield or high yield). In this sense, they can not be used to identify the most relevant meteorological drivers of substantial drops in crop yield (Hu et al., 2024). This portion of the spectrum has been refereed in the literature as yield failure (Webber et al., 2020), yield extreme (van Oort et al., 2023), yield loss (Ben-Ari et al., 2018) and yield shock (Zhu et al., 2021) among others. These low-yield events influence insurance payouts, investment strategies in agriculture, and even government-level policy decisions concerning food security (Kalkuhl et al., 2016; Zhou et al., 2022; FAO, 2023b). Therefore, this thesis specifically focuses on understanding and modeling the meteorological drivers of yield shocks, with the goal of supporting more targeted and risk-aware decision-making in climate-agriculture systems.

Additionally, for the adequate application of statistical models, it is crucial to overcome the specific challenges that can be noticed in the literature. First, identifying relevant predictors is not straightforward, as it requires prior knowledge of crop vulnerability, since not all extreme weather leads to yield loss and vice versa (Smith, 2011; van der Velde et al., 2012). Many studies rely on aggregated climate indicators such as mean temperature or total precipitation (Beillouin et al., 2020; Webber et al., 2020), while others use threshold-based metrics derived from statistical definitions (Schmitt et al., 2022). These statistically defined variables help standardize and compare extreme weather events across regions by

quantifying their frequency and intensity (Zampieri et al., 2017). However, the specific advantages of using either simple or more complex variable types remain unclear (Ben-Ari et al., 2016). Therefore, this thesis analyzes to what extent more complex variables can enhance both our understanding and the predictability of crop yield losses.

The second limitation of statistical models concerns data availability. The recent European literature has pointed the importance of sub-seasonal (i.e. monthly scale) weather and climate variability on substantial losses (Ben-Ari et al., 2018; Webber et al., 2020), lacking a standard comparison at the European level. Conversely, Zhu et al. (2021) attempted to study the influence of seasonal drivers (i.e. 3 month-aggregated) on regional scale, disregarding potential national differences. In combination, addressing the climate influence on substantial drops in yield at finer temporal and spatial scale have not been attempted. Recently, hybrid datasets combining satellite and ground observations have shown potential for improving spatial assessments of environmental impacts on crops, though their application remains limited (Iizumi and Sakai, 2020; Kim et al., 2021). Thus, this thesis utilizes the Global Dataset of Historical Yields (Iizumi and Sakai, 2020), a gridded dataset based on satellite and reported yield data, which provides higher data availability across the European domain and thereafter can enhance model robustness. This study focuses on two major crops: maize and winter wheat. Ultimately, a standard country-to-country comparison of the most important climate drivers of yield shock is provided.

The final point regarding statistical models relates to their application. Traditionally, these models have been used in agriculture to assess impacts under present climate conditions. However, with ongoing global warming, the average climate conditions along with the nature of extreme weather events is expected to shift (IPCC, 2023). Subsequently, this would trigger changes in agricultural suitability and crop yield variability across Europe (Bednar-Friedl et al., 2022). To explore future impact of climate change on crop yield, Global Climate Models (GCMs) downscaled through Regional Climate Models (RCMs) are commonly used, which have the potential to capture future climate signals and variability. While these models have typically been applied in conjunction with CSMs (Webber et al., 2018), their integration with statistical models remains largely unexplored. Thereby, this study also investigates how the risk of maize and wheat yield shocks may evolve under future climate scenarios using a statistical modeling approach.

This thesis is organized as follows. Chapter 2 presents the theoretical background, covering general meteorological, agricultural, and statistical modeling concepts. Chapter 3 outlines the research gaps and formulates the research questions. Chapter 4 describes the datasets and their pre-processing. Chapter 5 details the methodology and statistical models employed. The results are presented in three chapters: Chapter 6 investigates the added value of predictor definition complexity; Chapter 7 examines country-to-country variability across Europe in the present climate; and Chapter 8 extends the analysis to future climate change scenarios. Finally, chapter 9 summarizes and remarks the main outcomes of this thesis. It finalizes with discussion on the methodological choices, limitations and future research considerations.

2 Theoretical Background

This chapter establishes the basis for understanding the motivation, methodology, results, and discussions of this thesis. As the work relates components of climate, statistics, and agriculture, the foundations of each discipline are first explained individually, followed by a discussion of their interactions. The chapter starts with an overview of general meteorological background concepts, a description of climate in Europe, and the suitability of agriculture in the country (Section 2.1). Section 2.2 illustrates how several environmental factors influence the growth and development of plants. These concepts are further described in Section 2.3, with a focus on the two major crops of this thesis (maize and winter wheat). Section 2.4 explains the specific techniques used to assess weather and climate impact on agriculture, and with a special focus on statistical models. Finally, Section 2.5 introduces the concept of a climate model.

2.1 General meteorological background and the European climate

The climate system (illustrated in Figure 2.1) is a dynamic and interconnected framework comprising five primary components: the atmosphere, hydrosphere, cryosphere, land surface, and biosphere. These components are in constant change, and interact with each other, making the system highly non-linear. Solar radiation is the most significant source of energy income and fluctuations. The atmosphere is a thick layer of gases (composed by several sub-layers) that surrounds the earth and is held by gravitational force. Some of these gases (the most renamed are Carbon Dioxide CO_2, methane CH_4 and water vapor H_2O) absorb and emit long-wave radiation, keeping the average surface temperature around 15 °C. The local variation of the concentration of these gases as well as the presence or absence of clouds (composed by H_2O in the three phases) produce local changes in the radiative budget.

The Earth's translation motion, quasi-elliptical shape and 23.5° axial tilt drive the seasonal cycle of the incoming solar radiation (Figure 2.2). In June, when the Northern Hemisphere is tilted toward the Sun, it receives more direct sunlight and longer daylight hours, resulting in warmer weather. In contrast, in December, when the Northern Hemisphere is tilted away from the Sun, the sunlight is less direct and daylight hours are shorter, leading to cooler temperatures. During the transition to autumn, days gradually become shorter, while in spring, as the Northern Hemisphere begins to tilt back toward the Sun, the days lengthen again.

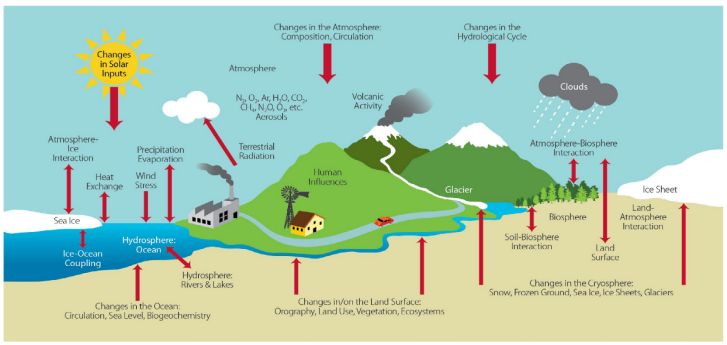

Figure 2.1: Schematization of the climate system. Reprinted from Figure 1 in Le Treut et al. (2007), *Cambridge University Press.*

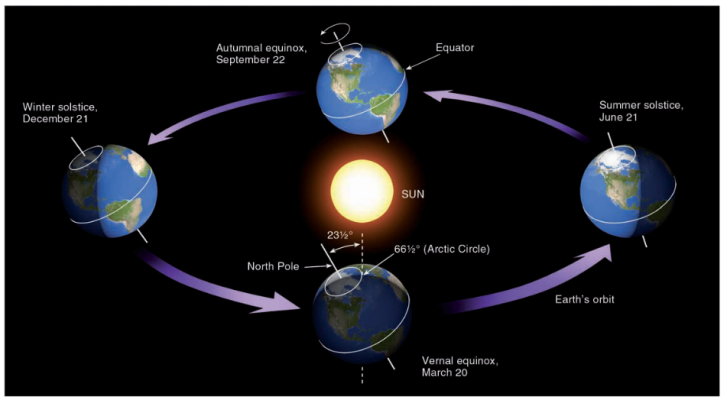

Figure 2.2: Earth's orbit around the Sun and seasons. Reprinted from Figures 3.3 in Ahrens (2009), *Brooks/Cole, Cengage Learning.*

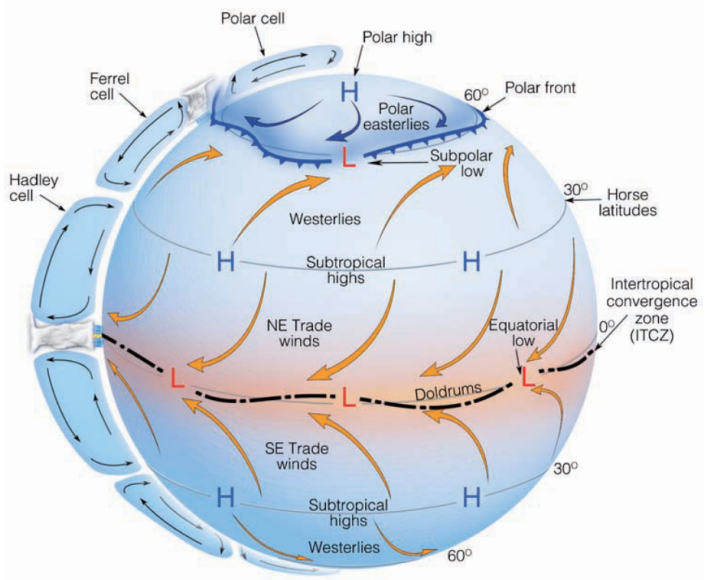

Figure 2.3: idealized wind and surface-pressure distribution over a uniformly water-covered rotating Earth. Reprinted from Figure 10.2 in Ahrens (2009), *Brooks/Cole, Cengage Learning.*

The Earth's shape and rotation produce a meridional imbalance in energy and heat, with higher temperatures near the equator than at the poles. This imbalance, combined with the Coriolis effect, drives the formation of large-scale atmospheric circulation patterns (Figure 2.3). These patterns are organized into three main cells in each hemisphere: the Hadley, Ferrel, and polar cells. The Hadley and polar cells are thermally direct, with warm air rising in low latitudes and cold air sinking at high latitudes, while the Ferrel cell, located in the midlatitudes, is thermally indirect. These vertical motions play a central role in shaping global precipitation: ascending branches of the circulation, found near the equator and around 60° latitude, promote convection and high rainfall, whereas descending branches, such as those near 30° and the poles, suppress convection and are associated with dry regions. From the surface branches of these cells emerge dominant wind systems: the trade winds (easterlies) close to the Equator and the westerlies in the mid latitudes.

2.1.1 Climate in Europe

Europe is a highly fragmented and heterogeneous landmass that constitutes the western part of the Eurasian continent. It has long peninsulas like the Iberian Peninsula, mountain ranges like the Alps, the Pyrenees or the Scandinavian range, and surrounding islands (like Iceland or the British Isles). Europe has coastlines on the Arctic Ocean and the Baltic Seas in the north, the Caspian Sea to the southeast, the Black Sea and the Mediterranean Sea in the south, and the Atlantic Ocean to the west. The southernmost points in Europe (south Iberian Peninsula, southern Italy and some islands in the Mediterranean Sea) are around the latitude 36°N. In contrast, the northernmost points (northern Norway and Iceland) are roughly at 70°N. The landmass also features distinct geological areas like the central European Uplands, highly-loess concentrated soil mass in the Great European plain and major sources of freshwater such as the Rhine basin.

Figure 2.4a and b display the seasonal average temperature and total precipitation respectively for Europe. Conventionality and orography strongly influence the climatology of the region. In general, southern regions are characterized by warmer temperature and drier conditions throughout the year. Here, recurrent droughts and prolonged dry periods are usual, with precipitation absent during a whole season (Casanueva et al., 2014; Moemken and Pinto, 2022). In contrast, the northern regions features colder temperatures with high cloud coverage and precipitation throughout the year (Peña-Angulo et al., 2020). In addition to this, continentality and topography also alter temperature and precipitation patterns locally. Eastern Europe experience strong interseasonal variability, with very high temperatures in summer but with values easily plunging below 0 °C in winter. The Scandinavian mountain range is the wettest region in the continent with cumulative rain reaching more than 300 mm or even 400 mm. The Alps, located in central Europe, also feature cold temperatures winter and high rainfall, especially during summer and autumn.

Besides the seasonal climatology, the European in-season (or sub-seasonal) climate is influenced the displacement of air masses (Figure 2.5; Kallos et al., 2007; Lépy and Pasanen, 2017). These are extended regions of approximately homogeneous characteristics in terms of temperature and humidty (Ahrens, 2009). Air masses are classified by their origin, in terms of latitude (Tropical, Equatorial, Polar, Arctic or Antarctic) and topography (Continental or Maritime); depending on the region these feature warm/cold or humid/dry

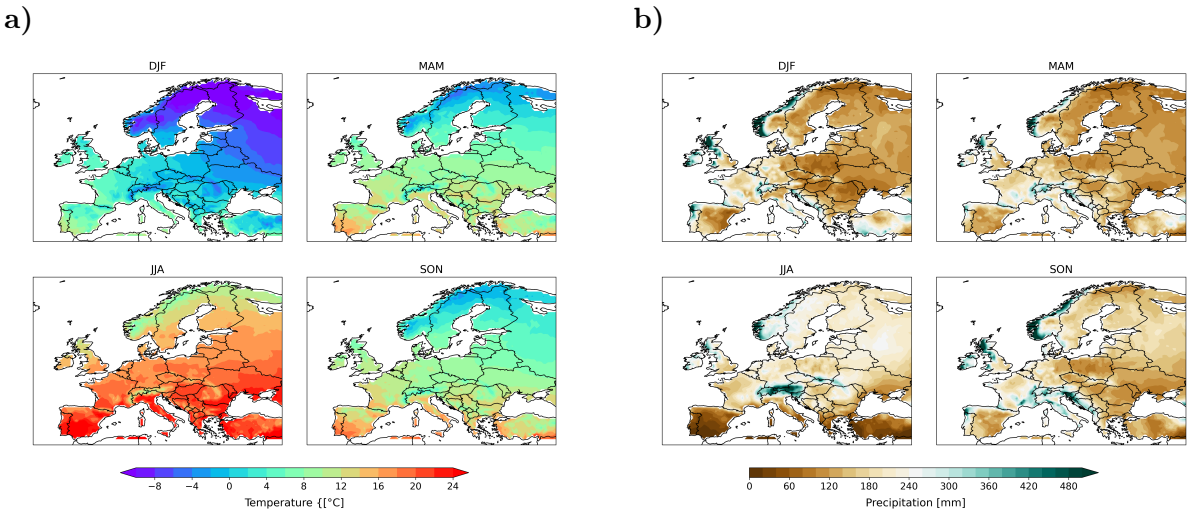

Figure 2.4: Seasonal average temperature (a) and total precipitation (b) for winter (DJF), summer (JJA), spring (MAM) and autumn (SON). The values are computed using daily average temperature and total precipitation data from the ensemble version v27.0e of E-OBS (Cornes et al., 2018) using the 1981-2021 period.

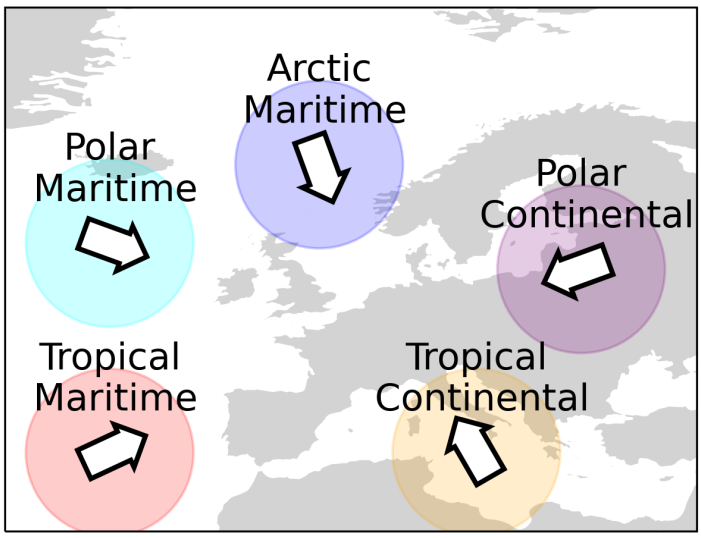

Figure 2.5: Schematization of air masses around Europe.

conditions. The Tropical Maritime air mass coming from the Atlantic Ocean is characterized by warm and humid temperatures, whereas the Tropical Continental coming from northern Africa is dry and warm. The Polar Maritime and Arctic Maritime are characterized by cold temperatures and humid conditions, while the Polar continental has rather dry conditions. The frequency, presence and characteristics of air masses as well as the advection changes depending on the season.

Air masses are transported by wind. This process is also known as advection, which plays a crucial role in modifying the weather conditions of the region they reach (Trigo et al., 2002; Pithan et al., 2018; Kautz et al., 2022). In particularly, the movement of airmases is

modulated by spatial air pressure distribution. As an example, the meridional preassure gradient in the north Atlantic Ocean modulates the westerly winds intensity (Trigo et al., 2002). Typically, a higher air preassure difference between the subtropical preassure and the polar region brings relatively humid, warm air, resulting in higher temperatures and precipitation, whereas a weakening of the gradient leads to drier and cold conditions. Another example atmospheric blocking, a persistent high-pressure system in the mid- and high-latitude regions. This phenomenon disrupts the typical zonal (west-to-east) flow of the westerly winds, causing them to shift into a meridional (north-south) pattern. As a result, air masses move meridionally, which can lead to prolonged weather extremes (Kautz et al., 2022). Notable events associated with atmospheric blocking include the 2002 European floods, the 2003 European heatwave, the 2012 European cold wave, and the 2018 European heatwave.

Figure 2.6a displays the monthly interannual variability of mean temperature in Europe. Between November and March, central, eastern, and northern Europe experience interannual variability exceeding 3 °C. For precipitation, between October and March, the monthly interannual variability exceeds 60 mm in north Scandinavia, north Great Britain, Portugal, Italy, and the Alps. From the centre of western regions (including western France) until eastern areas (including Slovakia and western Ukraine), precipitation can vary from 40 mm to 60 mm. In contrast, from April to October, the variability reduces, generally between 1 °C and 3 °C across Europe. The monthly precipitation variability (displayed in Figure 2.6b) is also notable. This greater variability is generally due to stronger transitions between NAO phases during the winter months compared to summer (Trigo et al., 2002; Hurrell et al., 2003).

Due to global warming, Europe has experienced strong changes in its climate. Although there is regional variability, temperature increases have become evident for the entire region (Watson et al., 1997; Krauskopf and Huth, 2020). Furthermore, global warming is also related to an increasing severity and frequency of several weather extremes such as heatwaves (Russo et al., 2015; Lhotka and Kyselý, 2022). The regions in the northern half of Europe have experienced an increase in annual rainfall; extreme precipitation and stream flows have also become more severe in central and northern Europe (Madsen et al., 2014). In contrast, droughts have become more frequent, longer and more severe in the Mediterranean region (Spinoni et al., 2015). With ongoing climate change and considering business-as-usual climate scenarios, extreme weather events are expected to increase in terms of frequency and severity (Watson et al., 1997; Beniston et al., 2007; Seneviratne et al., 2021).

2.1.2 Agriculture in Europe

Ramankutty et al. (2002) and Licker et al. (2010) assessed the global land suitability for agriculture. These studies found that the European continent, among other regions in the world, is highly suitable for agriculture, especially for some of the major crops like wheat or maize. What sets Europe (mainly Western Europe) apart from the rest of the world is the region's exceptionally high actual reported yields. This is also illustrated in Figure 2.7, where a relatively high yield in the European Union can be observed compared to the other continents for almost all the crop groups. The reason is attributed to advanced agricultural management and technology in European countries, which have made significant strides in

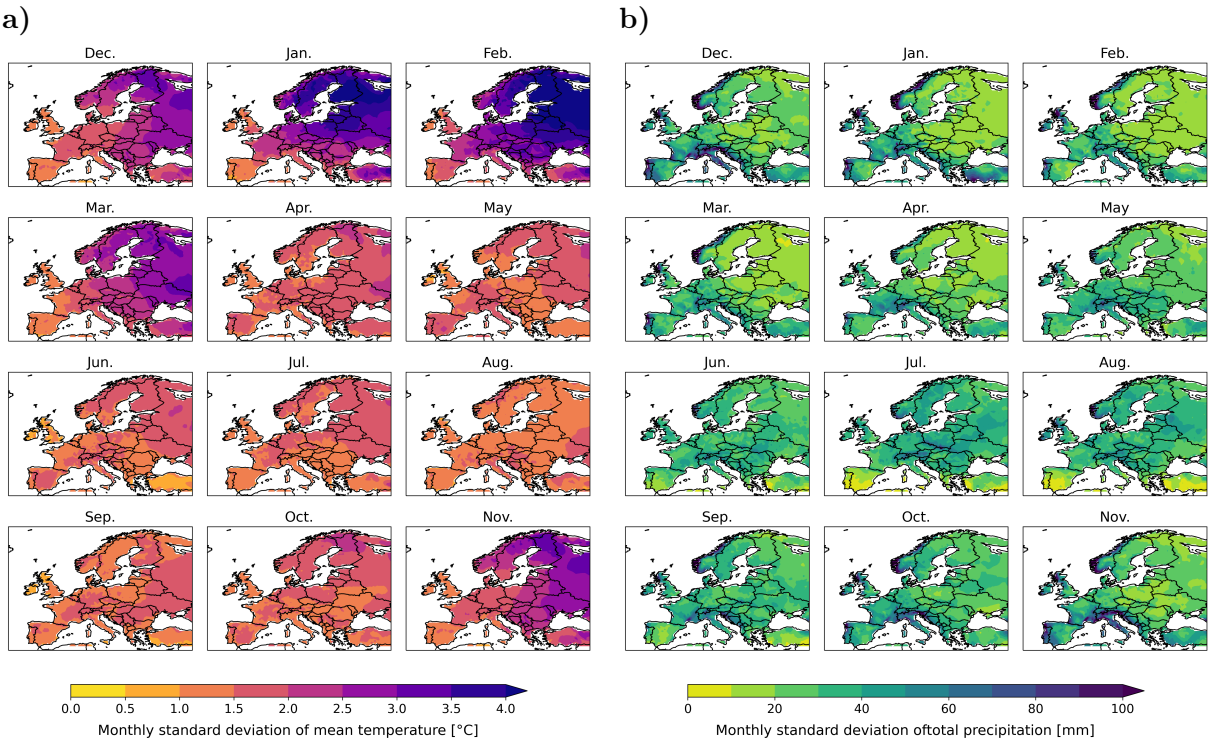

Figure 2.6: Same as Figure 2.4 but for the monthly standard deviation of mean temperature (a) and total precipitation(b). Values are calculated by first computing the monthly mean temperature (and total precipitation) and then computing the interannual standard deviation by month.

technological improvements related to genetic improvements and management practices, like nitrogen implementation or irrigation (Licker et al., 2010; Pujol Andreu, 2011). In 2021, for example, Europe contributed more than one-third to worldwide wheat, potatoes, oil rapeseed and oil sunflower production, and roughly a tenth of maize production (FAO, 2023a).

However, the recent increasing of extreme weather events in Europe has a direct impact on the agricultural sector (Figure 2.8). Some of the most widely studied stressors are droughts, heatwaves, frosts and floods (Brás et al., 2021). The European heatwave of 2003, for example, was characterized by both dry conditions and elevated temperatures that hit several regions during June and August (Fontana et al., 2015). The agricultural sector was severely affected across central European countries, with losses of about 10% in total wheat production and 21% in total maize production, with some districts having reported a reduction of more than 50%. In 2007 in England, he estimated losses in flooded areas were about 40% in cereals (Posthumus et al., 2009). Multiple extreme weather events in 2016 led to a national loss of 27% in wheat in France (Ben-Ari et al., 2018). These impacts will likely increase under future climate change scenarios (Bednar-Friedl et al., 2022).

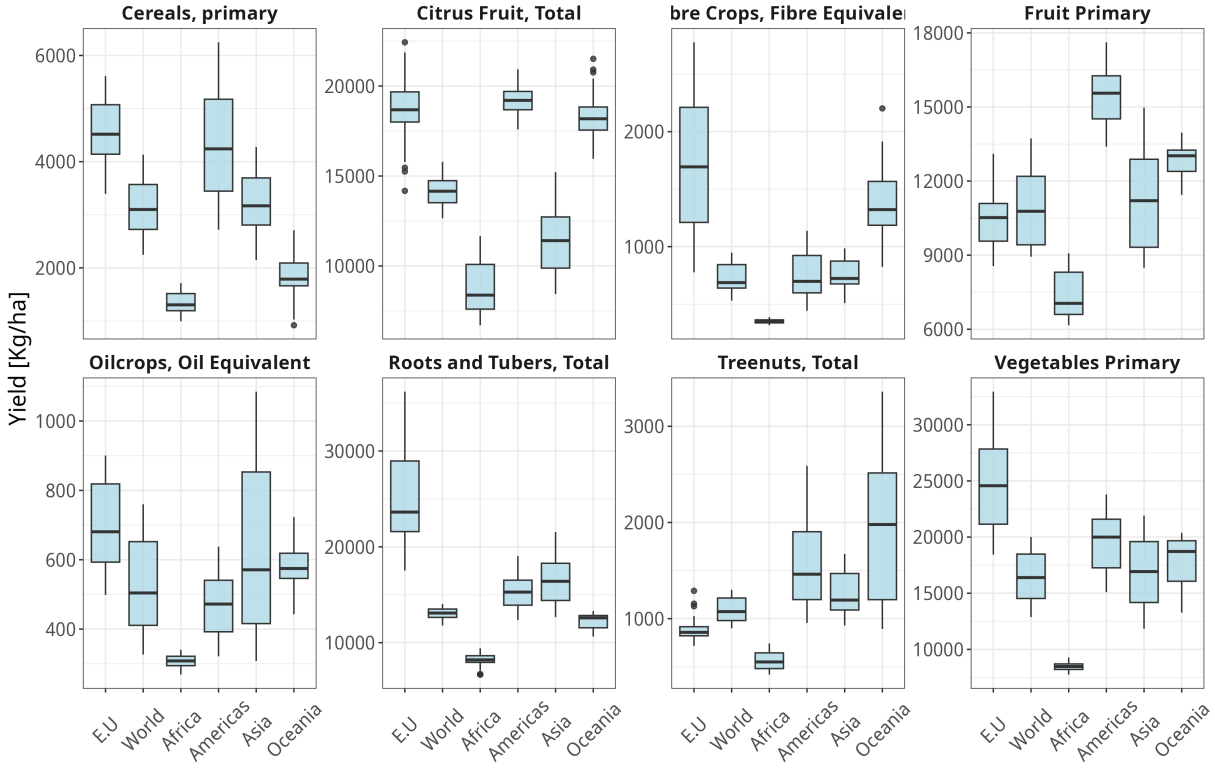

Figure 2.7: Distribution of crop yield for main crop groups for each continent and for the European Union (E.U). Data ranges from 1980 to 2020 and is obtained from FAO (2024a). For the definition of each crop group, see FAO (2022).

2.2 Environmental factors influencing crop growth and development

In Section 2.1, the climate in Europe and its suitability for agricultural practice are described. To understand how weather and climate influence crop yields, this section focuses on the environmental elements that affect plant physiology.

In botany, there is a difference between the concept of growth and development. Growth refers to the accumulation of biomass, weight, height or volume, and it is a quantitative value that can be measured. Development is a qualitative process that refers to changes in the morphology of the plant, aiming for the reproduction and perpetuation of the species. Development is related to the succession of visible (and also invisible) changes, which are referred to as phenological stages (associated with the successive observed phenomena). When assessing agricultural productivity, process related to both growth and development are equally relevant to understand. Several environmental factors modulate these processes.

The three most relevant factors modulating growth and development are radiation (specially the visible spectrum from radiation), temperature and water. Radiation is associated with growing and flowering, water plays a crucial role in growing, and temperature is a crucial modulator in the metabolic processes of plants (i.e. modulates growth and

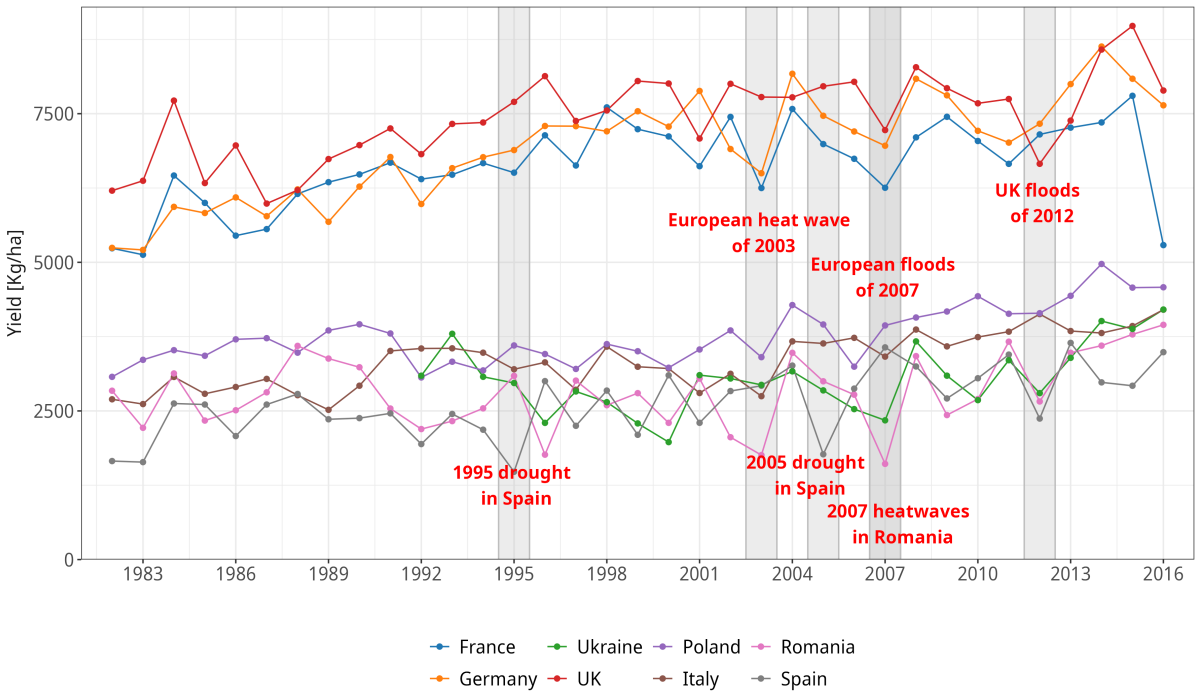

Figure 2.8: Wheat yield series for major producers in Europe (in colours) and documented weather and climate extreme in the region (red text). Data is obtained from FAO (2024a).

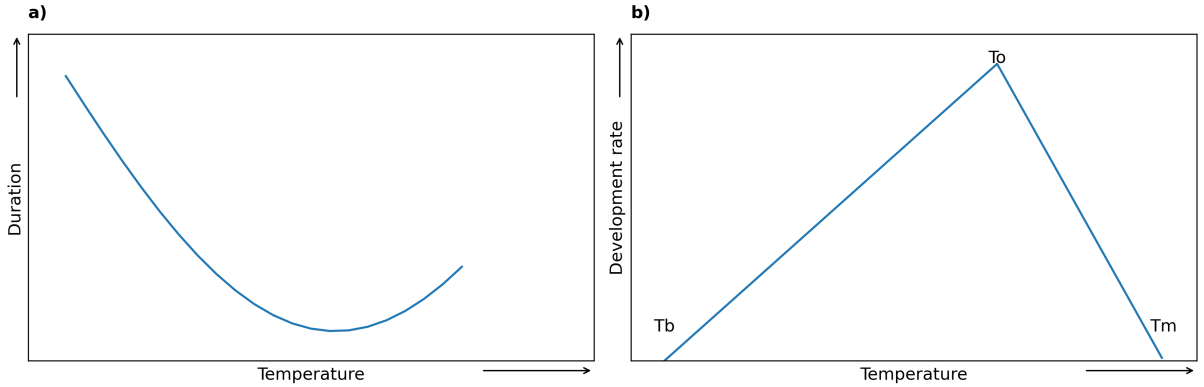

Figure 2.9: Idealized response of duration (a) of a phenological stage and development rate (b) to temperature. T_b refers to base temperature or also minimum temperature, T_o to optimal temperature, and T_m to maximum temperature. Adapted from Figure 2.4 in Andrade and Sadras (2002), *National Institute of Agricultural Technology (INTA)*.

development). Additionally, the soil properties like texture and chemical composition, and atmospheric composition (including CO_2, O_2, ozone O_3 and H_2O or most specifically relative humidity), play relevant roles in growth and impact. The following subsections provide a detailed description of these factors.

2.2.1 Temperature

Temperature is the most relevant factor in determining a plant's suitability in a region. Under proper light conditions, temperature is the determinant factor for development. Furthermore, with adequate water provision and light, temperature becomes the determinant factor for growing.

Temperature thresholds

A way to understand the effect of temperature is by considering temperature thresholds. These cardinal points (cardinal temperatures) delimit plant survival, growth and development. Temperature thresholds are practically unique for each individual plant, process and phenological stage (Porter and Gawith, 1999; Luo, 2011). Plants can only develop under specific temperature conditions.

Figure 2.9 schematizes the idealized duration of a phenological stage as a function of temperature. The duration decreases with lower temperature up to a certain point, after which it begins to rise again. Figure 2.9b illustrates the corresponding development rate (Duration^{-1}). The development rate increases from a so-called base temperature (T_b) up to a point of maximum rate, referred to as the optimal temperature (T_o); beyond this point, it declines sharply until it ceases entirely above the maximum temperature (T_m). In general, the inequality $T_m - T_o < T_o - T_b$ holds, indicating that plants typically tolerate cooler temperatures (relative to T_o) better than excessively high ones. This non-linear relationship also characterizes growth or biomass accumulation.

Lethal temperatures

Lethal temperatures refer to the thresholds (lower and upper thresholds) at which the effect of temperature becomes damaging or lethal. This threshold varies depending on the species and even to the phenological stage, as well as the exposure's duration, frequency and magnitude. Early lab studies focus on the temperatures at which plants can not survive (Porter and Gawith, 1999). However, a high frequency of very high temperature (or very low temperature) can produce physiological alterations in the plant and cause losses in quality or yield (Barlow et al., 2015). Winter crops (meaning that their growing cycle takes place mainly during winter) have typical thresholds of $-15\,^{\circ}\text{C}$ to $0\,^{\circ}\text{C}$ as a lower threshold and around $40\,^{\circ}\text{C}$ to $45\,^{\circ}\text{C}$ as an upper threshold, whereas summer crops (meaning that their growing cycle takes place mainly during spring and summer) have typical lethal temperatures of $-5\,^{\circ}\text{C}$ to $0\,^{\circ}\text{C}$ and $40\,^{\circ}\text{C}$ to $50\,^{\circ}\text{C}$.

Vernalization

Some types of plants (especially long-season crops like winter wheat) require cold exposure for later blooming. This process is called "vernalization", and if these plants are sown in spring (after winter), flowering can be delayed or even aborted. Vernalization is a cumulative process that accelerates flowering over long days. This process is crucial since it allows to delay flowering after winter and, in this way, avoid frost damage in the sensitive periods (Trevaskis, 2010). Vernalization response occurs only at temperatures around or above freezing; optimal temperature typically ranges between $0\,^{\circ}\text{C}$ and $10\,^{\circ}\text{C}$.

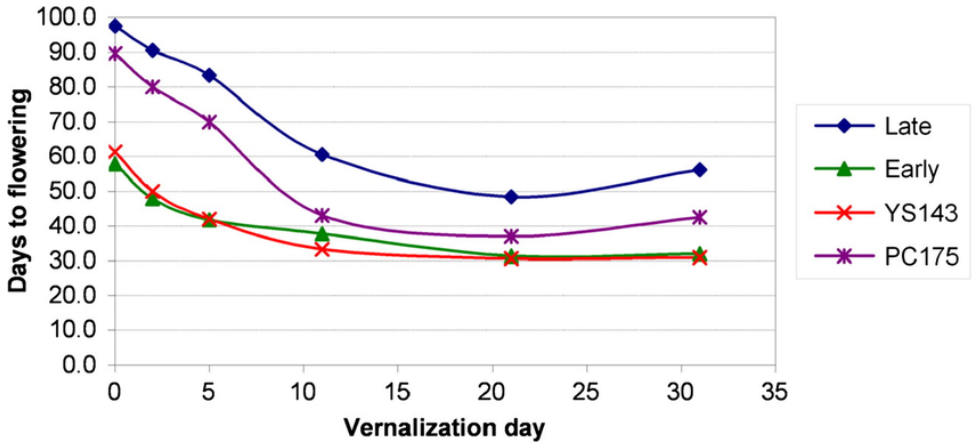

Figure 2.10: Effect of vernalization on flowering time obtained in a set of experiments with different populations of rapes (See Zhao et al., 2010, for the setup and details of the experiment). Reprinted with permission from Figure 3 in Zhao et al. (2010), *Journal of Experimental Botany, Oxford Academic*.

Vernalization is exemplified in Figure 2.10 for rapes, where flowering time is depicted as a function of vernalization days for different populations of rapes. For all the experiments, days to flowering reaches minimum when vernalization days approaches 20. In contrast, the number of days to flowering is maximized when vernalization is null.

2.2.2 Water, transpiration and evapotranspiration

Water is essential for growing and for regulating the temperature inside the plant. Water makes up most of the mass of plant cells. It is the most abundant and also considered the most limiting factor for growing.

The water movement form the roots to the whole plant is possible due to transpiration, which refers to the release of water vapour from the leaves into the atmosphere. Transpiration is only feasible when there is a difference between the water vapour content in the atmosphere and in the intercell space on the leaves (which is usually close to saturation). Therefore, when the air is dry (or the relative humidity is low), atmospheric demand for water is high and thus transpiration increases. Transpiration also works as a cooling mechanism for plants. Evapotranspiration integrates both evaporation and transpiration (Allen et al., 1998) and depends on several factors: the atmospheric demand for water (i.e. relative humidity), temperature, soil moisture, foliar area (the total area covered by leaves), type of plant, and the development stage. Soil moisture refers to the water content in the soil, and it relates to the available water for plants. Soil moisture mainly increases with precipitation and decreases with evapotranspiration. In agriculture, irrigation is a common practice to maintain good water balance, especially in critical periods of plant growth (Attri et al., 2022).

2.2.3 Radiation, photosynthesis and photosynthesis pathways

Several botanical processes are influenced by radiation. Here, we delve into the one correspondent to the spectrum between 400 mm to 700 m. This is also called Photosynthetically

Table 2.1: List of agricultural weather hazards and potential damages.

Hazard	Potential damage
Frost	Metabolic halt, risk of plant cell death.
Chilling	Photosynthesis inhibition
Heatwave	Heat stress, photosynthesis inhibition.
Drought	Plant growth inhibition, increasing risk of heat stress.
Pests	Physical damage
Disease	Biomass loss, quality loss
Floods and Water logging	Reduced nutrient uptake efficiency, increasing risk of pests and disease proliferation.
Hail	Physical damage

Active Radiation (PAR) and coincides with the largest portion of energy emited by the sun. Photosynthesis is the process by which plants can synthesise glucose ($C_6H_{12}O_6$) and release oxygen (O_2) by using water (H_2O), carbon dioxide (CO_2) and PAR. In the environment, energy is obtained from solar radiation, water from soil moisture, and CO_2 from the air.

As previously discussed, factors like water availability and temperature are also critical in regulating plant growth. However, how plants respond to these environmental conditions varies depending on their adaptation to specific habitats. These differences are reflected in the three main photosynthetic pathways: C3, C4 and CAM. Depending on the pathway, it enables plants to optimize their growth and survival in diverse environments.

Most land plants (∼85%) are C3 plants, which directly use CO_2 from the atmosphere during photosynthesis. These plants, such as wheat, grapes, oats, and berries, are common in mid and high-latitude regions. However, they face a trade-off between taking up CO_2 and limiting water loss through their stomata. In dry conditions, stomata are close to conserving water, which reduces CO_2 uptake and limits photosynthesis. High temperatures can exacerbate this by reducing transpiration, leading to heat stress. C4 and CAM plants are better adapted to hot and dry environments. C4 plants, like maize and sugarcane, initially fix CO_2 into four-carbon compounds, allowing photosynthesis to continue even when stomata are partially closed. CAM plants, common in desert areas, fix CO_2 at night when temperatures are colder. While these pathways are more water-efficient, they require more energy, meaning that C4 and CAM plants need more sunlight to thrive.

Figure 2.11 displays the CO_2 assimilation as a function of leaf temperature for C3 and C4 plants, with data gathered by (Yamori et al., 2014). The information for CAM plants should be ignored due to a lack of comparable experiments (specifically, only experiments during the night were considered; Yamori et al., 2014). In general, C3 plants have relatively higher CO_2 fixation in low temperatures compared to C4 plants. In contrast, C4 plants have much higher CO_2 fixation in warmer environments compared to C3.

2.2.4 Weather hazards and stressors

In addition to the biophysical relations described above, there is a list of weather and climate adversities which act as stressors and can produce severe damages in plants, or reduce drastically crop production. These stressors (summarized in table 2.1) can manifest singly, or simultaneously, and the impact can be cumulative (Bevacqua et al., 2021; Nóia Júnior et al., 2023). A detailed description of these stressors is provided below.

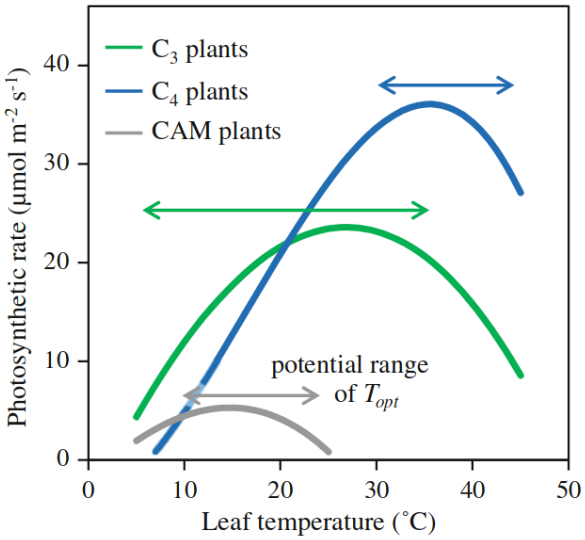

Figure 2.11: Typical temperature responses of photosynthesis in C3, C4 and CAM plants. Temperature responses of photosynthesis are pooled from the published data and are averaged in C3, C4 and CAM plants. The information for CAM plants should be ignored due to lack of comparable experiments (Yamori et al., 2014). Reprinted with permission from Figure 4 in Yamori et al. (2014), *Photosynthesis Research, Springer Nature.*

Heat stress: It refers to any temperature elevation that can cause permanent injuries to growth and development in the plant (Ul Hassan et al., 2022). Heat stress occurs tipically when the plant can not compensate the temperature differences with the environment. This occurs either when ambient temperature is suffitiently high to cause severe damages (i.e. above maximum temperature, Figure 2.11), or when transpiration is limited due to water scarcity. The effect of high temperature in plants are numerous (dos Santos et al., 2022). One of the most important is the sharply reduction in photosynthesis rate as well as the carbohydrate reserves (Taiz and Zeiger, 2002). Generally, C3 plants are more sensitive to C4 plants and CAM. Events of heat stress are observed during heatwaves, and can last during several days or weeks (Fink et al., 2004).

Frost and chilling: Frost refers to the period in which air temperature drops below the freezing point (0 °C). In this case, ice formation can occur inside the plant, causing severe damages or killing. The impact depends on the temperature, water vapor content, total exposure and the specie. Chilling refers to low temperatures which are not below the freezing point, but are still detrimental for the plant. In this sense, detrimental is relative to the specie itself, with temperatures ranging between 0 °C to 15 °C. Typically, plants with heat tolerance tends to be highly sensitive to low temperatures.

Drought and water stress: It is one of the major abiotic stressors in agriculture and also one of the most studied ones (dos Santos et al., 2022). Drought refers to a prolonged and sustained water deficiency compared to normal conditions (Mishra and Singh, 2010). Thought related between them, the definition of drought varies depending on the discipline (e.g. meteorological drought, agricultural drought, hydrological drought). In agriculture,

it refers to the substantial soil water scarcity that hinders crop growth or can even be lethal. Additionally, as previously mentioned, drought can also cause increase in the risk of heat stress due to limiting transpiration. However, the underlying impacts are complex and still under research (dos Santos et al., 2022). Events of drought typically last from weeks to months (Rousi et al., 2023).

Water logging and high precipitation: Water logging occurs when the amount of water in the soil is above the field capacity, producing an extra layer of water over the surface. This usually takes place after prolonged periods of precipitation. Water logging can lead to soil's chemical composition alteration, hypoxia (shortage of oxygen or anoxia), nutrient leakage and anatomical alteration (Maryam and Nasreen, 2012). Furthermore, waterlogging at the beginning or end of the season can constrain field operations by delaying sowing or limiting harvesting (Gobin, 2010; Olesen et al., 2012; Van Oort et al., 2012). In addition to water logging, extended precipitation periods are linked to reduced radiation and less photosynthesis, pest and disease proliferation(Nóia Júnior et al., 2023).

Hail: It refers to the solid precipitation spheroidal, conical or irregular in form, and generally with 5 mm of diameter or more (American Meteorological Society, 2012). Hailstorms are a mesoscale phenomenon, with severe and localized impact, which ranges from foliar loss (i.e. leaves loss), fruit loss and stem breackage.

Pests and diseases: Pests refer to a living being that has a nutritional relationship with a plant. Disease refers to a physiological alteration within the plant affecting homeostasis and, in some cases, producing visible morphological modifications. Although pests and disease are not a climatic hazards per se, their proliferation relies on the weather and climate conditions. Disease and pests outbreaks are influenced by temperature and humidity (Tho et al., 2019), or after long precipitation events (Rowlandson et al., 2015). Their spatial proliferation also depends on wind (Xu and Ridout, 2001).

2.3 The importance, the growth and the development of maize and wheat

The previous section focuses entirely on environmental factors influencing the growth and development of plants in general. This section examines the crops studied in this thesis: maize and wheat.

Maize and wheat plants are considered major crops since they play a crucial role in food security and development (Leff et al., 2004; FAO, 2024a). These plants are two of the most important crops in the world in terms of production, along with sugar cane and rice (FAO, 2024a). Both cereals are essential nutritional sources and are utilized for animal forage and ethanol fuel generation (Ranum et al., 2014). Europe accounts for over a third of the worldwide wheat production, meaning that any substantial drop in European wheat production can lead to teleconnected supply losses (d'Amour et al., 2016). Roughly 10% of global maize production comes from Europe and is mainly used in internal and intercontinental trade (Wu and Guclu, 2013). In general, maize production and yield

Table 2.2: Summary of the main differences between maize and winter wheat.

	Maize	**Winter wheat**
Planting	∼Spring	∼Autumn
Harvesting	∼Summer	∼Summer
Lethal temperatures	Max.: ∼45 °C Min.: ∼−2 °C	Max.: ∼45 °C Min.: ∼−15 °C
Optimal Temperature	∼20 °C to 25 °C	Planting: ∼20 °C Middle of cycle: ∼0 °C to 10 °C End of cycle: ∼20 °C
Vernalization	No	Yes
Water requirements (High yield)	∼500 mm to 800 mm	∼450 mm
Most sensitive period	Around flowering	Tillering (vernalization) Around flowering

losses in Europe lead to market instability and increases in importations (Chatzopoulos et al., 2020).

Table 2.2 summarizes the main differences between wheat and maize. Both crops adapt and evolve in different regions, resulting in distinct characteristics. The following sections explain the fundamental reasons for their global importance as well as the growth and development of each crop.

2.3.1 Maize

Maize (*Zea mays*), also called corn, is one of the most important crops in the world, in terms of production (FAO, 2024a). This crop is used for human consumption and fuel production and also serves as raw material for many industries, such as the food or textile industry (FAO, 1992). However, the major use is for animal feeding. The oldest archaeological evidence from maize domestication was found in Mexico and later spread through the American continent (Piperno et al., 2009; Tenaillon and Charcosset, 2011). There is evidence that it was introduced to Europe from the Caribbean in the late 15^{th} century and from North America during the 16^{th} century. The large-scale molecular analysis shows that most of the southern European maize is related to Caribbean maize, which is more adapted to warmer climates, whereas central European maize is more related to north American maize, which is more adapted to temperate climate (Tenaillon and Charcosset, 2011). Additionally, successful breeding techniques and hybridization have led to a substantial increase in maize yield during the second half of the 20th century (Tenaillon and Charcosset, 2011).

Maize yield is determined by the plant density (number of plants per area), the number of cobs per plant (usually between 1 and 2), the total number of kernels (grains) per cob, and kernel weight. In a field, the total number of grains and grain weight is estimated by sampling, producing both underestimation and overestimation (Ngoune Tandzi and Mutengwa, 2020). Maize yield is estimated differently for different purposes. When using

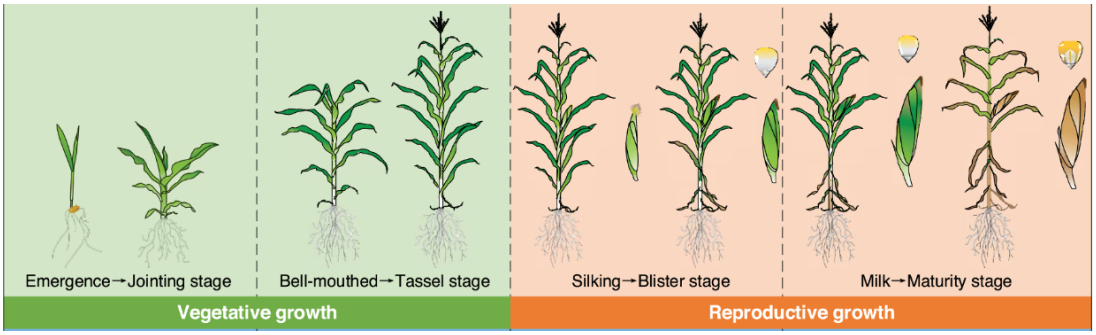

Figure 2.12: Phenological stages of maize. Adapted with permission from Figure 3 in Wan et al. (2022), ©*Elsevier*.

maize for animal feeding, for example, farmers harvest all aerial parts of the plant, chop them, and transport them into silos for fermentation (also called "silage maize").

Growth and development of maize

Maize has a cycle ranging between 3 and 5 months (FAO, 2024b). It is also considered a summer crop, with sowing dates typically in spring and harvest during late summer in mid-latitude regions. The most widely used scale to identify the stages of development is the one developed by Ritchie and Hanway (1986), also illustrated in Figure 2.12. It consists of two main stages, the vegetative stage and the reproductive stage, and their subdivisions. The beginning of the reproductive stage also refers to flowering. The stages do not overlap. However, the growth of the reproductive parts of maize already starts during the early part of the cycle.

Environmental factors influencing maize growth and development

The suitability of maize is mainly constrained by three factors: frost, soil moisture, and temperature (Maton et al., 2007). The seeds of maize require warm and humid conditions to emerge; dry and cold conditions at sowing can delay emergence by up to two weeks or even prevent it altogether (Smith and Hamel, 1999). As a C4 plant, maize is well-adapted to high-light environments and can continue photosynthesizing under high-temperature conditions (Crafts-Brandner and Salvucci, 2002).

Figure 2.13 illustrates the temperature thresholds of maize for each development stage, extracted from Sánchez et al. (2014). Overall, there are small changes in the sensitivity of maize to temperature along the cycle. The maximum development rate is around 27 °C to 30 °C, and the maximum temperature is about 40 °C at the beginning of the cycle, which decreases to 35 °C by grain filling. The minimum temperature is always close to 10 °C in the whole cycle. The lethal minimum temperature is −1.9 °C, whereas the lethal maximum temperature is around 46 °C.

Depending on the climate, maize requires between 500 mm and 800 mm of water for high yield (FAO, 2024b). The maximum sensitivity to environmental conditions is around flowering when the total number of kernels is determined. During this stage, lack of water, in addition to sunlight restriction, can sharply reduce the total number of kernels,

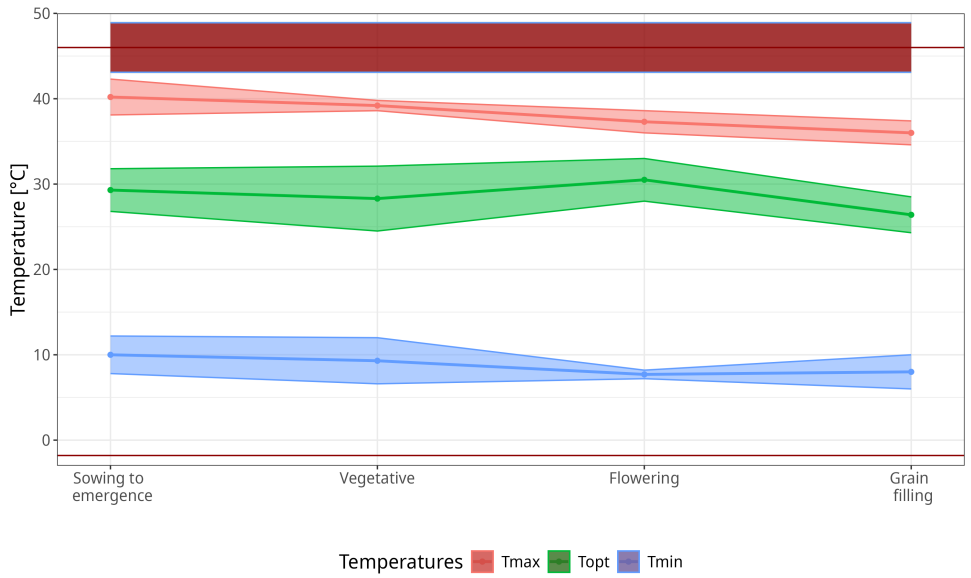

Figure 2.13: Estimated temperature thresholds of maize for each stage, obtained from Sánchez et al. (2014). The minimum or base temperature ($Tmin$, blue), Optimal temperature ($Topt$, in green), maximum temperature ($Tmax$, in red) and lethal temperatures (horizontal dark red) are illustrated. The opaque represents the average value, and the corresponding shades illustrate the standard error.

i.e. yield (Andrade et al., 2000; FAO, 2024b). This also refers to the critical period of maize (Andrade and Sadras, 2002).

2.3.2 Wheat

Wheat is one of the major crops in the world and ranks as the fourth most important crop in terms of production (FAO, 2023a). What sets wheat apart from other crops is its remarkable adaptability to different climates, as it is cultivated in both tropical regions and very high latitudes. Wheat is considered a significant source of carbohydrates, proteins, and fibres (Shewry and Hey, 2015). Apart from most common varieties, wheat can be classified as "winter wheat" and "spring wheat". Wheat was first domesticated around 10,000 BC in the Middle East (de Sousa et al., 2021). Through natural hybridization and anthropogenic selection, new wheat varieties emerged, leading to the development of the most common forms today: "common wheat" or "bread wheat" (*Triticum aestivum*) and "durum wheat" (*Triticum turgidum* var. *durum*). Wheat yield is determined by the total number of grains per area.

Growth and development of wheat

The variety of our interest is winter wheat, which is a long-day plant and has a cycle ranging from 180 to 250 days (FAO, 2024c). It is considered a winter crop, which means that it is planted during autumn, its main vegetative cycle takes place during winter, and it is harvested in early summer. The most widely used scale to determine the phenological stages is the Zadoks scale (Zadoks et al., 1974, also illustrated in Figure 2.14), which

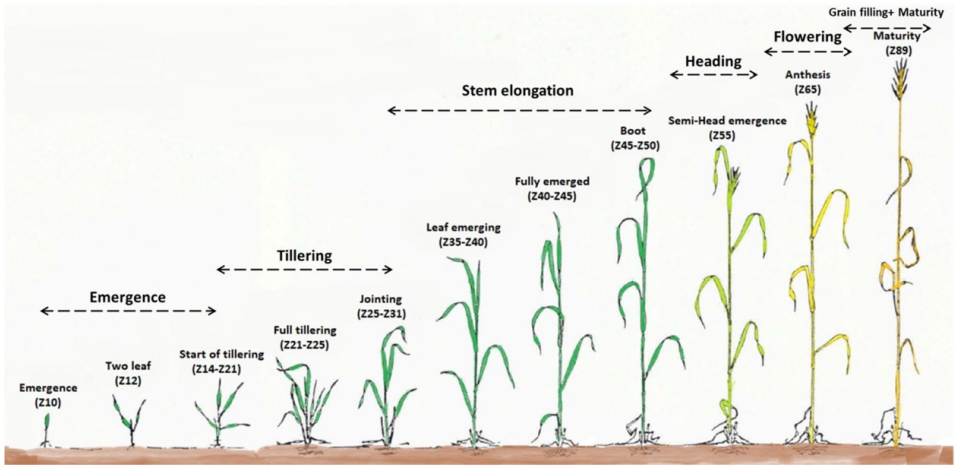

Figure 2.14: Phenological stages of winter wheat. Reprinted with permission from Figure 2 in Mamassi et al. (2023), *©CC BY 4.0*.

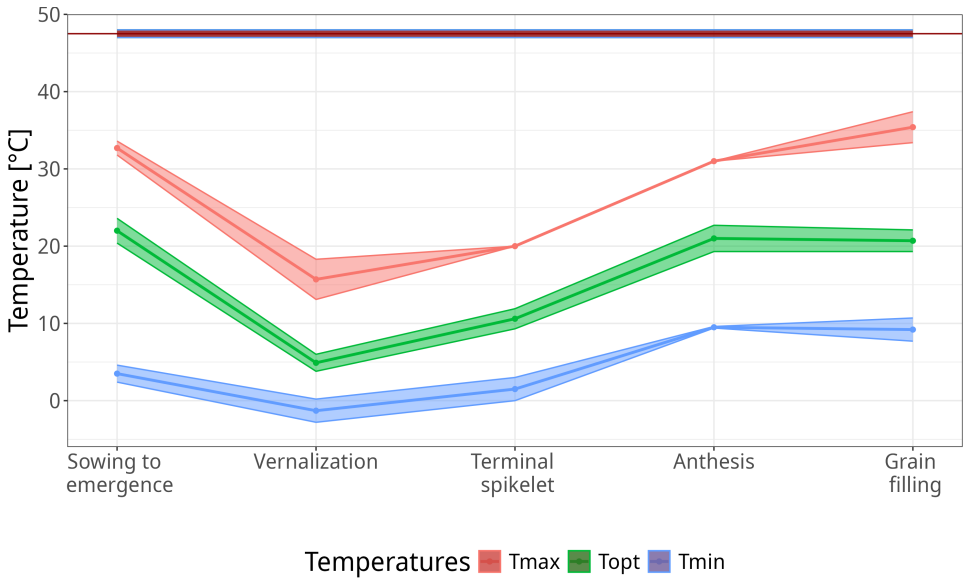

Figure 2.15: Same as Figure 2.13, but for wheat. The data is obtained from Porter and Gawith (1999).

consists of 10 main stages that can overlap. During the tillering stage (Figure 2.14, wheat undergoes vernalization.

Environmental factors influencing wheat growth and development

In contrast to maize, wheat has a longer cycle and can be exposed to several hazards throughout the year. Wheat has a higher tolerance to cold exposure but a lower tolerance to high temperatures. Furthermore, it requires vernalization. Therefore, if temperatures during tillering (Figure 2.14) are not cold enough (between 0 °C and 10 °C), flowering can be delayed or aborted. The number of tillers produced during tillering strongly depends on the duration of the phase. Earlier sowing enables longer tillering, potentially producing

more tillers and, thereafter, spikes. As wheat is a C3 plant, it does not perform well under hot-dry conditions.

Figure 2.15 displays the temperature thresholds for the cycle of wheat. The minimum, optimal and maximum temperatures increase from vernalization (vegetative stages) until anthesis. At early stages, minimum temperatures are close to 0 °C, until reaching 10 °C during anthesis and grain filling. Maximum temperature (Tm) is close to 20 °C during the vegetative stage until reaching 35 °C in grain filling. The lethal minimum temperature is −17 °C, whereas the lethal maximum temperature is around 46 °C.

In Europe, wheat plantation requires between 150 mm and 450 mm depending on the area (Supit et al., 2010). Water requirements are usually low until the reproductive stages and grain-filling period are reached. Generally, winter wheat is not irrigated, although some parts in the Mediterranean region and France implement irrigation (Zhao et al., 2015).

The most sensitive state (the critical period) for determining wheat yield is between 20 days before anthesis and 10 days after anthesis. During this period, low radiation, very low temperatures, very high temperatures, and water deficit limit the number of grains and the size, which determine the potential yield of the plant (Curtis et al., 2002).

2.4 Common approaches in agricultural meteorology

The previous section provides the bases to understand how weather and climate influence growth and development of plants, exemplifying the case of maize and wheat. This knowledge has been assured using mostly three methodologies: Field experiment-based studies, process-based crop models, also called crop simulation models (CSM), and statistical models.

Field experiments rely on direct measurements and, when variables are well controlled, offer highly reliable insights into specific climate-crop relationships. However, they are often costly, logistically challenging to implement, and geographically constrained, limiting the ability to generalize results beyond the study area.

CSMs are highly developed models, based on first-principled equations and parametrizations. They are used to assess the physiological responses of a specific crop to climate drivers through the control of other factors such as management, soil properties and nutritional availability, among others. CSMs are very useful for evaluating potential benefits of developing new technologies (Jones et al., 2017b) and evaluating alternative management for both present and future climate scenarios (Andarzian et al., 2015; Knox et al., 2016; Siebert et al., 2017). In addition, CSMs are also used for providing real-time crop yield forecast information, as the Joint Research Center (JRC) of the European Commission does in the European domain (European Commission. JRC, 2020).

Notwithstanding this, CSMs are prone to some drawbacks. First of all, their representation of extreme weather impact is limited (Barlow et al., 2015). By way of explanation, they fail to accurately represent losses linked to high precipitation extremes (van der Velde et al., 2012), extreme temperatures (Barlow et al., 2015) and the wide range of pests and disease species that damage crops (Jones et al., 2017a). Additionally, CSMs are based on empirical evidence of weather-related agricultural response in specific regions, and require

calibration for different areas (Zampieri et al., 2018). Lastly, they require extensive data input which may not be readily available (Hu et al., 2024).

The gaps from CSMs are bridged by statistical models (Zampieri et al., 2018). These are based on direct observations or reported data and, without assuming previous knowledge, they can potentially provide insight into new unknown relations between the environment and crop yield. Additionally, as an advantage over experimental research, it can cover extended regions, providing additional robust spatial comparison (Hu et al., 2024).

Rather than being competitors, these approaches complement each other (Hu et al., 2024). Since the methodology of this thesis relies heavily on statistical models, a detailed description of these models follows.

2.4.1 Statistical learning and machine learning

Even thought statistical and machine learning are referred as different concept, their definition is actually entangled. The difference between statistical modeling and machine learning lies in their fields of origin: statistical modeling originates from statistics, whereas machine learning comes from computational science. Broadly speaking, statistical modeling encompasses tools used to understand data (James et al., 2021), while machine learning includes methods that enable computers to learn from data (Mahesh et al., 2020). Generally, the goal of statistical learning is inference, whereas machine learning focuses on prediction. Machine learning tends to be associated with higher complexity and lower interpretability. However, there is now a vast number of tools that make machine learning models interpretable, as described in Chapter 5. Both statistical modeling and machine learning can be divided into supervised and unsupervised learning (Mahesh et al., 2020; James et al., 2021). In supervised learning, there is an expected outcome or response (e.g., linear regression or Random Forest), while unsupervised learning seeks patterns in the data (e.g., principal component analysis).

Together, these approaches involve exploring data, inferring certain behaviors, or making predictions (Tredennick et al., 2021). The following section focuses on the theoretical framework of statistical learning as described in James et al. (2021).

2.4.2 Definition of statistical models

Statistical methods assume a relationship between a set of variables X and a variable to be predicted y (also called the predictand). This relation is represented by the function f and is given in the form of (Equation 2.1):

$$y = f(X) + \epsilon_{ir} \tag{2.1}$$

where ϵ_{ir} refers to the irreducible error (that comes from e.g. instrumental errors). The underlying aim of statistical models is to estimate a function $\hat{f}$ which attempts to be as closed as possible to the real function f (Equation 2.2):

$$y = \hat{f}(X) + \epsilon_r + \epsilon_{ir} = \hat{f}(X) + \epsilon \tag{2.2}$$

where ϵ_r represents the error due to incorrect modelling, and ϵ is the sum of the two type of errors.

In general, statistical methods can be classified into two groups: parametric approaches and non-parametric approaches. The first group assumes that f has a specific structure based on parameters or coefficients. For example, if we assume that y has a linear response to X, Equation 2.2 can be written as (Equation 2.3).

$$y = \beta_0 + \beta_1 x_1 + \beta_2 x_2 + \ldots + \beta_k x_k + \epsilon \tag{2.3}$$

where β_0 is the independent fixed parameter and $\beta_1 ... \beta_k$ are the fixed parameters associated to each predictor $x_1 ... x_k$. $\beta_0 ... \beta_k$ are usually estimated with algorithms that attempt to reduce ϵ like ordinary least squares. Parametric approaches can also assume other types of relation, such as polynomic and exponential, and can also include the combination of several predictors. This method is generally more practical as it is eassy to interpret and estimate. However, the proposed structure lacks flexibility and may not provide the most accurate representation of f.

Non-parametric approaches involve direct estimation of the function f without assuming a specific structure beforehand. Therefore, these methods are more flexible than parametric approaches and tend to approximate the true function f more closely. This group includes methods such as Random Forest, which is described in Chapter 5. However, a major drawback of non-parametric methods is their requirement for a large number of observations to achieve accurate estimation. Furthermore, their high flexibility can lead to overfitting and poor performance on unseen data, as discussed later in this section.

2.4.3 Binary classification models

Statistical models can be applied for either predicting a quantitative variable or a qualitative (binomial) one. In the context of agriculture, statistical models can be used to study significant drops in crop yield. This are refereed in the literature as yield loss (Ben-Ari et al., 2018), bad year (Vogel et al., 2021), yield failure (Webber et al., 2020) or yield shock (Zhu et al., 2021; Ma and Zou, 2024). This type of events are specially detrimental for stakeholders as they lead to financial instability and losses in food supply (Kalkuhl et al., 2016; Cottrell et al., 2019; Zhou et al., 2022). The use of models targeting yield shock prediction allows the identification of the key drivers in the specific scenario of losses.

When the target variable follows a binary distribution (i.e., categories 0/1), the objective is to predict the probability of occurrence of one category (usually y=1 y=1). This probability function can be expressed as follows (Equation 2.4):

$$P(y = 1 \mid X) = \pi(X) \tag{2.4}$$

where $\pi(X)$ is the probability function of the event $y = 1$ given the predictors X. In this case, $\pi(X)$ must lie between 0 and 1. Therefore, approaches such as linear regression cannot be directly applied (as exemplified in Figure 2.16, green dashed line). For binomial

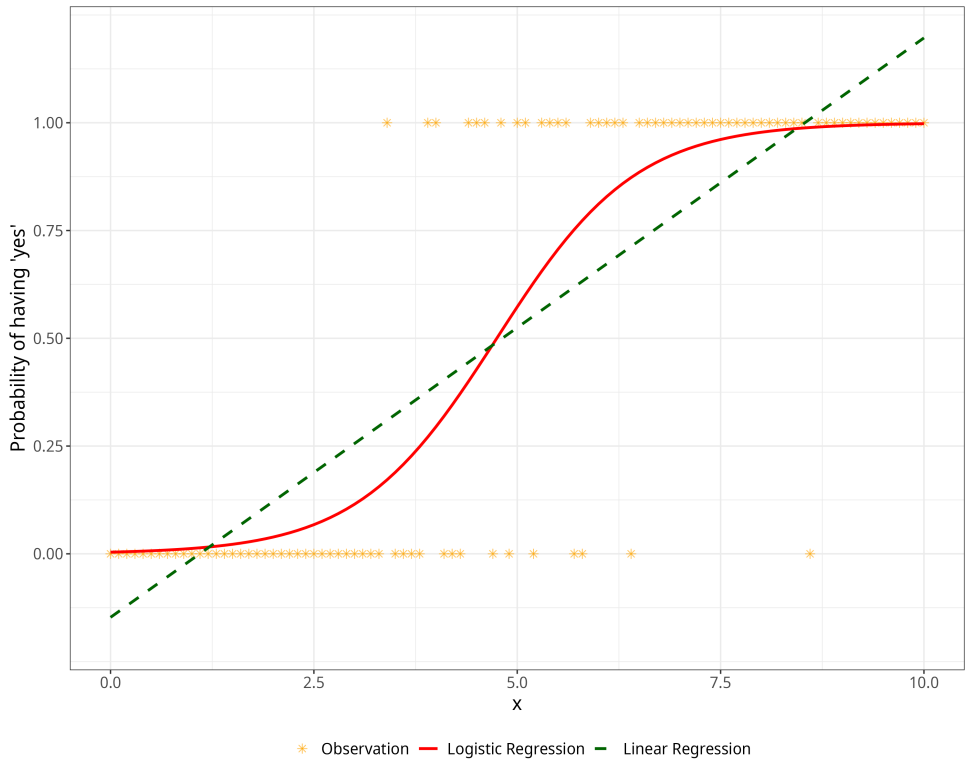

Figure 2.16: Comparison of linear and Logistic regression models for binary prediction. Probabilities (from 0, i.e. 0% to 1, i.e. 100%) of "yes" as a function of x by using a logistic regression model (red line) and a linear regression model (green dashed line). The observations (orange) denote 0 if the value is "no" and 1 if the value is "yes". Models are trained by using a predictor x with random values ranging from 0 to 10 and a binomial predictand "yes"/"no".

outcomes, a commonly used parametric approach is logistic regression, which is given by (Equation 2.5):

$$\pi(X) = P(y = 1 \mid X) = \frac{e^{\beta_0+\beta_1 x_1+\beta_2 x_2+\ldots+\beta_k x_k}}{1 + e^{\beta_0+\beta_1 x_1+\beta_2 x_2+\ldots+\beta_k x_k}} \tag{2.5}$$

Logistic regression is exemplified in Figure 2.16 (red line). In this case, logistic regression provides a natural framework for binary-classification problems. Additionally, Equation 2.5 can be rewritten in a linear regression–like structure, resulting in (Equation 2.6):

$$\log\left(\frac{\pi(X)}{1-\pi(X)}\right) = \beta_0 + \beta_1 x_1 + \beta_2 x_2 + \ldots + \beta_k x_k \tag{2.6}$$

where $\log\left(\frac{\pi(X)}{1-\pi(X)}\right)$ is called the *log-odds* or *logit*. This transformation has no restrictions and allows the implementation of parametric approaches such as linear modeling.

The coefficients of the logistic regression model are typically estimated using the method of maximum likelihood, which involves maximizing the following function (Equation 2.7):

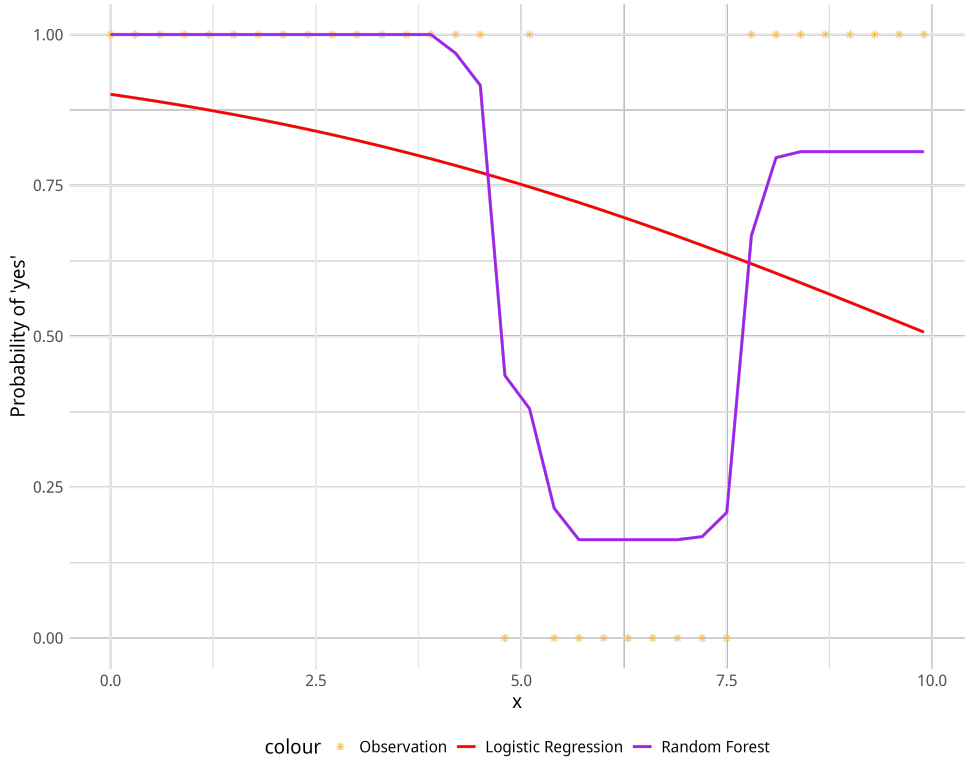

Figure 2.17: Comparison of Random Forest model and Logistic regression model for binary prediction. Probabilities (from 0, i.e. 0% to 1, i.e. 100%) of "yes" as a function of x by using a logistic regression model (red line) and a Random Forest model (violet line). The observations (orange) denote 0 if the value is "no" and 1 if the value is "yes". Models are trained by using a predictor x with random values ranging from 0 to 10 and a binomial predictand "yes"/"no".

$$\max_{\beta_0,\ldots,\beta_k} \left\{ \sum_{i=1}^{N} \Big[y_i \log(\pi(x_i)) + (1 - y_i) \log(1 - \pi(x_i)) \Big] \right\} \tag{2.7}$$

where N represents the total number of observations and $\pi(x_i) = P(y_i = 1 \mid x_i)$. This is the *log-likelihood function*, which is maximized when the predicted probabilities $\pi(x_i)$ closely match the observed outcomes y_i.

While Equation 2.5 and 2.6 assumes a linear relationship between the predictors and the logit, this assumption may not always hold. Figure 2.17 illustrated how logistic regression and a Random Forest model predict a simulated binomial variable. In the example, when $x < 5$ and $x > 7.5$, the $y = yes$. Therefore, the logistic regression (red line) struggles with accurate predictions since a non-linear relation exists between x and y. In contrast, Random Forest, which is a more flexible tool, can get closer to the observations. In cases where non-linear interactions are present, non-parametric approaches, such as classification trees, can of0fer advantages by accommodating more complex relationships.

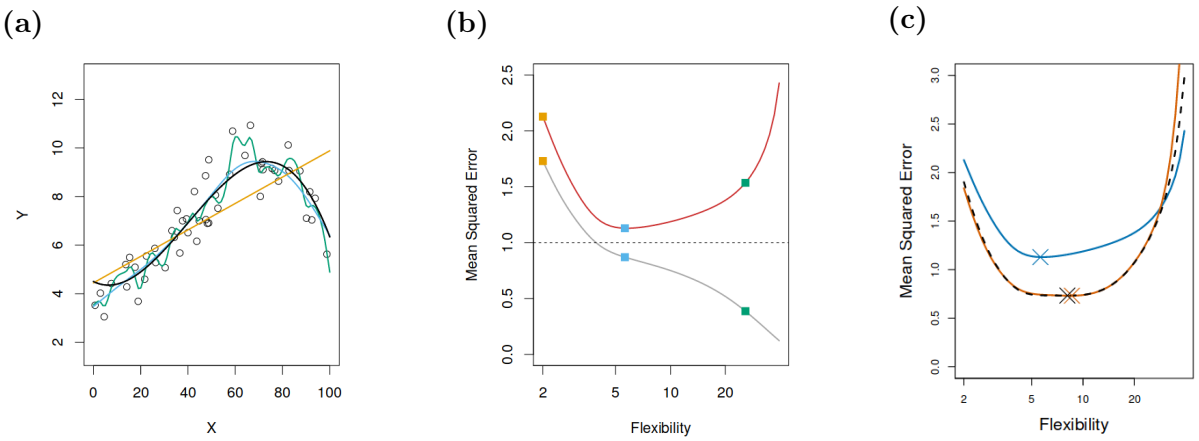

Figure 2.18: (a) Data simulated from a true function f (black). Three estimates of the f are shown: a low-flexible model (orange curve), a medium-flexible model (blue) and a high-flexible model (green). b() error obtained by using the training data (grey curve) and independent test data (red curve) as a function of flexibility; squares represent the training and test error for the three models shown in (a). (c) Test error is obtained from the original models (blue, similar to a red line in (b)) and by using cross-validation methods (dashed lines). Reprinted with permission from Figures 2.9 and 5.6 in James et al. (2021), *©2021 Springer*.

2.4.4 The bias-variance tradeoff and cross validation

When building a model, only a fraction of the observations, referred to as the training data, is used instead of the entire sample. Since the model is built on this set, its accuracy is typically very high when predicting outcomes from these observations. However, the model's utility is assessed by testing it against a previously unseen dataset. In this case, models with high accuracy on the training data often exhibit low accuracy on new data. Such models are described as having low bias but high variance, as they lack consistency across different training sets.

This phenomenon is illustrated in Figure 2.18a and b, where the performance of three models (low-flexible in yellow, mid-flexible in blue, and high-flexible in green) represent the true function (black line) and to predict unseen data. The high-flexible model is the one that gets closer to the observations; the medium-flexible model is the closest one to the true function. When analyzing the performance of these models for the training data (grey line) and test data (red line) in Figure 2.18b, the high-flexible model has the lowest errors when modelling the training data but is also the less accurate one when using the test data. In contrast, the medium-flexible model, though with higher error from training data, has the lowest test error. Therefore, modeling implies a trade-off between flexibility to represent the training observations and capacity to predict unforseen observations.

One way to reduce the variance of models is by building an ensemble of models based on subsamples of the original. For this, there are several tools that are based on data split (like cross-validation) or sub-sampling methods (like bootstrapping). In some cases, especially in machine-learning methods, these tools are included within the model construction. This process is common in statistics since the output average of the models

has a lower variance than the individual ones (We exemplify these concepts in Chapter 5). The three models attempt to represent the true function (black line). In the example of Figure 2.18, when readjusting the models using cross-validation (Figure 2.18c), the performance of all of them increase.

2.5 Climate models

As mentioned in section 2.1, there is vast literature supporting the evidence of ungoing global warming and climate change (Calvin et al., 2023; IPCC, 2023). The comprehension of climate variability and future prediction is feasible owing to the development of climate models, which we describe below.

2.5.1 Global climate models

Climate models are representations of the climate system based on parametrizations, physical laws and measured data. They are used to study the existent interactions and explore the changes in the climate system under different scenarios. Climate models have been used to quantify the evolution of the past and present climate as well as to estimate possible scenarios for the future (Stocker, 2011).

In the IPCC reports, for example, climate models are used to explore plausible future scenarios and to establish the impact associated with then, as well as the possible mitigation and adaptation strategies (Figure 2.19; IPCC, 2023). Future climate scenarios are based on the influence of human activity on climate. The concentration of Atmospheric greenhouse gases (GHG) induce changes in global temperature by increasing inward radiation flux (also called radiative forcing) and subsequently influencing the components of the climate system (Figure 2.19 bottom row). The resultant simulations can be used for assessing extreme weather and the impact in different sectors like in the agricultural one.

The possible climate pathways are based on a set of concentration and emission pathways, which entail a set of plausible socioeconomic decisions throughout the years. The Coupled Model Intercomparison Project (CMIP) was launched by the World Climate Research Program and aims to provide a standardized format for the Global Climate Models (GCM; Eyring et al., 2016). The core set of runs from phase 5 of CMIP (CMIP5) appraise different Representative Concentration Pathways (RCP) scenarios (Moss et al., 2010; Taylor et al., 2012; Collins et al., 2013; Edenhofer et al., 2014). There are in total four RCPs (RCP2.6, RCP4.5, RCP6 and RCP8.5); each of them contemplates a range of possible emission scenarios, but converges to a similar net radiation forcing by 2100.The RCP8.5, for instance, considers a pathway of progressively increase in GHG emission, reaching a value of $8.5\,\mathrm{W\,m^{-2}}$ by 2100, compared to pre-industrial levels. The RCP2.6 (high mitigation scenario), in contrast, is a scenario of progressively reduction in CO_2 emissions, converging to radiative forcing of $2.6\,\mathrm{W\,m^{-2}}$ by 2100, compared to pre-industrial levels. Later, CMIP phase 6 (CMIP6) developed a new set of pathways called Shared Socioeconomic Pathways (SSP). These contemplates both qualitative and quantitative features of societal future, and accounts for a wider spectrum of possible future socioeconomic pathways (also illustrated in Figure 2.19 by different colourlines; Chen et al., 2021).

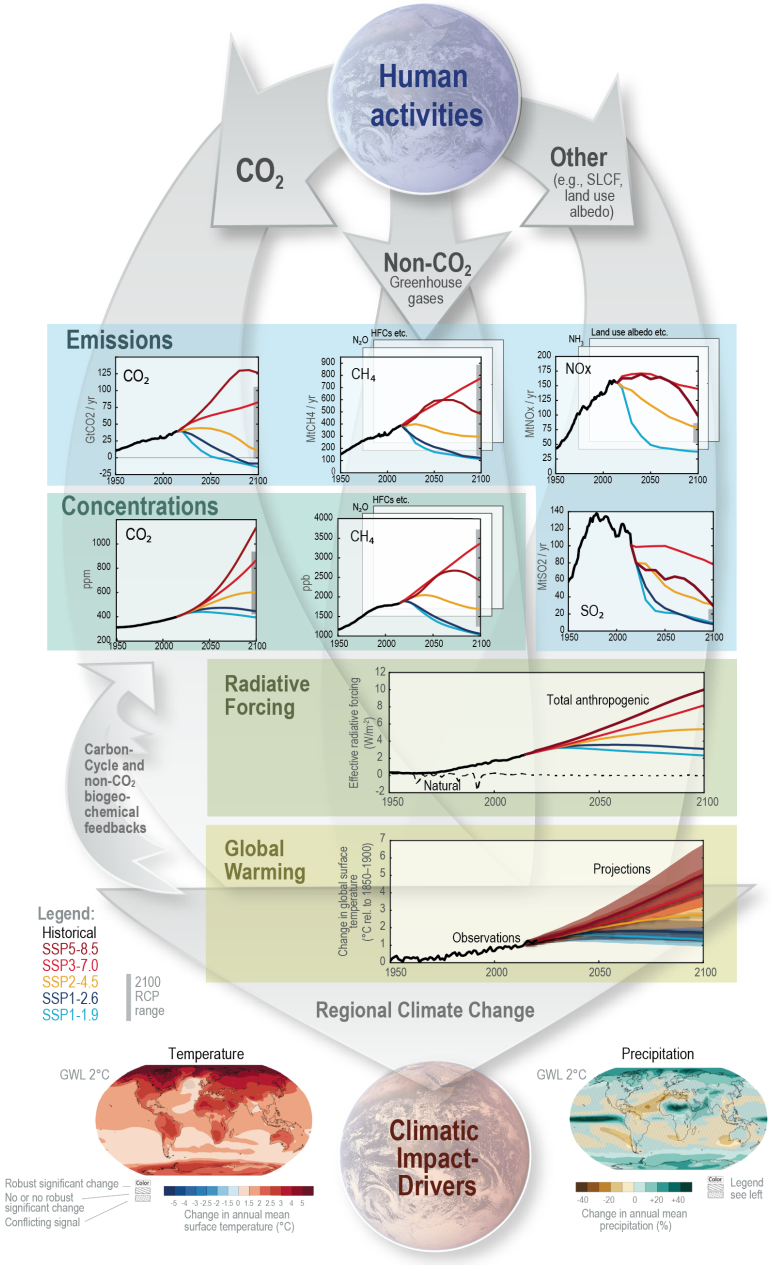

Figure 2.19: Schematization of the climate change study process, starting from anthropogenic emissions, to changes in atmospheric concentration, to changes in Earth's energy balance (*forcing*), to changes in global climate and ultimately regional climate and climatic impact-drivers. Shown is the core set of five Shared Socio-economic Pathways (SSP); carbon dioxide (CO_2) emissions (panel top left, $\mathrm{Gt\,yr^{-1}}$), methane (CH_4) emissions (middle) and sulphur dioxide (SO_2), nitrogen oxide (NO_x) emissions (top right, all in $\mathrm{Mt\,yr^{-1}}$); concentrations of atmospheric CO_2 (ppm) and CH_4 (ppb), second row left and right; effective radiative forcing for both anthropogenic and natural forcings ($\mathrm{W\,m^{-2}}$), third row; changes in global surface air temperature (°C) relative to 1850–1900, fourth row; maps of projected temperature change and changes in annual-mean precipitation at a global warming level (GWL) of 2 °C relative to 1850–1900. Reprinted from figure TS4 in IPCC (2023), *Cambridge University Press*.

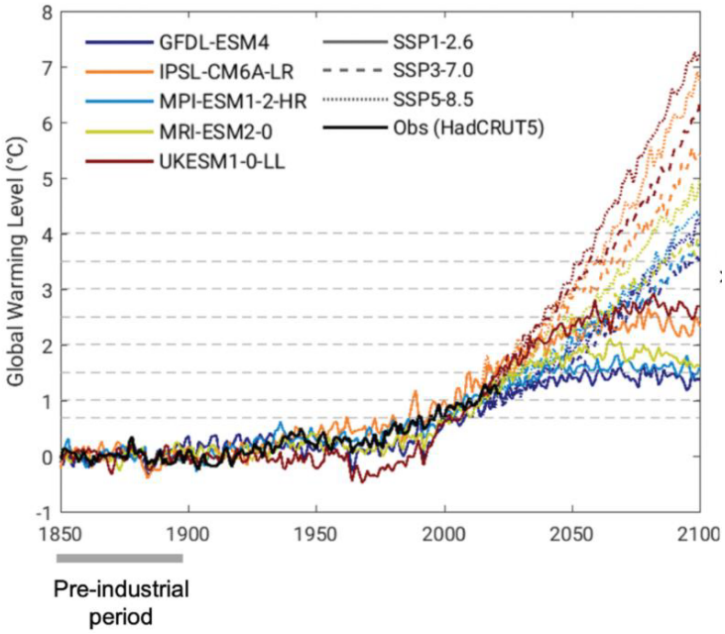

Figure 2.20: GLobal warming level relative to pre-industrial period for five GCMs (colors) and three emission scenarios (line style), and for the observational data (black line). Adapted from Figure 1 in Ruane et al. (2024), *Willey*.

In cliamte modeling, it is common to use multiple models rather than a single one. The IPCC report fifth assessment based on CMIP5, for instance, was based on a set of nearly 20 different Global Simulation Models, or General Circulation Models (GCM, Collins et al., 2013). The difference between models rely on the evolution of GHG emission and concentration, land use and land cover changes as well as model formulations and computational efficiency among others. This is also illustrated in Figure 2.19 (fourth row), where for each SSP there is a range of uncertainty in the global surface temperature evolution. The use of a multi model ensemble approach provides higher robustness through the consideration of all possible scenarios.

In the IPCC sixth report, the concept of global warming levels (GWL) were incorporated (Chen et al., 2023). GWL refers to the period in which the global temperature reaches certain threshold compared to pre-industrial levels. Instead of analyzing the temporal evolution of the GCMs, this approach focuses on the changes under certain GWL, which is calculated for each model individually (Vautard et al., 2014). GWL vary across different GCMs owing to, as previously mentioned, changes in the parallelization and assumptions in the socioeconomic decisions. This is also exemplified in Figure 2.20, where we see when different GCMs (in colors) for several SSP (line style) reach a correspondent GWL. In this case, for instance, the difference between models reaching 3 °C warming level can be greater than 20 or 30 years. This method, however, has been widely utilized since the impacts of climate change are apparently independent from emission scenario or GCM but rather GWL (Chen et al., 2023).

2.5.2 Regional climate models

Though GCMs (Global Climate Models) provide reliable information at the global scale, they often fall short in capturing local or regional-scale climate phenomena, such as the influence of complex topography, land-sea interactions, and localized weather systems. Consequently, Regional Climate Models (RCMs) have been developed to refine GCM outputs and provide higher-resolution projections over specific regions (Giorgi and Jr, 2015). The basic approach of RCMs is to retain the large-scale forcing provided by a GCM, such as long-term trends in greenhouse gas concentrations, as boundary conditions. These are then used to dynamically simulate regional climate by incorporating more detailed representations of surface features and atmospheric processes.

To standardize and advance regional downscaling efforts globally, the World Climate Research Programme initiated the Coordinated Regional Downscaling Experiment (CORDEX), with regional branches focusing on specific domains (Figure 2.21). EURO-CORDEX, for instance, addresses the European region using RCMs with spatial resolutions of $0.44° \times 0.44°$ (standard setup) and $0.1° \times 0.1°$ ($\sim$11 km), which significantly improve the representation of regional climate characteristics (Jacob et al., 2014). This increased resolution enables more accurate simulation of localized phenomena, such as orographic precipitation and regional wind patterns.

In general, three primary approaches to downscaling have been developed: statistical-empirical methods, dynamical downscaling (or nesting), and statistical-dynamical downscaling (SDD). Statistical methods rely on historical relationships between large-scale atmospheric variables from GCMs and local observations to infer finer-scale climate behavior. While computationally efficient, these methods may overlook dynamically evolving processes. In contrast, dynamical downscaling embeds an RCM within a GCM, allowing the RCM to receive boundary conditions updated over time, thereby providing a physically consistent simulation of regional climates. though at higher computational cost. SDD represents a hybrid strategy that reduces computational demands by using statistical techniques to classify GCM outputs into representative weather patterns, then running the RCM for each pattern separately.

2.5.3 Systematic biases and adjustment methods

An important consideration when working with climate model outputs is the application of bias correction techniques (Maraun and Widmann, 2018). Climate models, particularly GCMs and RCMs, often exhibit systematic errors when compared to observed climate data. These biases, commonly inherited from the driving GCM, can affect not only the mean state but also higher-order statistical properties such as variability, trends, and distribution shapes (Hall, 2014). From a statistical perspective, a bias refers to a systematic deviation between the simulated and observed datasets for a given variable (Maraun, 2016).

Bias correction aims to adjust the simulated data so that its statistical characteristics more closely match those of the observed records. Typically, this involves identifying and correcting persistent discrepancies through statistical transformations. These corrections are based on a comparison between a historical reference period of the model output,

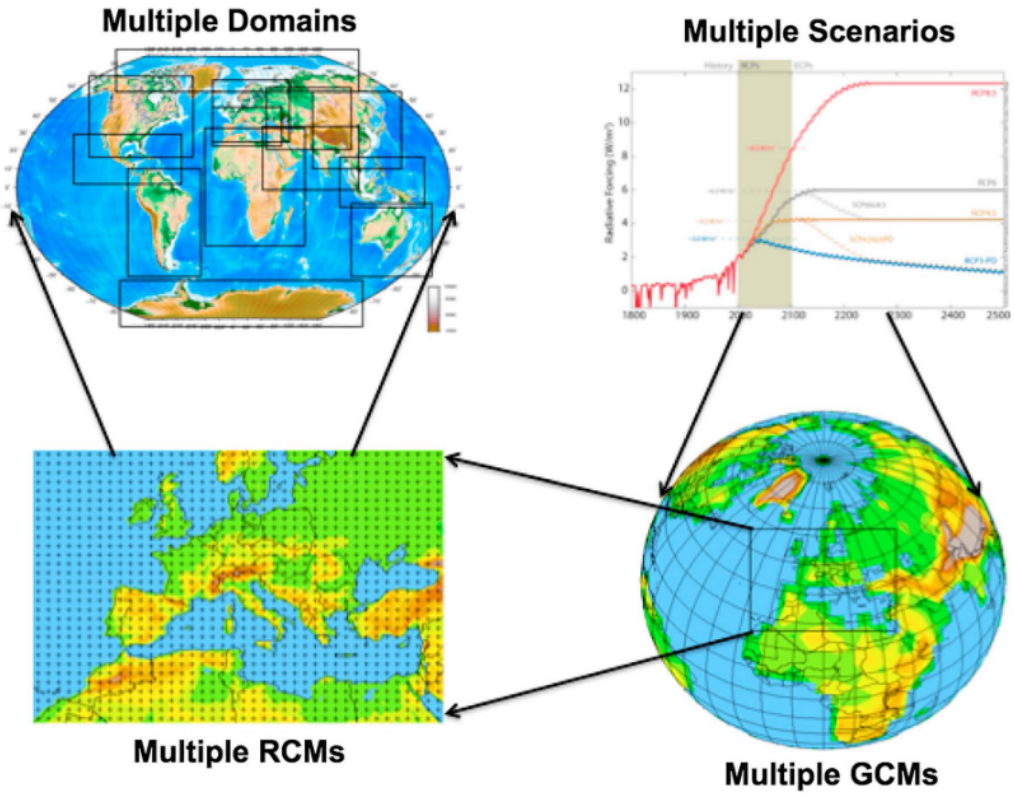

Figure 2.21: Conceptual framework for the experiments planned under the Coordinated Regional Downscaling EXperiment (CORDEX). RCM = regional climate model; GCM = global climate model. Reprinted with permission from Figure 7 in Giorgi (2019), *Wiley*.

often referred to as control data, and corresponding observed climate data. Once trained on this baseline period, the bias correction method is applied to future projections to improve their realism and usability, particularly for impact studies and decision-making in climate-sensitive sectors.

There are several methods to tackle bias correction (Teutschbein and Seibert, 2012). Below, we describe three methos commonly used.

Linear scaling

Linear scaling is the simplest bias correction method. Specifically it aims to correct the differences in the expected value, i.e. the average value (also called first order correction). If $\overline{X_{obs}}$ the mean of the observations X_{obs}, $\overline{X_{cont}}$ the mean of the control data X_{cont} and X_{sim} the simulation data (which can be in effect similar to the X_{cont} or future projection data),. Then, the adjusted simulated data X_{BCsim} can be written as (Equation 2.8):

$$X_{BCsim} = X_{sim} + (\overline{X_{obs}} - \overline{X_{cont}}) \tag{2.8}$$

or also by considering a multiplication factor (Equation 2.9):

$$X_{BCsim} = X_{sim} + \frac{\overline{X_{obs}}}{\overline{X_{cont}}} \tag{2.9}$$

In general, the additive form of the equation is more common for temperature-based variables, with low variance, whereas the multiplicative form is more common for precipitation (higher variability).

Empirical Quantile Mapping

Another method which has been very popular in the literature is Empirical Quantile Mapping (EQM). The advantage that it has over other methods is that it adjust certain simulated data based on the quantiles; in this way, it does not assume any previous theoretical distribution of the data (Teutschbein and Seibert, 2012). Quantile mapping adjust the distribution by each single estimated quantile q, which is obtained from the empirically-estimated cumulative distribution function F. For a certain value x_q of of the variable to be adjusted, the qth quantile is then given by (Equation 2.10):

$$q = F(x_q) \tag{2.10}$$

From this, the inversed empirical distribution function F^{-1} can be written as (Equation 2.11):

$$x_q = F^{-1}(q) \tag{2.11}$$

By using the two equations above, the adjusted value x_s can be written as (Equation 2.12):

$$x_{BCsim} = F_{obs}^{-1}(F_{sim}(x_{sim})) \tag{2.12}$$

where the suffix *obs* refers to the observation and *sim* to the simulated data. By itself, EQM is not adequate for climate projection data adjustment. This is because the projected data ussually falls outside the scope of the original distribution, and this method adjust back to the original historical distribution.

Quantile Delta Mapping

Cannon et al. (2015) introduced two methods that adjust quantiles while keeping the model projections: Detrend Quantile Maping (DQM) and Quantile Delta Mapping (QDM). The description of QDM (which is utilizes in this thesis) is provided below.

Let's call *sim* the simulated data associated to future projection and *cont* to the historical data. For a given value x_{sim}, the quantile q_{sim} is defined as (Equation 2.13):

$$q_{sim} = F_{sim}(x_{sim}) \tag{2.13}$$

With F_{Proj} the cumulative distribution function of the future projected data. Next, the difference between the historical data and the future data for q_{Proj} is calculated as (Equation 2.14):

$$\delta = x_{sim} - F_{cont}^{-1}(q_{sim}) \tag{2.14}$$

Or it is also calculated in the multiplicative way (Equation 2.15):

$$\delta = \frac{x_{sim}}{F_{cont}^{-1}(q_{sim})} \tag{2.15}$$

With F_{cont}^{-1} the inversed cumulative distribution function of the historical data. Finally, the adjusted value x_{sProj} is obtained by (Equation 2.16):

$$x_{BCsim} = F_{Obs}^{-1}(q_{sim}) + \delta \tag{2.16}$$

or for the multiplicative (Equation 2.17):

$$x_{BCsim} = F_{Obs}^{-1}(q_{sim}) * \delta \tag{2.17}$$

Similar to Linear scaling, the suffix *sim* can refer to both historical or projected data. As a matter of fact, if the historical data is used (i.e. $sim = cont$), QDM becomes similar to EQM.

3 Research Questions

As mentioned in Chapter 1 and Chapter 2, statistical models have the potential to bridge the knowledge gap that raises from CSMs by revealing previously unseen interactions. In contrast to the traditional aim of understanding crop yield variability, this thesis focuses on substantial losses (also refereed throughout the thesis as "yield shock"), which are the drivers of food insecurity and finantial instability. The first objective is to understand to what extent complex-defined weather variables or predictors can enhance predictability skill on a study case of silag emaizeyield shock in Germany. Second, a comparison of climate drivers of maize and wheat yield shock across European countries is performed. Finally, the changes of yield shock risk under future climate scenarios is evaluated. The results addressing these aims are presented in Chapter 6 to 8.

The thesis workflow is summarized in Figure 3.1. Initially, the focus is on comparing the advantages and disadvantages of variable selection in statistical models for assessing weather influence on crop yield losses. The representation of climate drivers in statistical models is rarely examined, particularly in the context of significant yield losses (Beillouin et al., 2020). Thus, the aim is to address this gap by comparing the use of simple versus complex climate variables in a case study on silage maize yield shocks in Germany. For this, two statistical approaches are evaluated: the Least Absolute Shrinkage and Selection Operator (LASSO), a linear method that optimizes performance by penalizing and shrinking coefficients, and Random Forest, a non-parametric model that combines multiple decision trees to capture complex patterns. Thus, the first research question is as follows:

Research Question 1 (RQ1)

To what extent does increasing the complexity in the definition of climate predictors improve the performance of silage maize yield shocks predictions in Germany?

RQ1 is answered in Chapter 6. The results show that when using LASSO, a combination of simple and complex predictors enhances model performance. In contrast, with Random Forest, models perform equally well regardless of the pre-selection of predictors. This is because Random Forest captures non-linear interactions.

The second research question addresses the challenge of data limitations and model robustness in assessing climate impacts across European countries. For the first time, the Global Dataset of Historical Yields (GDHY), a gridded dataset based on satellite and observed yield information, is employed to enable standardized comparisons across the

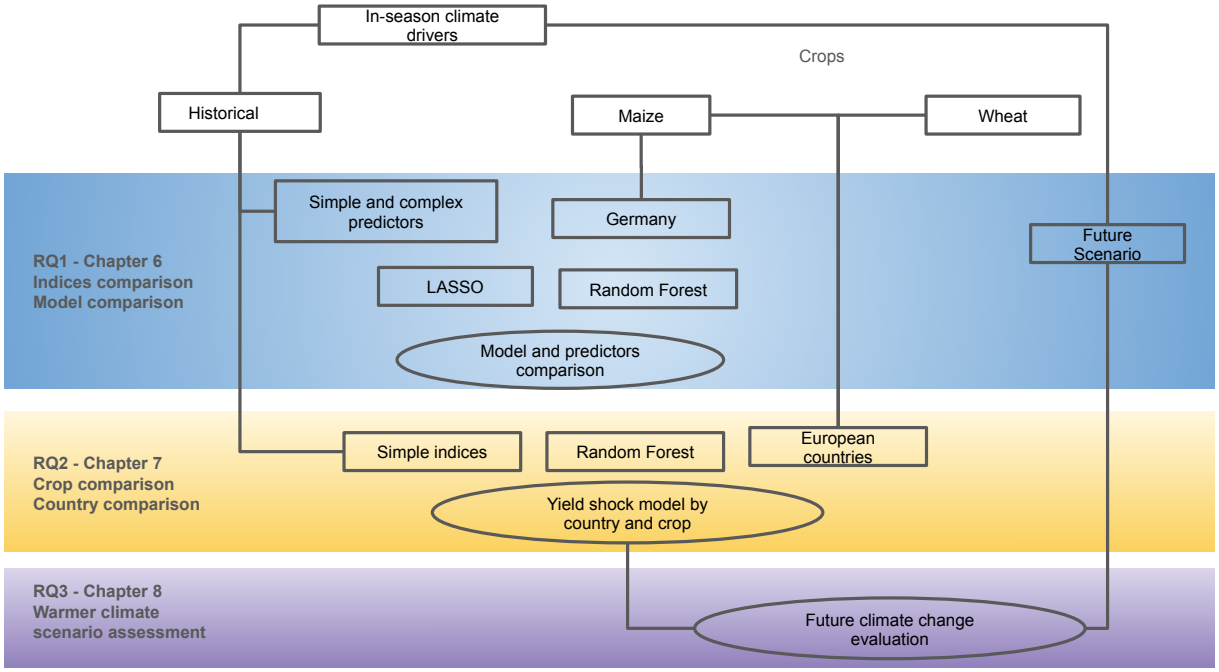

Figure 3.1: Schematization of thesis workflow summary, data used and research questions by chapter. The squared boxes includes method and data inputs, whereas the circled ones the correspondent analyses associated with the research question.

continent. Based on the findings in Chapter 6, the analysis exclusively applies Random Forest models using simple predictors. The focus is on three major maize-producing countries in Europe (France, Romania and Spain) and six for winter wheat (France, Germany, Poland, Romania, Spain and the UK). The study identifies and quantifies the influence of key in-season climate drivers on crop yields across these countries. Therefore, the research question remains as follows:

Research Question 2 (RQ2)

What are the country-to-country variations in the in-season climate drivers of maize and winter wheat yield shock across European countries?

RQ2 is answered in Chapter 7. The results displays the high spatial and crop variability of weather and climate influence on maize and wheat yield shock. We find that cold, warm, dry and wet conditions can have similar impact depending on the country.

Finally, the third research question examines how crop yield risk may evolve under future climate scenarios. Ongoing global warming raising concerns about changes in key agricultural stressors (Bednar-Friedl et al., 2022). Chapter 8 offers a novel perspective by applying statistical models to assess future climate impacts on major European crops. To explore this, an ensemble of GCMs from CMIP5, downscaled through the CORDEX framework, is used to project future climate conditions. The statistical crop models developed in Chapter 7 are then employed to assess which predictors are associated with

increased or decreased probabilities of maize and winter wheat yield shocks in a warmer climate. Thus, the research question remains as follows:

Research Question 3 (RQ3)

How would the risk of maize and winter wheat yield losses vary across Europe in a warmer climate from a statistical modeling perspective?

The answer of RQ3 is in Chapter 8, which highlights the importance of temperature and precipitation signal on a warmer climate. Maize yield shocks are mainly driven by drier conditions, though precipitation signals are uncertain, while for winter wheat, higher temperatures generally increase yield loss risk.

In summary, Chapter 6 establishes the fundamental requirements for a robust and simple model, specifically to assess the influence of sub-seasonal climate drivers on substantial losses. Chapter 7 expands the analysis to the European domain and compare two crops, which are different in their physiology. Finally, Chapter 8 explores the changes in the risk of losses and the attributions under warmer climate. By focusing solely on yield losses, we identify the key weather drivers of food insecurity and market instability in the context of agriculture. Furthermore, it supports the development of targeted adaptation strategies for maize and winter wheat at the national scale. Ultimately, this thesis advances the basis for assessing agricultural vulnerability under present and future climate change.

4 Datasets and Data Transformation

This chapter describes the datasets utilized in the thesis. The two crop datasets are introduced first (Section 4.1): the reported yield data extracted from the German Statistical Office and the Global Data of Historical Yields (GDHY), developed by Iizumi et al. (2014) and Iizumi and Sakai (2020). The crop yield data classification process is then explained, in which continuous yield data is transformed into categorical yield shock/no yield shock data, a method applied to both datasets. Subsequently, the meteorological data is presented (Section 4.2), specifically the ensemble version of the meteorological observational dataset E-OBS, which is used to study the impacts under present climate conditions. This data is used to create sub-seasonal weather and climate indices. Finally, future climate scenario models are introduced (Section 4.3) to investigate the potential impacts of climate change on crop yields. Additional details related to this chapter are provided in Appendix A.

4.1 Crop data

The crop datasets employed in this thesis contain exclusively crop yield information, expressed in units of mass per area ($kg \cdot ha^{-1}$). Given their differing spatial resolutions, temporal coverage, and geographic domains, each dataset is utilized for distinct purposes. The first dataset focuses on silage maize yields in Germany (Section 4.1.1), available at the district ("Landkreis") level for the period 1999 to 2020. This high-resolution regional dataset is used to address RQ1, which centers on a methodological comparison (Chapter 6). The second dataset, the GDHY (Section 4.1.2), provides gridded global data on maize and winter wheat yields from 1982 to 2016. Its spatial scope make it suitable for a robust country-to-country analysis of weather impacts on major staple crops (RQ2, Chapter 7 and RQ3, Chapter 8).

As this thesis focuses on substantial drops in yield, both datasets are transformed to yield shock. This approach serves to identify the most common weather and climate patterns observed during significant losses in agriculture. These are the ones that have a strong impact on food security, finance and therefore are relevant for various sectors.

4.1.1 Silage maize in Germany

The crop yield dataset is extracted from the Statistical German Office database "Regionaldatenbank Deutschland" (Statistisches Bundesamt (Destatis), 2025). Silage maize yield data for the period 1999 to 2020 is used at the district level ("Landkreis"), corresponding

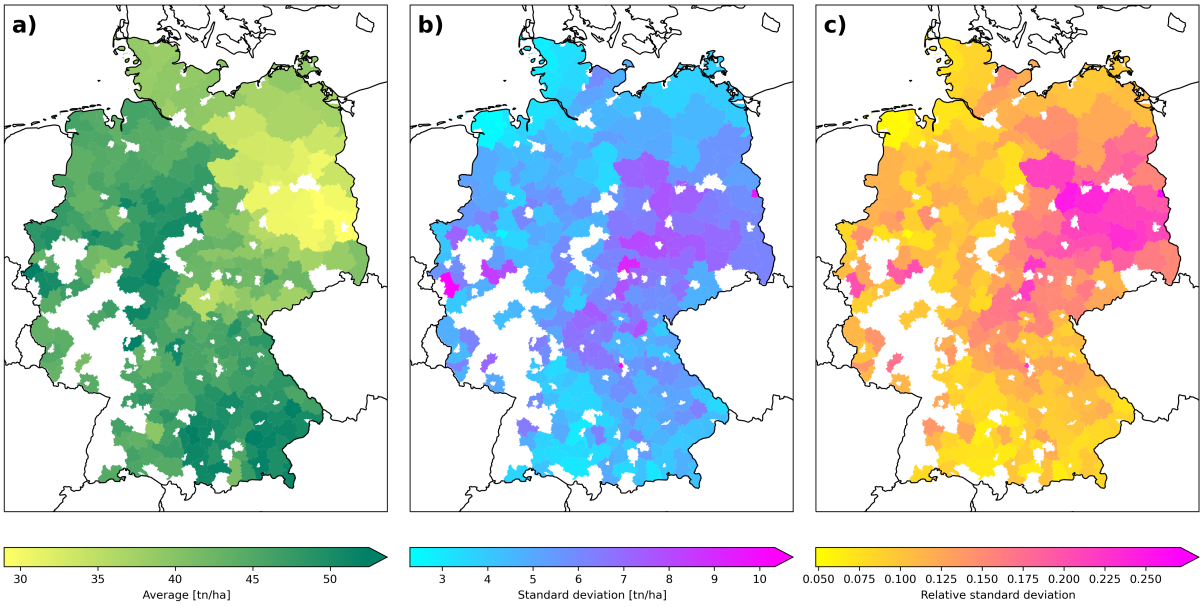

Figure 4.1: Average silage maize yield (a), standard deviation (b) and relative standard deviation (defined as *standard deviation/average*, c) per district in Germany in the 1999-2020 period. The statistics are calculated after removing districts with less than 21 values of data (districts in blank do not satisfy the filter).

to the NUTS3 resolution (Eurostat, 2025). Locations with more than 10% missing values (i.e., more than two years of missing data) are excluded. This filtering process results in a dataset comprising 242 time series, each with at least 21 annual yield values.

Figure 4.1 displays the climatology of silage maize yield data in Germany. The average values of silage maize yield in Germany (Figure 4.1a) range between roughly $30\,\mathrm{t\,ha^{-1}}$ and $50\,\mathrm{t\,ha^{-1}}$, with higher values in western and southern Germany and lower values in northeastern Germany. This spatial difference occurs due to the sandy soil characteristic of the region, which reduces field capacity and tends to reduce the overall yield (Section 2.2; Gebauer et al., 2022; Schmitt et al., 2022). The variability of yield along the years (standard deviation, Figure 4.1b) is mostly homogeneous in the country. However, the relative variability of silage maize yield (Figure 4.1c) is higher in central-eastern Germany, mainly due to the relatively lower values in average maize yield.

4.1.2 Global Dataset of Historical Yields

This data is used in Chapter 7 to assess the impact of sub-seasonal weather and climate conditions on maize and winter wheat yield across European countries.

Iizumi et al. (2014) developed a global gridded dataset for major crops, also called the Global Dataset of Historical Yields (GDHY; Iizumi and Sakai, 2020). This is a global gridded dataset of major crops based on a combination of satellite data and nationally reported yield data. The newest version has a resolution of $0.5° \times 0.5°$ and can distinguish between seasonal winter and spring varieties (Iizumi and Sakai, 2020). The GDHY is built by using the following datasets as input:

- Yearly nationally reported yield data obtained from FAO (2024a).
- Grid-cell net primary production (NPP), calculated using satellite-based products and crop-specific radiation use efficiency.
- Global gridded dataset of crop planting and harvesting date around the 2000s (Sacks et al., 2010).

The development of the dataset proceeds the following steps for each grid cell:

1. Fitting of normal distribution for planting and harvesting date (to account for temporal variability and management at specific locations).
2. Accumulation of NPP along the growing season (between planting and harvesting date).
3. Adjustment of FAO country yield for secondary cropping system use (Secondary cropping system refers to the practice of planting a shorter season variety within the same year, which is very common in tropical regions).
4. Combination of crop-specific grid NPP with FAO country yields.
5. Repetition of step 4, but for secondary cropping systems.

The satellite-based NPP gives reasonable information on the above-ground biomass of the crops, whereas the harvesting practices and yield data report politics are strongly dependent on the country. In other words, the temporal variation in modelled yields followed those in the FAO data, whereas the spatial variation within a country follows that in the NPP data (Iizumi et al., 2014).

This thesis uses version 1.3 of the GDHY (Iizumi and Sakai, 2020), which has yearly data on major crops from 1982 until 2016, with a resolution of $0.5° \times 0.5°$. The dataset has free access and can be downloaded from the PANGAEA repository (Iizumi, 2019). The original datasets distinguish between spring wheat (with the growing period in spring), winter wheat (with the growing period throughout winter and spring), maize, rice and soybean. Since this thesis aims to compare crops with different season length, the analyses centers on two crops: Maize, which is typically planted in early spring and harvested in late summer, and winter wheat, which is planted in early autumn and harvested in summer (Chapter 2).

Overview of maize yield data in Europe using the GDHY

Figure 4.2 displays the average and standard deviation values of maize yield in Europe. Maize yield ranges between $4\,\mathrm{t\,ha^{-1}}$ and $16\,\mathrm{t\,ha^{-1}}$ for most of Europe, except for Galicia (northwestern Spain), with values over $24\,\mathrm{t\,ha}$. The values are rare and much higher than Spain's average national reported values (Supplementary Figure A1). However, this difference is probably due to the relatively high NPP in the country (Neumann et al., 2016), which produces much greater values of maize yield in that region. Additionally, the relative variability remains quite similar in the whole European domain. We also observe that neither Germany, Ukraine nor Poland (top maize producers in Europe, Supplementary Figure A1) are present in the data.

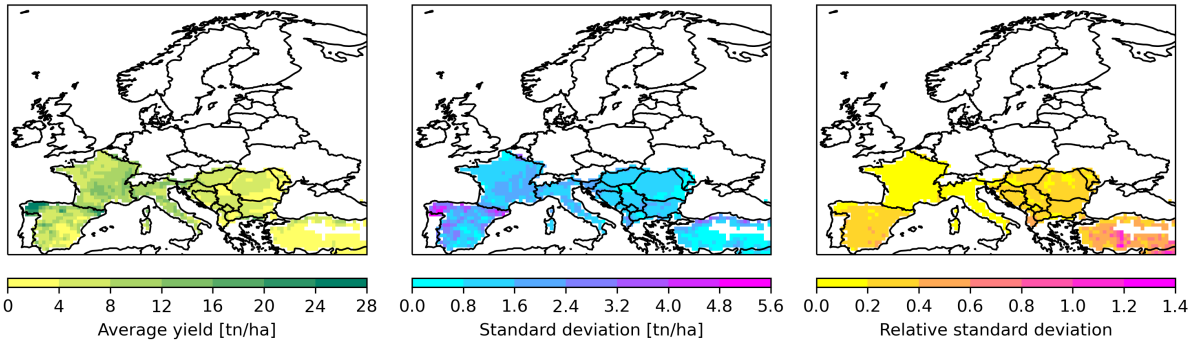

Figure 4.2: Maize yield data from GDHY (Iizumi and Sakai, 2020). Average yield (a), standard deviation (b) and relative standard deviation (c) for the European domain in the 1982-2016 period.

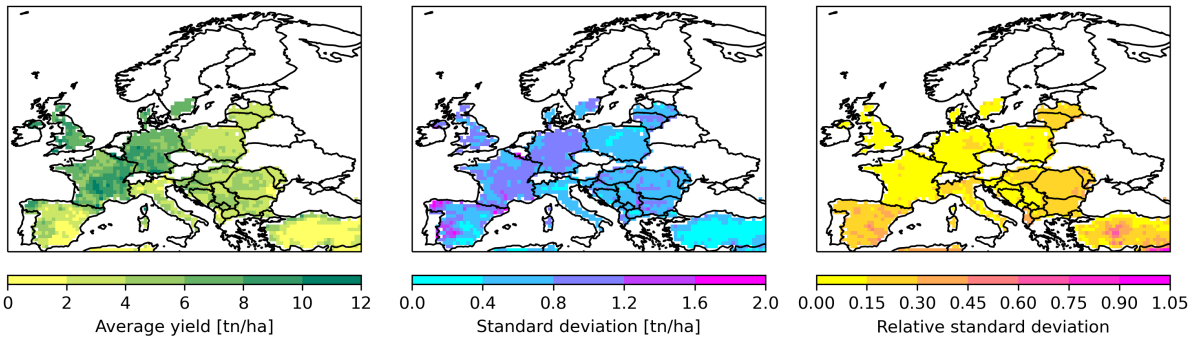

Figure 4.3: Same as Figure 4.2, but for winter wheat.

Given the data availability, sample size (number of grids per country), and importance in terms of production at the European level (Figure A1), the target countries are:

GDHY Maize yield. Studied countries

• France • Romania • Spain

Overview of winter wheat yield data in Europe using the GDHY

Figure 4.3 displays the average, standard deviation and relative standard deviation for winter wheat yield using the GDHY. The highest values of winter wheat yield are found in central and northwestern Europe, whereas the lowest ones are in southern and eastern Europe. Similar to the case of maize, the region of Galicia in Spain presents a higher yield than the rest of Spain. In high-.yield areas, the values range between 6 t ha^{-1} and 12 t ha^{-1}, which can be outstanding for some grids (similar to maize, due to the relatively high NPP values within the country). Winter wheat yield variability ranges between 0 and 2 t ha^{-1} per year, whereas the relative variability is relatively homogeneous in the domain (between 15% and 30%).

Given the sample size, importance in terms of production at the European level (Figure A2), and regional variability in terms of climate, the six target countries are:

GDHY winter wheat yield. Studied countries

• France • Germany • Poland • Romania • Spain • The UK

4.1.3 The definition of yield shock

The following description of yield data transformation is common for all crop yield datasets. Silage maize yield shock (defined below) is described and used in Chapter 6, whereas maize and winter wheat yield shock series across European countries are described in Chapter 7.

As previously mentioned, crop yield has experienced a long-term positive trend associated with technological improvements over the decades (Chapter 1). This is especially observed in the GDHY for most of Europe (Figure A3). Additionally, political context and policy implementations also produce a long-term effect on agriculture and could have either negatively or positively influenced crop yield data (Micu et al., 2017). In this context, it is hard to disentangle the impact of climate drivers. Therefore, removing trend is generally recommended (Shi et al., 2013).

Furthermore, crop yield data is spatially heterogeneous since other static and temporal non-environmental sources of crop yield variability exist, such as management and spatial soil properties variability. Given that the focus is on individual countries, the data first must be detrended and standardized, so thereafter, the individual series range on similar values and have similar variability.

Detrending and standardization is a common practice and has been implemented in many previous studies (Ben-Ari et al., 2018; Ceglar et al., 2016; Beillouin et al., 2020; Zhu et al., 2021). The process usually consists of modelling the yield data series solely as a function of time t and then applying the following equation (Equation 4.1):

$$y_{DetStd,j} = \frac{y_{obs,j} - y_{trend,j}}{y_{trend,j}} \tag{4.1}$$

Where j refers to the specific location (district or grid, depending on the dataset), thus the detrending is applied to individual series (in our case, location or grid point). y_{DetStd} is the detrended and standardized yield, y_{obs} is the observed yield and y_{trend} is the long-term modelled yield. There are several approaches to model y_{trend}. The most common in the literature is based on locally weighted scatterplot smoothing (LOESS or LOWESS; Ceglar et al., 2016; Ben-Ari et al., 2018; Beillouin et al., 2020; Lischeid et al., 2022). LOESS is a non-parametric regression tool that properly captures the long-term behaviour and variance of magnitude and is not sensitive to outliers (Cleveland, 1979), showing to be the most appropriate approach for detrending yield data (Lu et al., 2017). After detrending and standardizing, yield is not treated as a general continuous positive variable but rather as a variation from the expected long-term behaviour.

Since this thesis focuses on the impact of climate and weather on individual countries, the yield series are grouped by country. In the case of silage maize in Germany, all the data

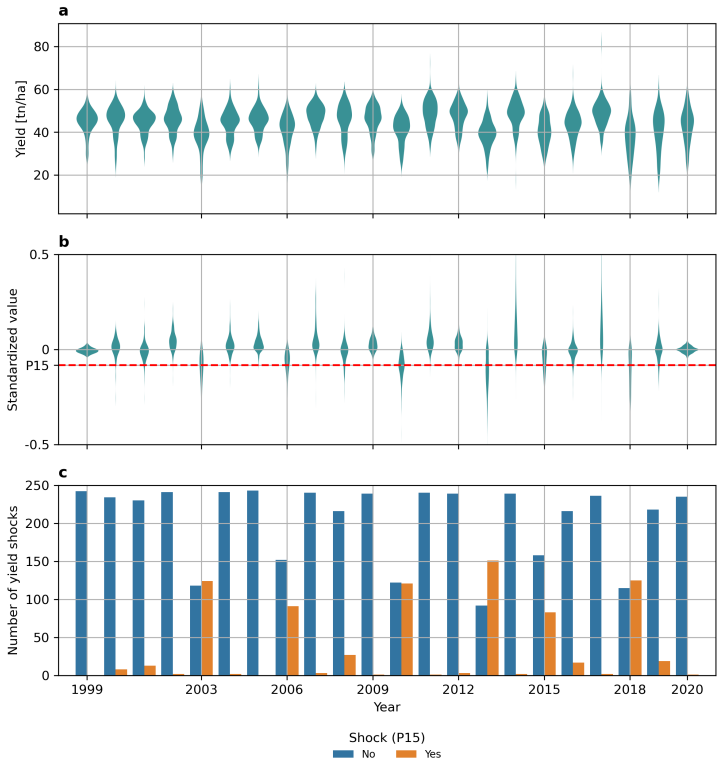

Figure 4.4: Yield data transformation for silage maize yield in Germany. (a) Year-to-year distribution of silage maize yield for the entire sample, (b) year-to-year distribution of standardized yield, horizontal red line corresponds to the global 15$^{\text{th}}$ percentile (c) number of "yield shock" (orange bars) and "no yield shock" (blue bars) per year.

is treated as coming from a single distribution, whereas in GDHY, the data is grouped by the individual countries.

Finally, the definition of yield shock is applied. For this, the data is discretized to distinguish between cases of substantial drop in yield and the opposite. The 15$^{\text{th}}$ percentile of the domain's detrended and standardized data is computed. Subsequently, if the value falls below the 15$^{\text{th}}$ percentile, the data is re-defined as "yield shock". In contrast, if the value exceeds the 15$^{\text{th}}$ percentile threshold, the data is re-defined as "no yield shock". In this way, the continuous distribution is converted into a binary yield shock/no yield shock distribution. Typical threshold values range between the 5$^{\text{th}}$ and 20$^{\text{th}}$ percentile for yield shock (Webber et al., 2020; van Oort et al., 2023).

The yield data transformation is exemplified and illustrated for silage maize yield in Germany in Figure 4.4. The first panel (a) displays the year-to-year distribution, where we observe high dispersion within the yearly samples. In the second panel (b), the series is already detrended and standardized with Equation 4.1. In this case, the data is much less dispersed than the original observations. Furthermore, Figure 4.4b includes the 15$^{\text{th}}$ percentile (horizontal red line) that is used to categorize the data into yield shock and no yield shock. Finally, Figure 4.4c displays the year-to-year frequency of yield shock reports (in orange) and no yield shock reports (in blue).

4.2 Meteorological data

Meteorological data is essential for understanding the influence of weather and climate on crop yield shocks. The analysis done in present climate (RQ1 and RQ2, Section 4.2.1 and 4.2.2, Chapter 6 and Chaptern 7) are based on the ensemble version v23.1e and 27.0 of E-OBS (Cornes et al., 2018). E-OBS is a gridded observational dataset, with a resolution of $0.1° \times 0.1°$ ($\sim$11 km), based on interpolated European meteorological station data. Daily maximum, minimum and average temperature data as well as the daily total precipitation data are extracted. Thereafter, the climate indices are calculated. These are based on precipitation data and temperature data, and attempt to work as proxis of the most common drivers of yield shock. The first set of climate indices (use to assess silage maize yield shock in Germany) spam different definitions which contemplate average state of climate, frequency and magnitude of extreme weather events. Given the conclusions from RQ1 (Chapter 6), the climate indices are redefined and simplified for the followup chapters (Chapter 7 and Chapter 8).

4.2.1 Climate indices for silage maize yield shock in Germany

The climate indices described below are used in Chapter 6 to assess the weather and climate drivers of silage maize yield shock in Germany.

The first set of climate indices is based on daily maximum temperature, minimum temperature and total precipitation from 1998 to 2020. A total of 11 climate indices (Table 4.1) are calculated. These indices are partially based on previous literature (Vogel et al., 2019; Schmitt et al., 2022) and attempt to represent the most studied weather and climate extreme events (drought event, extreme precipitation, cold and high temperatures). In particular, the aim is to compare the impact of frequency (e.g. number of warm days) and magnitude (e.g. cumulative heat) of unusual weather conditions apart from the most commonly used variables (average temperatures and cumulative precipitation). All the percentiles required for defining the indices are calculated using 1998-2020 as the base period. For the cumulative-precipitation-based variables ($SPltm05$ and $SPgt05$), monthly total precipitation is computed and standardized within the same months of the study period by fitting a Gaussian distribution. This yields a "Standardized Precipitation" (SP), which resembles the widely-known Standardized Precipitation Index (McKee et al., 1993), but focuses on the accumulation of a single month. The standardized precipitation during wet months ($SPgt05$) and standardized precipitation during dry months ($SPltm05$) are obtained by adjusting the original SP values.

Since maize is roughly planted around April in different parts of Germany and harvested around September, the range from April to September is considered. This gives a total of 66 climate indices (i.e. eleven indices $\times$ six months).

Figure 4.5 displays the correlation matrix between climate indices for each month. Among the considered variables, co-linearity is evident. To distinguish the predictive capabilities of simple versus complex variables and to reduce spurious correlations, six different groups of predictors are constructed (Figure 4.6): a group of simple variables (*Simple*, Figure 4.6a), consisting of total precipitation (PP), mean maximum temperature (TX), and mean minimum temperature (TN); a group of frequency-based variables (*Frequency*, Fig-

Table 4.1: List of climate indices utilized to study silage maize yield shock in Germany.

Variable	Short name	Description
Total precipitation	PP	Monthly total precipitation
Number of dry days	$PPlt1$	Number of days with precipitation below 1 mm
Number of wet days	$PP90p$	Number of days with precipitation above the wet days-based 90th percentile
SP during dry months	$SPltn05$	Monthly standardized precipitation when the value is below -0.5
SP during wet months	$SPgt05$	Monthly standardized precipitation when the value is above 0.5
Mean maximum temperature	TX	Monthly mean maximum temperature
Number of warm days	$TX90p$	Number of days with daily maximum temperature above the monthly 90th percentile
Cumulative heat	$TX90pDD$	Cumulative daily maximum temperature during warm days
Mean minimum temperature	TN	Monthly mean minimum temperature
Number of cold nights	$TN10p$	Number of nights with daily minimum temperature below the monthly 10th percentile
Cumulative cold	$TN10pDD$	Cumulative daily minimum temperature during cold nights

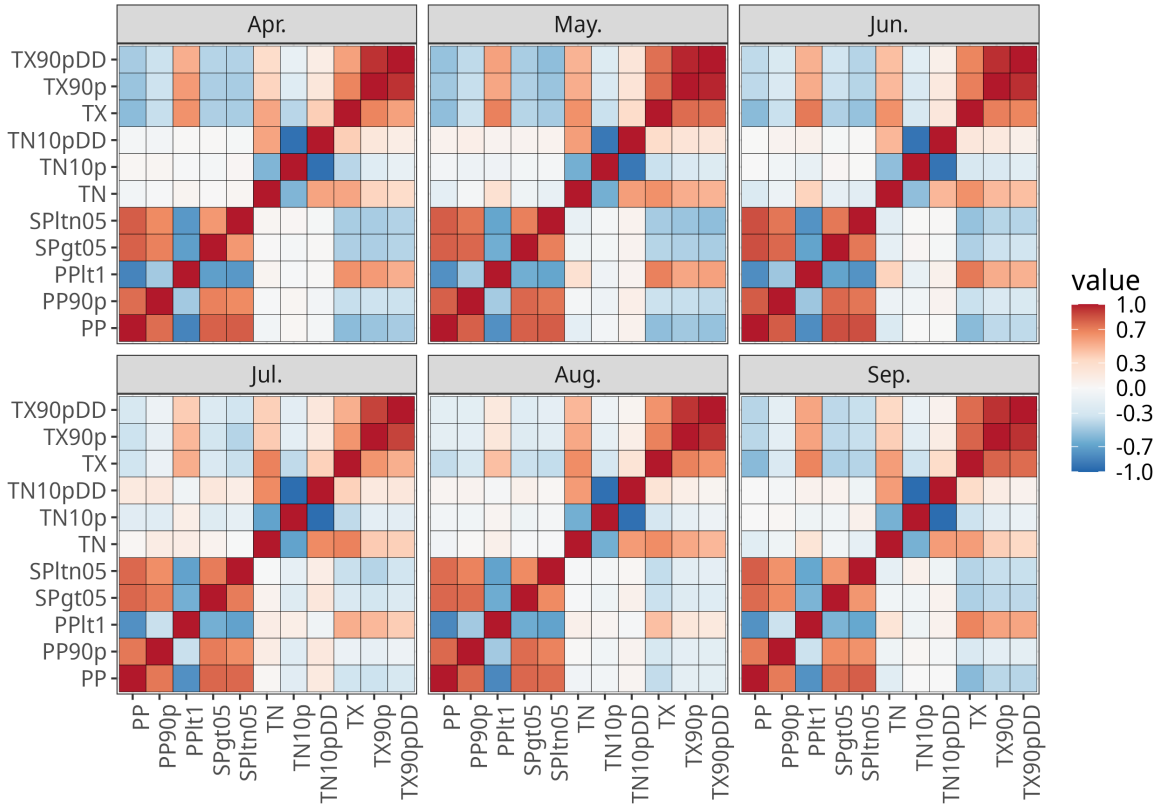

Figure 4.5: Spearman correlation between climate indices for each month (in panels).

ure 4.6b), including the number of warm days ($TX90p$), number of cold nights ($TN10p$), $PP90p$, and the number of dry days ($PPlt1$); a group of cumulative-based variables (*Cumulative*, Figure 4.6c), incorporating accumulated heat ($TX90pDD$), accumulated cold ($TN10pDD$), $SPgt05$, and $SPltm05$; and a group using all variables together (*All*, Figure 4.6d).

In addition, two groups are generated using a step-wise variable reduction method (James et al., 2021). The step-wise algorithm selects an optimal subset of predictors by iteratively adding or removing variables based on a specific criterion, typically an information criterion or statistical test, to identify the best-performing model with a reduced num-

Figure 4.6: Set of selected variables of each group (by panel) before modelling. The considered variables appeared in blue squares, while the not-considered variables in blank.

ber of variables. This method requires computation of a "null model" (a model with no predictors) and a "full model" (a model containing all predictors). In this case, both are based on a logistic regression model, consistent with Equation 2.5. The model selection is made using a Bayesian Information Criterion, which measures how well the model fits the data as well as the number of predictors required, which helps avoid overfitting (James et al., 2021 and Appendix A). The fifth and sixth group are based on the Forward mode of Step-wise (*Forward*, Figure 4.6e) and the Backward mode (*Backward*, Figure 4.6f). From the 66 variables, 18 predictors remain in the Forward group, while Backward counts 18 predictors.

4.2.2 Climate indicators for the GDHY

The climate indices described below are used to assess the weather and climate drivers of maize and winter wheat yield shock in Europe in present climate (in Chapter 7) and in future climate scenarios (in Chapter 8).

Table 4.2: List of climate indices utilized to study maize and winter wheat yield shock across European countries, using the GDHY.

Variable	Short name	Description
Mean temperature	$Tmean$	Monthly average temperature
Diurnal temperature range	DTR	Monthly mean diurnal temperature range
Total precipitation	$RRsum$	Monthly total precipitation

Daily maximum temperature, minimum temperature, mean temperature, and total precipitation are extracted for the period 1981 to 2016 with a spatial resolution of $0.1° \times 0.1°$ ($\sim$11 km). Additionally, the daily diurnal temperature range is calculated by subtracting the daily minimum temperature from the daily maximum temperature. Since the GDHY dataset has a resolution of $0.5° \times 0.5°$, the meteorological data is re-gridded using bilinear interpolation to match the GDHY resolution. To reduce day-to-day variability, a 3-day moving mean window is applied to the datasets. Table 4.2 displays the climate indices considered when focusing on maize and winter wheat yield shocks across European countries. The selected predictors at this stage include monthly mean temperature ($Tmean$), monthly diurnal temperature range (DTR), and monthly total precipitation ($RRsum$).

Planting and harvesting dates differ for maize and winter wheat; therefore, the month ranges considered for each crop vary. For maize, which is sown between March and May and harvested around September, the period from April to September is used. This results in a total of 18 climate indices (i.e., three indices $\times$ six months). For winter wheat, planted during autumn and harvested around summer of the following year, the period from October to August is considered, resulting in 33 climate indices (i.e., four indices $\times$ eleven months).

4.3 Future climate model data

To investigate the effect of climate change on crop yield shocks, future modeled climate data is used. As mentioned in Chapter 2, Global Climate Models (GCMs) can project changes in climate by considering different socioeconomic pathways and climate variability. Additionally, Regional Climate Models (RCMs) downscale GCM outputs to provide future climate projections at finer spatial resolutions. This data also requires adjustment to match the distribution of observed data.

4.3.1 GCM-RCM model chains

The focus is placed specifically on the RCP8.5 scenario, which represents a high-emission pathway and aligns with current observations (Schwalm et al., 2020). To enhance the robustness of subsequent modeling, results are based on eight GCM-RCM model chains (Table 4.3). Following the CORDEX standard framework (Chapter 2), all data have a spatial resolution of approximately 11 km and daily temporal resolution. For all GCM-RCM model chains, the ensemble member *r1i1p1* and version *v1* are used, except for the ICHEC-EC-EARTH models (using members r12i1p1 v1) and the CNRM-CERFACS-

Table 4.3: List of cGCM-RCM model chains and their correspondent period for GWL2 and GWL3.

GCM-RCM chain	GCM	RCM	GWL2	GWL3
CNRM-CERFACS-CNRM-CM5_CLMcom	CNRM-CERFACS-CNRM-CM5 (Voldoire et al., 2013)	CLMcom-CCLM4-8-17 (Rockel et al., 2008)	2029-2058	2052-2081
CNRM-CERFACS-CNRM-CM5_KNMI	CNRM-CERFACS-CNRM-CM5 (Voldoire et al., 2013)	KNMI-RACMO22E (Meijgaard et al., 2008)	2029-2058	2052-2081
ICHEC-EC-EARTH_CLMcom	ICHEC-EC-EARTH (Hazeleger et al., 2012)	CLMcom-CCLM4-8-17	2026-2055	2051-2080
ICHEC-EC-EARTH_KNMI	ICHEC-EC-EARTH	KNMI-RACMO22E	2026-2055	2051-2080
IPSL-IPSL-CM5A-MR_KNMI	IPSL-IPSL-CM5A-MR (Dufresne et al., 2013)	KNMI-RACMO22E	2028-2057	2040-2069
MPI-M-MPI-ESM-LR_CLMcom	MPI-M-MPI-ESM-LR (Giorgetta et al., 2013)	CLMcom-CCLM4-8-17	2029-2058	2052-2081
MPI-M-MPI-ESM-LR_KNMI	MPI-M-MPI-ESM-LR	KNMI-RACMO22E	2029-2058	2029-2058
NCC-NorESM1-M_KNMI	NCC-NorESM1-M (Bentsen et al., 2013)	KNMI-RACMO22E	2031-2060	2057-2086

CNRM-CM5_KNMI model chain (using member *r11i1p1 v2*). Each member contains a historical period (1950–2005) and future projections (2006–2100). The historical period corresponds to the time frame during which the model was trained, while the projection period covers the future scenario. Since the GDHY dataset begins in 1982, the historical period is limited to 1982–2005, with future projections spanning 2006–2100.

To record the changes in future climate simulations, the definition of Global Warming Levels (GWLs, Chapter 2) is applied. The GWLs are calculated for each GCM independently (Table 4.3; Fortems-Cheiney et al., 2017; Teichmann et al., 2018; Moemken and Pinto, 2022) following the methodology of Vautard et al. (2014). In this case, the GWLs are calculated relative to the pre-industrial period 1881–1910 by selecting the year when the 30-year rolling global mean temperature reaches either 2 °C or 3 °C. This thesis focuses on GWL+2 °C (GWL2) and GWL+3 °C (GWL3), and compare the outputs with the historical period (1982-2005).

4.3.2 Data transformation and bias correction

The data replicates the climate indicators calculated for Chapter 7 with some additional adjustments. Figure 4.7 displays the model transformation process, including bias correction and predictor computation. From the simulations, the daily precipitation and daily maximum, minimum, and mean temperatures are extracted. The diurnal temperature range is calculated by subtracting the daily minimum temperature from the daily maximum temperature. Additionally, all simulated daily precipitation values between 0 mm and 0.1 mm are converted to 0 mm. This is referred to as drizzle correction (Moemken and Pinto, 2022; Lazoglou et al., 2024) and is applied to remove the model's tendency to overestimate the occurrence of light precipitation events. Next, the data is remapped to match the GDHY grid and subjected to a 3-day running mean to remove synoptic-scale variability (Section 4.2.2). Following this, the simulations undergo bias correction using two methods: Linear Scaling and Quantile Delta Mapping (QDM, Teutschbein and Seibert, 2012; Maraun, 2016 and Chapter 2). This produces two separate chains for each bias correction method, resulting in a total of 16 RCM-GCM-bias-corrected (RCM-GCM-BC) model chains.

After bias correction, climate indices defined in Section 4.2.2 are computed individually for each simulation: monthly mean temperature ($Tmean$), total precipitation ($RRsum$), and diurnal temperature range (DTR). Consequently, the output consists of 16 independent simulation datasets (Figure 4.7).

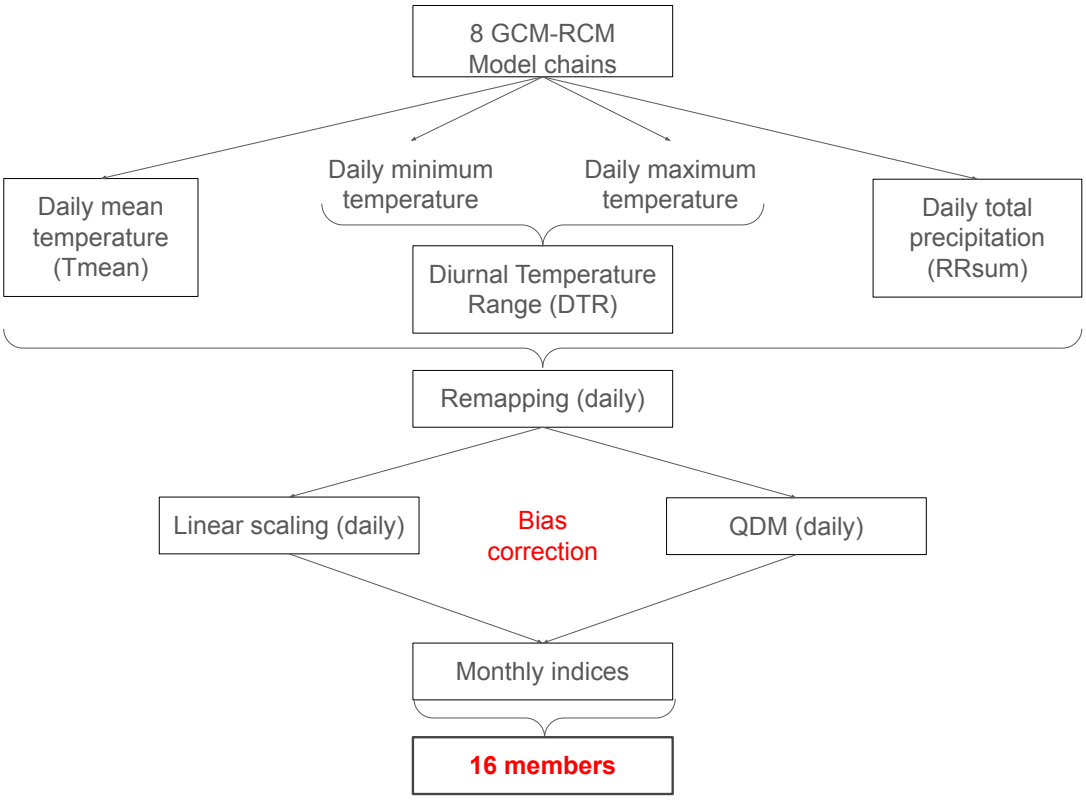

Figure 4.7: Schematic overview of the processing chain for bias adjustment and climate indicators calculation.

The simulations before and after bias correction are evaluated against the reference E-OBS dataset for the historical period (1982–2005). The evaluation is based on two statistical metrics: mean bias (Equation 4.2) and mean relative bias (Equation 4.3). For a set of observations $x_{obs,i}$ and corresponding simulations $x_{sim,i}$, the metrics are defined as follows:

$$\text{Mean Bias} = \frac{1}{N}\sum_{i=1}^{N}(x_{sim,i} - x_{obs,i}) \tag{4.2}$$

$$\text{Mean Relative Bias} = \frac{\text{Mean Bias}}{\bar{x}_{\text{obs}}} \quad \text{with } \bar{x}_{\text{obs}} = \frac{1}{N}\sum_{i=1}^{N} x_{\text{obs},i} \tag{4.3}$$

The performance is addressed at different aggregation levels. By all means, the analysis is centered on differences across months, GCM-RCM model chain, domain and the data in its totality. The results are displayed and discussed in Chapter 8.

5 Statistical Modelling

This chapter outlines the methodologies employed in this thesis. Specifically, the approaches used to identify the influence of climate indicators on crop yield shock (both maize and winter wheat) are described. First, composite analyses are introduced (Section 5.1), which elucidate the behavior of weather and climate drivers during years of yield shock in Europe. Next, LASSO (Section 5.2), a linear parametric method, is presented to study silage maize yield shock in Germany. Following this, Random Forest (Section 5.3), a non-parametric machine learning model, is introduced and applied to analyze the weather and climate drivers of silage maize yield shock in Germany as well as maize and winter wheat yield shock across European countries. The final section describes the models' setup for the specific cases of this thesis.

5.1 Composite analysis

As a first step, the state of the climate during yield shock and no yield shock years is depicted using composite analysis. This approach provides an initial overview of how certain data behave under specific conditions. In this case, selected climate indicators during yield shock years are compared against those during no yield shock years. Despite its simplicity and not being a statistical model per se, composite analysis offers an initial insight into the impacts of individual predictors and the expected outcomes for subsequent models. Results from composite analyses are presented in Chapter 6 and Chapter 7.

To compare the predictors, positional estimators (specifically the median and interquartile range) are illustrated for both yield shock and no yield shock years. A second comparison relies on the cumulative distribution along with the the two-sample Kolmogorov-Smirnov test (K-S test; Wilks, 2006). The Kolmogorov-Smirnov is based on the maximum difference between the cumulative distribution functions of the two samples tested. This test is a is a popular alternative to the two-sample T-test, as it does not assume prior knowledge of the data distribution.

5.2 Statistical modelling with LASSO

The first statistical model applied in this thesis is the Least Absolute Shrinkage and Selection Operator (LASSO; Tibshirani, 1996). LASSO is a parametric model based on linear regression that aims to find the best model while regularizing coefficient values. A key feature of LASSO is that, through regularization, some predictor coefficients can

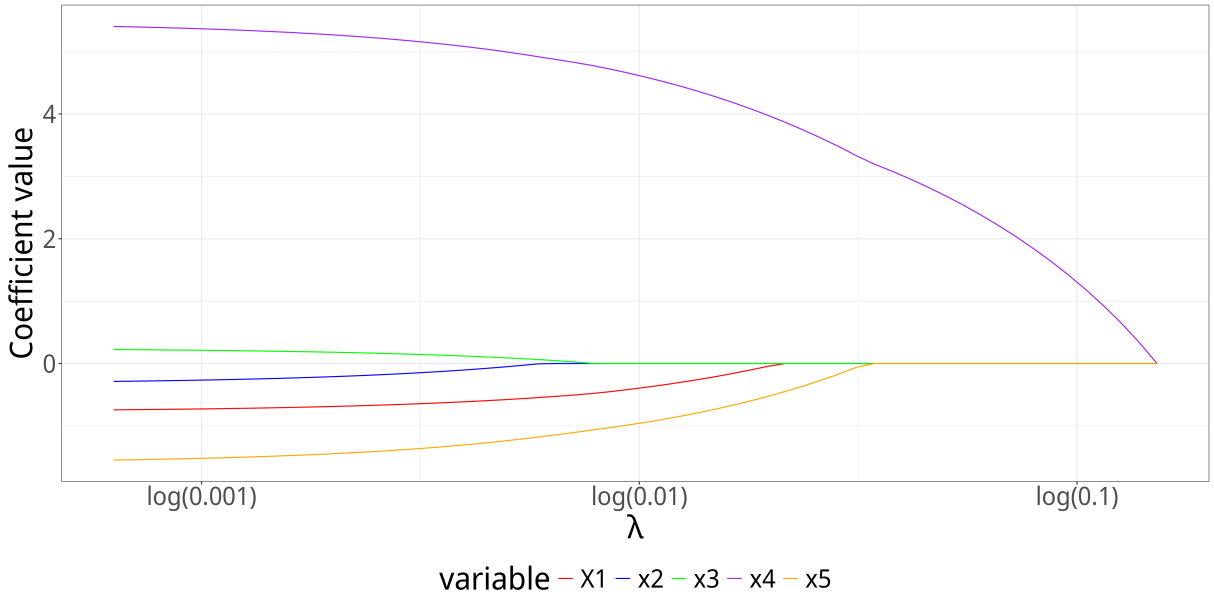

Figure 5.1: Example of LASSO's mechanism. Five random variables $x1...x5$ are used to predict a binary "yes"/"no" variable. The plot illustrates the predictor's coefficient values as a function of the tuning parameter λ. The relation is based on Equation 5.1.

be shrunk to zero, effectively performing variable selection. LASSO is primarily used in Chapter 6 to analyze key predictors of silage maize yield shock in Germany.

5.2.1 Description of LASSO

LASSO can be adapted for binary classification problems by applying the logistic regression model, as described in Equation 2.5. In this case, the coefficients are estimated by maximizing the following criterion (Equation 5.1):

$$\max_{\beta_0,\beta_1...\beta_k} \{\underbrace{\sum_{i=1}^{N}[y_i log(P(x_i;\beta_0,\beta_1...\beta_k)) + (1-y_i)log(1-P(x_i;\beta_0,\beta_1...\beta_k))]}_{\text{Log-likelihood}} - \underbrace{\lambda \sum_{j=1}^{k}|\beta_j|}_{\text{Penalty}}\} \tag{5.1}$$

Where the first term represents the log-likelihood. Here i refers to an observation (in our case, a specific time and location), and N is the total number of observations in the sample. The variable y_i is the binary outcome, taking the value of 0 (no yield shock) or 1 (yield shock), and $P(x_i;\beta_0,\beta_1...\beta_k)$ is the probability function that depends on the parameter $\beta_1...\beta_k$, the predictors $x_1...x_k$ (associated with each parameter), and an intercept term β_0. For a given i, the log-likelihood is maximized when P is close to 1 for $y_i = 1$ or P close to 0 for $y_i = 0$.

The second term in Equation 5.1 is called the "penalty term", which is the sum of the absolute values of the coefficients $\beta_0, \beta_1...\beta_k$ weighted by a tuning parameter λ. The way this term works is illustrated in Figure 5.1. It is observed that the larger the value of λ,

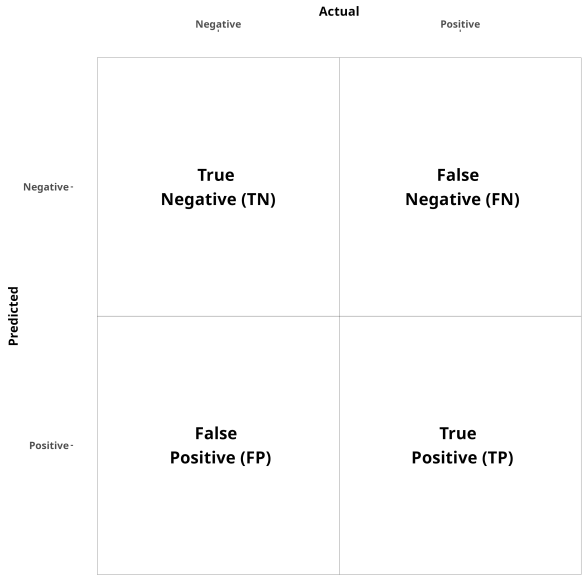

Figure 5.2: Schematized of a confusion matrix.

the smaller the values of $\beta_1 ... \beta_k$. Thus, in LASSO, the parameters to be estimated are $\beta_0, \beta_1 ... \beta_k$ and λ. Both are typically determined together through cross-validation.

5.2.2 Model performance with Mathews Correlation Coefficient

Several metrics exist to assess the performance of a binary regression model (Assel et al., 2017; Chicco and Jurman, 2020). The evaluation employed in this thesis is based on the Matthews Correlation Coefficient (MCC; Matthews, 1975). The MCC is a symmetric coefficient designed for assessing binomial or classification model performance. This metric is chosen because of its sensitivity to imbalanced data, allowing consideration of broader data distribution scenarios and providing more comprehensive information than other metrics (Chicco et al., 2021).

MCC is calculated using the values obtained from a confusion matrix (Figure 5.2), where TN refers to true negatives (actual negatives that are correctly predicted negatives), TP refers to true positives (actual positives that are correctly predicted positives), FP refers to false positives (actual negatives that are wrongly predicted positives) and FN refers to false negatives (actual positives that are wrongly predicted negatives). Then, MCC can be written as follows (Equation 5.2):

$$MCC = \frac{TP \times TN - FP \times FN}{\sqrt{(TP + FP)(TP + FN)(TN + FP) + (TN + FN)}} \tag{5.2}$$

MCC increases when either $TPxTN$ increases or $FPxFN$ decreases. This means that a high model performance requires high numbers of both TP and TN while having low numbers of both FP and FN. An MCC equal to 1 implies a perfect model, whereas an MCC equal to -1 means that the model does not hit any single value. A value close to 0 implies a performance similar to random guessing.

5.2.3 Variable importance in LASSO

Given that LASSO is based on a linear regression. The importance of each variable is easily addressed by comparing the coefficients values. $\beta_1 ... \beta_k$. When considering Equation 2.6, the estimated coefficients are related to the linear increase/decrease of the term $log(\frac{p(y=yes)}{1-p(y=yes)})$.

However, this approach faces a limitation. Since the coefficients are related to the magnitude and scale of their corresponding predictors, it is unfeasible to compare them directly. Therefore, it is common practice to either normalize the data or standardize it to maintain the predictors' distribution within a comparable scale. Once the data lies on a similar scale, for a given variable X_j, we can convey variable importance as the coefficients β_j.

5.2.4 Predictor's contribution to low and high probabilities

Once a model with LASSO is built, it is possible to apply new data to estimate the contribution to low and high probabilities of either yes (in our case, yield shock) or no (no yield shock). This is straightforward by using Equation 2.6 and calculating the individual contribution to the $log(\frac{p(y=yes)}{1-p(y=yes)})$ (Equation 5.3):

$$Contribution_{l,k} = \beta_k * \hat{x}_{l,k} \tag{5.3}$$

where $Contribution_{l,k}$ is the contribution for each observation l and each predictor k, and $\hat{X}$ is the data for each observation and predictor. This approach enables the identification of the most important predictors for a specific datasets and quantifying the actual contribution to either high or low probabilities of either yes or no.

5.3 Statistical modelling with Random Forest

The second statistical model utilized in this thesis is Random Forest (Breiman, 1998). Random Forest is a machine learning method widely used due to its flexibility and high predictive skill. This tool has been previously used in extreme weather-related crop impact studies in Europe and showed exceptionally high-performance skill (Vogel et al., 2019; Beillouin et al., 2020). Random Forest is utilized in Chapter 6 to analyze silage maize yield shocks and in Chapter 7 to examine maize and winter wheat yield shocks across Europe. Later, the models obtained are applied in Chapter 8 for investigating future climate change impacts.

5.3.1 Description of Random Forest

Random Forest is based on the decision tree algorithm (Figure 5.3). Since the predictand, yield shock, is a binomial variable in this research (yield shock/no yield shock), a binary classification approach is described.

In detail, Random Forest functions as an ensemble of decision trees (Figure 5.4). They are built by iteratively constructing individual trees using a subsample of the training dataset, selected through the bootstrapping sampling method. The complementary data

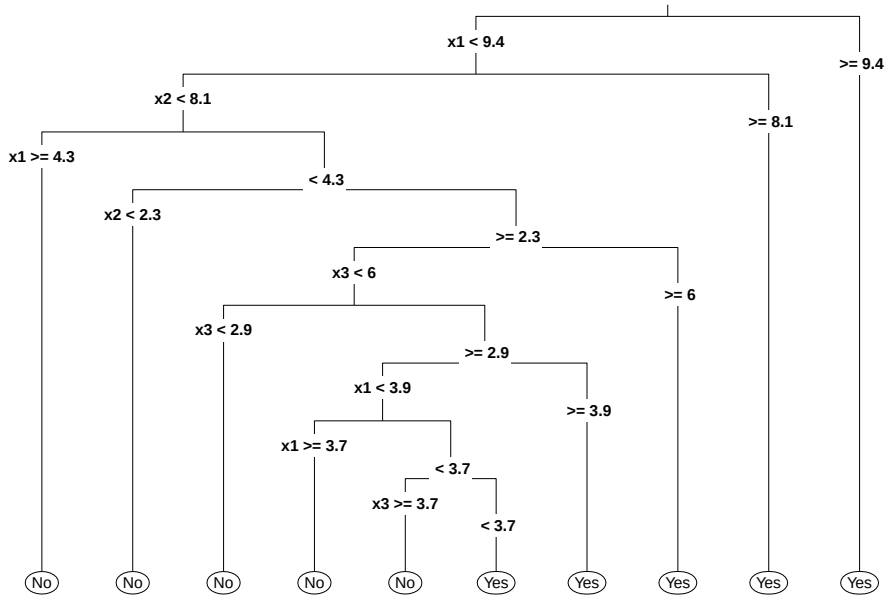

Figure 5.3: Schemtization of a decision tree. This example is produced by using four random predictors x1...x4 and a binary predictand Yes/No. Decision trees consist of recursive splitting until a value of "Yes" or "No" is finally obtained. The decisions between the branches of the trees are called "nodes". The final node is called "terminal node".

not used to create a given tree is called Out-Of-Bag (OOB) data. During forest construction, OOB data can be used to make predictions, which may be probabilistic or a single class determined by majority vote across the trees. The OOB error rate is defined as (Equation 5.4):

$$ClassificationError = \frac{TotalMisclassifications}{TotalObservations} \tag{5.4}$$

Thus, Equation 5.4 takes values close to 0 with high accuracy and close to 1 with high misses. Increasing the number of trees T reduces the error rate. Typically, models with more than 500 trees are already stable (having low error and low variance, Chapter 2). The OOB error can be considered a cross-validation error (James et al., 2021). Furthermore, Equation 5.4 can be used to measure the accuracy of independent data, which is not used to make the model.

5.3.2 Variable importance in Random Forest

In the process of building trees, variable importance can also be addressed. When building a tree, the most utilized approach for determining node splits is the Gini index G (Equation 5.5):

$$G = 2p(1-p) \tag{5.5}$$

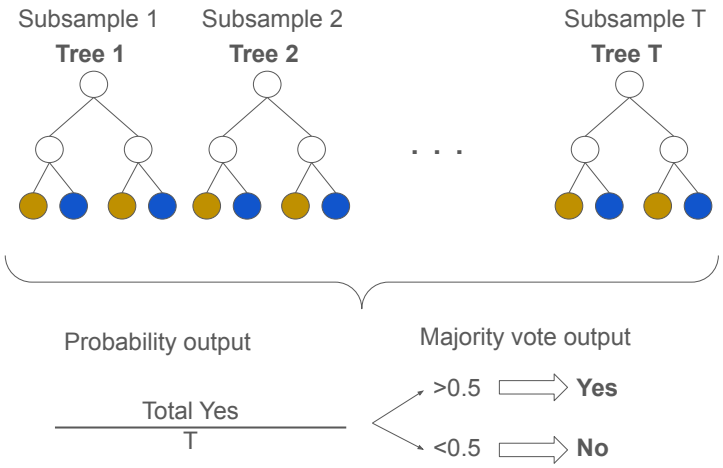

Figure 5.4: Schemtization of Random Forest and outputs of the model. Random Forest is obtained by producing a total of T decision trees (which are similar to Figure 5.3). The predictand yes/no is obtained either as a class proportion or decided by majority vote.

Where p refers to the proportion of either the class yes/no. Therefore, the Gini index measures the purity of the node. In this context, purity refers to the proportion (i.e., the higher the proportion of a single class, the higher the purity of the node).

One way to determine the importance of predictors in Random Forest is by using the Gini index impurity (Equation 5.5). During tree construction, the total decrease in the Gini index caused by splits on a specific predictor is recorded and then averaged across all trees. A larger decrease indicates greater importance of that predictor. This metric is also known as the mean decrease in Gini index or Gini importance.

5.3.3 Partial dependence plots

The mean decrease in the Gini index provides information on variable importance but does not reveal the actual effect of the target predictor. To address this, partial dependence plots are utilized (Friedman, 2001; Goldstein et al., 2015). Partial dependence plots are used to illustrate the relationship between a target feature (or a subset of features) and the predicted outcome of a machine-learning model. They help to show how the probabilities of a certain class change as a function of individual predictors.

To define partial dependence plots, let s be the target predictor of interest and C be the set of all other features (the complement of s). The partial dependence function, $\hat{f}_s$ represents the average predicted outcome when the feature s takes different values, with all other features held constant (Equation 5.6):

$$\hat{f}_s = \frac{1}{N} \sum_{i=1}^{N} \hat{f}(x_s, x_{C,i}) \tag{5.6}$$

Where N is the total number of observations, x_s is the vector of the predictor s, $x_{C,i}$ are the predictors C for the observation i, and $\hat{f}$ the estimated function (in this case, obtained by using Random Forest). Partial dependence plots are a practical way of making black boxes understandable and are commonly used to explain model behaviour in agriculture and extreme weather-related studies (Vogel et al., 2019; Beillouin et al., 2020).

5.3.4 Shapley values

Partial dependence plots provide an average view of how the probabilities of yield shock depend on selected predictors. However, they do not show the marginal contribution of each predictor to the predicted probabilities. This distinction is especially important when interpreting the individual influence of predictors on unseen (test) data. To address this limitation, Shapley values are introduced (Shapley et al., 1953; Molnar, 2020).

A Shapley value represents the average marginal contribution of a feature across all possible coalitions of predictors. This allows us to quantify each predictor's contribution relative to the average predicted probability. For example, if the average probability of yield shock is 20% and the predicted probability for a new instance is 45%, the Shapley values sum to the difference of 25%, distributed according to each predictor's individual contribution. However, a Shapley value does not equal the change in prediction caused by simply removing the feature; rather, it is the average contribution across all possible feature combinations.

One limitation of Shapley values is that they are estimated by permuting feature values, which can generate potentially unrealistic instances, particularly when predictors are correlated. Another limitation is that they are computationally expensive, so in practice, approximate methods are usually applied.

5.4 Models' setup

This section describes the specific setups for each study. Chapter 6 compares LASSO and Random Forest models using similar setups. Chapter 7 builds upon the outcomes and limitations identified in Chapter 6, refining the approach by focusing exclusively on Random Forest. Finally, Chapter8 applies the models developed in Chapter 7 to future climate scenarios, integrating additional tools to evaluate projected impacts. Detailed descriptions of each chapter's setup follow below.

5.4.1 LASSO for maize yield shock in Germany

The silage maize yield data described in Section 4.1.1 is used after transformation into yield shock and no yield shock categories (Section 4.1.3). Additionally, the set of predictors from Section 4.2.1 is employed. Models are computed separately for each defined group of variables. Since the coefficients $\beta_1 ... \beta_k$ from LASSO depend on the magnitude of the predictors (Section 5.2.3), all predictors are first rescaled to the range $[-1, 1]$. This step ensures all predictors share the same unit range while preserving their distribution (Ali et al., 2014).

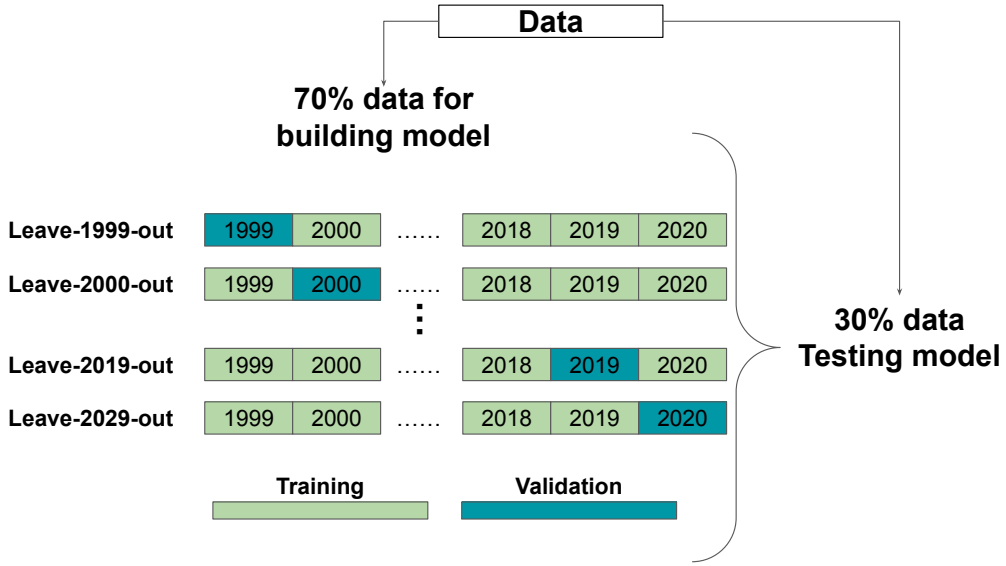

Figure 5.5: Schematization of model set-up when analysing weather and climate drivers of maize yield shock in Germany. The data is first split into random 70% for building the model and 30% for testing the model. The model construction consists of leaving one year out (blue) and validating the individual model against the year. The resulting model is the one that reduces the error to the minimum. Finally, the model is tested against the remaining 30% of data.

The model setup for LASSO is illustrated in Figure 5.5. The data is first randomly split, allocating 70% for training and 30% for testing. LASSO is computed using the *glmnet* package in R software (Friedman, Jerome et al., 2021). The tuning parameter is selected via a customized cross-validation method known as "leave-one-year-out cross-validation" (Wang et al., 2020; Tredennick et al., 2021). This procedure involves building a model while excluding all observations from a particular year and evaluating a range of values for λ. The model's accuracy is then validated against the omitted year. This process is repeated for each year. Cross-validation is performed using the *cv.glmnet* function, which produces two main outputs: *Lambda.min*, the tuning parameter that minimizes the cross-validation error, and *Lambda.*1*se*, which corresponds to the most regularized model within one standard deviation of *Lambda.min*. All models are estimated using *Lambda.*1*se* to balance model complexity and predictability.

Once models are built for each set of variables, variable importance is compared across them. To estimate the relevance of climate drivers explaining silage maize yield shock, a qualitative analysis is performed, focusing explicitly on the variable importance ranking for each group and addressing similarities and differences among them.

Next, the test data is used to assess the performance skill of each model via the Matthews Correlation Coefficient (MCC) (Section 5.2.2). To construct the confusion matrix, a threshold is required to split the predicted probabilities; a common choice is 50%. This implies that predicted probabilities above (below) 50% are labeled as yield shock (no yield shock). However, this threshold can be biased, particularly with imbalanced data.

Therefore, MCC is calculated for each model across a set of 20 equally spaced thresholds ranging from 0 (0%) to 1 (100%), i.e., threshold $= 0, 0.05, 0.1, 0.15, \ldots, 1$. When interpreting results, a threshold closer to 0% represents a more pessimistic view, while one closer to 100% represents a more optimistic view.

Finally, the best model is selected based on the Matthews Correlation Coefficient (MCC), and the contribution of climate drivers to historical silage maize yield losses is investigated (Section 5.2.4). As an initial step, year-to-year probabilities of yield shock are calculated using the test data and compared with reported observations (illustrated in Figure 4.4c). Next, the years are ranked from the worst (highest predicted probabilities of yield shock) to the best (lowest predicted probabilities of yield shock) by averaging predictions per year. The six worst years (referred to as "bad years") and the six best years (referred to as "good years") are then selected based on these average predicted probabilities. Finally, the contributions of the variables to the predicted high and low yield shock probabilities are quantified and compared (Section 5.2.4).

5.4.2 Random Forest for maize yield shock in Germany

Since the aim is to compare the outputs with those obtained using LASSO, most of the methods are repeated (Section 5.4.1, Figure 5.5). First, the data is randomly split into 70% for training and 30% for testing (using the same sets defined in Section 5.4.1). The training data is used to compute a Random Forest model for the six groups of variables derived from Section 4.2.1. These models are trained using the *train* and *trainControl* functions from the `caret` package in R (Kuhn et al., 2023). The number of trees is set to 500, and the leave-one-year-out validation method is employed to identify the best model and the optimal number of features m within the range of 7 to 12.

For each model, the variable importance ranking is examined using the mean decrease in the Gini index (Section 5.3.2). Subsequently, the model's performance skill is evaluated by computing the MCC on the test data. Finally, year-to-year probabilities of yield shock are estimated as described in Section 5.2.4. Because Random Forest is constructed from decision trees, variable contributions cannot be explored in the same manner as with LASSO. Instead, partial dependence plots are used to illustrate how the probabilities of yield shock depend on each predictor, complemented by visualizations of the variables' distributions during the "good" and "bad" years.

5.4.3 Random Forest for crop yield losses across Europe

The set-up and outputs for assessing weather and climate drivers of yield shock across European countries are illustrated in Figure 5.6. Unlike the previous method, an ensemble of Random Forest models is performed to incorporate uncertainty from the input data. For this, a Random Forest ensemble is computed for each country and dataset by employing a leave-one-year-out approach (similar to Section 5.4.1 but maintaining separate models, Figure 5.6a). Since the GDHY dataset covers the period from 1982 to 2016, this approach results in an ensemble of 35 models per country (e.g., one model trained on 1982–2015 and tested on 2016, one model trained on 1982–2014 plus 2016 and tested on 2015, etc.). The function *randomForest* from the `randomForest` package in R is used (Breiman and

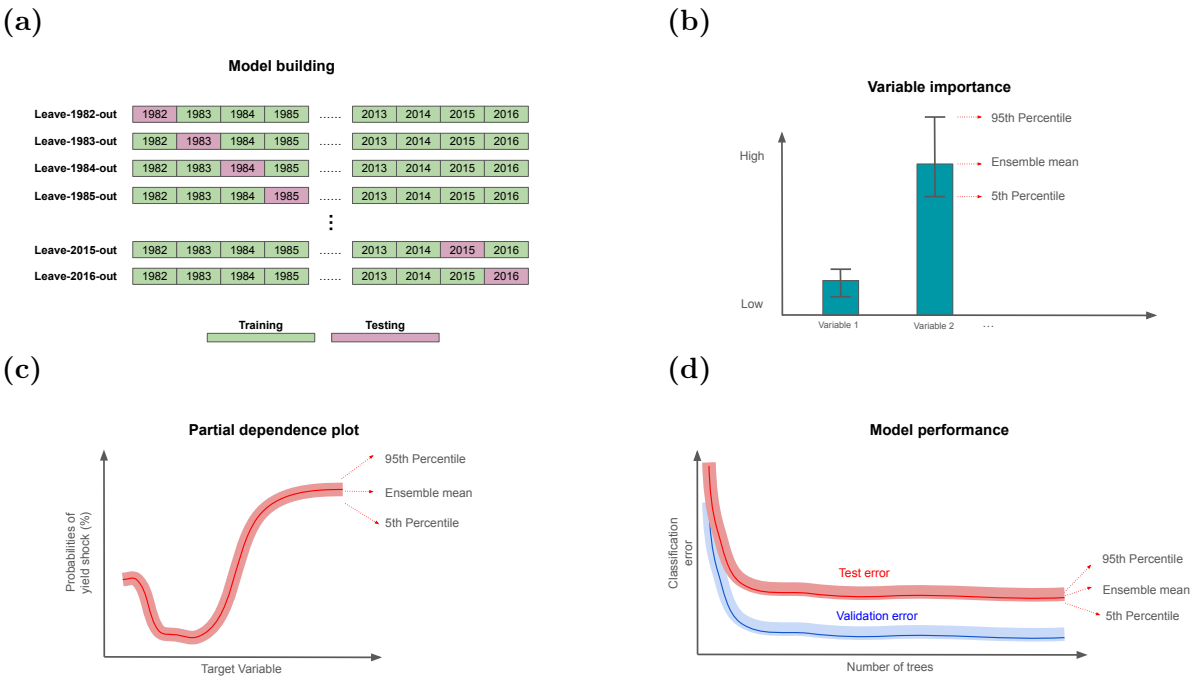

Figure 5.6: Schematization of model set-up and outputs when analysing weather and climate drivers of winter wheat yield across European countries. (a) leave-one-year-out model building process, (b) Variable importance schematization with uncertainty. (c) Illustration of partial dependence plots with uncertainty. And (d) Classification error as a function of number of trees for the validation or OOB error (blue) and for the test data (red).

Cutler, 2022). The number of trees is set to 500, while the number of features is kept at the default value of $\sqrt{\#}$ predictors.

For each ensemble, variable importance is calculated using the mean decrease in the Gini index (Section 5.3.2). Additionally, the marginal effect of each predictor is quantified through partial dependence plots (Section 5.3.3). Since each country has a total of 35 Random Forest models, results are summarized by plotting the ensemble mean and uncertainty ranges represented by the 5^{th} and 95^{th} percentiles of all models (Figure 5.6b,c).

Both the OOB error (validation error) and test error are recorded (Figure 5.6d). Predictability skill of the ensemble is assessed by testing each model against the left-out year (e.g., the model trained on 1982–2015 is tested on 2016; the model trained on 1982–2014 plus 2016 is tested on 2015). Performance is evaluated using the error rate defined in Equation 5.4.

Finally, years with low accuracy are identified for each country. The causes of low accuracy are investigated by examining specific model outputs, analyzing partial dependence plots, and reviewing the climatology of the identified years.

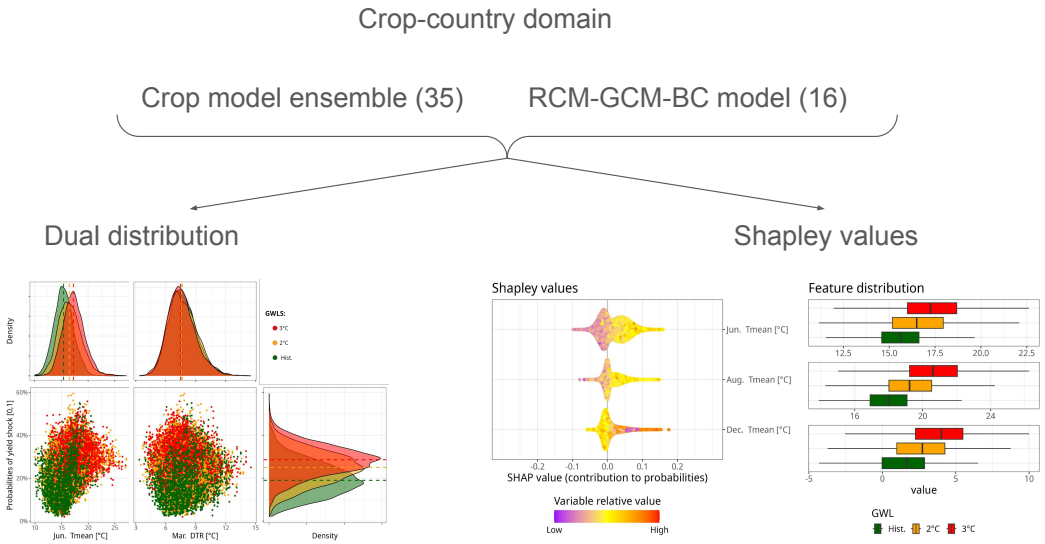

Figure 5.7: Schematization and exemplification of model outcome in future climate change scenario. For each crop-country domain, the use the 16 RCM-GCM-Bias Correction (BC) model chain (16 models) as input on the leave-one-year-out ensemble model (35 models) are used. The predicted probabilities are assessed in two different ways. The first one (left plot) display the dual distribution analysis, exemplified for the case of two predictors in winter wheat yield shock in Germany during the historical period (green), GWL2 (orange) and GWL3 (red). The second approach (right plot) analyze side by side the Shapley values using GWL2 and GWL3 data (left panel), and the shift in distribution's predictors on the correspondent periods (right panel).

5.4.4 Random Forest for crop loss in warmer climates

Once the models are established for present climate data, they are applied to future climate scenarios to predict changes in yield shock probabilities. These results are presented in Chapter 8, where the drivers of changes under GWL2 and GWL3 (Section 4.3) are also investigated in comparison to the historical period.

Figure 5.7 illustrates the two approaches considered to assess the climate drivers of changes in yield shock risk under warmer climate scenarios. For each crop-country model ensemble developed in Chapter 7, future climate change data (Section 4.3) are used as input data. Given the leave-one-year-out ensemble comprising 35 models and the RCM-GCM-BC ensemble with 16 datasets, a total of 560 individual predictions per grid and year are obtained, ensuring relative independence. To evaluate the influence of predictors on changes in probabilities, two approaches are utilized, which are described below:

- **Dual distribution relation.** This approach focuses on the top variables identified using the Gini index. Based on information derived from partial dependence plots (Chapter 7), changes in yield shock can be attributed to variations in these top variables. For example, suppose the Random Forest ensemble and partial dependence plots indicate that $Tmean$ in June increases the probability of winter wheat yield shock in Germany. If both the probability of yield shock and $Tmean$ in June

increase under GWL2 and GWL3, this would suggest that changes in yield shock are due to the changes in $Tmean$ in June. It is important to note that this approach is based on causality rather than casualty.

- **Shapley values and changes in variable distribution.** Shapley values are estimated separately for GWL2 and GWL3. For a given GWL, crop, and country, the probabilities of yield shock are calculated, allowing estimation of changes in probabilities compared to a baseline (average values in the historical period). Attribution is then studied based on the behavior of individual variables in each specific case. Taking the example of winter wheat in Germany, this approach can reveal whether the changes in probabilities are associated to the ones in $Tmean$ in June.

Shapley values are calculated using the *Fastshap* package in R (Greenwell and Greenwell, 2020). The *Shapviz* package is employed to visualize the results (Mayer and Stando, 2025). By default, the criterion for determining the most important variable in these packages is the average of the absolute Shapley values, expressed as $\frac{1}{N}\sum_{i=1}^{N}|s_i|$, where N denotes the total sample size. Given the large size of the dataset (approximately 6.72×10^7) and the high computational cost of the method, Shapley values are computed on a sub-sample of 300 observations per input data, per GWL and per leave-one-year-out model (i.e., 35 models). The baseline is defined as the average probability of yield shock during the historical period for each leave-one-year-out model.

6 Model Comparison of Climate Drivers of Silage Maize Yield Shock in Germany

This chapter aims to answer the RQ1:

To what extent does increasing the complexity in the definition of climate predictors improve the performance of silage maize yield shocks predictions in Germany?

Additionally, the influence of climate drivers on silage maize yield shock is described and discussed. First, an overview of the silage maize yield shock series in Germany is provided, the most extreme years are identified, and the recorded weather reports during those years are reviewed. Furthermore, differences between the selected weather and climate drivers during yield shocks and no yield shocks are described (Section 6.1). Next, the results obtained by LASSO and Random Forest are compared. Analyses are always conducted separately for each method. Variable importance (Section 6.2), predictability skill (Section 6.3), and contributions to high and low predicted probabilities of yield shock (Section 6.4) are compared. Following this, a physical interpretation of the model outputs is provided by describing the physiological response (Section 6.5). The chapter concludes with a summary of results, discussion of methodological choices, and answering RQ1 (Section 6.6). The information of this chapter is further supported by Appendix B.

6.1 Overview of yield shock series and composite analysis

This first section focuses on the climatology of yield shock and the chosen climate drivers. Yield shock are defined by using the 15^{th} percentile of yield deviations from the whole domain (as described in Chapter 4). In detail, the aim is to evaluate to what extent the years with high yield shock numbers match extreme weather events in the studied period (1999-2020). The second step is to analyze the behavior of the eleven climate indicators (displayed in Table 4.1 and described in Section 4.2.1) during yield shock and no yield shock using composite analysis.

Yield shock series

First, the characteristics of the silage maize yield shock series in Germany are described. The year-to-year distribution is shown in Figure 6.1 (similar to the one shown in Figure 4.4c). The shocks are mostly concentrated in six years: 2003, 2006, 2010, 2013, 2015,

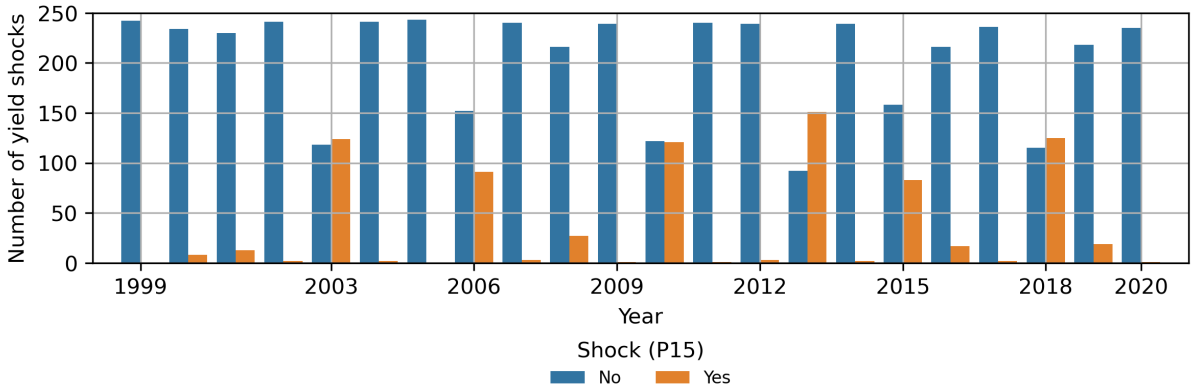

Figure 6.1: Year-to-year silage maize number of yield shock (orange) and no yield shock (blue) in the whole domain.

and 2018. During these years, the number of losses exceeds 50 (i.e., more than 20% of the total domain). These years also coincide with those reported by Webber et al. (2020).

The spatial distribution of yield shock for the identified years are shown in Figure 6.2. As a general view, the shocks during 2006, 2010 and 2018 are mostly concentrated in central and northern Germany. The year 2003 shows high density of losses in central and eastern Germany. During 2013, losses are identified throughout the whole country, especially in northwestern Germany. Finally, in 2015, we see a relatively low number of districts with losses, which are mostly located in southern eastern Germany.

In the identified years, extreme weather events were also reported in the area (Lhotka and Kyselý, 2022). The year 2003 was characterized by anomalously hot and dry conditions during June and August in central Europe (Fink et al., 2004). Similarly, extreme high temperatures were reported during July 2006 (Rebetez et al., 2009). During 2010, warmer-than-average summer temperatures were recorded throughout Western and Central Europe, with values of at least 3 °C warmer than average in Germany (Blunden et al., 2011). 2013 presented several anomalies throughout spring and summer, with extremely cold and wet conditions in early spring, late snowfalls and floods in wide areas of the country and the exceptional hailstorm of 27th and 28th July (Blunden and Arndt, 2014). During the year 2015, unusual strong and long-lasting heatwaves were reported in Central Europe (Blunden and Arndt, 2016). Finally in 2018, Germany experienced one of the driest and warmest years from the last century, reporting temperature record breaking throughout spring and summer in different regions (Blunden and Arndt, 2019; Rousi et al., 2023).

Composite analysis

The link between climate anomalies and silage maize yield shocks can be rapidly inspected by using composite analysis. For this, the climate indicators defined in Table 4.1 are used.

Figure 6.3 presents the climatology (median and interquartile range) of the selected predictors for yield shock years (orange) and no-yield-shock years (blue). The most pronounced differences occur in June, July, and August, characterized by warmer and drier condi-

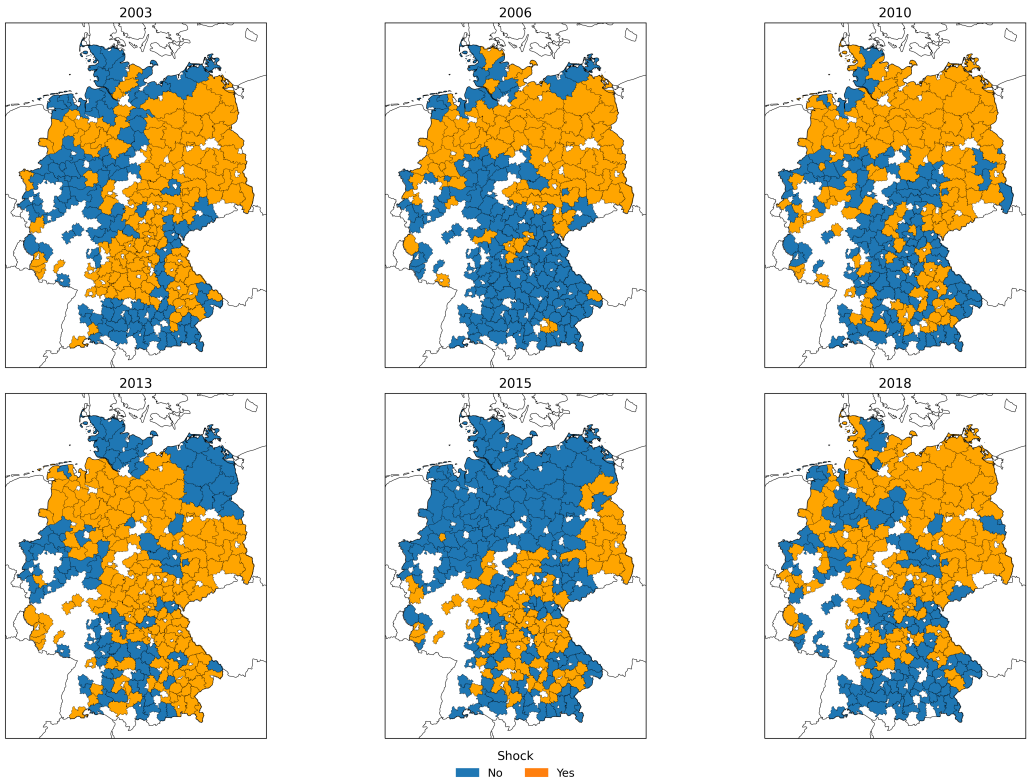

Figure 6.2: Spatial distribution of yield shocks for the top six worst years (in panels).

tions during yield shocks. Specifically, these cases exhibit relatively lower values of PP, $PP90p$, and $SPltm05$, and higher values of $PPlt1$. Similarly, increased values of TN, TX, $TX90p$, and $TX90pDD$ are observed, alongside lower $TN10p$ and $TN10pDD$. The largest deviations during yield shock years occur in July, where the median of PP is approximately 45 mm lower, and $PPlt1$ and $TX90p$ are about 13 d and 3 d, respectively. Additionally in this month, TX is 2 °C higher and TX90pDD is between 5 °C d and 35 °C d higher.

Moreover, in April, higher values of $TN10p$ and lower values of $TN10pDD$ (with considerable variability in the interquartile range) are evident. This is also observed in September for both variables.

According to the K-S test, almost all predictors present statistically significant differences between years of yield shock and no yield shock (not shown). It is only for $PP90p$ and $SPgt05$ in April, $SPltm05$ in May, and $PP90p$ and $SPgt05$ in September, where there is no statistically significant difference between the two cases.

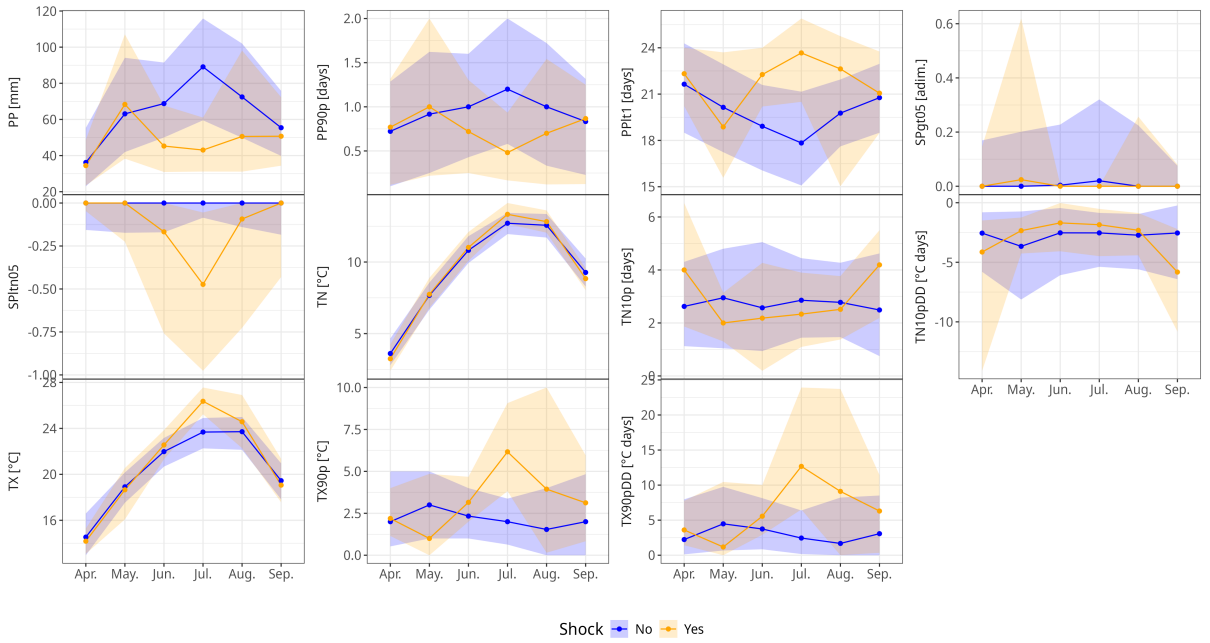

Figure 6.3: Climatology of the selected predictors during yield shock (orange) and no yield shock (blue). The opaque lines represent the median, and the shades represent the interquartile range. Since $SPgt05$ and $SPltm05$ are standardized values, they are adimensional ("adim.").

6.2 Comparison of variable importance between groups

This section compares the general pattern of the meteorological variables that explain silage maize yield shock probabilities. The results are organized by method and the illustrations show the comparison by variable group.

LASSO

Figure 6.4 illustrates the coefficient values obtained for each group of variables. The name of the models corresponds to the predefined set of predictors. When the colour is red (blue), an increase in the value of the corresponding variable leads to a higher (lower) yield shock probability. Coefficients which are either null or not included are not displayed in colours. The coefficient values are presented in Table B.1, sorted by decreasing absolute value. First of all, a reduction in the total number of predictors in comparison to the original inputs is observed (Figure 4.6). The approach with LASSO reduces the total number of variables from 18 to 11 in group *Simple*, 24 to 7 in *Frequency*, 24 to 11 in *Cumulative*, 66 to 21 variables in group *All*, 18 to 14 in *Forward* and 18 to 15 in *Backward*.

Overall, the six groups agree on two sets of factors. The first one is that hot-dry conditions during July and August increase the probability of maize yield shock. The primary predictor for the six groups is maximum temperature-related variables in July. This is illustrated in a positive coefficient of TX (i.e. higher maximum temperature, higher probability of yield shock), $TX90P$ (i.e. higher number of warm days, higher probabilities

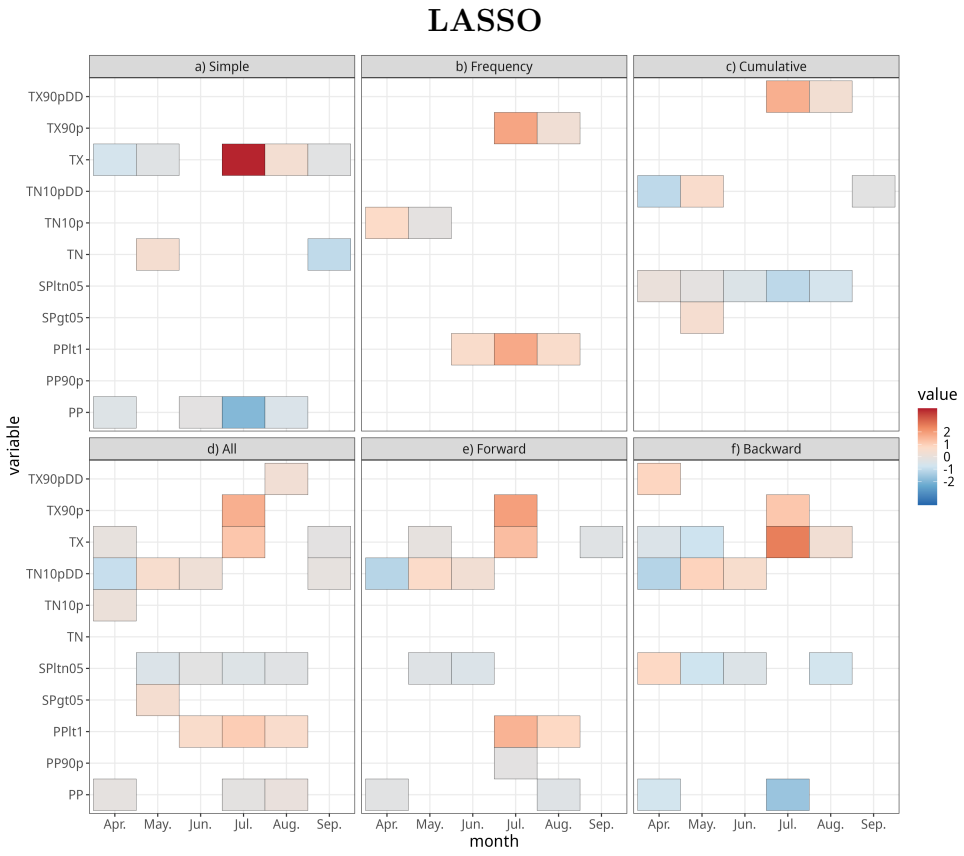

Figure 6.4: Coefficient values by variable group (in each panel) in LASSO. The coefficient names (y-axis) refer to the variables in Table 4.1. Months (x-axis) are represented by their number. Variables that are either excluded from the group or not selected by LASSO are in blank.

of yield shock), and $TXD90pDD$ (i.e. higher cumulative heat, higher probabilities of yield shock) in groups *Simple*, *Frequency*, and *Cumulative*, respectively. Groups *All* and *Forward* select $TX90p$ in July as the most important variable. The group *Backward*, on the other hand, chooses TX in July as the most important variable (second most relevant variable in group *All* and third in group *Forward*). In addition, in the same month, reduced precipitation increases the probability of maize yield shock. This is shown in the negative coefficient of PP (i.e. the less precipitation, the higher probabilities of yield shock) in groups *Simple* and $SPltm05$ (i.e. the more negative the value, the more the probabilities of yield shock) in group *Cumulative*, and *Backward*, and in the positive coefficient of $PPlt1$ (the higher the number of dry days, the higher the probabilities of yield shock) in groups *Frequency*, *All* and *Forward*. Lastly, hot and dry conditions in August increase the probability of yield shock, though the importance of predictors in this month has a lesser impact.

As a second general pattern, cold temperatures during April increase the probability of silage maize yield shock. The key variables change depending on the group, but the predictors show similar patterns. In group *Simple*, a negative coefficient of TX in April can be noted, whilst in group *Frequency*, it is illustrated in the positive coefficient of $TN10p$ (i.e., the more number of cold nights, the highest the probability of yield shock).

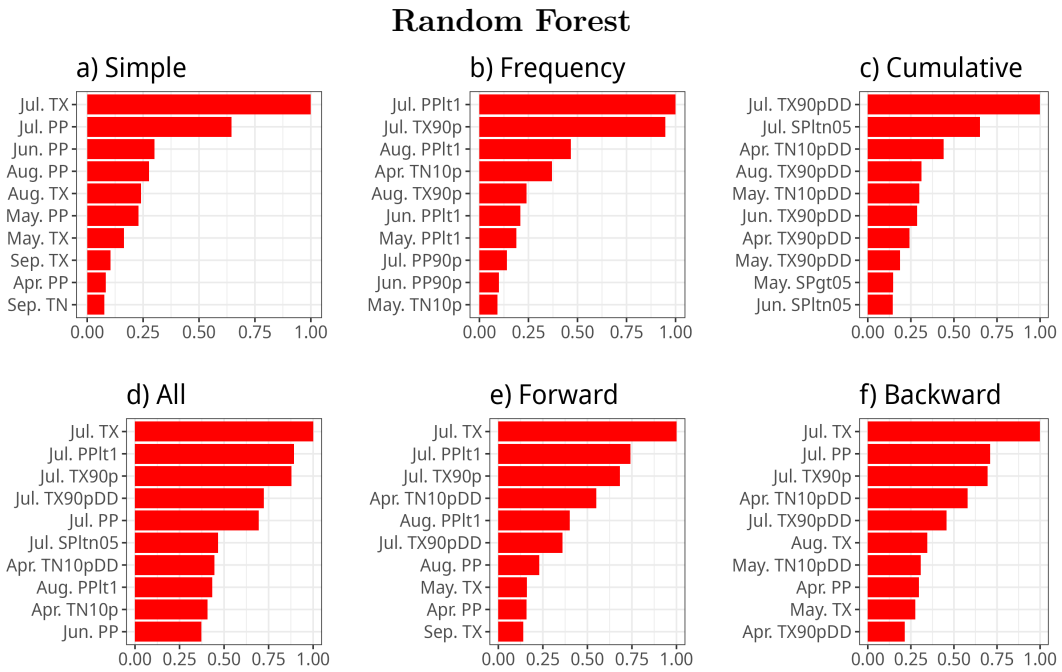

Figure 6.5: Relative variable importance of the Random Forest models by group (in panels). Only the top 10 variables per group are displayed. The variable importance is normalized between 0 and 1 to make it comparable between groups.

In groups *Cumulative*, *All*, *Forward* and *Backward*, the negative effect of cold temperatures in April is illustrated by a negative coefficient of $TN10pDD$ (i.e. the more cumulative cold, the higher the probabilities of yield shock). We also observe this pattern in May (particularly with $TN10pDD$) but to a lesser extent.

Random Forest

Figure 6.5 illustrates the relative variable importance of the top 10 predictors per group (in panels). Due to the nature of variable importance in Random Forest, the direction of the relationship (positive or negative) with silage maize yield shock cannot be determined. The plot only indicates how influential each variable is on model performance.

As expected, the six groups exhibit patterns similar to those obtained using LASSO, with July-based variables being the most important across groups. This is particularly evident in the group *All*, where the top six variables are exclusively July-based. This pattern arises because Random Forest does not perform variable selection or filtering as LASSO does. The most important predictors in each group are maximum temperature-based variables in July. However, unlike the LASSO results, TX holds relatively greater importance than $TX90p$ for the three hybrid groups (*All*, *Forward*, and *Backward*). Additionally, precipitation-based variables in July show high relevance, such as PP for groups *Simple* and *Backward*, $PPlt1$ for *Frequency*, *All*, and *Forward*, and $SPltm05$ for *Cumulative*.

The subsequent set of variables changes depending on the group, but in general, either August or April-based predictors seem to be the most important. Similar to LASSO, in the case of April-based variables, the most relevant predictor for all the groups, except for

group *Simple*, is a minimum temperature-based variable, i.e. $TN10p$ for group *Frequency*, $TN10pDD$ for group *Cumulative*, *All* and *Forward* and *Backward*. In the case of the group *Simple*, August, May and September-based variables (PP and TX) appear as the most relevant after July-based predictors.

6.3 Comparison of predictive skill between set of variables

The next step involves comparing the performance of predicted probabilities between the different sets of variables. This is achieved by evaluating and describing the predictive skill of each method individually using the Mathews Correlation Coefficient (MCC, Chapter 5).

LASSO

Figure 6.6 illustrates the performance skill obtained with MCC for all models throughout the different thresholds. As a general observation, the MCC is positive for all models and thresholds, which means that the six model performances are better than random guessing. Moreover, a peak in performance in the six groups is observed when the probability threshold is between 20% and 30%, depending on the model. The hybrid groups (*All*, *Forward* and *Backward*) present superior predictive skills than the other groups (*Simple*, *Frequency* and *Cumulative*). This becomes evident when considering thresholds between 30% and 80%. The group *Backward* (red line) is the one with the overall highest performance, though the difference can be considered negligible.

Random Forest

Figure 6.7 displays the model performance by using MCC for each group with Random Forest. Similar to the results obtained by using LASSO (Figure 6.6), the MCC is positive for all models and thresholds; additionally, the peak in performance is between 20% and 40%, depending on the model.

In contrast to the results obtained with LASSO, no group demonstrates a clearly superior performance in the Random Forest models. All groups show comparable predictive skill for thresholds below 40%. Between 40% and 65%, the groups *All* and *Frequency* exhibit a slight improvement relative to the others, though the difference is minimal.

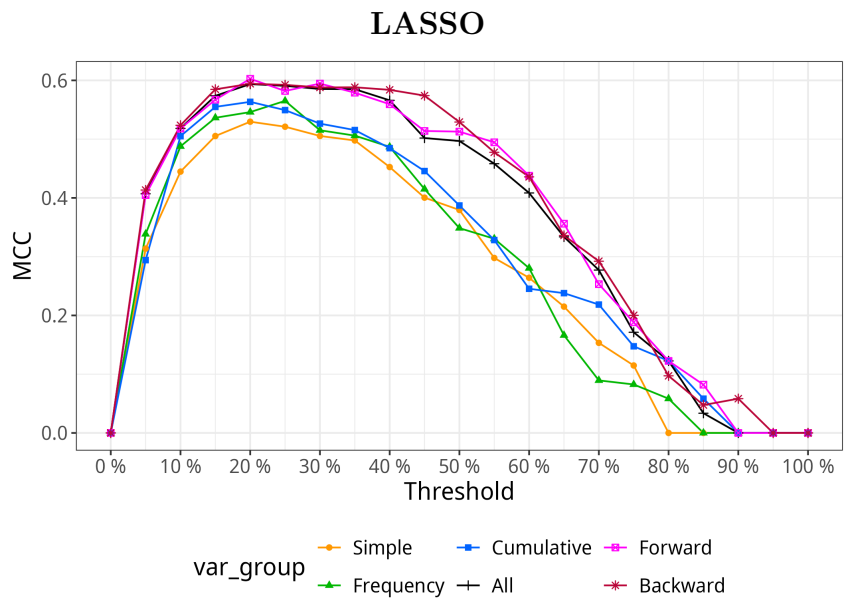

Figure 6.6: Mathews correlation coefficient (MCC) for each variable group (by colour) using LASSO. The threshold (x-axis) chosen to determine the confusion matrix is in percentage.

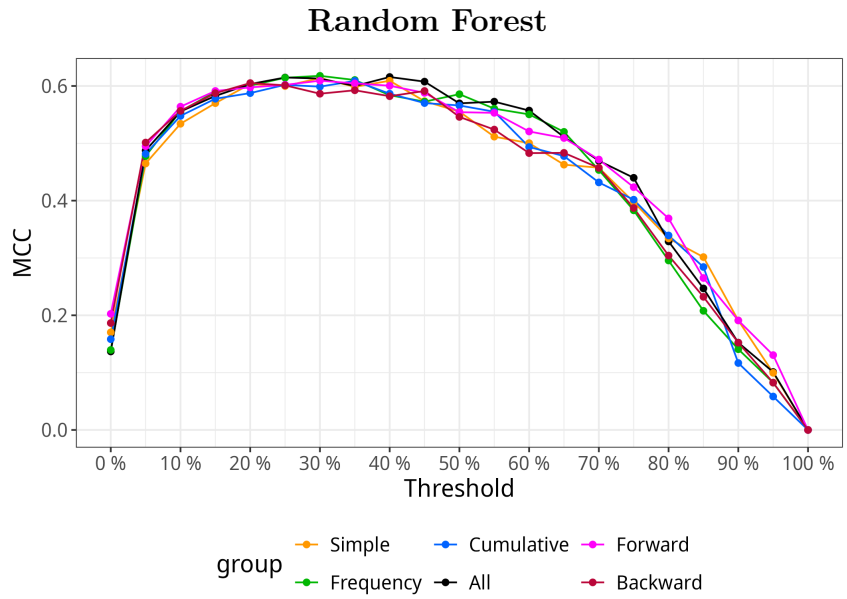

Figure 6.7: Same as Figure 6.6, but using Random Forest.

6.4 Year-to-year prediction and variable contribution during historical losses

As a final step, the factors contributing to both high and low predicted probabilities of yield shock are examined. In particular, the six years with the highest risk (also called "bad years") are compared to those with the lowest (referred as "good years"). As in

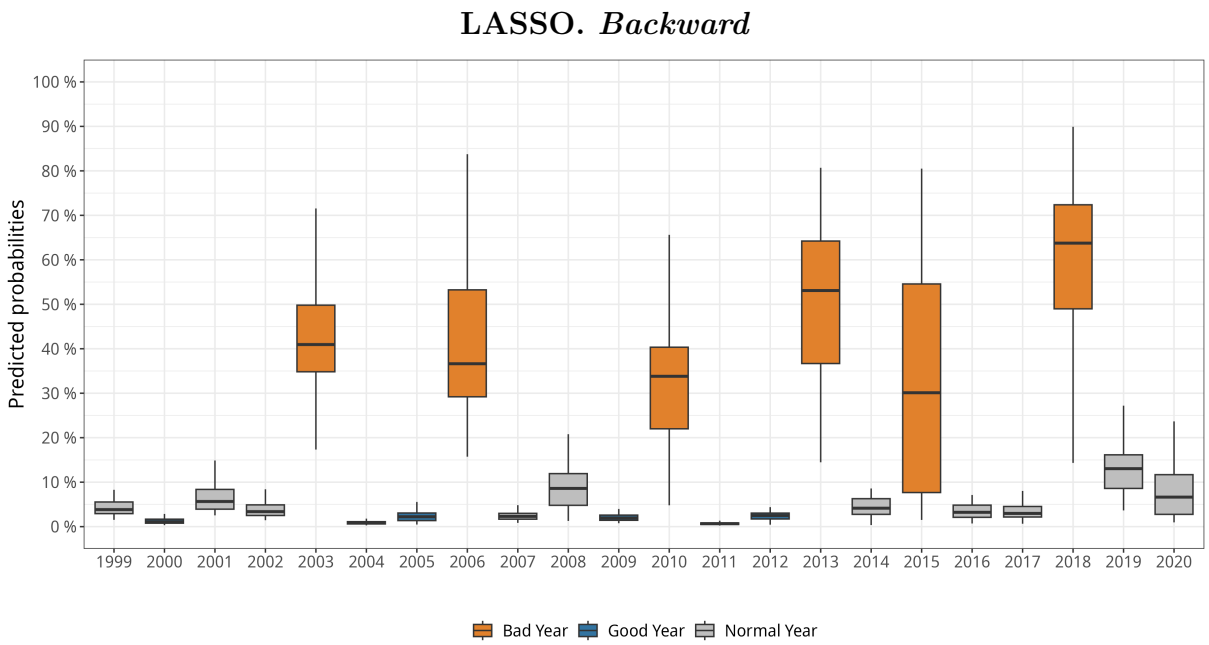

Figure 6.8: Year-to-year distribution of the predicted probability in group *Backward* using LASSO. Orange-coloured boxplots correspond to the six bad years, and blue-coloured to the six good years.

earlier sections, the analysis is performed separately for both LASSO and Random Forest models.

LASSO

Since the model obtained using the group *Backward* outperforms the others, the remaining analysis focuses solely on this group. Figure 6.8 presents the year-to-year distribution of predicted probabilities of yield shock. Years with higher and lower predicted probabilities correspond closely to the reported observations of yield shock in Figure 6.1. The years 2003, 2006, 2010, 2013, 2015, and 2018 exhibit the highest predicted yield shock probabilities (orange-colored boxplots in Figure 6.8, referred to as bad years), which coincide with the largest numbers of reported yield shocks (orange bars in Figure 6.1). Among these, 2018 shows the highest predictions. Conversely, the years 2000, 2004, 2005, 2007, 2009, and 2011 (blue-colored boxplots in Figure 6.8, referred to as good years) have the lowest predicted yield shock probabilities. This pattern also holds for the groups *All* and *Forward* (Supplementary Figures B1 and B2). Subsequently, composites of variable contributions are created using these two sets of years to compare factors contributing to lower or higher probabilities.

The comparison between the variable contribution to the predicted probabilities is presented in Figure 6.9. The variables in the x-axis are sorted by variable importance (as in Table B.1 for group *Backward*). If the values are positive (negative), then the corresponding variable contributed to increasing (decreasing) probabilities of yield shock. The most noticeable difference is observed in temperature-based variables in July and in April. For Tx and PP in July (first and second variable), the contribution during bad years is

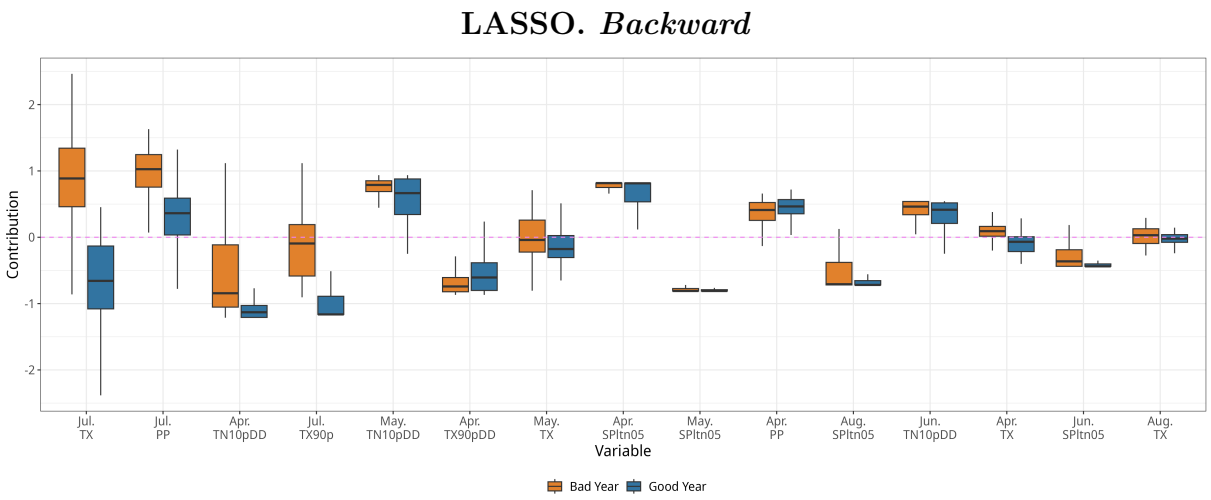

Figure 6.9: Composite distribution of the variable contribution to the predicted probabilities in group *Backward* using LASSO. The variables in the x-axis are organized by absolute coefficient values (as in Table B.1). The dashed-horizontal violet line indicates a null contribution. Composites are made using the bad years (orange-coloured boxplots) and the good years (blue-coloured boxplots).

mostly positive (i.e. higher logit values), whereas for the good years, this is negative. For $TX90P$ (fourth variable), the overall contribution during good years is entirely negative, whereas it is close to 0 during bad years. Furthermore, the distributions reveal a relatively positive contribution of $TN10p$ during April. For the remaining variables, there is no apparent difference between bad years and good years. These patterns are also observed for groups *All* and *Forward* (Supplementary Figure B3 and B4 with their corresponding variable importance rank).

Random Forest

Given the similarity in variable performance among the Random Forest models, only the case of group *Simple* is analyzed. Figure 6.10 displays the year-to-year predicted probabilities of yield shock *for group Simple* by using Random Forest. Similar to LASSO, the highest predictions are, in order, 2018, 2013, 2003, 2010, 2015 and 2006 (bad years). The order slightly changes depending on the chosen group (table B.2). Additionally six groups are in agreement with the selected good years, which are 2004, 2005, 2009, 2011, 2012, and 2017 (good years).

Figure 6.11 presents the partial dependence plots for the Random Forest model based on group *Simple*, highlighting the top five variables along with their distributions during bad years (orange) and good years (blue). The probability of yield shock sharply increases with extremely low July TX, reaching approximately 40% when TX falls below 15 °C. However, at least 75% of observations during bad years show TX values above 20 °C, indicating that low July temperatures are not the primary characteristic of these cases. For the first two variables (TX and PP in July), hotter or drier conditions correspond to increased yield shock risk. The probabilities rise to about 40% when TX exceeds 28 °C or when PP approaches zero. Consistently, bad years exhibit generally hotter and drier

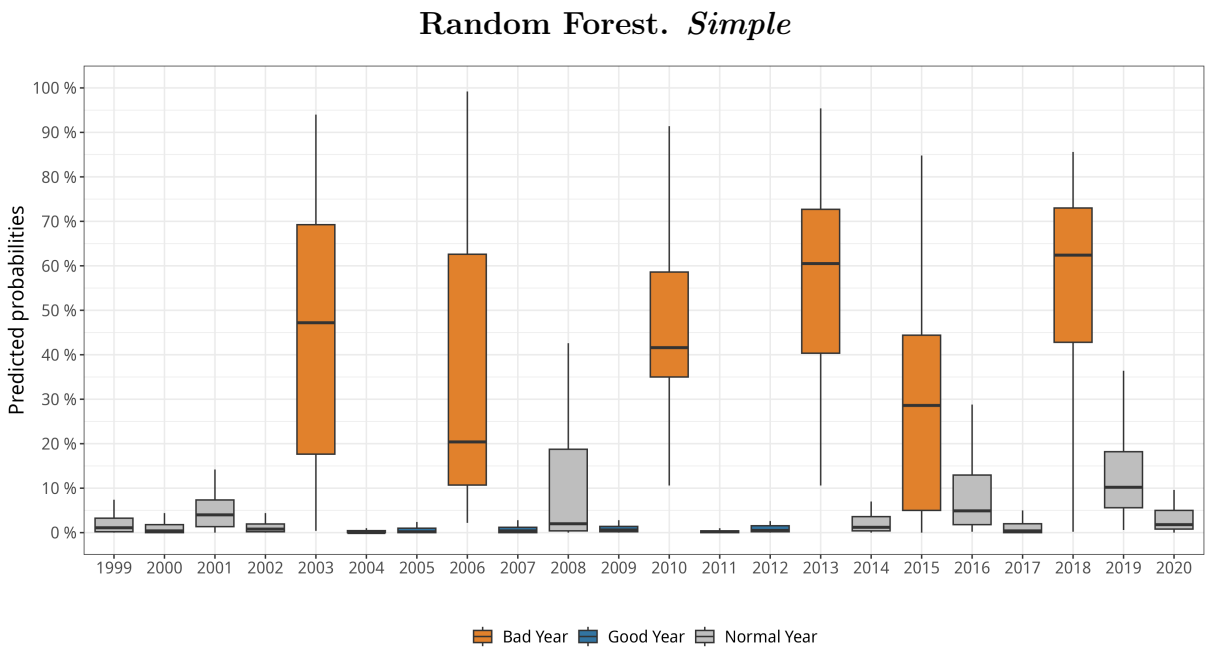

Figure 6.10: Same as Figure 6.8 for group *Simple* and Random Forest.

conditions compared to good years. Additionally, increased TX in August also elevates the risk of yield shock, reaching similar probability levels to the other variables.

Similar patterns emerge across other variables for the selected months in groups beyond *Simple* (Supplementary Figures B5 to B9). Higher temperatures (e.g., elevated $TX90p$ and $TX90pDD$) and drier conditions (high $PPlt1$) during July correlate with increased yield shock probabilities. Furthermore, elevated $TN10p$ and reduced $tn10pDD$ in April are associated with higher risk of silage maize yield shock.

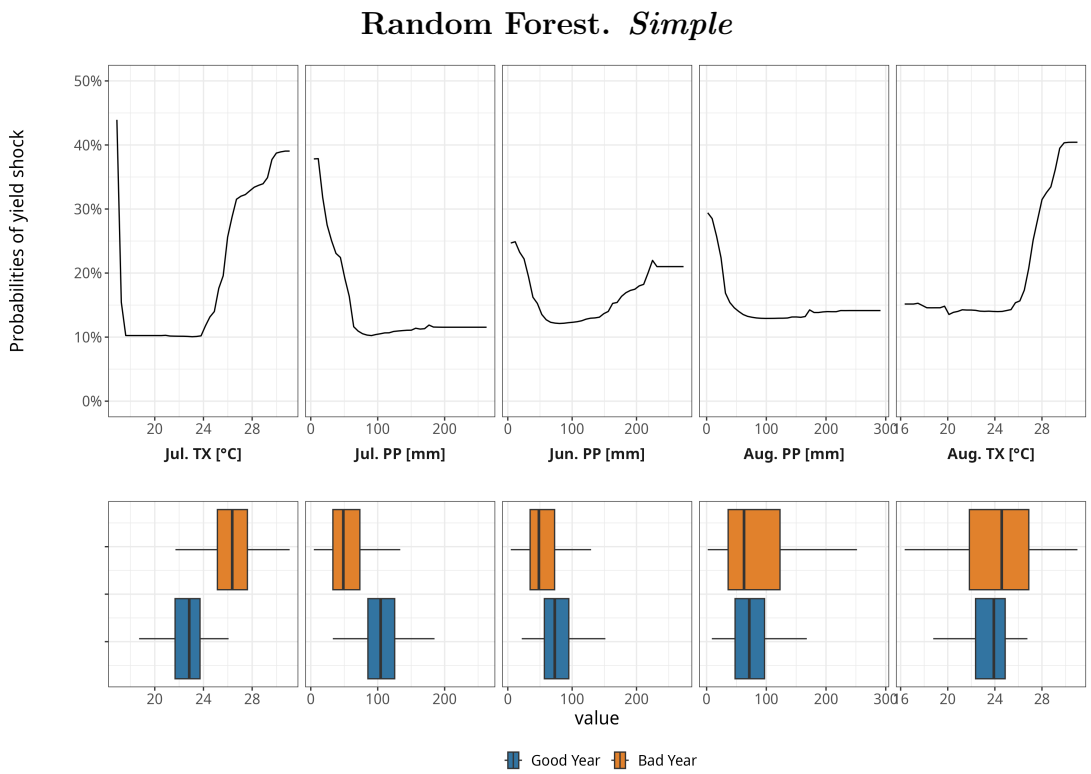

Figure 6.11: (top row) Partial dependence plots of the top 5 predictors obtained from group *Simple* and Random Forest. And (bottom row) the associated variable distribution during good years (blue) and bad years (orange).

6.5 Physiological response of silage maize yield shock to key climate drivers

The patterns identified by both LASSO and Random Forest models can be interpreted through the lens of maize physiology, highlighting how specific weather and climate conditions influence yield.

For both methods, higher temperatures and lower precipitation in July emerge as the most important factors influencing silage maize yield shock. Specifically, the number of warm days ranks as the most critical July-based variable. These findings align with the global-scale study by Vogel et al. (2019), but contrast with previous German studies (Gornott and Wechsung, 2016; Schmitt et al., 2022), which examined a range of weather and climate drivers focusing on general crop yield variability. Gornott and Wechsung (2016) identified evapotranspiration, calculated from maximum and minimum temperatures, as negatively impacting silage maize yields during August to October. Meanwhile, Schmitt et al. (2022) demonstrated a clear drought effect using soil moisture data aggregated by phenological stages. Disentangling the direct impacts of high temperature, evapotranspiration, and water deficit remains challenging. Extreme heat increases vapor pressure deficit, elevates soil water demand through enhanced carbon assimilation and transpiration rates, ultimately reducing water availability (Lobell et al., 2013). Thus, both temperature and precipitation must be considered when predicting yield shocks. Combined indices (e.g.,

Zampieri et al., 2017) offer a promising alternative by capturing compound-event drivers, reducing spurious correlations, and jointly assessing temperature and precipitation effects. Notably, irrigation can mitigate the adverse effects of hot and dry conditions, making it a vital adaptation strategy. Although maize irrigation is uncommon in Germany (Peichl et al., 2018; Zhao et al., 2015), it can substantially increase yields and sometimes represents the most critical management factor (Huynh et al., 2019).

As a secondary set of explanatory variables, anomalously low temperatures during April also increase the probability of silage maize yield shock. This pattern was similarly reported by Lischeid et al. (2022) using machine-learning models. While most agricultural climate research prioritizes temperature and drought, other extremes such as frost, low temperatures, or floods receive less attention (Cogato et al., 2019). However, maize seedlings are sensitive to early-season conditions, requiring warm and moist soils for optimal growth (Stone et al., 1999; Bechoux et al., 2000). Consequently, yield losses may be triggered by low temperatures above freezing (Sánchez et al., 2014; Vogel et al., 2019). To mitigate cold stress, farmers often delay planting dates (Parker et al., 2017), though this strategy can reduce yields by shortening the growing season (Baum et al., 2019).

When applying Random Forest, a decrease in TX during July is also observed to sharply increase the probability of silage maize yield shock. This pattern was similarly identified by Lischeid et al. (2022) using both Random Forest and Support Vector Machine models. Although high temperatures during the summer months generally impact maize negatively, cold conditions in July can reduce biomass accumulation and slow development rates. In such cases, the effects of high temperatures on silage maize yield tend to manifest later, particularly in August. However, in our analysis, TX values during July in bad years are not notably lower than those in good years. This suggests that, while very low July temperatures can have a strong impact, most silage maize yield shocks correspond to warmer July conditions. It is also noteworthy that LASSO regression is unable to capture this non-linear relationship between the predictors and silage maize yield shock.

6.6 Discussion and summary

This chapter investigates the added value of using both simple and complex variables through the application of LASSO and Random Forest methods. Key climate drivers associated with silage maize yield shock are identified, the best combination of variables in terms of predictive skill is determined, and the meteorological factors driving historical yield losses are examined.

The composite analysis reveals that silage maize yield shock features higher and drier conditions during summer as well as cold conditions during April and September. The information from the composite analysis provides a first overview of how the selected predictors behave during yield shock. However, this approach does not quantify the actual probabilities of yield shock. Additionally, it does not provide insight into non-linear interactions. To address these limitations, statistical models are applied to provide quantitative insights and to assess the relative importance and influence of the selected predictors.

With LASSO, the results from the MCC revealed that a combination of more complex and simple variables outperforms models with more traditional ones. The Step-wise selection model reduced the number of considered variables drastically, giving a coherent model with high prediction skills. Even though the capability of Step-wise prediction is widely criticized, it can be a powerful algorithm if it is supported by information criterion (Whittingham et al., 2006). These results cast light on the relevance of considering complex variables and using adequate variable selection methods to enhance predictability skills.

However, in contrast to LASSO, Random Forest models perform similarly regardless of the pre-selection of predictors. They perform equally well as the hybrid groups in LASSO. The advantage of Random Forest is that it does not require an increased number of predictors or more complex variable formulations to achieve high predictive performance. In contrast, LASSO necessitates a more sophisticated set of predictors to reach similar levels of robustness. Furthermore, Random Forest offers valuable interpretability through tools like Partial Dependence Plots and variable importance metrics, such as the Gini index, which provide deeper insights into the model's decision-making process. This makes Random Forest not only a powerful tool but also a relatively comprehensible one.

Lastly, we find that predicted probabilities matched the historical silage maize yield shock observations well. The six years with the highest predicted probabilities are 2003, 2006, 2010, 2013, 2015 and 2018. Despite all the predictors from the model, the strongest contribution to high probabilities of yield shock comes from temperature-based variables in July and cumulative cold in April. In the case of 2013, it is important to highlight that not all potential climate indicators are identified. In this year, there were mainly two extreme events reported: Extreme floods that took place at early June in northeastern Germany (Blunden and Arndt, 2014) and the severe hailstorms from 27^{th} and 28^{th}July impacting mainly northern Germany (around Hanover) and southern Germany respectively (Kunz et al., 2018). These events can have notable impacts at more localized level but are not identified by the model due to the nationally-aggregated and leave-one-year-out validation approaches. In this case, models with higher resolution (e.g. for each NUTS1 or bundesland) could be more useful. Furthermore the chosen climate indicators may serve as proxy of both extreme weather events (specially $PPgt90p$ and $SPIgt05$) but are not necessarily correlated. As a last point, exceptional cold temperatures in March were also reported (Blunden and Arndt, 2014) that, thought not included in the model, could have delayed the sowing of maize in some local farms.

Answer to RQ1

With the analysis performed in this chapter, the answer to RQ1 remains as follows:

RQ1: To what extent does increasing the complexity in the definition of climate predictors improve the performance of silage maize yield shocks predictions in Germany?
When using LASSO, hybrid groups (consisting on simple and complex-defined predictors) exhibit superior predictive skills. Regardless of the pre-selection of variables, warm and dry conditions during July and August, as well as cold conditions in April, increase the chances of silage maize yield shock in Germany. The number of warm days in July and cumulative cold in April have higher relevance among the variables within the corresponding months and within the groups that consider these variables.
In contrast to LASSO, the models obtained using Random Forest perform similarly regardless of the pre-selection of variables. The high flexibility of Random Forest provides the added value and thus, it is not entirely necessary to use more complex variables in this case. Additionally, it has the potential to reveal non-linear responses. Apart from the already-mentioned maize yield shock drivers, low maximum temperatures in July heightens the probability of yield shock.

In summary, this chapter demonstrates that model performance is influenced by both the definition of climate predictors and the choice of statistical method. While LASSO benefits from a broader set of predictors, particularly when combining simple and complex-defined variables, Random Forest consistently delivers high predictive skill regardless of the variable selection strategy. The chapter also identifies the key meteorological drivers associated with silage maize yield losses in Germany. Warm and dry conditions in July, as well as unusually low temperatures in April, are shown to increase the likelihood of yield shocks. Among these, high temperatures in July emerge as the most dominant driver of historical yield losses, according to the selected variables and modeling approach.

7 Spatial Heterogeneity of Agricultural Losses Across Europe

This chapter aims to answer the RQ2:

What are the country-to-country variations in the in-season climate drivers of maize and winter wheat yield shock across European countries?

The chapter analyses how climate drivers influence maize and winter wheat yield shock across major European producers. The countries studied for each crop are:

- **Maize**: France, Romania and Spain.
- **Winter wheat**: France, Germany, Poland, Romania, Spain and the UK.

The results are presented separately for maize and winter wheat across the sections of this chapter. The first section introduces the yield shock time series alongside documented extreme weather events within the corresponding regions (Section 7.1). This is followed by a climatological analysis of the selected predictors, highlighting differences between years with and without yield shocks (Section 7.2). The subsequent section presents the results from the Random Forest ensemble, beginning with an assessment of variable importance and their influence on yield shocks (Section 7.3), and continuing with an examination of the factors contributing to low predictive skill (Section 7.4). A physical interpretation of the model outputs and spatial heterogeneity of the impacts is then provided (Section 7.5). The chapter concludes with a summary and discussion, including a response to RQ2 (Section 7.6). Additional supporting material is available in Appendix C.

7.1 Overview yield shock series

As in Chapter 6, the analysis begins by describing the characteristics of the yield shock series. An initial connection between weather extremes and yield shocks is also established by examining reported events during the identified years.

The maize yield shock series is illustrated in Figure 7.1 for France(a), Romania(b) and Spain(c). These are presented as a fraction of the total domain for easy comparisons between countries. In France (Figure 7.1a), the proportion of yield shock is small throughout the years. It is specifically in 1990, 2003 and 2013 where the fraction of yield shock/no yield shock is over 75%. In Romania (Figure 7.1b), the distribution is even more uneven. Yield shocks are concentrated mostly in the years 1982, 2000, 2007, and 2012, where the proportion reaches almost 100% in the domain. In Spain (Figure 7.1c), in contrast,

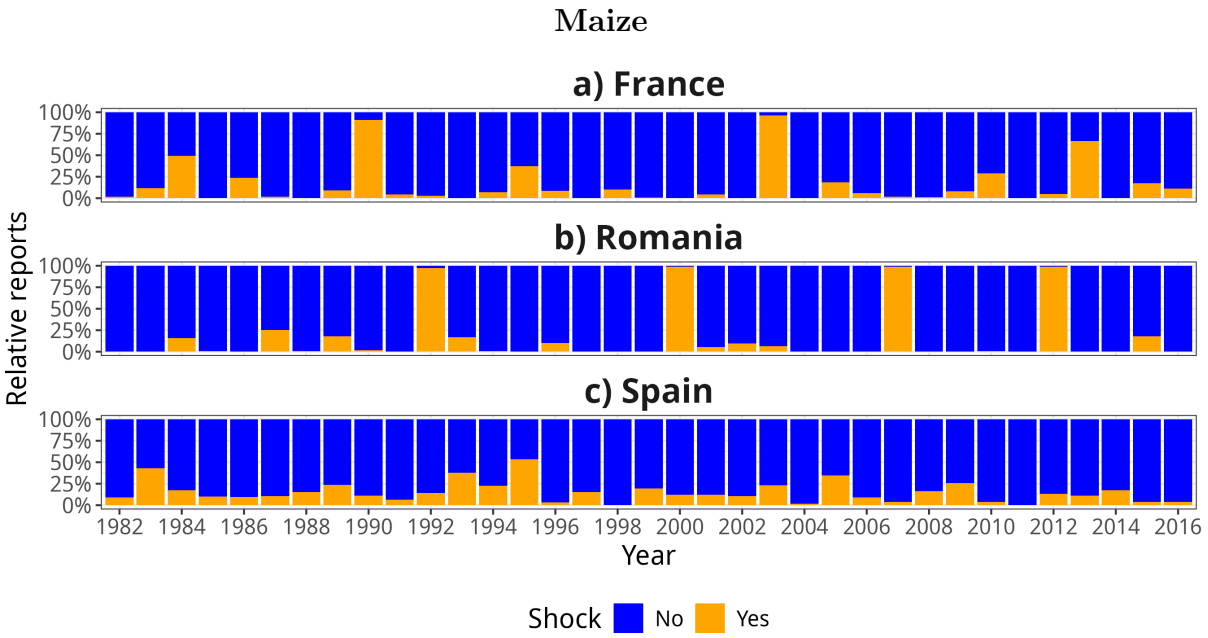

Figure 7.1: Year-to-year proportion of maize yield shock (orange) and no yield shock (blue). The proportion is calculated as the total number of grids with shock divided by the total number of grids of the country.

yield shock is approximately evenly distributed throughout the years, with only a high proportion (50%) in 1995.

Figure 7.2 displays the winter wheat yield shock and no yield shock series for France(a), Germany (b), Poland (c), Romania (d), Spain (e) and the UK (f). Overall, the cases are concentrated in a small number of years. The series for France displays around 50% yield shocks in 1986, 1987, 2010, and 2011, while there is almost 100% of cases in 2016. In Germany, yield shocks are more evenly distributed over the years, with 2003 being the only year with a peak of 50% of the cases. Poland has a high number in 1992, 2000 and 2003, with almost the entire country being affected in this last year. Romania sees nearly 100% yield shocks in 1996, 2003, and 2007. Spain only experience high proportions in 1995 and 2005. Finally, in the UK, yield shocks are relatively low, with 50% in 1987 and 2007, but nearly 100% of the yield shocks reports in 2012.

Many of the years with high proportions of yield shocks coincide with historical records of extreme weather events (Ben-Ari et al., 2018; van der Velde et al., 2018; Bevacqua et al., 2021; Moemken and Pinto, 2022). The European heatwave from 2003 extended throughout central Europe, impacting most of France, Germany and some regions in Poland (Fink et al., 2004). During 2007, the UK was hit by high precipitation events and floods, specially in the southern region (Levinson and Lawrimore, 2008), while Romania experienced one of the warmest years recorded since 1960 (Busuioc et al., 2007; Marcu and Borz, 2013). During 2012, the Uk recorded the third warmest March since 1910 whereas it experienced the wettest June in the 247-year England and Wales series (Blunden and Arndt, 2013). Finally, the year 2016 in France was characterized by extremely high temperatures during December but also extraordinary precipitation events at the end

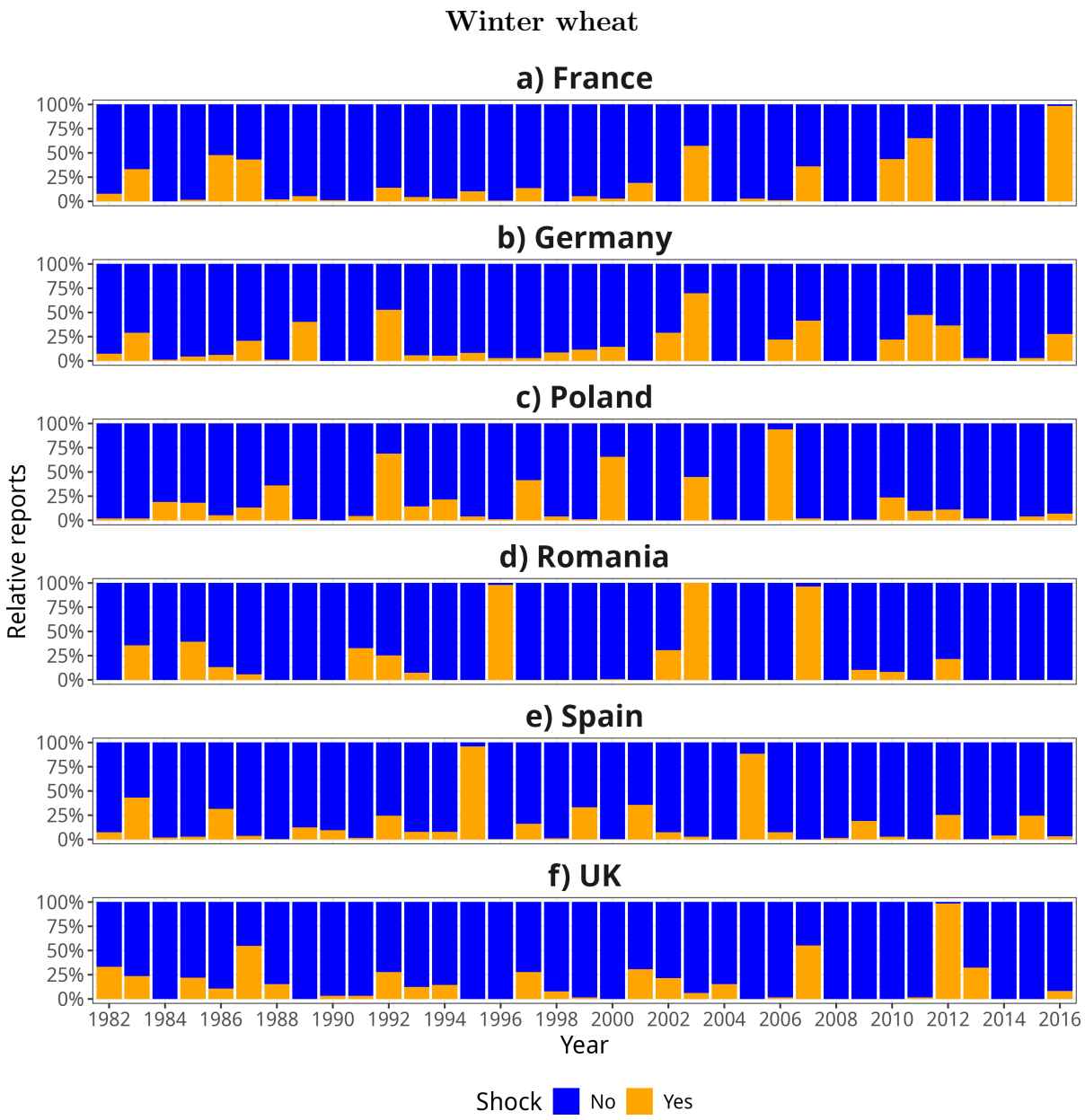

Figure 7.2: Same as Figure 7.1, but for winter wheat across the studied countries.

of May and beginning of June, with precipitation values exceding up to four times the climatology in some stations (Blunden et al., 2017).

7.2 Climatology and composite analysis of climate indicators

As a first step, the general variability of the selected climate indices (*Tmean*, *DTR*, and *RRsum*; Section 4.2.2) during yield shock and no yield shock periods is described. Initially, a climatology of the corresponding indices is provided and compared across the selected countries. Since the chosen predictors for maize yield shock span from April

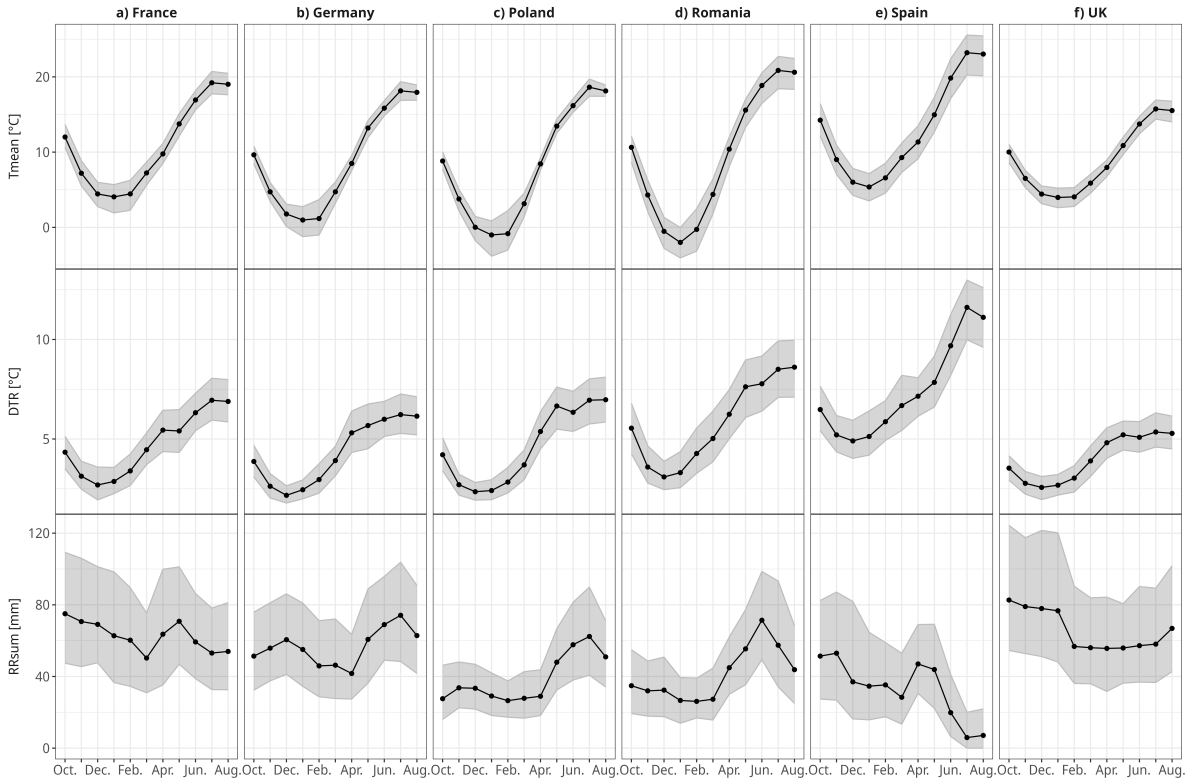

Figure 7.3: Series of median (opaque lines) and interquartile range (shade) for the three climate indicators (in rows) along the six countries (in panels).

to September, while those for winter wheat cover the October–August period, only the climatology for the latter group is analyzed here (see Appendix C for the case of maize).

Climatology of drivers

Figure 7.3 shows the climatology of selected climate indicators across the six countries. Naturally, $Tmean$ exhibits notable seasonal variability. Additionally, higher fluctuation in the winter months (i.e. higher interquartile range). In winter (Dec.,Jan., Feb.), we see $Tmean$ values of about 5 °C in France, Spain and the UK, and 0 °C in Germany, Poland and Romania. During the summer months (Jun., Jul., Aug.), the values rounds close to 20 °C in all the selected countries excepting Spain and the UK, where $Tmean$ can reach values of around 25 °C and 15 °C respectively. The DTR behaves similar for all the countries, i.e. lower values during winter and higher during summer. Alike to $Tmean$, all the countries (except Spain and the UK) present similar values of DTR during the winter months (∼2.5 °C) and in the summer months (∼7.5 °C). In the case of Spain, DTR presents higher intranual oscilation, with values of around 5 °C in winter and over 10 °C in summer, whereas the UK is the country with lower DTR variability, with values of 2.5 °C in winter and 5 °C. $RRsum$ pattern varies between countries. In France and Germany, precipitation oscillates around 40 mm to 100 mm per month throughout the year, whereas in Poland and Romania, $RRsum$ ranges between 20 mm and 40 mm in autumn and winter months and reaches values over 60 mm between June and July. Spain is the driest country, with values ranging between 40 mm and 80 mm from autumn to

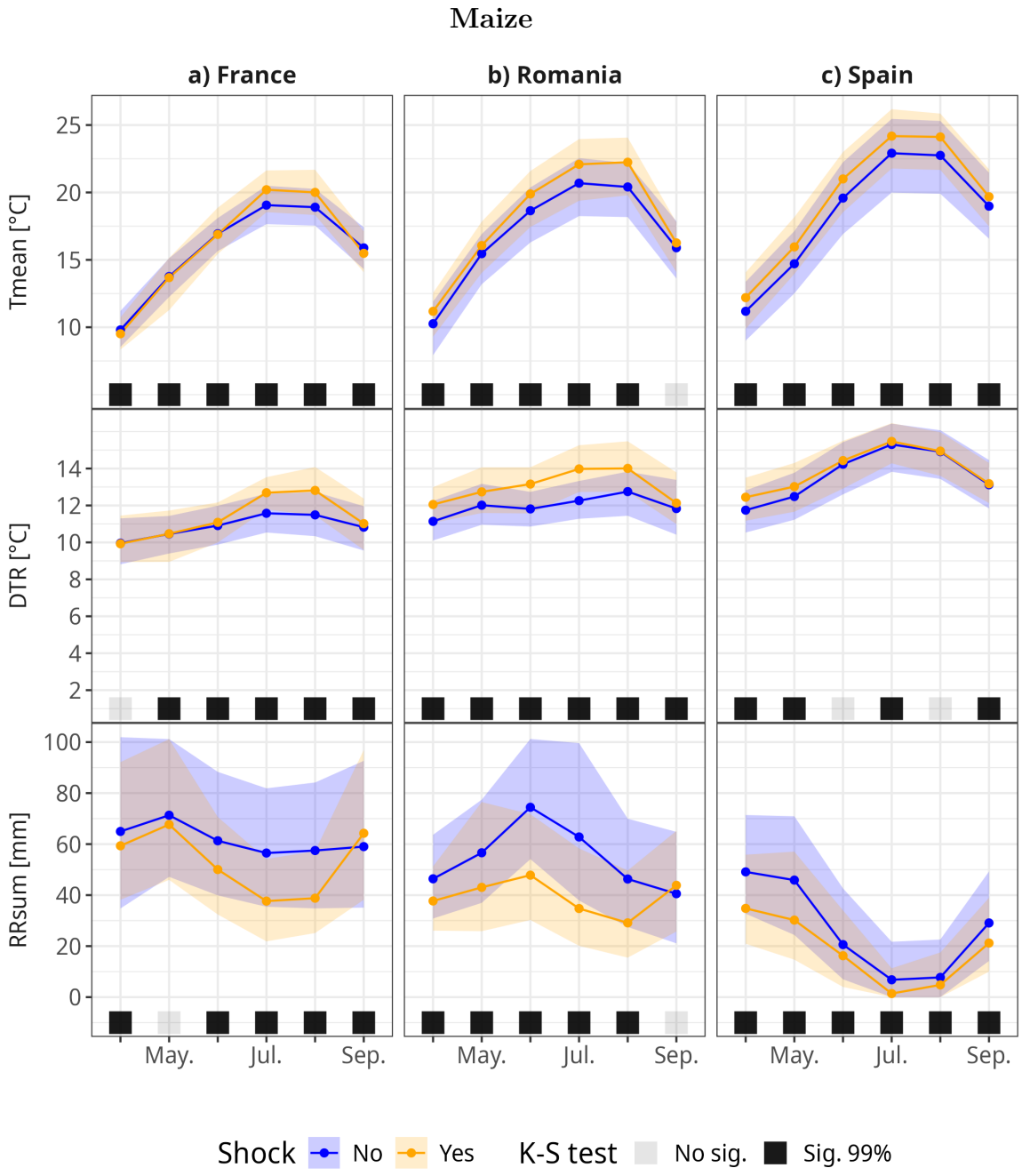

Figure 7.4: Median (opaque lines) and interquartile range (shade) of the selected climate indices during cases of maize yield shock (orange) and no yield shock (blue) for each country (in panels). Statistical significance by using the K-S test is presented in squares for a confidence level of 99% (black) and no significance (light grey).

spring months, and *RRsum* dropping to less than 20 mm in summer months. The UK has precipitation ranging between 60 mm and 120 mm per month throughout the year, with the highest *RRsum* from October to December.

Composite analysis for maize yield shocks

Figure 7.4 shows the difference between the average values of selected predictors during years of yield shock and no yield shock for the studied countries. For the cumulative distribution of the selected climate indicators for each country, see Supplementary Figure C2,C3 and C4 for France, Romania and Spain, respectively. In the three cases, years of yield shock are characterized by relatively higher $Tmean$, higher DTR, higher DTR, and lower $RRsum$ throughout the selected months. Additionally, according to the K-S test, almost all the predictors are statistically significantly different.

In France (Figure 7.4a), the most pronounced differences occur between July and August. During these months, the mean temperature ($Tmean$) and diurnal temperature range (DTR) are approximately 1 °C higher, while total precipitation ($RRsum$) is about 20 mm lower in years with yield shock compared to years without yield shock. To a lesser extent, reduced precipitation is also observed during May and June. Additionally, September shows a slight decrease in mean temperature alongside a modest increase in precipitation during yield shock years.

Romania (Figure 7.4b) presents substantial differences in the climate indicators during the whole cycle, with more distinction between June and July. In these months, $Tmean$ is around 1 °C to 2.5 °C higher during yield shock than no yield shock reports. Additionally find higher DTR throughout the cycle, with values ranging between 1 °C in April up to 2 °C in July. Alike the case of France, yield shock years feature lower $RRsum$ during the entire cycle, with the most notable difference in June and July (up to 40 mm in the median), but a shift in the behavior in September (i.e. higher $RRsum$ during yield shock years). In these months, $RRsum$ ranges between 20 mm and 70 mm during yield shock and between 40 mm and 100 mm during no yield shock. DTR is 2 °C to 3 °C higher and.

Spain (Figure 7.4c), though still significant, is the country which presents minor quantitative differences between the selected predictors during yield shock and no yield shock. In contrast to the other countries, the highest difference in $RRsum$ is presented at the beginning of the studied months, i.e. in April and May, where values are overall 10 mm lower during yield shock. DTR is also relatively higher, but the differences do not reach 1 °C. $Tmean$ is persistently around 1 °C higher during yield shock throughout the months.

Composite analysis for winter wheat yield shocks

Composite analysis are displayed in Figure 7.5 for the six countries (in panels). The results from the K-S test are presented as squares in the bottom part of the subplots for each variable and country. Overall, there are overlaps in the interquartile ranges, though there are differences in the median values of the selected predictors. According to the K-S test, there is a statistically significant difference between most of the climate indices distribution during cases of yield shock and no yield shock.

In France (Figure 7.5a), $RRsum$ behaves differently during years of yield shock and no yield shock, with higher precipitation from November and March but relatively lower in April. With less extent, relatively warmer conditions during November and December in cases of yield shock can be observed. Additionally, the country features slightly lower DTR and higher $RRsum$ during May and June.

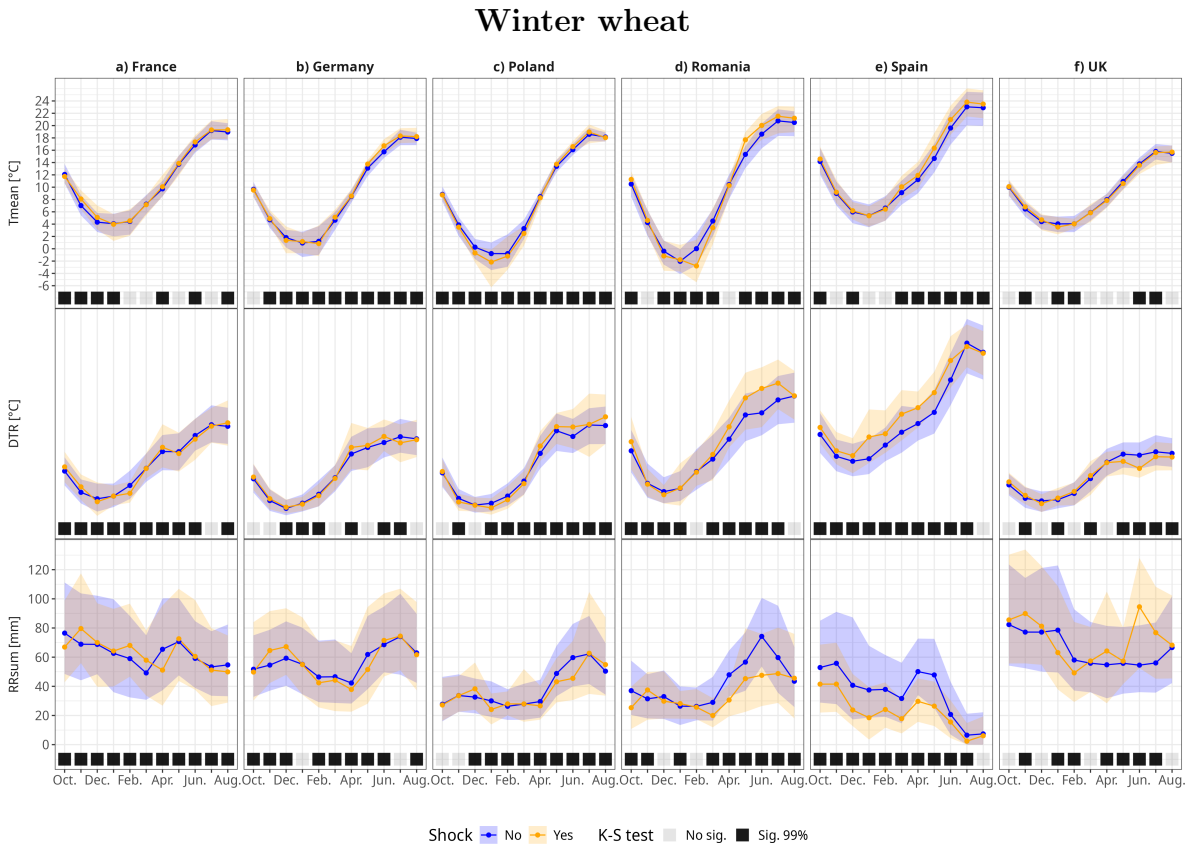

Figure 7.5: Same as Figure 7.4, but for winter wheat and the correspondent target countries.

In Germany (Figure 7.5b), *RRsum* is relatively higher, particularly between October and December, but presents slightly drier conditions between February and June. To a lesser extent, we observe slightly higher *Tmeans* between April and June during yield shock cases than in cases with no yield shock.

Similar to Germany, in the case of Poland (Figure 7.5c), *RRsum* during years of yield shock is slightly lower during spring months (between April and June). Moreover, *Tmean* between December and February is slightly lower during cases of yield shock, while in April and June, DTR is relatively higher.

Romania (Figure 7.5d) presents substantial differences in the climatology during years of yield shock and no yield shock. *Tmean* tends to be lower during winter, with median values of $-5\,°C$ during yield shock cases and $0\,°C$ during no yield shock cases. The spring and summer months are more characterized by warmer, dryer and higher DTR conditions. The highest difference is observed in June, where the median of *RRsum* is 75 mm during years of no yield shock and 50 mm during years of yield shock.

Spain (Figure 7.5e) presents drier conditions during years of yield shock throughout the year, with differences of around 25 mm between years of yield shock and no yield shock in April and May. We also observe higher DTR, especially between December and June.

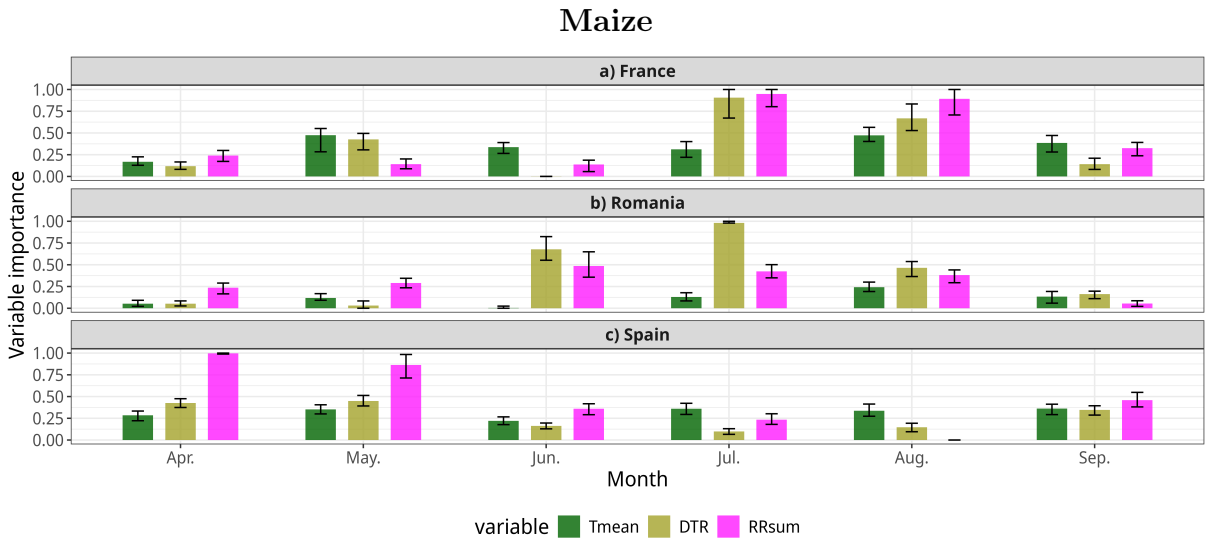

Figure 7.6: Variable importance in the Random Forest ensemble when assessing maize yield shock. Values are normalized for each country (in panels). Predictors are displayed by month (x-axis) and variable type (colour). The bar endings correspond to the average value of the Random Forest models, and the error bars correspond to the 5^{th}-95^{th} percentile uncertainty range.

Lastly, in the UK (Figure 7.5f), yield shock reports feature high DTR and higher precipitation during summer. This is especially evident in June, where the median of $RRsum$ during yield shock reports is almost 100 mm higher than in the case of no yield shock reports.

7.3 Determination of variable importance and impact

Building on the information from the previous section, notable climatological differences between yield shock and no yield shock conditions are established. This section analyzes the results obtained from the Random Forest ensemble, focusing specifically on identifying the most important drivers of yield shock under variable climate conditions.

Maize

Figure 7.6 shows the normalized variable importance by country for maize yield shock in response to the selected climate indices. The three countries exhibit distinct patterns in variable importance. Overall, variables based on total precipitation ($RRsum$) and diurnal temperature range (DTR) are markedly more influential than those based on mean temperature ($Tmean$). In France, DTR and $RRsum$ during July and August are highly important, followed by $Tmean$ in May, August, and September, which show similar relevance. In Romania, DTR and $RRsum$ in June and July are most significant, with $RRsum$ playing a somewhat lesser role; $Tmean$-based variables appear to have minimal relevance. In contrast, Spain differs from the other countries by showing high importance of $RRsum$-based variables in April and May.

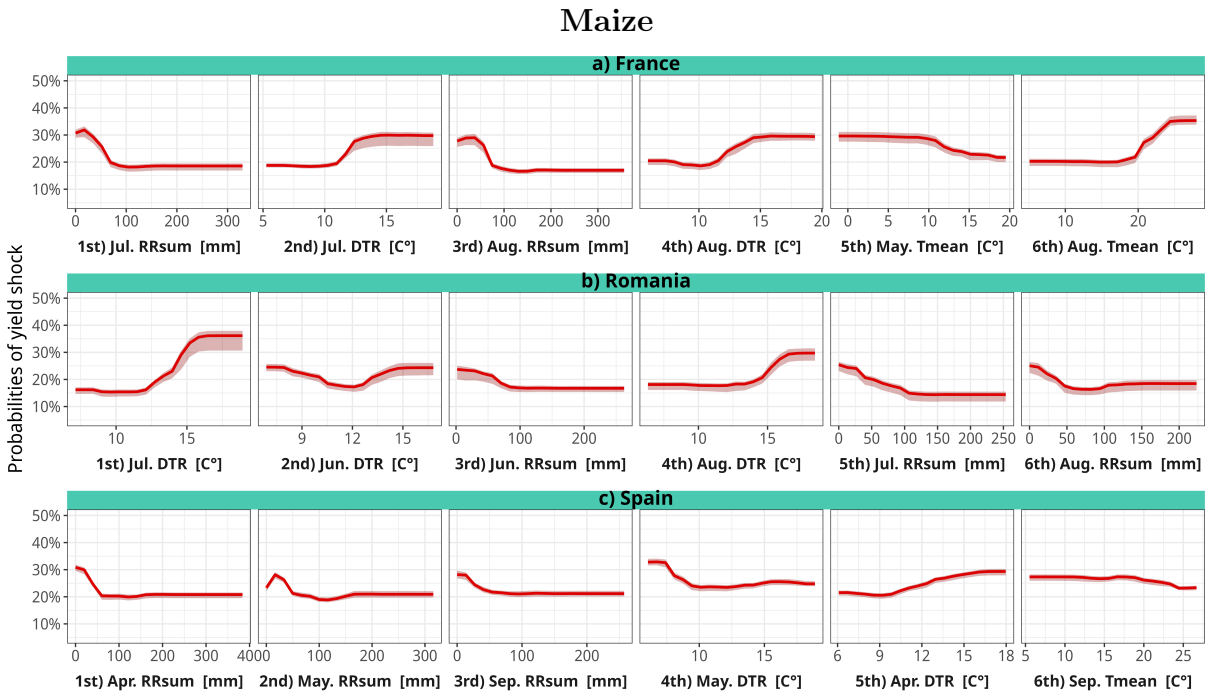

Figure 7.7: Partial dependence plots of the top six variables per country for maize. The rank is obtained by sorting the variable importance by descendant average value on Figure 7.6. The red opaque line corresponds to the ensemble mean of the Random Forest models, and the shade to the 5^{th}-95^{th} percentile uncertainty range.

Partial dependence plots are displayed in Figure 7.7 and for the top six most important variables per country. The plots present the average probabilities of yield shock as a function of each predictor (Section 5.3.3). Overall, the probabilities range between 15% to 35% approximately.

For the first four predictors in France (Figure 7.7a), the probabilities of maize yield shock increase from 20% to 30% when $RRsum$ drops below 100 mm and with DTR growing from 10 °C over 15 °C in July and August. From the 5^{th} and 6^{th} predictor, we see a slight increase in the risk with low $Tmean$ in May, but a notable increase (from 20% to 35%) with high $Tmean$ in August.

In Romania (Figure 7.7b), higher probabilities of maize yield shock are associated with increased diurnal temperature range (DTR) and reduced total precipitation ($RRsum$), particularly during July. When DTR exceeds 15 °C in July, the likelihood of yield shock rises from 15% to 35%. Additionally, a double-tailed effect is observed for DTR in June, where both unusually high and low values increase the probability of yield shock. Low $RRsum$ during the summer months further contributes to elevated risk.

In Spain (Figure 7.7c), the overall probability of yield shock remains below 25%. The risk increases up to 30% when April precipitation drops to zero.

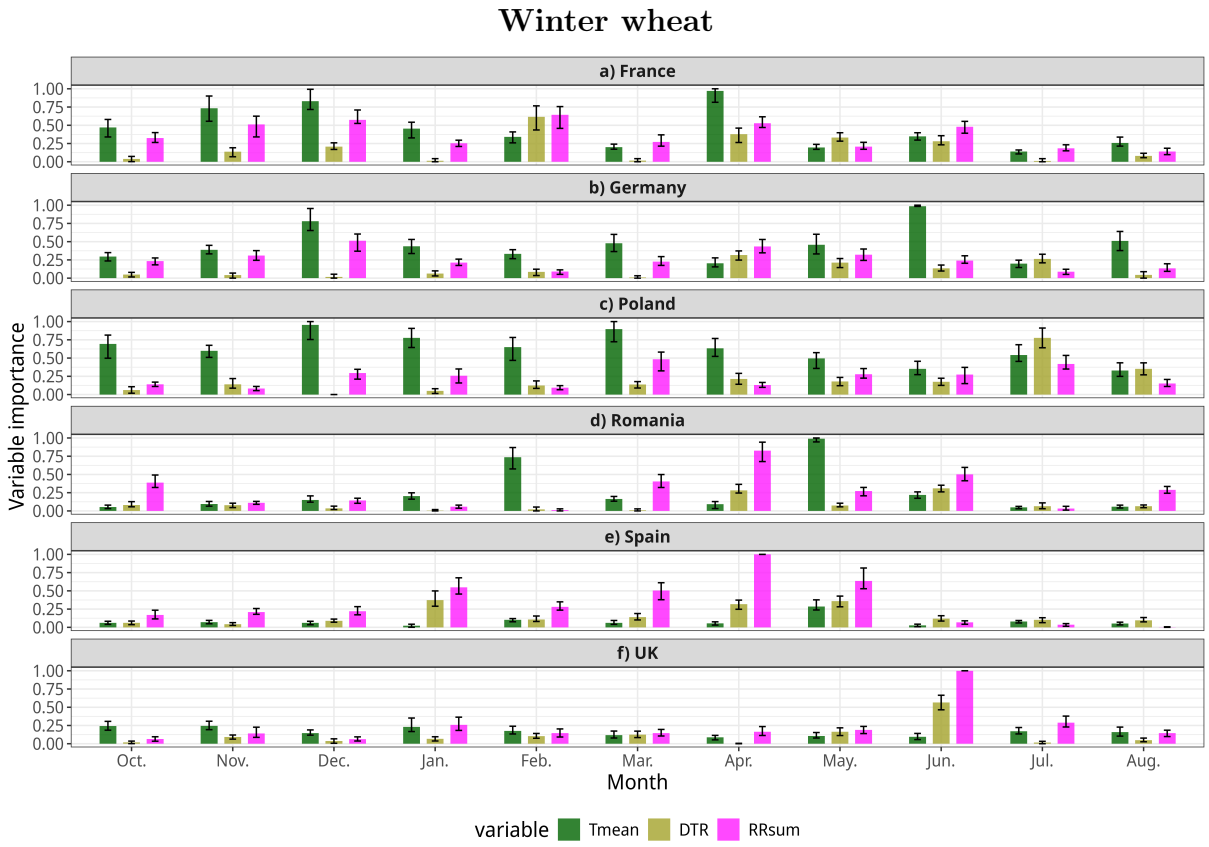

Figure 7.8: Same as Figure 7.6, but for winter wheat yield shock models and the correspondent countries.

Winter wheat

Figure 7.8 presents the average variable importance for each country, along with associated uncertainty ranges, for the winter wheat yield shock models. Significant differences emerge in the patterns of variable importance, with *Tmean*-based variables generally showing high relevance, while *RRsum* and *DTR* tend to have low importance in most countries. Notably, France, Germany, and Poland (Figures 7.8a–c) exhibit strong importance of *Tmean* during December, and to a lesser extent in November. Additionally, *Tmean* in April is highly relevant in France, and in June and August in Germany. In Poland, many predictors display similar importance within their uncertainty ranges. In Romania and Spain (Figures 7.8d and e), *RRsum* in April is notably important, with *Tmean* during February and May also showing high relevance in Romania. In the UK (Figure 7.8f), the Random Forest ensemble identifies *RRsum* and *DTR* in June as the only variables of high significance.

The variable importance is further explored by analysing the individual contribution to high or low probabilities of yield shock. Figure 7.9 shows the partial dependence plots of the four most important variables per country selected based on Figure 7.8. Given the unique characteristics, the analysis is done for each country separately.

In France (Figure 7.9a), the highest probabilities of winter wheat yield shock are associated with two key variables: mean temperature (*Tmean*) in April and December. For

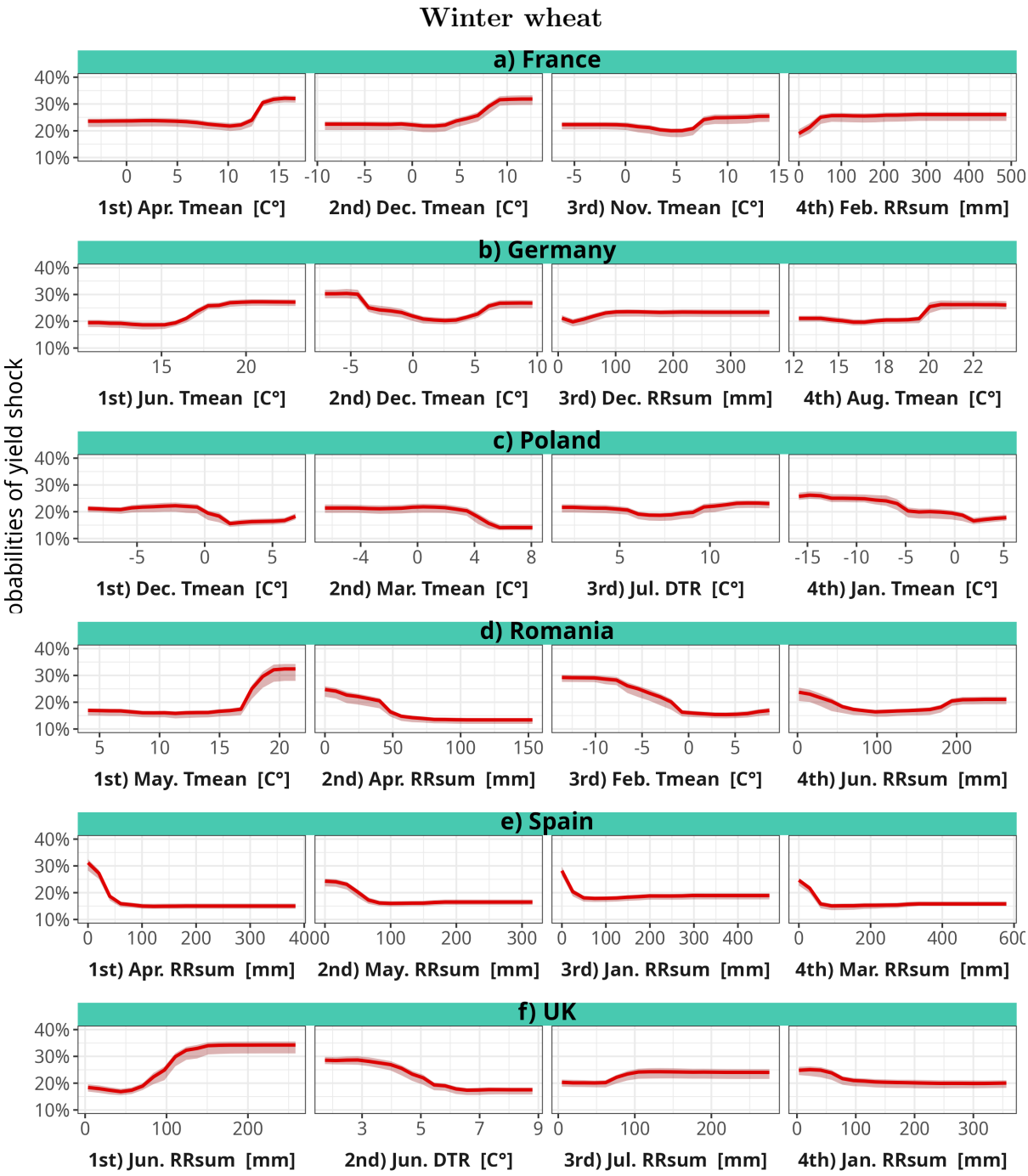

Figure 7.9: Same as Figure 7.7, but for the ensemble models assessing winter wheat yield shock. The rank is obtained from Figure 7.8.

both predictors, increasing temperatures correspond to elevated risk, reaching up to 30% probability at approximately 15 °C in April and 10 °C in December.

In Germany (Figure 7.9b), warmer June conditions increase the risk from 20% to 25%. Additionally, *Tmean* exhibits a non-linear relationship with yield shock, where values below −5 °C raise the probability from 20% to 30%, and values above 5 °C increase the

chances to 25%. Furthermore, $Tmean$ in August (the fourth most important variable) also shows an effect, with probabilities of yield shock increasing for $Tmean$ over 20 °C.

The Random Forest ensemble shows little impact from the selected climate drivers for Poland (Figure 7.9 c). The probability of yield shock rises to roughly 20% to 25% with decreasing $Tmean$ during December, March and January.

The results from Romania (Figure 7.9d), shows impact of dry, cold and hot conditions depending on the month: increasing $Tmean$ in May rises the risk up to 35%, while low $RRsum$ in April and $Tmean$ in February increases them to 30% and 35%, respectively.

In Spain (Figure 7.9e), drivers of yield shock are predominantly drier conditions during January and spring (March-May). The risk of yield shock abruptly heightens from 15% to 30% with scarce $RRsum$ in April and, to a lesser extent, in May and January.

Finally, the UK (Figure 7.9e) experience higher risks of winter wheat yield shock with high $RRsum$ in June and July as well as low DTR in July.

7.4 Performance of Random Forest ensemble

This section evaluates the performance of the Random Forest ensemble and examines individual models exhibiting low accuracy. The results for maize and winter wheat ensemble models are presented together, as the analysis and findings are similar for both crops.

Ensemble performance

Figure 7.10 display the OOB error and test error while building the Random Forest model for winter wheat (See supplementary Figure C5 for maize). For each model during the Random Forest building, the OOB is recorded. Within the same process, the leave-one-year-out dataset is used as test data to calculate the model performance against the independent one. The ensemble reaches stability after considering 100 trees, and the value converges to 0.1 in all the models. Therefore, the ensemble produces reliable results when considering 500 trees. On average, the test error converges to 0.15 in each country. This means that the ensemble of models presents 85% of accuracy when using unforeseen data. However, there is high uncertainty when taking the uncertainty into account. This is specially notable in the case of Romania for both crops (Figure 7.10d and Figure C5b).

To understand in detail the previous outcomes, we identify the individual years which present low accuracy within the ensembles. Figure 7.11 displays the distribution of error rate for each individual country model for both studied crops. The most inaccurate models (with an error rate above 0.5) are labelled with the corresponding tested year in red. For both crops, the interquartile range of the individual countries ranges between 0 and 0.25, with the lowest values found in France for both crops. All the models present between one to five leave-year-out models where the error rate is above 0.5. For instance, in France for maize yield shock (Figure 7.11a), the model trained without the data from 2003 (i.e. tested against the year 2003) has an error rate close to 1. For maize, the years and models with low accuracy identified in each country are 2013, 1990 and 2003 in France and 2003, 2007, 1992, 2000 and 2012 in Romania; the resultant models in Spain present errors lower than 0.5. For winter wheat (Figure 7.11b), the years identified in each country are 2016,

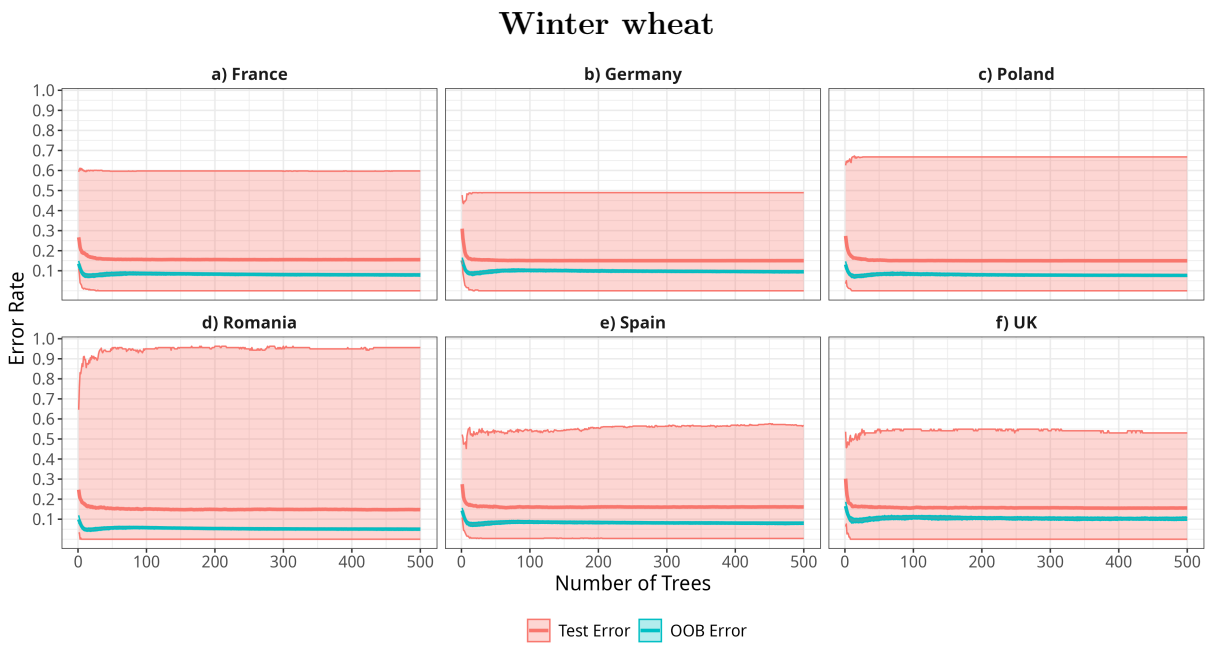

Figure 7.10: Error rate and test error as a function of number of trees for the ensemble of Random Forest models per country (in panels), using the maize yield shock data. The solid lines denote the average value between the models, and the shades represent the uncertainty range by using the 5^{th} and 95^{th} percentile. The Out-Of-Bag (OOB) error (turquoise) is built using the OOB sampling method from Random Forest (James et al., 2021), and the test error (red) is built by using the leave-one-year-out data.

2011 and 2003 in France; 2003 and 1992 in Germany; 2006, 1992 and 2000 in Poland; 2003, 1996 and 2007 in Romania; 1995 and 2005 in Spain; and 2012, 1987 and 2007 in the UK. All these years are also identified as extreme years, i.e. the proportion of yield shock reports is relatively high (Figure 7.1 for maize and Figure 7.2 for winter wheat).

Performance during extreme years

As a last point, we further explore the behaviour of the individual leave-extreme year-out models by analysing the partial dependence plots in conjunction with the data distribution of the target year and model. In this way, we can identify whether the model itself predicts high or low probability in during the target year.

We first investigate the example of 2003 in France for maize. Figure 7.12a displays the partial dependence plots for the three most essential variables in the Random Forest ensemble (in black, as depicted in Figure 7.7a) and for the leave-2003-out model (in red). Figure 7.12b displays the distribution of the correspondent top three variables for the studied period without considering 2003 (i.e. 1982-2002,2004-2016, grey boxplot) and for 2003 (red boxplot). During this year, the values of DTR and $Tmean$ in August (sixth variable, last column) are exceptionally higher than the climatology. When analysing the partial dependence plots, the impact of both predictors for the leave-2003-out model (red line) disappears. In other words, the model does not predict high probabilities of maize yield shock with sunny and warmer days in August.

(a) Maize

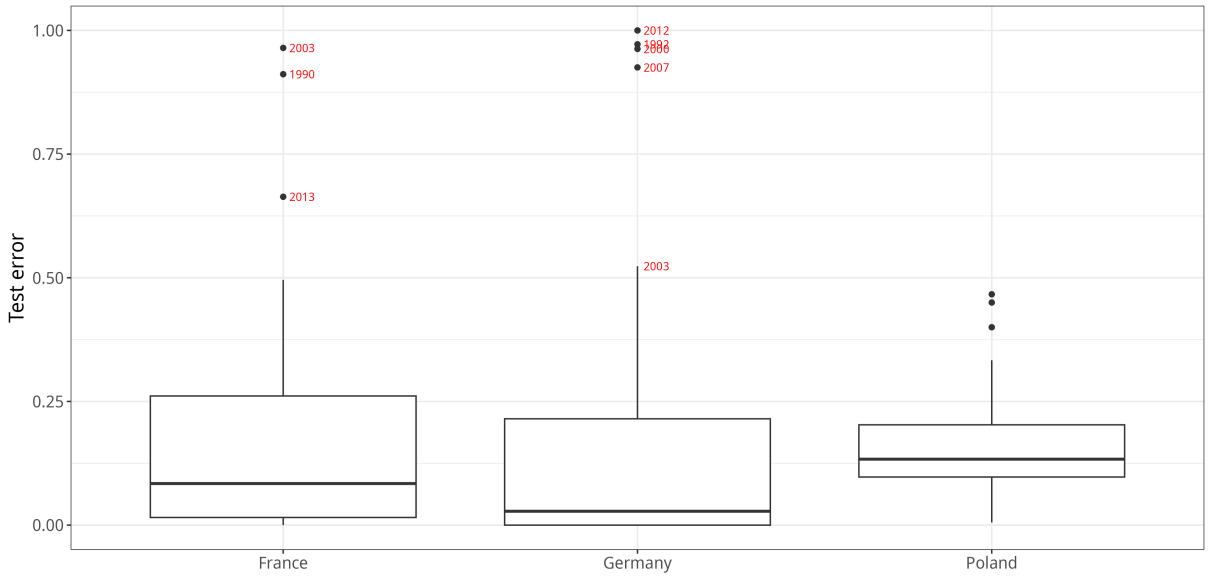

(b) Winter wheat

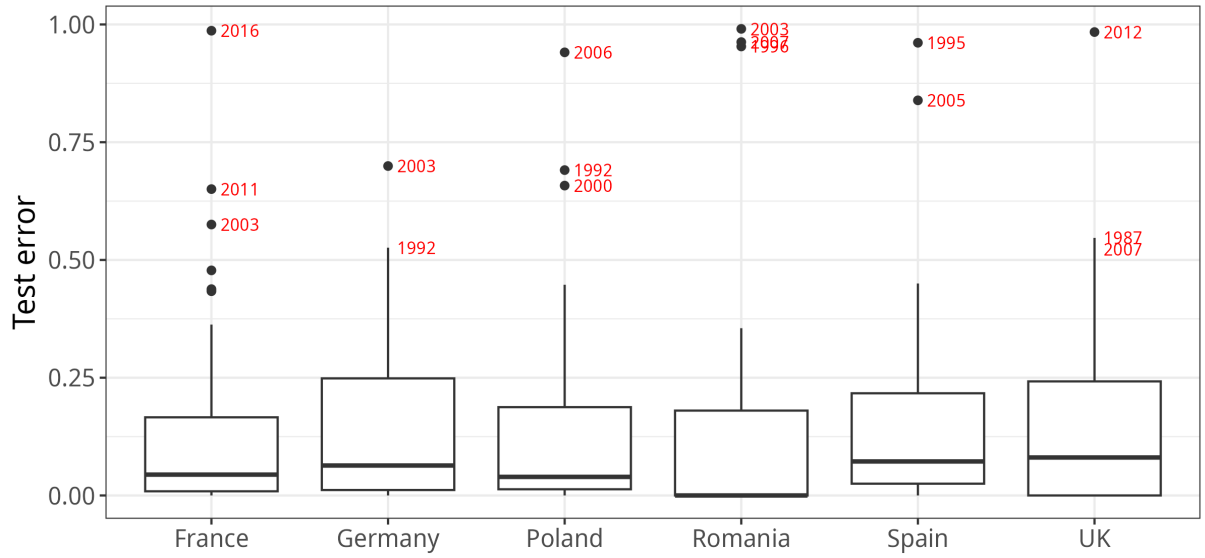

Figure 7.11: Test error distribution for each country. Year-out tests with classification errors higher than 0.5 are displayed in red. (a) for maize and (b) for winter wheat.

For the case of winter wheat, we analyse the example of 2012 in the UK. Figure 7.13a displays the partial dependence plots of the top three variables for the ensemble model (*RRsum* and *DTR* in June and *RRsum* in July, as shown in Figure 7.9f) and the individual model produced by leaving 2012 data out (red line). Figure 7.13b displays the distribution of the correspondent top three variables for the studied period without considering 2012 (i.e. 1982-2011,2013-2016, grey boxplot) and for 2012 (red boxplot). *RRsum* in June and July is notably higher than the climatology, while *DTR* in June is relatively lower. The partial dependence plots for the model trained without using 2012 (red line) quantify lower probabilities of yield shock than the ensemble means. A similar analy-

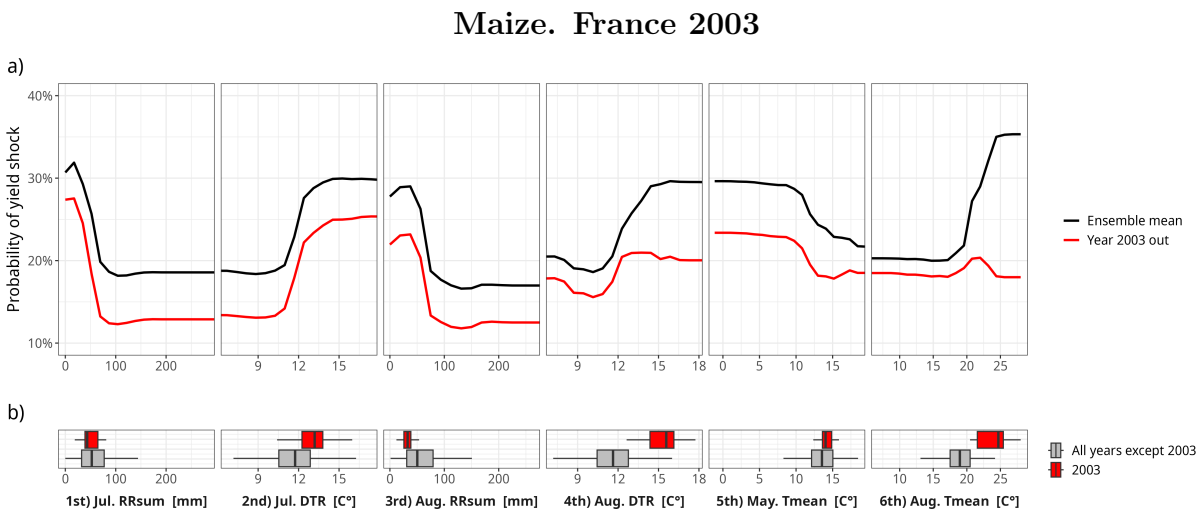

Figure 7.12: (a) Partial dependence plots for the three most important variables (according to Figure 7.6) for the ensemble model (black line) and the model leaving-2003-out (red line), and (b) data distribution during the studied period without considering 2003 (grey) and only for 2003 (red) in France for the top three variables.

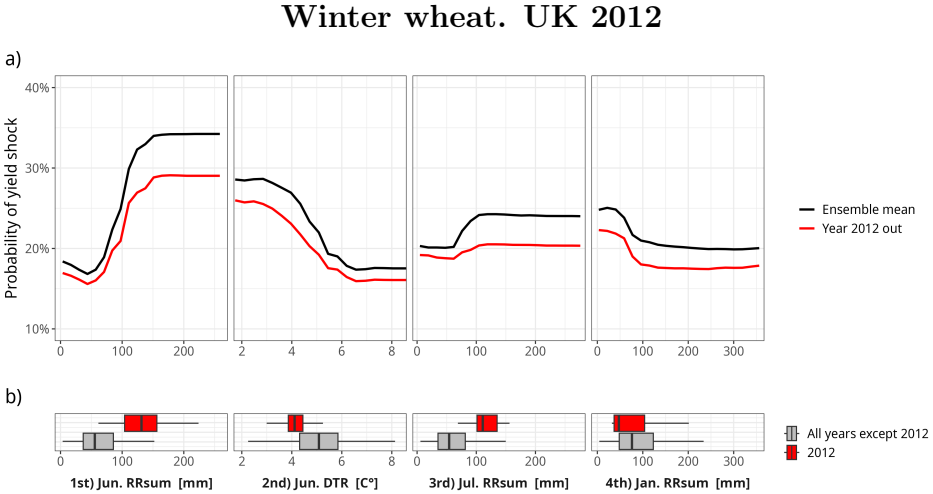

Figure 7.13: Same as Figure 7.12, but for winter wheat yield shock and the year 2012 in the UK.

sis can be done for the 2003 in Germany, displayed in Figure 7.14. In this case, the leave-2003-out model quantifies lower probabilities of yield shock for high *Tmean* in June and August compared to the ensemble model. According to the variable's distribution (Figure 7.14b), both *Tmean* in June and August have exceptional values during 2003.

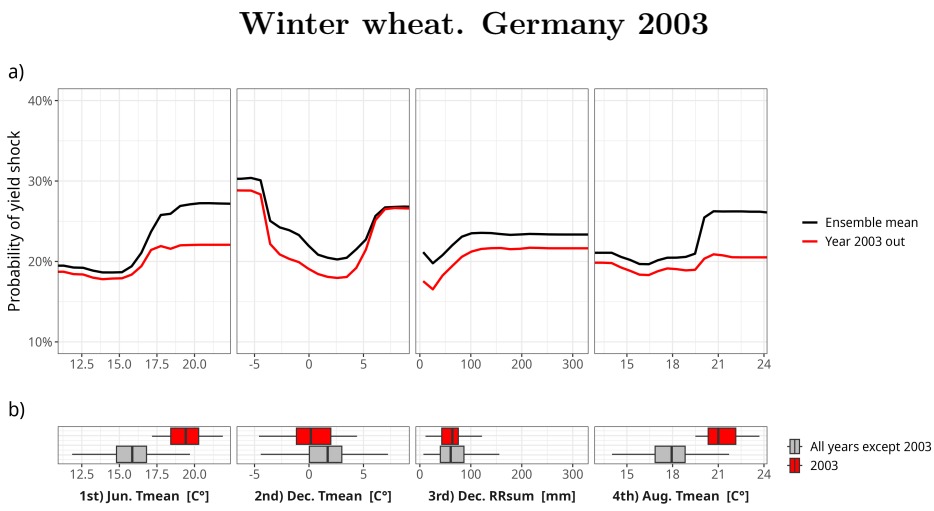

Figure 7.14: Same as Figure 7.12, but for winter wheat yield shock and the year 2003 in Germany.

7.5 Physiological response and spatial heterogeneity of the impacts

Both crops present notable differences in the most important climate indicators, even within the same country. In the case of France for instance, we find that for both maize and winter wheat, low *RRsum* and high *Tmean* in the individual summer months can lead to higher chances of yield shock, but we also point the impacts of low *Tmean* in maize and high *Tmean* in winter wheat during December. This is also the case of Romania. The differences in the physiological response also provides higher and lower sensitivity to years with extreme weather events reported. The heatwaves that hit France in 2003 were more detrimental to maize than winter wheat, and this is also observed in Romania but for the opposite case.

As we mentioned in Chapter 2, each crop has different characteristics, cycle length and thus sensitivity to weather. Considering the spatial heterogeneity in the climatology's domains, below we explore what causes high risk of yield shock in each case.

Maize

In the case of maize, the output impacts are similar in Romania and France whereas Spain shows different impact. In France, we find high impact of low precipitation and overall sunny days (i.e. high *DTR*) in July and August. The findings are in partial agreement with previous literature (Hawkins et al., 2013b; Ben-Ari et al., 2016), who specifically found higher importance of precipitation shortage during the late 20$^{\text{th}}$ century but a higher importance of hot days during the 21$^{\text{st}}$ century. The increasing application of irrigation and frequency of extreme temperatures during the last decades have changed the relative importance of precipitation and temperatures Hawkins et al. (2013b). In general, flowering, the critical period of maize, takes place during July in France (Olesen et al., 2012), which may explain the high relevance of predictors in the summer months.

We also find that lower temperatures during May can trigger high probabilities of maize yield shock in France. At first, these results may be striking since most of the literature targets high-temperature impacts. However, cold exposure (frost and chilling) can be critical for maize growth and yield for both early and late varieties (Caubel et al., 2018).

In Romania, the Random Forest ensemble model reveals a high impact from increasing diurnal temperature and dry conditions in summer months, especially in July and August. In general, DTR is linked to increasing maximum temperatures, decreasing minimum temperatures and dry conditions due to low cloud cover and possibly low precipitation. This result also agrees with previous literature in the studied area (Micu et al., 2017; Feng and Hao, 2020). Flowering generally occurs around the June and July months in Romania (Olesen et al., 2012); thus, dry-warm conditions in these months are detrimental to the crop. Furthermore, we find that low DTR in June (likely higher cloudy days) can increase the risk of maize losses in the country. Thought previous studies do not reveal our findings (Prăvălie et al., 2020; Călugăr et al., 2024), their methodology were mostly based on linear approaches or do not distinguish between causality and casualty. A high percentage of cloudy days can reduce the total radiation and thus be also detrimental for maize yield.

Interestingly enough, the most relevant variable in determining maize yield shock in Spain is low $RRsum$ during April. Irrigation is a common practice in Spain (Zajac et al., 2022). This may explain why our results do not reveal high importance of hot or dry conditions during summer.

Winter wheat

In Europe, there is evidence of extremely cold temperatures, heat waves, and dry and wet periods impacting winter wheat yield (Mäkinen et al., 2018). Though winter wheat has lower precipitation requirements than maize and a higher tolerance to low temperatures, the long season of the crop increases the crop's susceptibility to extreme weather. Winter wheat undergoes vernalization during the winter months. Therefore, warmer temperatures during these months can partially abort flowering or delay it (as an example, this phenomenon partially explains the losses of 2016 in France; Nóia Júnior et al., 2023). Furthermore, the lack of snow coverage during these months exposes the plant to detrimental low temperatures (Mäkinen et al., 2018). Anthesis in wheat in Europe is typically observed between May and June (Olesen et al., 2012; Oteros et al., 2015; Schmitt et al., 2022; Nóia Júnior et al., 2023). Higher temperature and drier conditions during this stage lead to fast development with low growth, whereas lower temperatures during this stage can delay the most ideal window for growth and can expose the crop to heatwaves and dryer conditions during the summer (Djanaguiraman et al., 2020; Du et al., 2022). Therefore, these months are generally critical for determining yield.

Overall, depending on the country and month, cold/warm conditions and dry/wet conditions are related to increasing probabilities of winter wheat yield shock. The climatological heterogeneity between countries may partially explain the differences in winter wheat yield shock drivers.

In France, winter wheat yield shock risk is linked to warmer conditions in April and warmer conditions during December. The study from Ben-Ari et al., 2018 also revealed a

strong influence from a higher number of days with maximum temperature between 0 °C and 10 °C during December, and Ben-Ari et al., 2016 noted that April is the month with the highest importance to explain yield loss. France presents high spatial heterogeneity within the country, and therefore, weather and climate drivers of yield shock could be rather region-specific (Ceglar et al., 2016).

In Germany, warmer conditions during June increase the probability of yield shock. Furthermore, we observe that both cold and warm temperatures during December are linked to a higher risk of losses. Schmitt et al., 2022 mentioned drought to be the most important factor, while Peichl et al., 2021 found high-temperature impacts in June but also negative wheat yield anomalies with higher soil moisture in March. Central regions, like Germany and France, experience both cold and warm temperatures in December, which are both detrimental for winter wheat (Ceglar et al., 2016; Mäkinen et al., 2018). Central regions, like Germany and France, experience both cold and warm temperatures in December, which are both detrimental for winter wheat (Ceglar et al., 2016; Mäkinen et al., 2018). Anthesis is typically observed around June (Schmitt et al., 2022), so higher temperatures in this month can be critical.

The results from Romania reveal that colder conditions in February, dry conditions in April and warm conditions in May are linked to higher probabilities of yield shock. The experimental study from Tayyar (2010) showed that negative precipitation anomalies and positive $Tmean$ anomalies during springtime shorten the grain filling period, resulting in earlier grain maturity and low yield. Due to the warmer climatology, maturity is reached around June (Croitoru et al., 2012), and the impacts of hot-dry conditions are likely seen during spring months. Additionally, temperatures in Romania during winter can drop below the freezing point, which can also halter the growth of the crop.

In Spain, drought conditions during the whole year (especially in April) are linked to an increasing probability of yield shock. These results were also obtained by Páscoa et al. (2017), which showed that negative precipitation anomalies during March, April, and May are linked to reduced wheat yield in the Iberian Peninsula. Prolonged periods of drought are typical in Spain and the Iberian Peninsula (Moemken and Pinto, 2022) and hence abrupt drops in yield are more likely due to such phenomenon (Bento et al., 2021). Flowering in Spain occurs in early spring (Oteros et al., 2015), and the crop is harvested between May and July. Therefore, drier conditions during early spring are the most detrimental effect observed.

Lastly, in the UK, we observe that strong precipitations in June and low DTR lead to higher yield shock probabilities. This is also highlighted by van der Velde et al. (2018) when assessing the historical loss of 2012 in the country. Posthumus et al. (2009) also mention significant agricultural losses during the summer floods of 2007. The UK is more humid throughout the year, and the likelihood of having yield shock due to high precipitation is higher in this area. Therefore, the risk of losses may be rather linked to drops in solar radiation (which is indirectly related to DTR and also to $RRsum$).

7.6 Discussion and summary

This chapter assesses the weather and climate drivers of maize and winter wheat yield shock across European countries. The three target countries for maize are France, Romania and Spain, and we include Germany, Poland and the UK for winter wheat. We explore the most important weather and climate indicators according to the leave-one-year-out Random Forest ensemble model and quantify the impacts. Finally, we investigate the behaviour of individual models within the ensemble, which show low accuracy.

We observe partial agreement between the composite analysis and Random Forest outputs. However, the composite analysis only shows the differences between years with and without yield shocks, missing non-linear patterns. Most of the climate indicators have statistically significant differences between yield shock and no yield shock cases, even though they are not apparent, for instance, for the $Tmean$ series in Germany in the case of winter wheat. Composite analysis serves as a first approach to disentangle how weather and climate drivers behave during years of yield shock. Nevertheless, we still require a more powerful tool to quantify and disentangle the impacts.

For the reasons mentioned above, we utilize a flexible and robust statistical model such as Random Forest, which enables us to identify the key drivers of yield shock and quantify their impact. The leave-one-year-out ensemble approach helps capture high-frequency drivers of yield shock and also the effects of weather extremes. This setup reduces the apparent impact of individual extremes (not shown), which is why the obtained probabilities by using partial dependence plots do not exceed 40%. This is particularly evident in Poland for the case of winter wheat, where composite analysis reveals strong negative anomalies, but the predicted probabilities of yield shock do not exceed 25%. Despite this, the leave-one-year-our ensemble approach enhances the robustness of the results by reducing the sensitivity to outliers.

For both crops, Random Forest ensembles have an overall high accuracy. However, when predicting extreme years, the performance is limited. This is illustrated by the examples of 2003 in France for maize, 2012 in the UK, and 2003 in Germany for winter wheat. The summer of 2012 in the UK was exceptionally wet, with some locations reporting their highest precipitation values in the last 200 years (Blunden and Arndt, 2019). The partial dependence plots for the leave-2012-out model present lower probabilities of high $RRsum$ in June and July and low DTR in June than the ensemble. Likewise, this can be observed in Germany and France, where $Tmean$ in June 2003 is exceptionally high compared to the climatology (Fink et al., 2004). Another example is the unprecedented warm December in 2016 in France (Figure C6; Ben-Ari et al., 2018) or the dry conditions in 1995 in Spain. Random Forest is a practical tool with high predictability in ecology (Cutler et al., 2007). However, it struggles with extrapolation beyond the historical evidence. This information provides insight into the uniqueness of these years, which are relevant in the ensemble to capture important variables in both years' high-yield shock reports. Single models should not be individually assessed, but rather, we should focus on the ensemble in conjunction.

Answer to RQ2

By considering the outcomes from this chapter, we answer the RQ2 as follows:

RQ2: What are the country-to-country variations in the in-season climate drivers of maize and winter wheat yield shock across European countries?
Maize yield shocks show similar weather-related impacts in France and Romania, with July–August conditions, particularly high diurnal temperature range (DTR) and low precipitation, being critical. In France, cold conditions in May and dry, sunny summers during flowering are key drivers. Romania shows sensitivity to summer highly-sunny and dry conditions, though cloudy (low DTR) Junes may also pose risks. Spain differs, with low spring precipitation in April being most important, likely due to widespread irrigation mitigating summer stress.
The climatology of the target countries plays a more important role when assessing weather and climate drivers of winter wheat yield shock. The risk of yield shock increases with warmer conditions in December in France and Germany. Romania and Poland experience colder winter months during yield shock years. Drier and warmer springs are typically observed in yield shock years in the studied countries. High chances of losses are especially seen for France, Romania and Spain. All countries except the UK see drier and/or warmer conditions in the summer months. The UK, in contrast, features higher rainfalls and a low diurnal temperature range during the summer months.

Unlike the analysis performed in Chapter 6 for silage maize yield in Germany, we incorporate a crop and spatial dimension to the problem. We observe notable spatial heterogeneity on the impacts, in this is probably due to the climatological differences between domains, though we find some common patterns. France and Germany have similar climates, although the temperatures during the winter months are lower in Germany (where we also see the impacts in winter wheat). Poland and Romania present the lowest temperature values during winter months, although during spring and summer months, Romania tends to be warmer, impacting both maize and winter wheat. Spain is the driest and warmest country in the study domain, and we see high impacts on dry conditions in both crops. Lastly, the UK is the wettest country and the one with the lowest diurnal temperature range and interannual temperature variability. The combination of both high rain and low diurnal temperature rain are the most detrimental for winter wheat according to the analysis presented in this Chapter.

8 Future Climate Change Influence on Crop Yield Shock

This chapter aims to answer the last research question of this thesis:

How would the risk of maize and winter wheat yield losses vary across Europe in a warmer climate from a statistical modeling perspective?

As in Chapter 7, the target domains are:

- **Maize**: France, Romania and Spain.
- **Winter wheat**: France, Germany, Poland, Romania, Spain and the UK.

The first section focuses on the historical period (1982-2005); it evaluates the climate models' capacity to capture the reference data and the predicted probabilities of crop losses (Section 8.1). The second stage concentrates on the future climate scenario. For this, the chosen climate drivers are evaluated in a warmer climate and compared to previous literature (Section 8.2). After that, the changes in crop yield shock and the plausible causes of them are addressed (Section 8.3). The following section concentrates on the physiological aspects of the risk changes (Section 8.4). Finally, Section 8.5 summarizes the whole chapter, discusses the methodological aspects and answers RQ3. The information from this Chapter is further supported by Appendix D.

8.1 Evaluation of historical simulations

The performance of historical simulations in representing climate drivers and yield shocks across Europe is assessed by comparison with the E-OBS ensemble mean dataset. The analysis focuses on the historical period (1982–2005), evaluating eight Global Climate Model-Regional Climate Model chains (GCM-RCM chain) against the corresponding predictors derived from the E-OBS reference. The evaluation begins by examining simulation biases for key variables ($Tmean$, DTR, and $RRsum$), highlighting differences across models, months, and countries. Both non-corrected simulations (referred to as NC) and those adjusted using two bias correction methods, Quantile Delta Mapping (QDM) and Linear Scaling, are considered. In the second part, the models' ability to reproduce the variability of maize and winter wheat yield shocks is analyzed for each country.

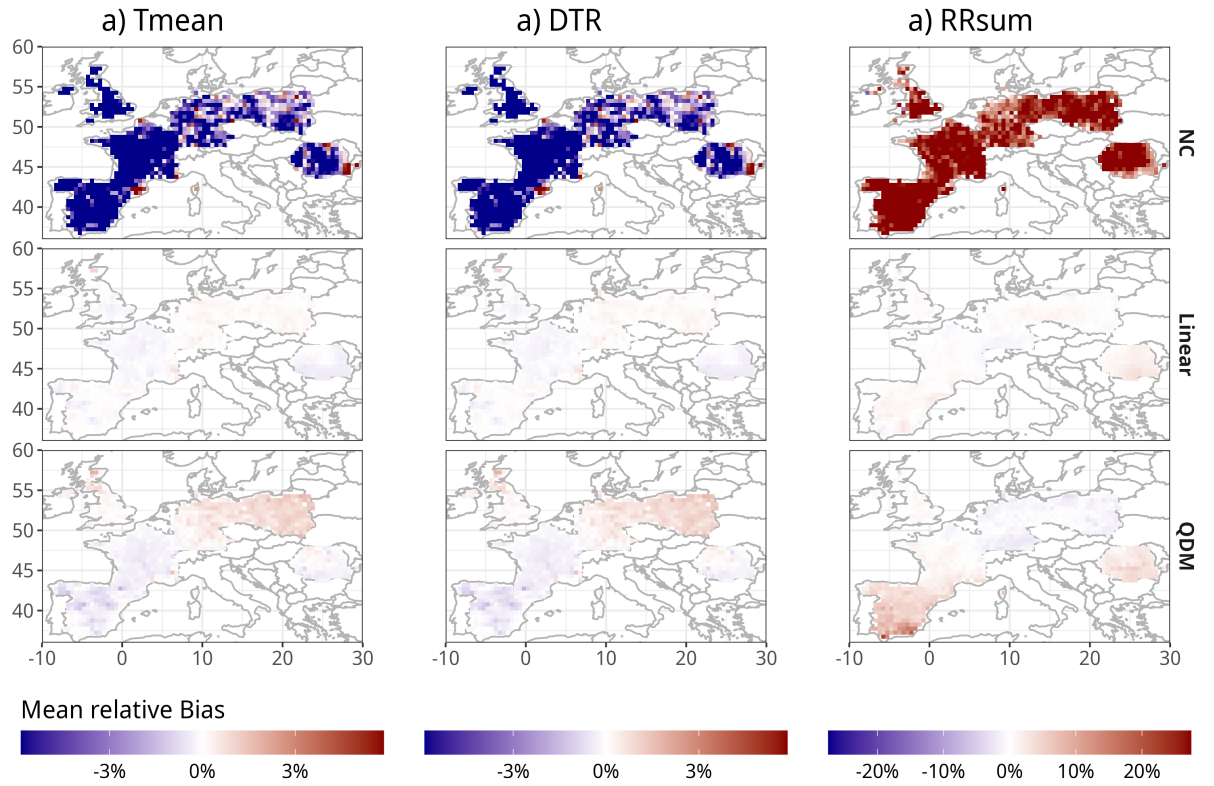

Figure 8.1: Average relative bias between the simulations and E-OBS data during the historical period (1982-2005) for each variable (columns) for data previously bias correction (NC), and after bias correction (Linear scaling and QDM, in rows). The relative bias is computed as the average bias for each month, variable, and model divided by the mean of the observed data. Then, the mean relative bias is computed by averaging the relative bias across months and subsequently across models.Finally the values are converted to percentage ($\times 100\%$).

8.1.1 Comparison of climate drivers

The average relative bias for each variable across months and models is displayed in Figure 8.1 (See Supplementary Figure D1 for the average bias). High overestimation of bias (or high underestimation) are represented with high tone of red (blue). Visibly, the simulations before being corrected present noticeable variance while values after bias correction drop to almost 0%. In general, the biases are slightly higher for QDM than for Linear scaling. More specifically, for $Tmean$ and DTR the ensemble simulation underestimate the reference data with more than 3% ($\sim$0.4 °C for both variables, Supplementary Figure D1). Both bias-correction methods display small underestimation of $Tmean$ and DTR in southern and western Europe (France and Spain), while the opposite can be observed for the remaining domain. For $RRsum$; the ensemble mean overestimate the reference data in the entire domain, for about 20% the average values (approximately 5 mm to 10 mm more, Supplementary Figure D1). In addition to this, the biases are

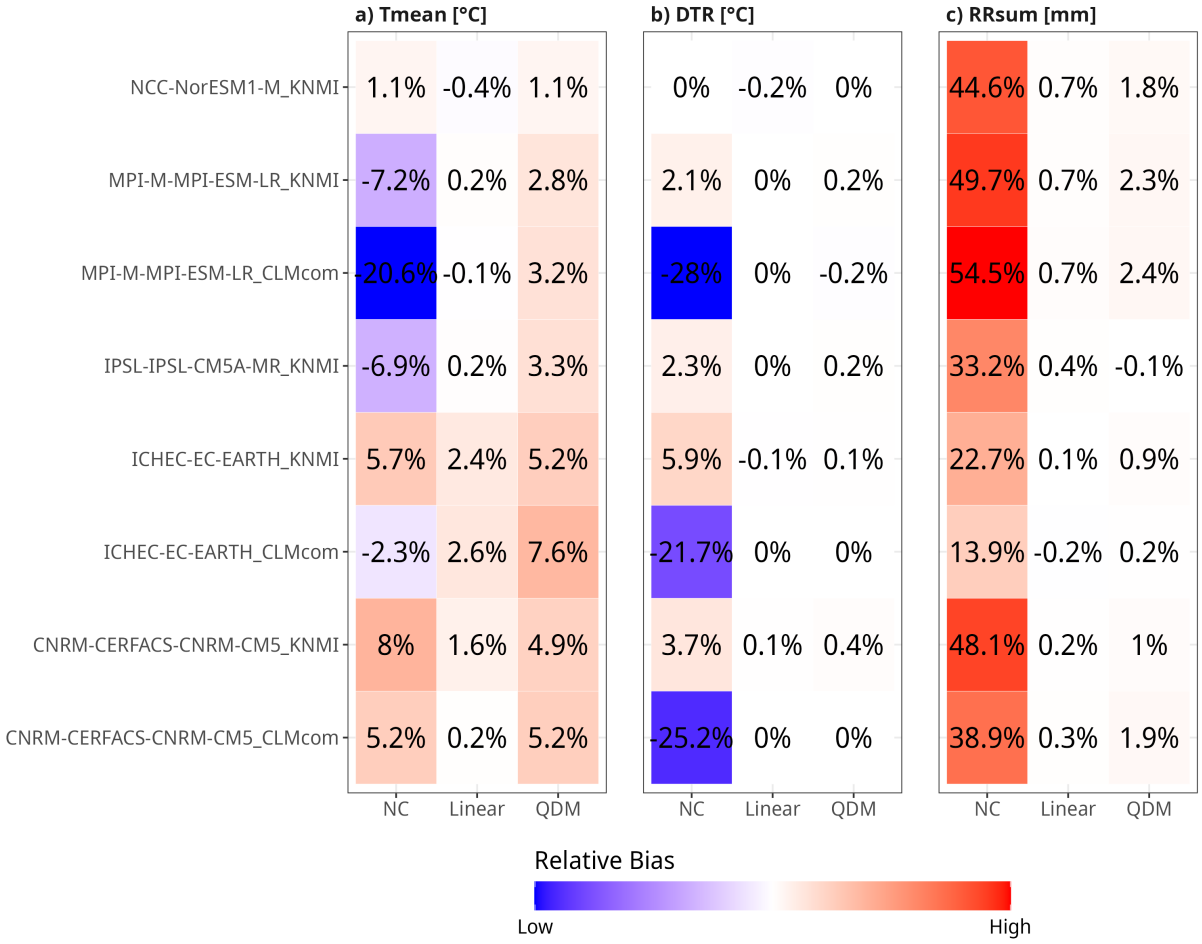

Figure 8.2: Average relative bias between the simulations and E-OBS data during the historical period for each variable (panels) for data previously bias correction (NC), and after bias correction (Linear scaling and QDM, in columns), and for each model (rows). The values (black text) are calculated by computing relative bias for each grid point, month and variable, and then averaging across the domain and months. The colorbar (blue-white-red) display the normalize bias per model (0% for white, underestimation in blue and overestimation in red).

contrasting to the other variables, with overestimation in the south and underestimation in central and northern Europe.

Aggregated relative bias per model is displayed in Figure 8.2. The values are calculated by averaging relative bias for each grid point, month and variable, and then averaging across the domain and months. Average relative bias changes depending on the model and variable. By way of example, the NCC-Nor-ESM1M_KNMI model before correction (NC) has -1% of bias for *Tmean* and around 44% for *RRsum*. The ICHEC-EC-EARTH_CLMcom presents average relative biases of around -2% for *Tmean* and *DTR* (higher than NCC-Nor-ESM1M_KNMI), and about 23% for *RRsum* (lower than NCC-Nor-ESM1M_KNMI). For all the cases, bias correction suppress the differences in the data to no more than 1% or 2%. Generally, there are slightly lower values (i.e. better

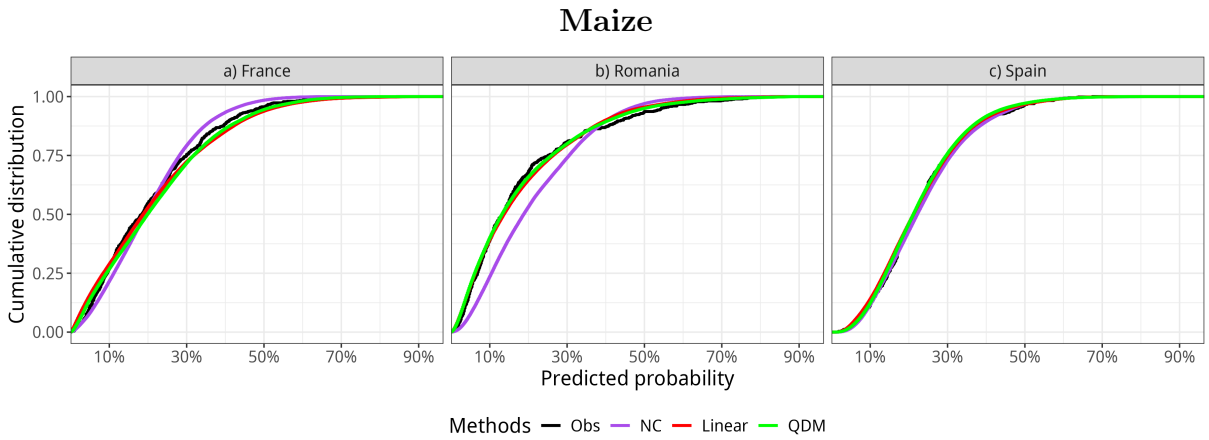

Figure 8.3: Cumulative distribution for the predicted probabilities of maize yield shock across countries (panels), methods (colors) and the observations (black). The probabilities are obtained using the historical period (1982-2005).

performance) for linear scaling than for QDM. The magnitude does not only depends on the chosen model but also on the month (Supplementary Figure D3).

8.1.2 Analysis in predicted yield shock probabilities

The second evaluation is based on comparing the predicted probabilities of yield shock using the simulations against the E-OBS data. For this, the models are evaluated individually (by RCm-GCM model chain) before and after bias correction (NC, Linear and QDM) for each country and for each leave-one-year-out model. In the case of E-OBS, the outputs are based on the year-out probabilities (for example, the input data of the year 2000 is only evaluated on the model trained without the year 2000, See Chapter 7 for more detail). In this way, the probabilities are not based on the data in which they were trained. The results are illustrated in the way of cumulative distributoin function, boxplots and time series (See Appendix D for the boxplots and time series).

Cumulative distribution of the probabilities of maize yield shock are displayed in Figure 8.3 for each country (panels). In the case of France and Romania (panel a and b) the curves of the predictions after bias correction (Linear in red and QDM in green) closely match the observations (black). In contrast, the results without correcting biases (blue) do not match the curves for these two countries. Specifically in the case of Spain (panel c) we do not observe substantial differences in the outputs regardless of correcting or not correcting the input data.

The similar analysis can be done for the case of winter wheat (Figure 8.4). For this crop, the differences between the simulation before correcting and the observations are more notorious than for maize in all the countries. Generally, the simulations tend to overestimate the probabilities of yield shock in all the countries except for Romania and Spain (panel d and f). For both Linear and QDM, the outputs match the observed predictions curves.

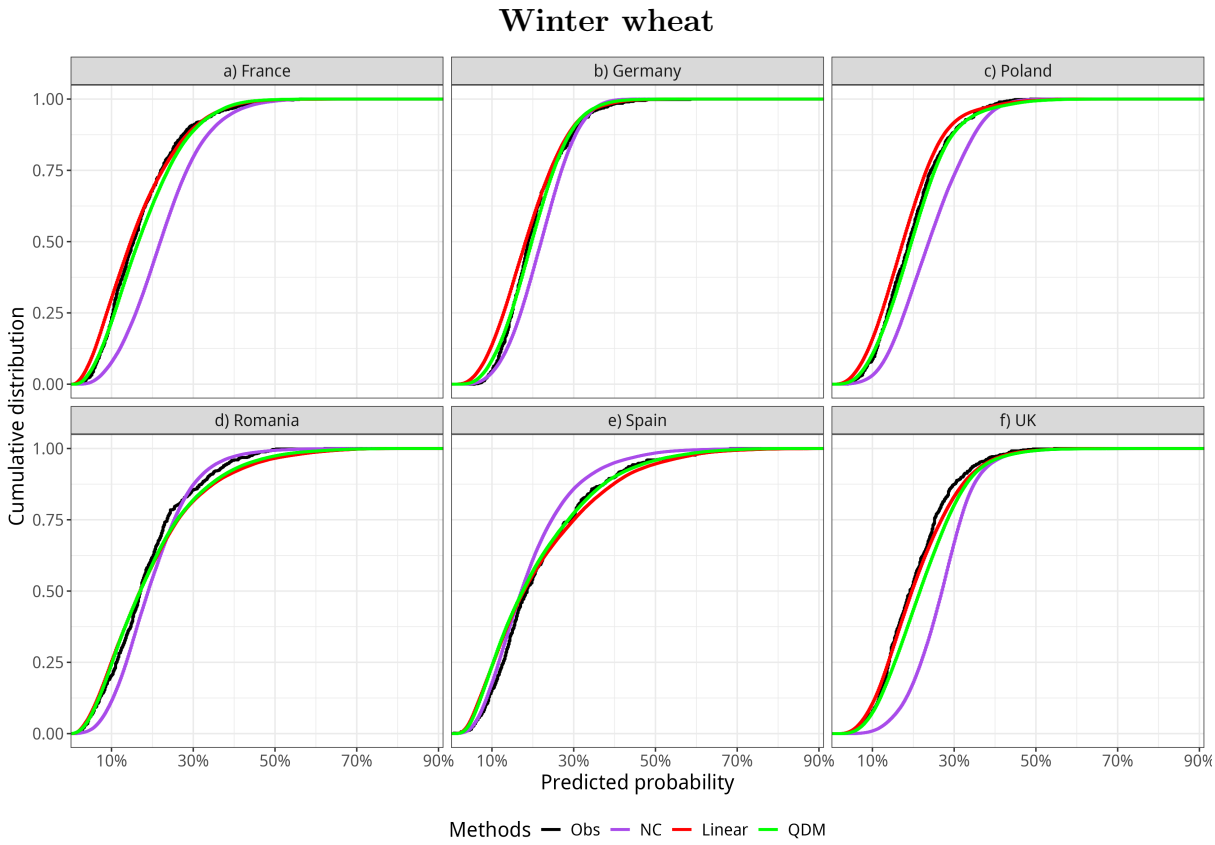

Figure 8.4: Same as Figure 8.3 but for winter wheat and the correspondent countries.

Summary of bias correction

Based on the findings from this section, both Linear and QDM bias correction methods demonstrate equivalent performance in approximating the observed historical data. This holds true when examining in-season climate drivers as well as when comparing the average predicted probabilities of crop yield shock. As a result, both correction methods are incorporated in an ensemble framework. The subsequent analysis is therefore based on sixteen (16) datasets, derived from eight RCM–GCM model chains combined with the two bias correction methods.

8.2 Changes in the climate drivers under global warming

The next step consist on evaluating the climate drivers in the future scenarios. Additionally, this section compares the results with the observed ones in previous literature to future climate extremes. For this, the average values of the indices are computed in a GWL2 and GWL3 (See Table 4.3) and compared against the mean values of the historical period (Supplementary Figure D9,D10 and D11). Given the differences in the signal across models, the agreement between these ones are evaluated by using the approach B from IPCC AR6 (Gutiérrez et al., 2021). This one establishes that there is high confidence

between model signal only when at least 80% of models agree on it (i.e. more than 12 models).

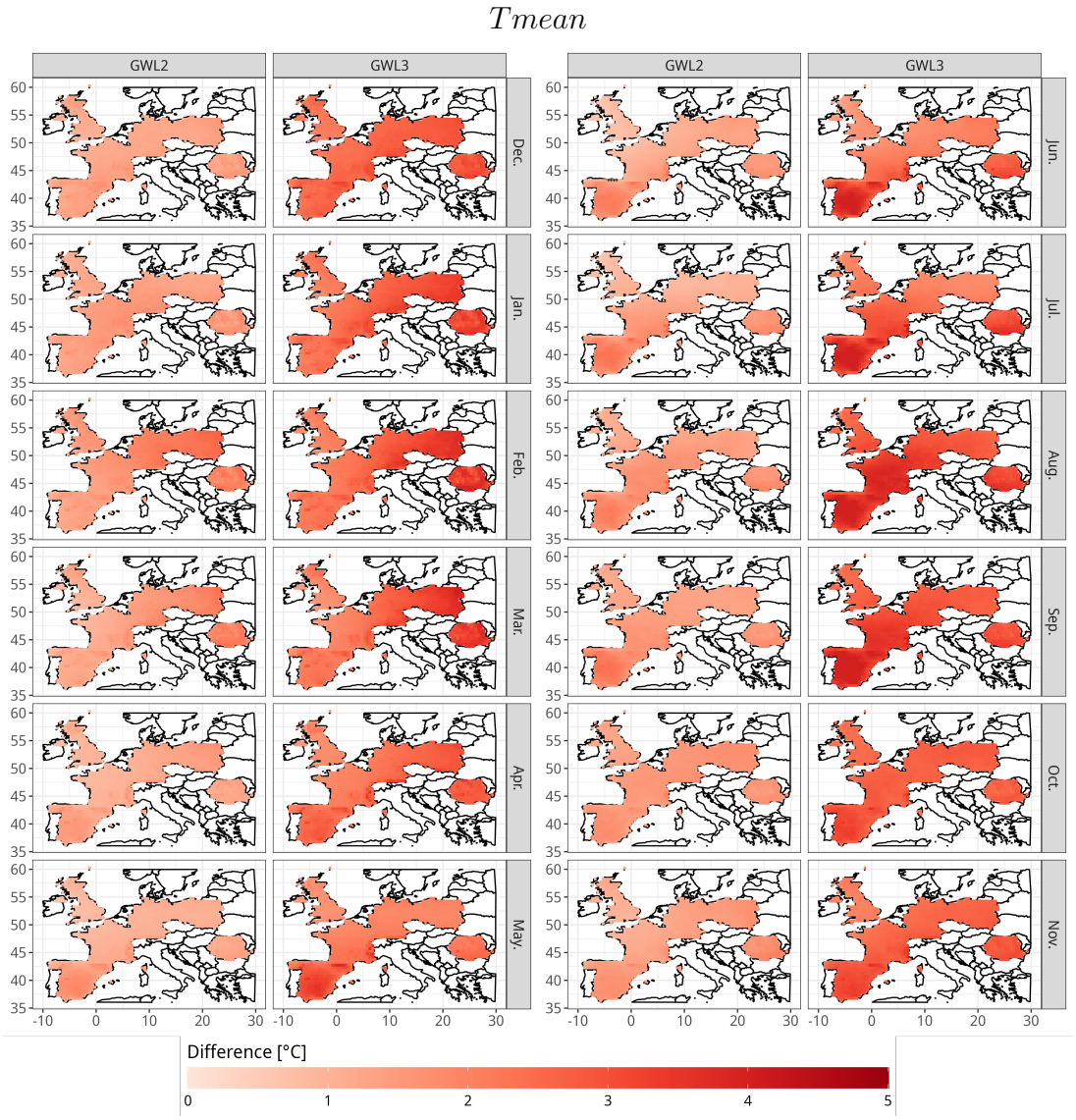

Figure 8.5: Spatial changes in average *Tmean* between GWL2 (column 1 and 3) and GWL3 (column 3 and 4) by months (Rows, December-May on the left and June-November on the right) compared to the historical period. The results display the average difference between mean values during GWL2 and GWL3 (obtained from Table 4.3) and the historical period (1982-2005) across each GCM-RCM model-bias correction chain (16 members in total). If the signal between models does not agree in more than 80% (i.e. more than 12 models), this is represented with an "x" point. The approach correspondent to Approach B of model robustness representation in IPCC AR6, described in Table 1 in Gutiérrez et al. (2021).

Annual temperature is expected to increase in whole Europe under RCP8.5 scenario with high model agreement (Jacob et al., 2014). Figure 8.5 display the monthly difference in the average *Tmean* between GWL2 and GWL3 compared to the historical period. At the monthly scale, the increase in temperature is likely stronger in a GWL3 than a GWL3.

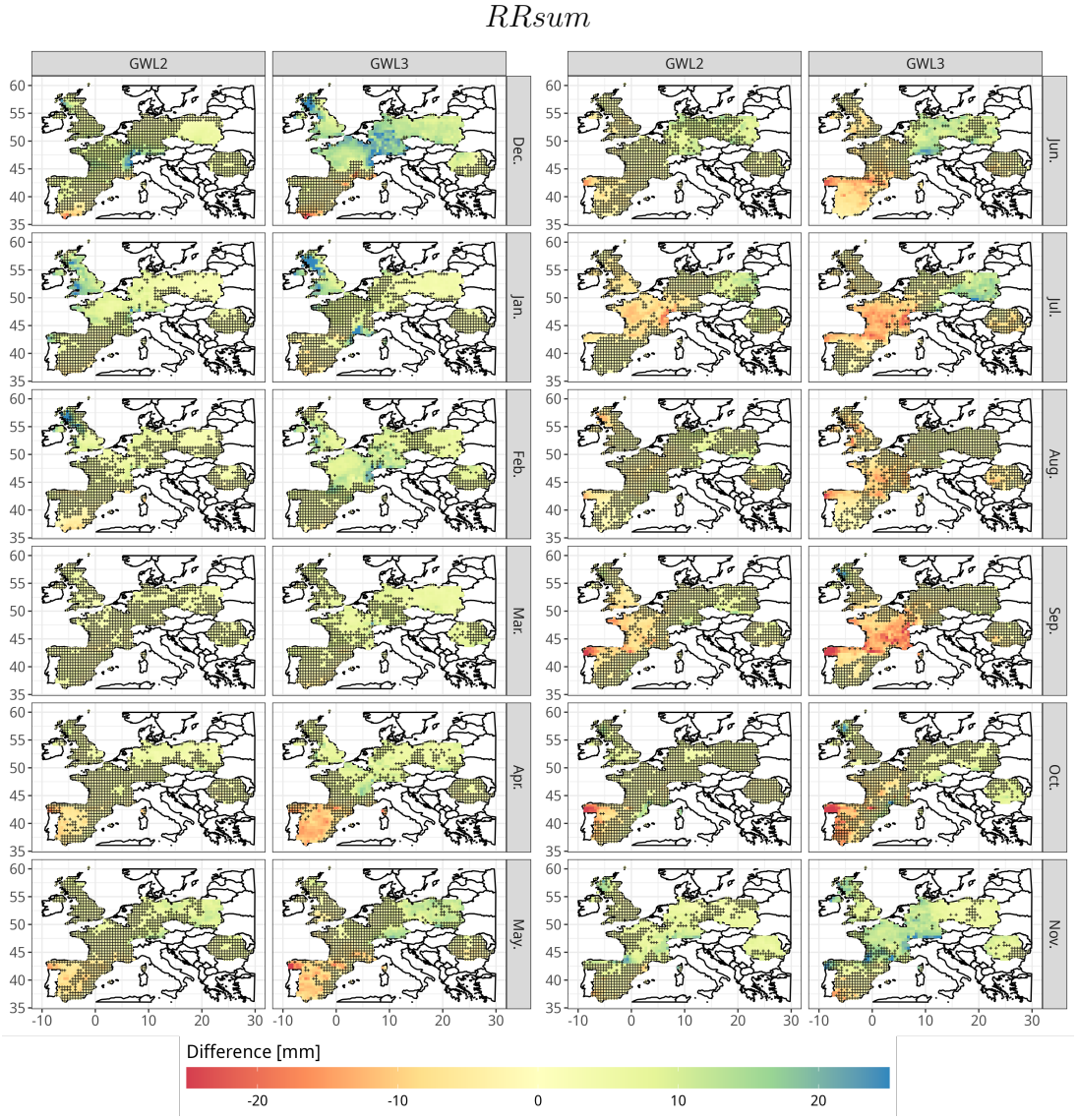

Figure 8.6: Similar to Figure 8.5 but for *RRsum*.

In fact, in some regions, values rise over 4 °C, suggesting warming higher than the global rate (Vautard et al., 2014). The highest difference are observed in Poland and Romania between January and April, and in Spain between June and October. The increase in Germany and France is higher during the transition months (March-May and September-November) compared to winter and summer. This is also in agreement with previous literature, pointing to higher warming rate as well as increase in frequency and intensity of heatwaves at the southern regions than central and norther regions (Jacob et al., 2014; Molina et al., 2020).

Precipitation is expected to increase in northern areas, mainly in winter, and decrease in central and southern Europe, especially in summer (Cardell et al., 2020; IPCC, 2023; Coppola et al., 2021). However, there is low agreement between models in the projected precipitation (Jacob et al., 2014). According to Figure 8.6, at a monthly scale, the overall results on *RRsum* suggest decrease in precipitation in the southern region (including southern France) and higher values in central and northern regions, but the model's signal

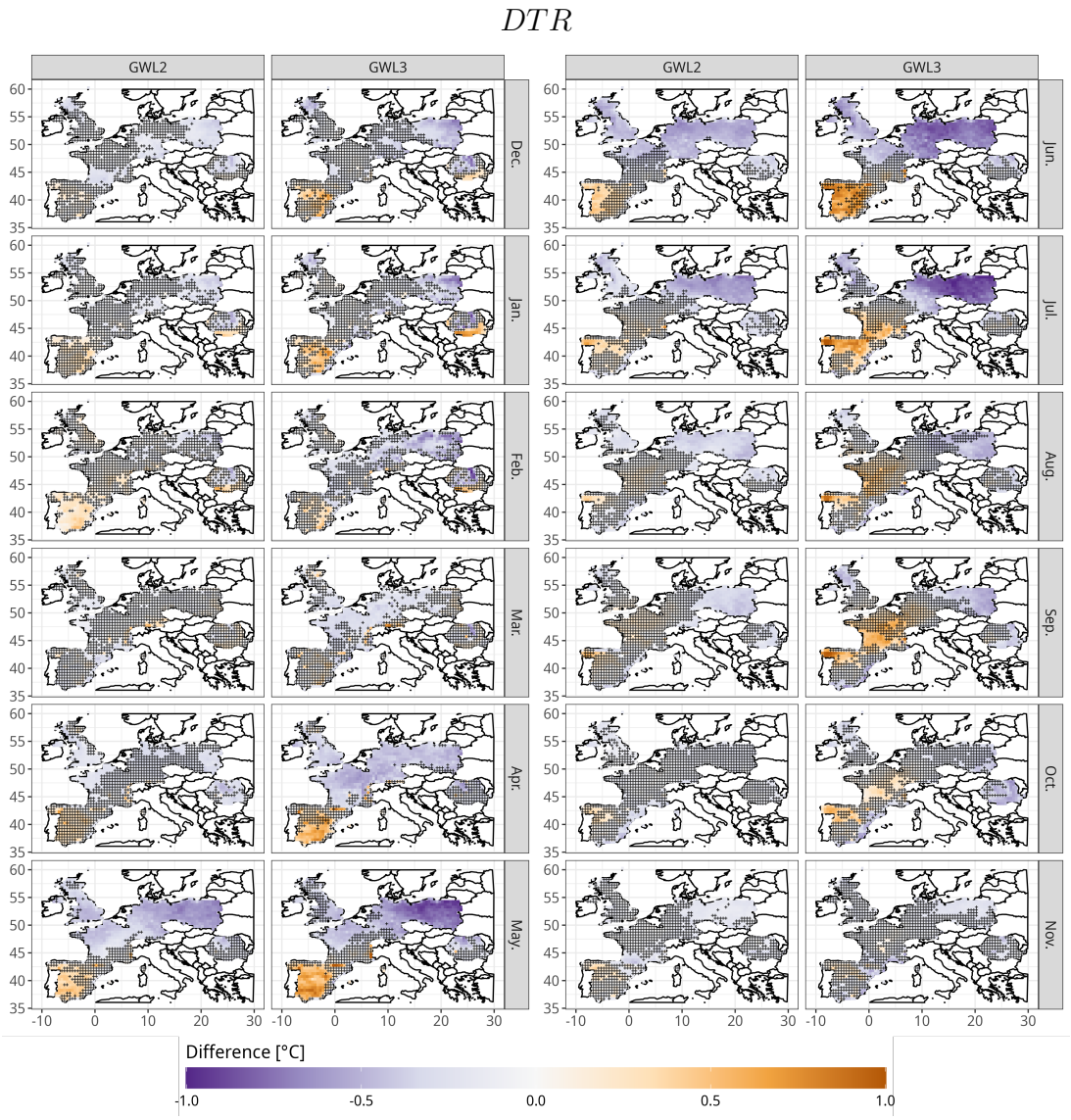

Figure 8.7: Similar to Figure 8.5 but for DTR.

is contrasting. More specifically under GWL2 we find agreement in a slight increase of $RRsum$ (10 mm to 20 mm) in central and northern Europe in January, and average lower values (~ -10 mm) in norther Spain and France in July. Generally, the rates are stronger in a GWL3 compared to GWL2, with also wider extension of model agreement. Between December and February, central and northern regions (Germany, Poland and the UK specially) become wetter (between 10 mm and 20 mm). Conversely in southern region (Northern Spain and southern France), $RRsum$ between March and August drops about 20 mm in a GWL3 compared to the historical period. It is important to consider that this results solely target the cumulative precipitation but not the frequency or the intensity of events, which can still be relevant. For example, the Mediterranean region would likely experience longer dry period but more intense extreme precipitation events (Coppola et al., 2021).

Finally, Figure 8.7 illustrate the changes in monthly DTR by GWL2 and GW3. It is only in some reginos in Spain and Poland where there is high agreement between model's

signal. Our results suggest a slight increase in DTR in southwestern Europe and a decrease in northeastern Europe, but the differences do not exceed 1 °C. Generally, the highest values are observed in Spain and southern France, between May and September whereas, within the same month rage, Poland features lower DTR values, specially in a GWL3 compared to GWL2. Diurnal temperature attempts to cover several atmospheric aspects. It is directly related to the difference between maximum temperature and minimum temperature, thus it also relates to the cloud cover and thereafter total solar incoming radiation. With drier conditions in the south, as previously discussed, there might be overall higher DTR associated with it. This is also supported by projected increase in surface shortwave radiation observed in these regions (Coppola et al., 2021). Conversely, the observed diminished DTR in the eastern (Poland) can be rather related to higher increase in minimum temperature compared to the rate projected for maximum temperature (Carvalho et al., 2021).

8.3 Drivers and yield shock risk under warmer climate

Once the future changes in drivers have been established, the next step is to analyze the trends and drivers of yield shocks under future climate conditions. This section evaluates the outputs of the leave-one-year-out ensemble model using the future simulation datasets. The analysis is organized in three stages for each crop: first, it examines the overall trends in the probabilities of yield shock; second, it investigates the apparent changes in the most relevant variables under GWL2 and GWL3 using the dual distribution approach (Chapter 5); and third, it identifies the variables responsible for higher or lower probabilities of yield shock under GWL2 and GWL3 using Shapley values. The full ensemble considered includes 8 GCM–RCM models × 2 bias correction methods × 35 leave-one-year-out Random Forest models, while for computational efficiency the outputs are based on sub-samples of the data.

8.3.1 Maize

Trend in probabilities

Figure 8.8 display the evolution in the probabilities of maize yield shock for the studied domain. Most of the change in the risk of losses are expected only at the end of the century. France (a) would experience slight increase in he mean probability vlaues, from 20% to 25%. In the historical period, average values range between 10% and 30% while after 2050 some years can rise up to 35%. However, the uncertainty does not change throughout the period. Average probabilities of maize yield shock in Romania (c) remain constant until 2040, when there is an approximately linear increase reaching 25% by te end of the century. Finally, in the case of Spain (c) probabilities of yield shock remain constant. In contrast to the other countries, the uncertainty narrows down by the end of the century.

A similar analysis can be conducted when comparing global warming levels (GWLs), as shown in Figure 8.9. In this case, the probabilities of yield shocks under GWL2 and GWL3 are compared against those observed during the historical period. Although the risk of yield shock increases under warmer climate scenarios, the magnitude of the

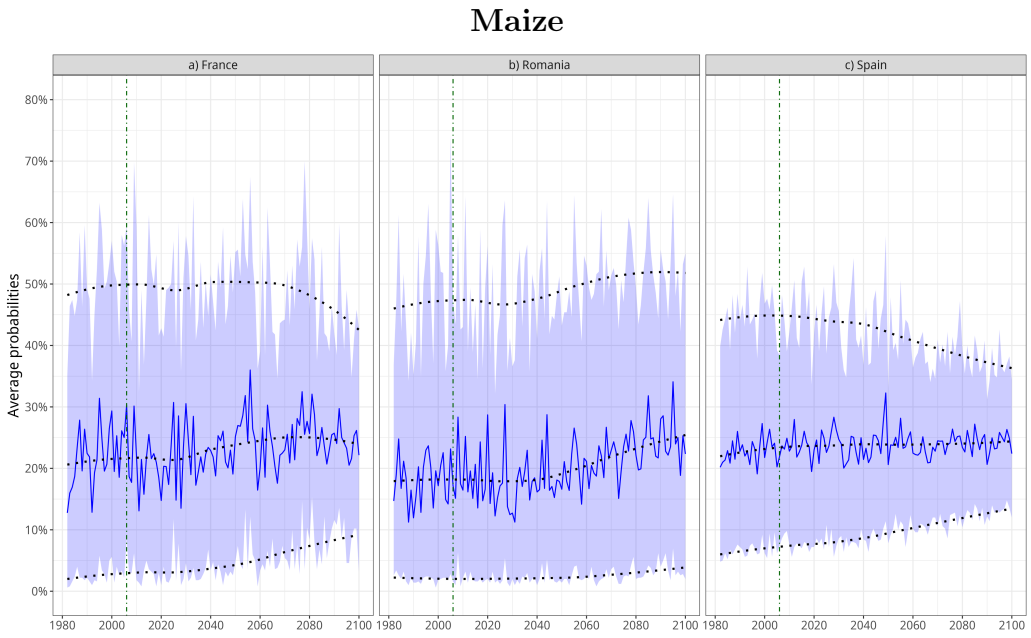

Figure 8.8: Probabilities of maize yield shock for each country (in panels) in the 1982-2100 period. Blue opac line represents the yearly average value, and the shade represents the 5^{th}-95^{th} percentile uncertainty form the ensemble. Black-dot lines display the long-term trend in the 5^{th} percentile, mean and 95^{th} percentile, obtained by LOEWSS (See Equation 4.1). Vertical green-dashed line in 2006 indicates the end of the historical period and the begining of RCP85 scenario. The probabilities are obtained by combining GCM-RCM models (8 models), the two bias correction methods (2 methods), and the leave-one-year-out ensembles (35 models).

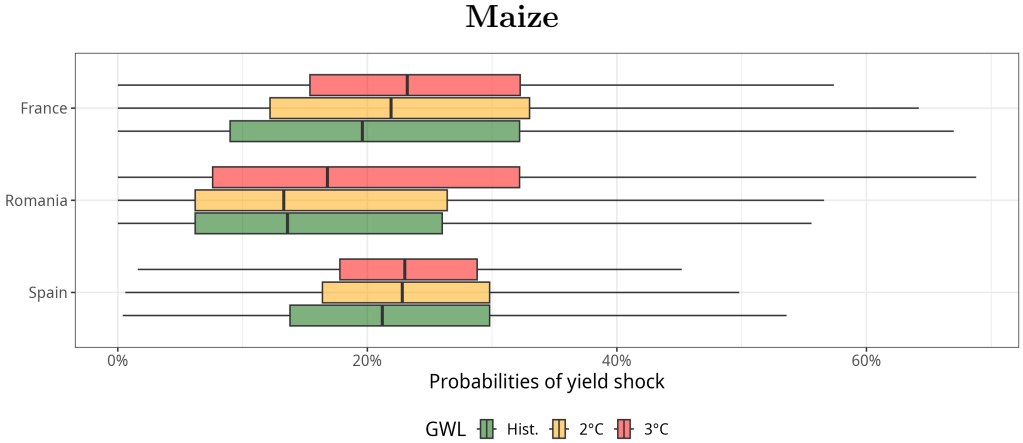

Figure 8.9: Maize yield shock probability distribution (x-axis) per country (y-axis) and per global warming level (colors). The historical period ("Hist.", green) correspondent to the 1982-2005 period. Boxplot mid line corresponds to the median of the distribution, the end of the boxes to the 25^{th}-75^{th} percentile and the end of the whiskers to the 5^{th}-90^{th} percentile. GWL periods are based on the Table 4.3 for each correspondent GCM-RCM model chain.

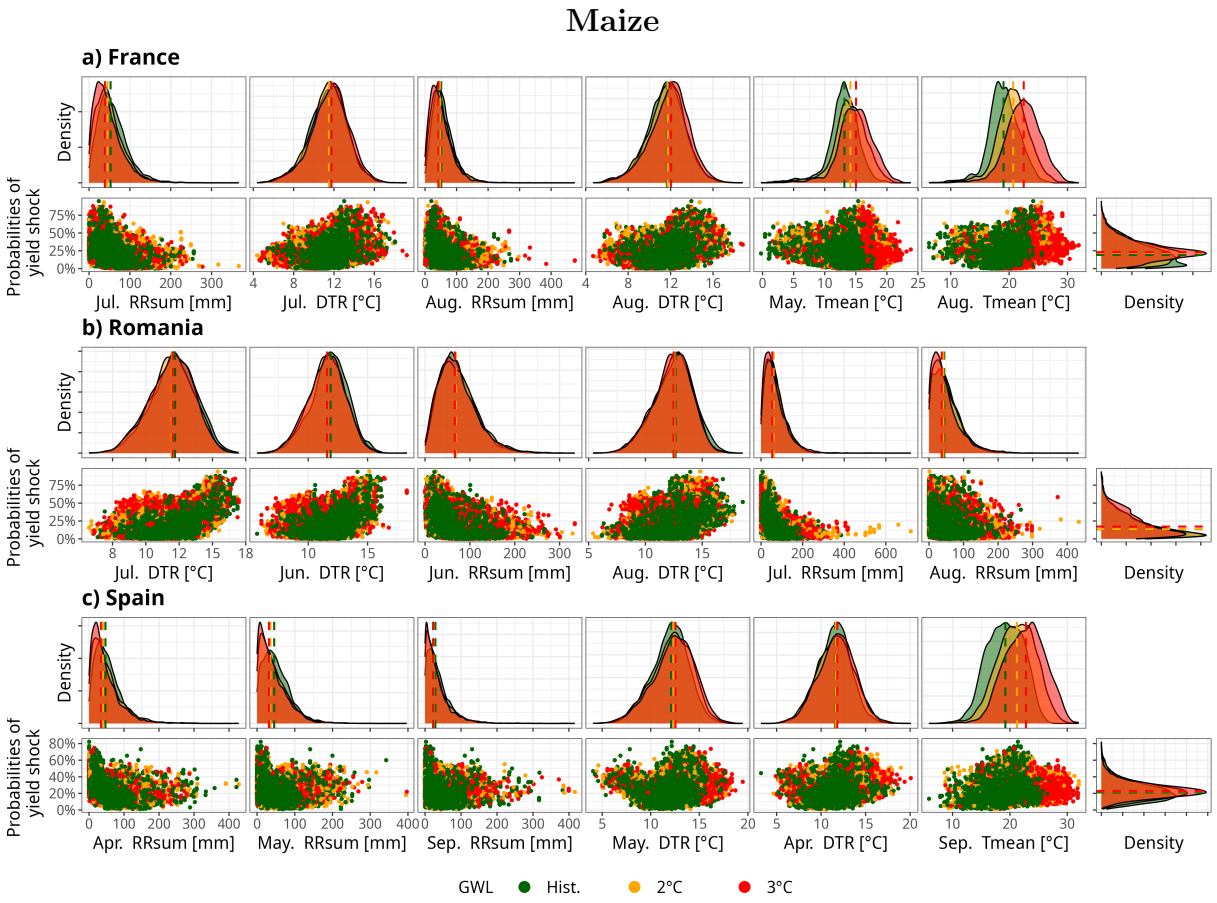

Figure 8.10: Dual distribution of the top three most important predictors of maize yield shock probabilities by country (a, b, c) for each GWL (shown in colors). Predictors are based on Figure 7.6 in Chapter 7. Top row: Density distributions for each variable (columns). Bottom row, left: Scatter plots between each variable (columns) and yield shock probabilities. Bottom row, right: Distribution of yield shock probabilities and average values for each GWL (horizontal dashed lines).

shift does not exceed 5% for any of the countries analyzed. For instance, France is projected to experience a higher risk of yield shock under both GWL2 and GWL3, with a concurrent reduction in uncertainty. In Romania, the increase in risk is particularly evident under GWL3, whereas little change is observed under GWL2. In the case of Spain, the median probability of yield shock is higher for both GWL2 and GWL3 compared to the historical period, but the values are similar between the two warming levels. Additionally, uncertainty is reduced under warmer climate scenarios.

Dual distribution

The analysis begins with information from the model ensemble by examining the most important predictors identified in Chapter 7. Figure 8.10 illustrates the relationship between the top three predictors (x-axis, by column) and the probabilities of yield shock (y-axis), shown for each GWL scenario and the historical period (distinguished by color). Generally, the predictor variables exhibit limited variation across GWLs. This is partic-

ularly evident in all variables based on DTR and $RRsum$. Notable shifts are observed only in $Tmean$ for May and August in France (panel a, fifth and sixth columns) and in $Tmean$ for September in Spain (panel c, sixth column), where higher values are seen under GWL2 and GWL3 scenarios. In France, probabilities of yield shock show a slight increase under GWL2 and GWL3, while in Romania (panel b), an increase is evident only under GWL3.

Shapley values

The results derived from Shapley value analysis are presented in Figure 8.11. For each country (panels a, b, c), the left panels display the top nine contributing variables under warmer climate conditions, along with their relative values (colorbar). The corresponding right panels show the distributions of these predictors during the historical period, GWL2, and GWL3. A country-specific analysis is provided below.

In the case of France (Figure 8.11a), eight of the top nine contributing variables are associated with the summer months (June, July, and August), with the exception of $Tmean$ in September. In general, higher values of $Tmean$ and DTR (represented by red dots), along with lower values of $RRsum$ (blue dots), are associated with positive contributions to the probability of maize yield shock. This indicates that, under these conditions, the expected probability of a yield shock increases relative to the historical baseline. Conversely, lower values of $Tmean$, higher values of $RRsum$, and, to a lesser extent, lower values of DTR are linked to reductions in yield shock probability. Notably, $Tmean$ appears consistently among the top contributing variables and exhibits a strong negative influence on the probability of yield shock under extreme conditions. In particular, maximum values of $Tmean$ in September during GWL2 and GWL3 scenarios show a more pronounced negative contribution than any other predictor. An examination of the variable distributions (right panel) reveals a clear upward shift in all $Tmean$-based variables (first, second, sixth, eighth, and ninth rows) under GWL2 and GWL3. The most significant increase occurs in August and September (top two variables), where the interquartile ranges of GWL3 and the historical period do not overlap. For the $RRsum$-based variables (third and fourth rows), a moderate shift toward lower values is observed under warmer scenarios. In contrast, the DTR-based variables (fifth and seventh rows) exhibit minimal change in distribution across climate scenarios.

In Romania (Figure 8.11b), the highest influences arise from predictors associated with June and July. As observed in France, high values of $Tmean$ and DTR (indicated by red dots), along with low values of $RRsum$ (blue dots), contribute to elevated probabilities of maize yield shock relative to the historical baseline. The most significant contribution is attributed to DTR in July (first row), where peak values are associated with an increase in yield shock probability of up to 0.3 (i.e., 30%). In contrast, $Tmean$ in September (ninth row) contributes negatively to yield shock probability at high values, though its overall impact is smaller compared to the primary predictors. The distribution of variables in Romania (right panel) indicates a general warming trend under GWL2 and GWL3, though the magnitude of change is less pronounced than in France. For example, while $Tmean$ shows moderate increases, there is a slight reduction in $RRsum$ under warmer scenarios and minimal change in the distribution of DTR-based variables.

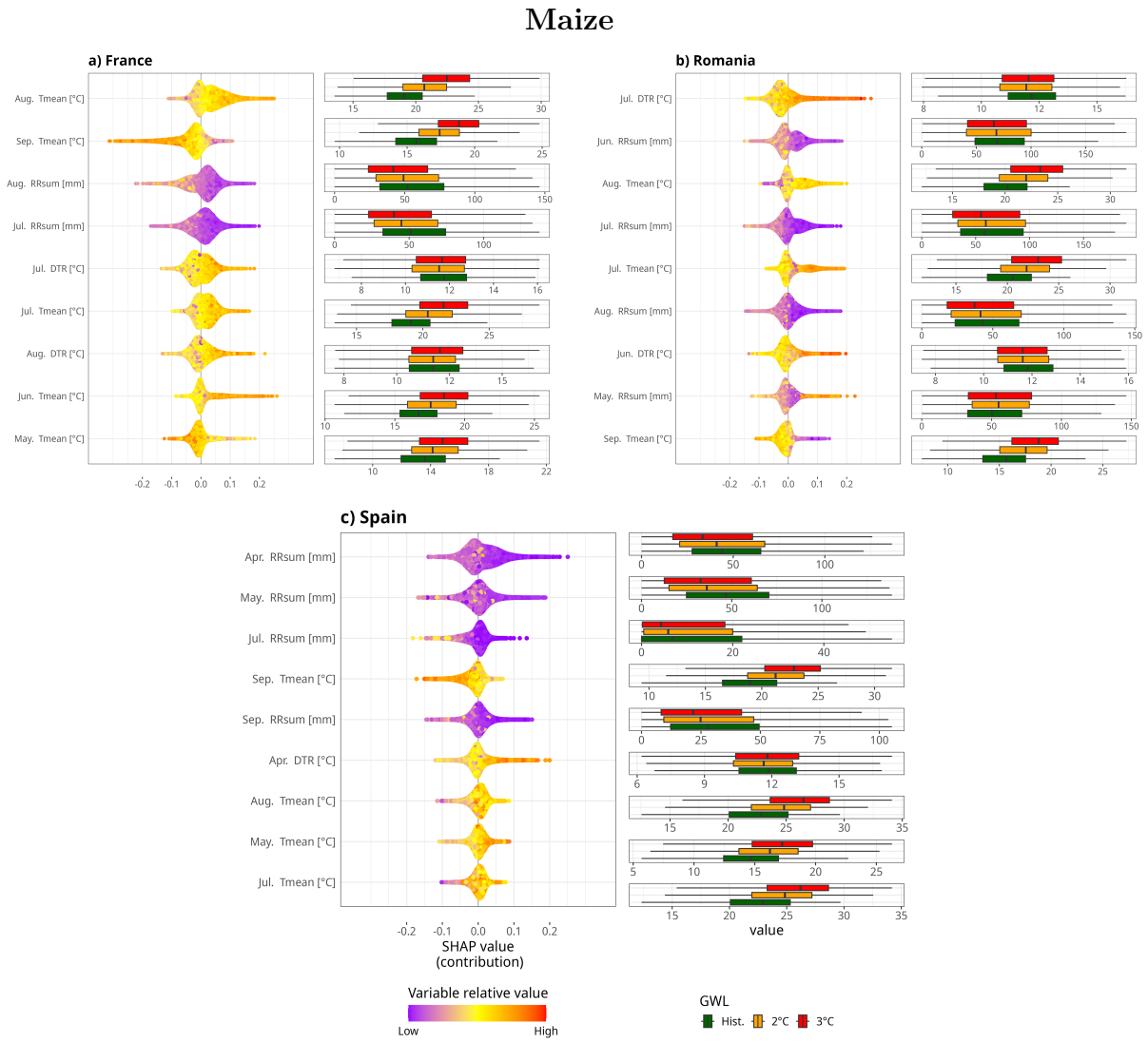

Figure 8.11: For each country (a,b,c) and maize yield shock: Top nine contributors (left panel) Shapley values values and relative feature value (in colors), and (left panel) variable distribution during the historical period, GWL2 and GWL3 (colors).

In Spain (Figure 8.11c), the top three contributing variables are *RRsum* in April, May, and July. Consistent with patterns observed in other countries, warmer, drier conditions and higher *DTR* values are associated with increased probabilities of maize yield shock. However, the Shapley values in Spain are generally lower than in France and Romania, rarely exceeding 0.15. A notable exception is *RRsum* in April, where extremely low values during GWL2 and GWL3 are linked to a substantial increase in yield shock probability. The distribution of variables (right panel) reflects similar trends to those observed in France and Romania. Drier conditions, represented by *RRsum* in April, May, July, and September (first, second, third, and fifth rows) as well as warmer conditions, captured by *Tmean* in May, August, and September (fourth and seventh to ninth rows), are more likely under GWL2 and GWL3 scenarios.

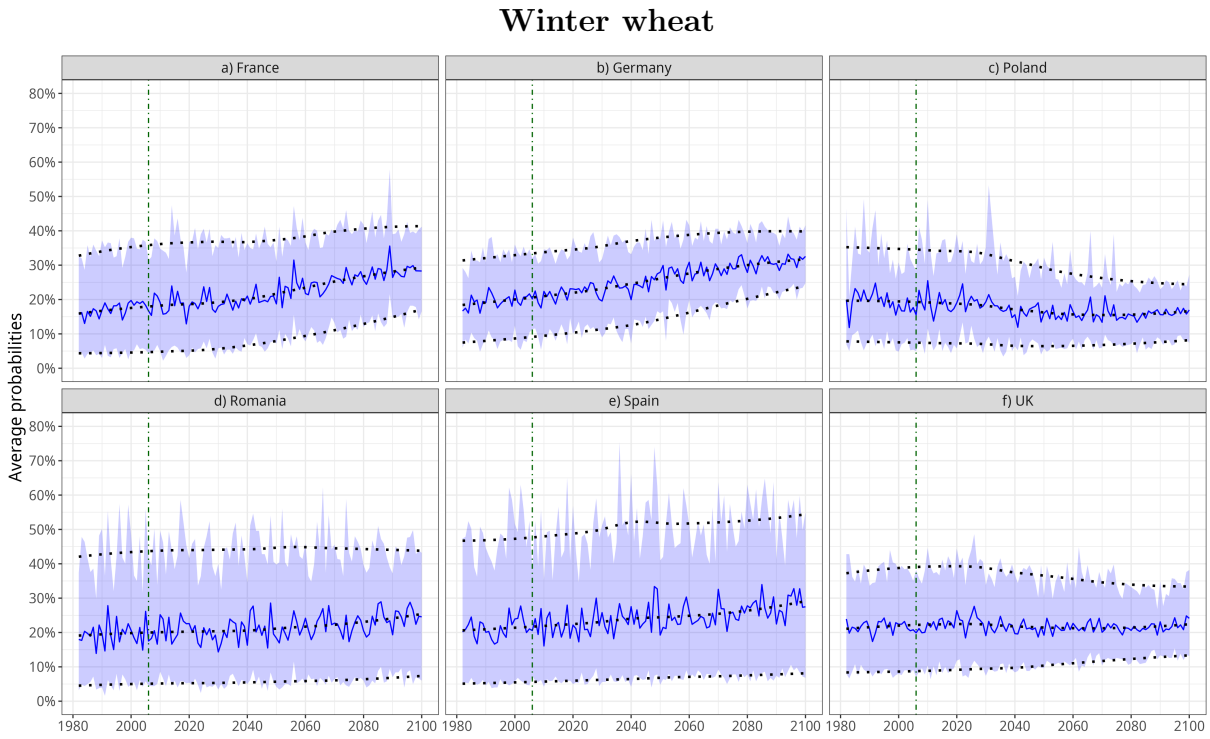

Figure 8.12: Similar to Figure 8.8 but for winter wheat and the correspondent domain (in panels).

8.3.2 Winter wheat

Overall trends in probabilities

The probabilities of winter wheat yield shock (Figure 8.12) display strong changes during the century. France and Germany (panel a and b) present similar behavior, with pseudo-linear trend and 10% increase in the risk observed by the end of the century. In contrast to the case of maize, the uncertainty along the century is smaller; values up to 5-30% in the beginning of the century and 10-40% at the end of the century in Germany, while in France the uncertainty rise form 10-30% to 20-40%. Poland (panel c) is the only country presenting visible negative trend in the risk of losses. Average probabilities decrease from 20% to 15%. Additionally, the uncertainty range also narrows down from 10-50% to 10-20%. In the case of Romania and Spain (panel d and e), probabilities of winter wheat yield shock only present slight increase by the end of the projections (no greater than 5% comparing the end of the century and the historical period). Uncertainty in Romania range constant values of 5-45%, while in Spain the uncertainty is slightly bigger (5-50%). Finally, in the UK (panel f), probabilities of yield shock remain constant, with an uncertainty range of 5-35% and a slight narrowing by the end of the century.

When comparing GWL against the historical period (Figure 8.12), the behavior is contrasting across countries. France and Germany would experience drastically increase in the risk of yield losses under GWL2 and GWL3 respectively. For both countries, the 5^{th}-95^{th} percentile range remains unchanged, but the median increases by 5% under GWL2 and almost 10% for GWL3 compared to the historical. On the other hand, the probabilities of yield shock in Poland slightly diminish under warmer climate, as well as the

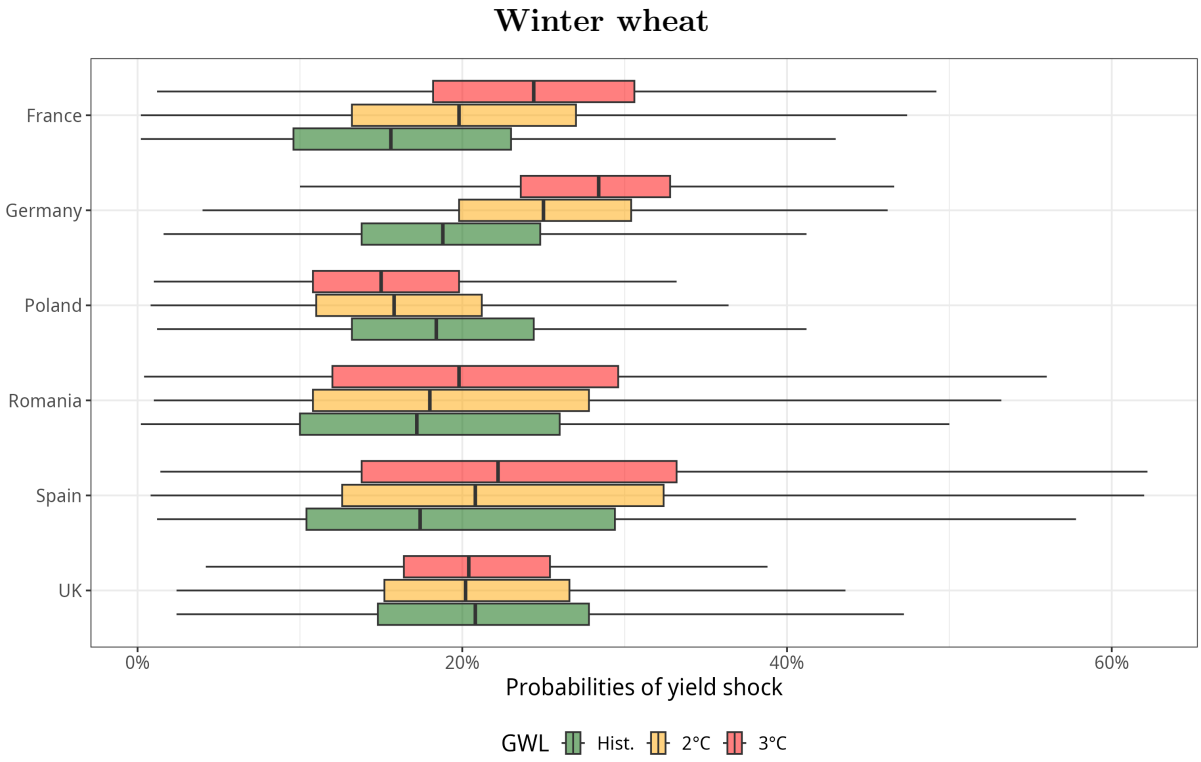

Figure 8.13: Same as Figure 8.9 but for winter wheat.

uncertainty range. For both Romania and Spain, the risk of losses are overall higher under warmer climate, with higher values for Spain. Finally, thought the risk of losses in the UK does not change under warmer climate, the uncertainty would be reduced under GWL2 and GWL3 respectively.

Dual distribution

Figure 8.14 and Figure 8.15 illustrate the relationship between the top three predictors (x-axis, by row) and the probabilities of winter wheat yield shock across different Global Warming Levels (GWLs), distinguished by color. Compared to maize, winter wheat displays more pronounced differences in both the predicted probabilities of yield shock and the distribution of predictors between the historical period, GWL2, and GWL3. These differences are particularly evident in *Tmean*-based variables, which exhibit clear distributional shifts under warming scenarios.

In France (Figure 8.14a), *Tmean* in April and December shows a marked shift toward higher values under GWL2 and, more prominently, under GWL3. This is accompanied by an increase of approximately 10% in the median predicted probability of yield shock in GWL3 compared to the historical period. A similar pattern is observed in Germany (Figure 8.14b), where *Tmean* in June and December (first and second columns) increases progressively with warmer climate, and the median probability of yield shock rises to nearly 30% under GWL3.

In Romania and Spain (Figure 8.14c and Figure 8.15d), the predicted probabilities of yield shock also increase under GWL2 and GWL3, although to a lesser extent than in France

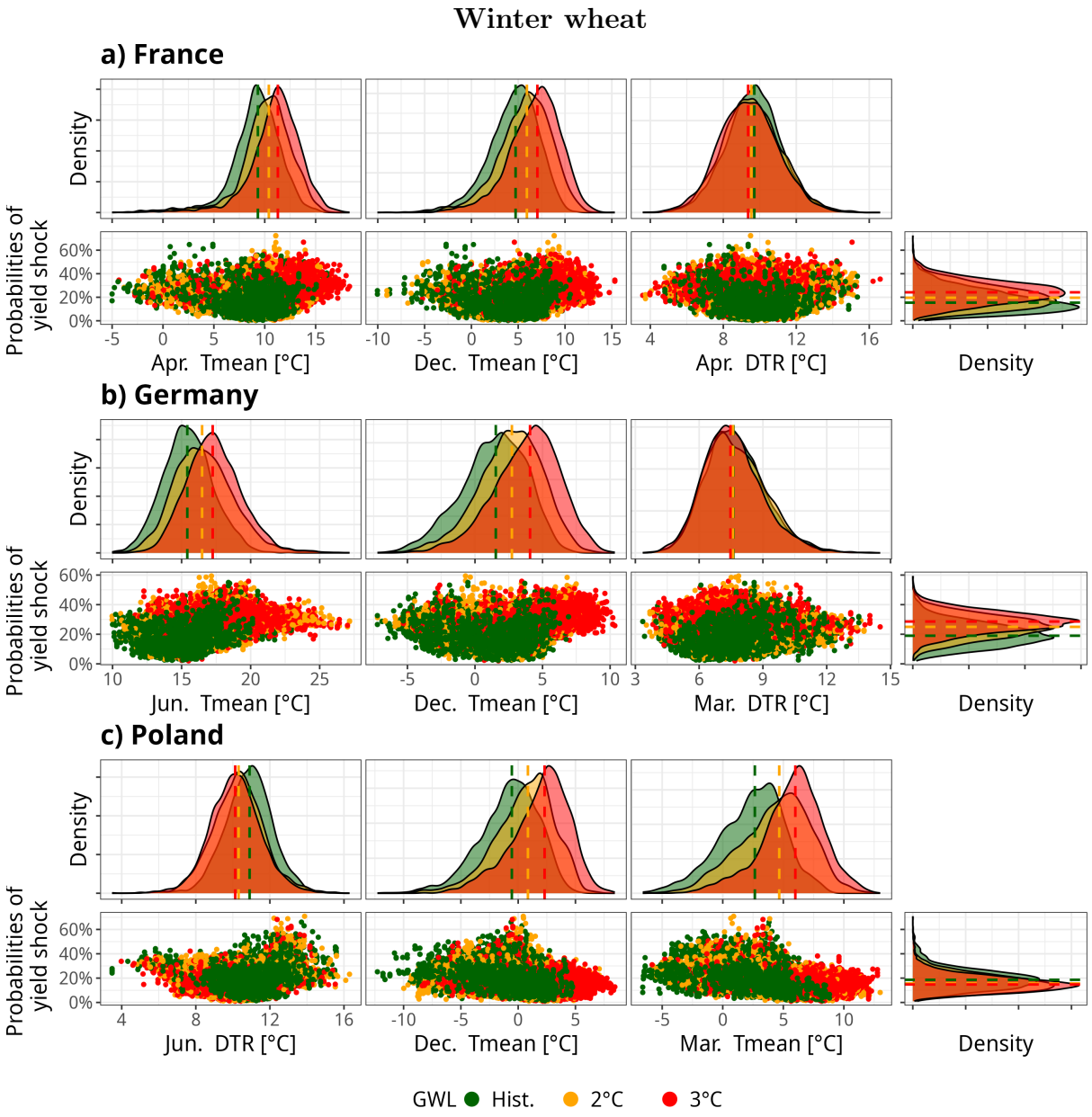

Figure 8.14: Similar to Figure 8.10 but for winter wheat and top three predictors for France, Germany and Poland (panel a,b,c).

or Germany. In Spain, slight reductions in *RRsum*-based variables are noted, alongside higher values of *Tmean* in May and February (panel d, first and third columns). Poland (Figure 8.15e) presents a contrasting pattern: *Tmean* in December and March shows increases, yet the probabilities of yield shock decrease under GWL2 and GWL3, with little difference between the two warming levels.

In the UK (Figure 8.15f), no notable differences are observed in either the top predictors or the predicted probabilities of yield shock across scenarios, suggesting a relatively stable response under projected warming.

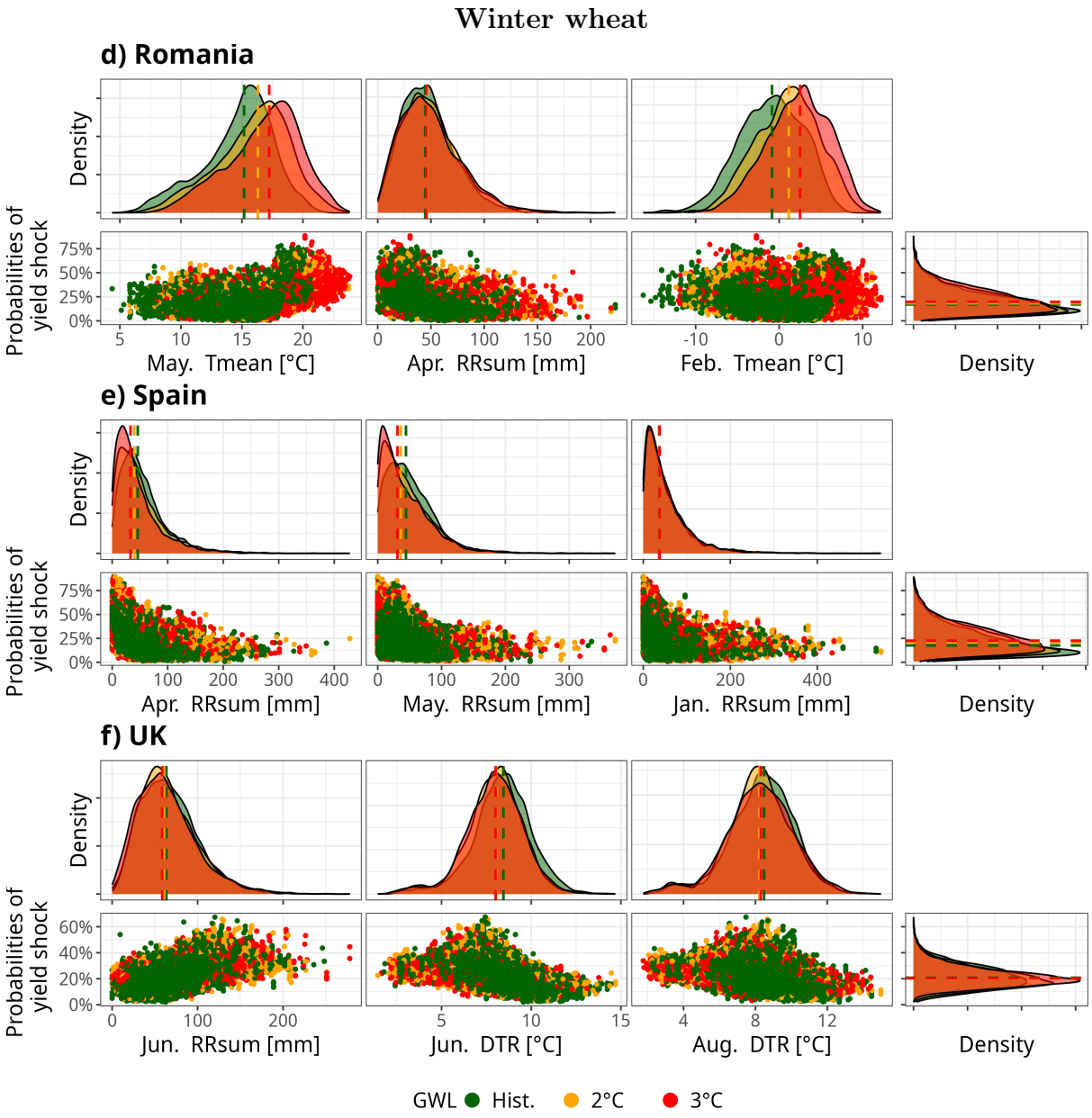

Figure 8.15: Similar to Figure 8.10 but for winter wheat and top three predictors for Romania, Spain and the UK (panel d,e and f).

Shapley values

The results obtained by Shapley values are shown in Figure 8.16 for each country (a-f). The left panel display the distribution of Shapley value for the top three contributors as a function of their relative values (from low values in blue, mid values in yellow and high value in red). The top contributors is calculated by considering both the average in the absolute Shapley values for each predictor during GWL2 and GWL3 together. As a general view, most of the contributors are similar to the ones obtained by using Gini index. The Shapley value are relative to the baseline obtained by computing the historical data in each leave-one-year-out model, which results in average values of 0.2 (i.e. 20%).

The contributions in most extreme shows values of 0.25 which can be translated on an expected increase in 25% to the probabilities of yield shock or, conversely, a decrease. Below, each country is analyzed separately.

In France (Figure 8.16a), the top three contributors to changes in the probabilities of winter wheat yield shock are $Tmean$ in December, $Tmean$ in October, and DTR in February. According to the Shapley values, high values of $Tmean$ in December (indicated by yellow to red dots) are associated with increased probabilities of yield shock, with contributions reaching up to 0.2. These elevated values of $Tmean$ are more frequent under GWL2 and GWL3 scenarios. To a lesser extent, high values of $Tmean$ in October (second row, red dots) are associated with slightly negative Shapley values. Despite this, a consistent increase in $Tmean$ for October is observed under GWL2 and GWL3, similar to the trend seen in December. In the case of DTR in February (third row), the relationship is inverse: high values are linked to lower probabilities of yield shock, while lower values tend to contribute positively. However, the distribution of DTR in February remains relatively unchanged across GWL2, GWL3, and the historical period. Among the top nine contributing variables (Supplementary Figure 8.14a), $Tmean$ in April also stands out. High values of this variable contribute positively to the probability of yield shock and align with a noticeable increase in its distribution under both GWL2 and GWL3 scenarios.

The top three contributors in Germany (Figure 8.16b) are $Tmean$ in June, August and December. For the three variables, higher values (yellow and red dots) contribute to relatively positive probabilities of winter wheat yield shock. We also see that low values of $Tmean$ in December (blue dots) contribute further higher probabilities. The three variables increase under GWL2 and GWL3. This is specially notable in August, where there is no overlapping in the interquartile range between GWL3 and the historical period.

In Poland (Figure 8.16c), the top three contributors to changes in the probabilities of winter wheat yield shock under GWL2 and GWL3 are $Tmean$ in October, December, and March. Additionally, $Tmean$ in January ranks among the top four contributing variables (Supplementary Figure D12c). For all four variables, high values of $Tmean$ contribute negatively to the probability of yield shock, whereas low values contribute positively, though with a smaller magnitude. All four months are projected to experience higher $Tmean$ values under GWL2 and GWL3 scenarios. This shift is particularly pronounced in October and March, where the interquartile ranges of GWL3 and the historical period do not overlap, indicating a substantial warming trend in these months.

In Romania (Figure 8.16d), under GWL2 and 3, the most important contributors to changes in the probabilities of winter wheat yield shock are $Tmean$ in May, $RRsum$ in April and $Tmean$ in February. This also coincides with the results by using Gini index (Chapter 7 and Figure 8.14d). From the Shapley values distribution, $Tmean$ is characterized by two groups: High concentration of relative low values (yellow and blue dots) reduce the probabilities of yield shock (between 0 to -1) whereas a more spred of high values (yellow to red) contribute positively (between 0 to 0.3). Additionally, when analysing the variable distribution (panel b), the values of this predictor in a GWL2 and GWL3 are progresively higher. In the case of $Tmean$ in February (third variable), high values (red dots) contribute slightly negatively, whereas low values (blue dots) increase

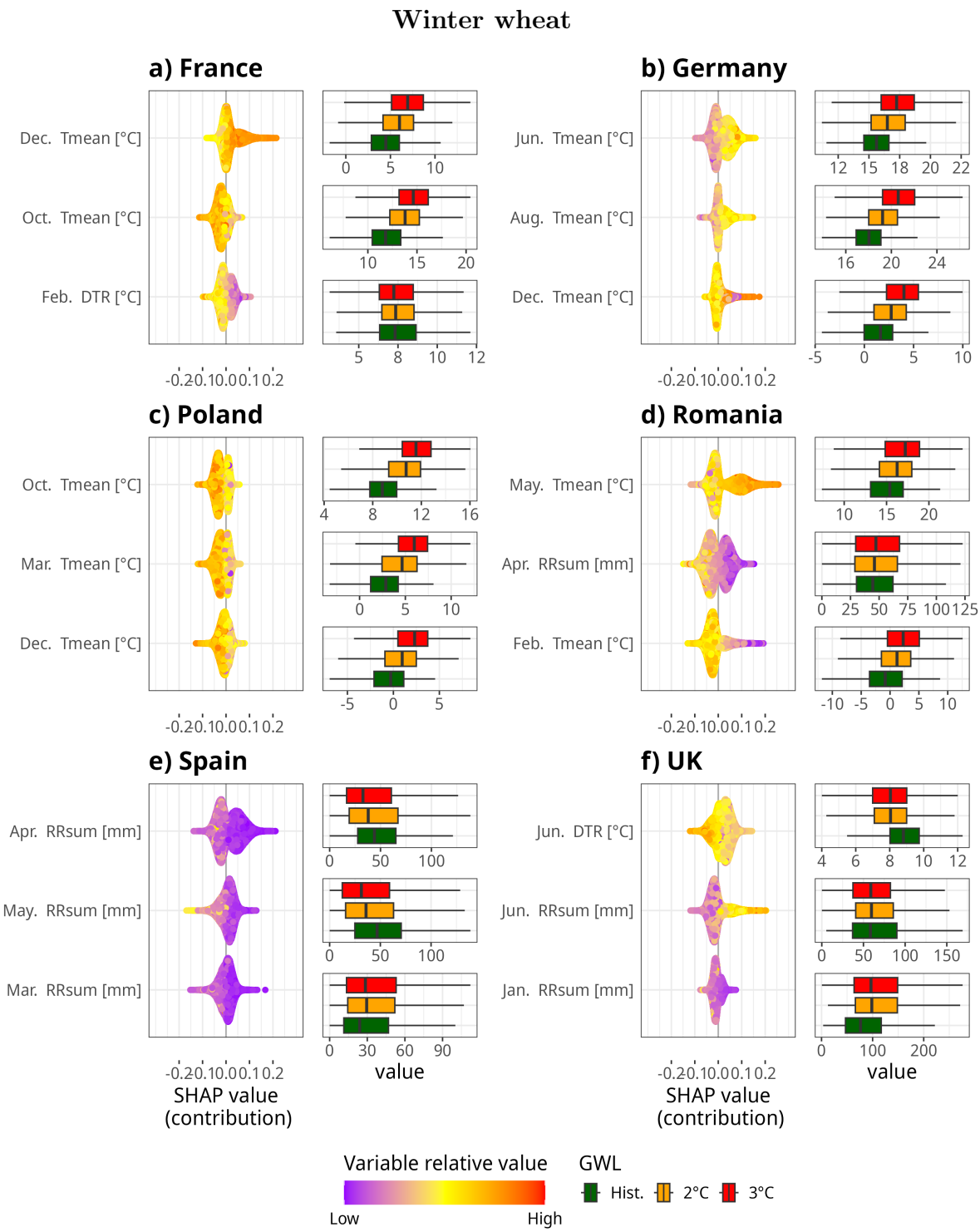

Figure 8.16: Similar to Figure 8.10 but for top three variables and winter wheat for the corresponding studied countries.

the probabilities of yield shock, thought the data spread is less concentrated; similar to the case of *Tmean* in May, the values in February are likely higher in a GWL2 and GWL3. For *RRsum* in April, we find a dual distribution behavior, with high values (red)

contributing negatively and low values (blue) positively; there are not apparent differences in the *RRsum* distribution under GWL2 or 3 compared to the historical.

In Spain (Figure 8.16e), the top contributing variables to changes in winter wheat yield shock probabilities are *RRsum* in April, May, and March. Analysis of the variable distributions reveals a slight shift toward lower *RRsum* values in April and May under warmer climate scenarios, with slightly lower values under GWL3 than GWL2. In contrast, *RRsum* in March shows a slight increase under both GWL2 and GWL3 compared to the historical period. Additionally, *RRsum* in January exhibits strong positive Shapley contributions (Supplementary Figure D13e); however, no clear distinction is observed in its distribution across the different warming levels.

Finally, in the UK (Figure 8.16f), no substantial changes are observed in the top contributing variables between the historical period and the GWL2 or GWL3 scenarios. The primary contributors include *RRsum* and *DTR* in June, with *RRsum* in January also showing moderate influence. Among these, only *DTR* in June displays a slight shift toward lower values under warmer conditions, with similar behavior under both GWL2 and GWL3.

8.4 Physiological response to future climate warming

Due to global warming, sagroclimatic zones in Europe have shifted towards northern areas, and this would likely continue under a 2 °C warming scenario according to RCP8.5 (Ceglar et al., 2019b). This translates in an extentio in the growing season (which opens the opportunity for new cropping systems), reduction in the risk of frost and increase in heat stress (Ceglar et al., 2019a; Cardell et al., 2020; Coppola et al., 2021). Consequently, the probabilities of maize and winter wheat yield shock in future warmer climate scenarios could be attributed to a different physiological process compared to the present climate. This section provides an in-detailed discussion for each crop, domain and compares the results with previous literature.

Maize

The contrasting signals in *RRsum* and *DTR* and the high agreement in *Tmean* may explain the probability trends. According to the ensemble of Random Forest models employed in this chapter, probabilities of maize yield shock are not expected to increase more than 5% in the regions, with a high level of uncertainty. One of the possible explanations of such small changes leans on both the high importance of *RRsum*-based variables on the domains and the low agreement in the signal. This may also explain the high uncertainty in the year-to-year probabilities (Figure 8.8). Furthermore, the model agreement in the changes of in-season precipitation within countries is contrasting. Consequently, the signal in the probabilities would likely vary at sub-national scale.

Despite what is mentioned above, warmer and drier conditions throughout the summer months would still lead to higher risk of losses in France and Romania. Thought there is little documentation on the future impact of climate change in maize yield in both domains, there is agreement on slight decrease in overall yield variability (Bednar-Friedl et al., 2022). In the case of Romania, however, the losses are mostly attributed to higher

DTR in July (translated to average higher sunny days), which would not change in the future. Higher summer temperatures increase the risk of heat stress, water use and reduce growing season length (van der Velde et al., 2012; Hawkins et al., 2013a; Ben-Ari et al., 2016). Some of these effects can be compensated by adequate adaptation measures like targeting mostly optimal cycle duration and sowing dates (Parent et al., 2018).

According to the results obtained in this chapter, Spain would experience slight increase in maize yield shock risk. The impact of climate change in Spain can be actually two-fold (Rey et al., 2011). On the one hand, drier conditions would lead to both higher atmospheric water demand (i.e. evapotranspiration) and lower water availability for maize. This is in agreement with our results, that display the high importance of *RRsum*. On the other hand, increases in average temperature reduces the growing season length, which subsequently leads to overall lower water use and water deficit. In this way, the potential losses in yield are compensated by the reduction in water demand (Rey et al., 2011). In this conditions, irrigation can actually lead to even increase in some parts of the country. However, the increase in longer drier periods and generally lower precipitations would compromise water supply for irrigation (Iglesias et al., 2003).

Furthermore, the results from Shapley value display the influence of warm Septembers in France and Spain. Specifically, it suggest that warmer conditions in the month would lead to lower probabilities of yield shock. Grain filling in maize ussually coincides with August and September, with harvesting between late September and October. Low temperatures in this phenological stage can lead to lower starch cumulative rate, ultimately reducing yield (Guo et al., 2022; Xu et al., 2024). In contrast, high temperatures in this month, which are not as harmful as summer months, can lead to optimal development rate (Katsenios et al., 2021). In this sense, warm conditions in September can lead to temperatures in September expected under GWL2 and GWL3 respectively can actually lead towards lower risk of losses. On the other hand, it is also true that the shortening in growing season length questions the influence of late summer temperatures on yield variability (Rey et al., 2011; Parent et al., 2018). Thus, while late-season warmth may offer some mitigation against yield shocks, its overall impact remains uncertain.

Winter wheat

The probabilities of winter wheat yield shock across the domains display higher consistence between models (Also depicted in Supplementary Figure D8). Generally, the most important drivers of yield shock are *Tmean*-based predictor. The consistence positive sign among models may explain the clear trend observed in France, Germany, Poland and Romania. In the case of Spain, which relies mostly on *RRsum*-based predictors, the low agreement between models' signal may explain the high uncertainty presented in the probabilities (Figure 8.12e). We do not find strong changes in yield shock probabilities in the UK, but neither strong signal on the variables.

High temperatures during December in France and Germany would likely increase the risk of winter wheat losses in these countries. With higher temperatures in winter, the vernalization requirements are less likely to be fulfilled (Wu et al., 2017). In the case of France for instance, this is also pointed by Ben-Ari et al. (2018) that predicted a negative trend in the number of vernalizing days (i.e. number of days with daily temperature

between 0 °C and 10 °C) under RCP8.5 scenario. As winter becomes warmer, the suitable areas of winter wheat with sufficient vernalization days would likely diminish (Martin et al., 2025). This would require the exploration of new varieties or considering alternative crops. In addition to this, in Germany, as well as in Romania and Poland, there would still be events of low temperature in winter. This is illustrated for instance in the case of *Tmean* in December (as is shown in FIgure 8.16). where low temperature can equally contributes towards higher probabilities of yield shock in the country. Hence, future adaptation will demand varieties and management practices resilient to both insufficient vernalization and occasional extreme cold.

Higher temperatures in spring months contribute towards increasing risk of losses in France, Germany and Romania. As heatwaves become more intense, the impact of heat stress, specially during anthesis would likely increase (Martin et al., 2025). Moreover, increasing temperatures would lead to enhanced development rate, potentially reducing mass accumulation (Senapati et al., 2020), which is expected for the three countries (Cuculeanu et al., 1999; Trnka et al., 2015). However, in some cases this can be an advantage, since early maturity can reduce the exposure of wheat to the summer temperatures (Rezaei et al., 2015; Le Roux et al., 2024). Addressing these trade-offs will require models that simulates growing season length, which lies beyond the scope of this chapter. In any case, this does not negate the negative impacts that can arise from higher temperatures in summer months.

In contrast to the other countries, the probabilities of winter wheat yield shock in Poland would diminish or likely remain similar under warmer climate. In fact, the country is expected to experience an increase in relative yield (Bednar-Friedl et al., 2022). Under GWL2 and GWL3 in an RCP8.5 scenario, increases in temperature and precipitation would make the country more suitable for growing wheat. Given the increase in *Tmean* throughout the year, the risk of losses due to frost would strongly diminish. This strengthen the evidence that northern Europe would become more suitability for agriculture in future climate change (Ceglar et al., 2019b). This is also observed in Romania with *Tmean* during February, where warmer conditions within the months would contribute to lower probabilities of losses. However, as it happens in Germany, the occurrence of low temperatures contributing to risk of losses would be diminished but not necessarily dissipated. Additionally, high temperatures in October tends to contribute towards lower risk of losses, which is observed in Poland as well as France. Warm conditions at the earliest stage can contribute to more optimal seeding conditions (Le Roux et al., 2024).

The risk of losses in Spain are mostly attributed to relatively lower precipitation during spring, It is important to notice that our results point to *RRsum* in March, April and May as most crucial indicators, suggesting the influence of cumulative seasonal rain (Trnka et al., 2015). Although irrigation can partly offset these impacts, its effectiveness will be constrained by declining water availability (Bednar-Friedl et al., 2022). By comparison, the projected increase in mean temperature (*Tmean*) during May contributes less to the probability of yield shocks than dry conditions (Supplementary Figure D13f). However, it is possible that our models underestimate the role of heat stress, as maximum temperature was not explicitly included as a predictor.

Finally, for the case of the UK, we find no significant trends in the risk of losses. The previous literature in the UK is particularly contrasting (Harkness et al., 2020; Putelat et al., 2021). The results from Clarke et al. (2021) point to the loss increase due to drought stress, whereas Putelat et al. (2021) suggest similar risk compared to present climate. In particular, these studies are based on the CSM Sirius (Jamieson et al., 1998), which does not account for heavy rain as stressor and may be limited to the local calibration (Zampieri et al., 2018). Conversely, Harkness et al. (2020) focuses on the stressors and states that "hotter and drier summers would improve sowing and harvesting conditions and reduce the risk of lodging". Our results are based on the historical evidence of yield losses, which is independent from the previous approaches. Given that the total precipitation would remain constant under GWL2 and GWL3, the risk of winter wheat yield shock in the UK would likely remain similar in the future compared to present climate.

8.5 Discussion and summary

Given the statistical-based crop models developed in Chapter 7, this chapter addresses the question of whether the risk of losses would change under warmer climate scenarios and the potential attributions. For this, it is necessary to employ bias correction on the GCM-RCM model to thereafter address the changes in the future scenarios. The results are also discussed by considering the physiological aspects of crops and the knowledge according to previous literature.

Regardless of the month, model and country, QDM and Linear scaling perform similarly. Specifically, to our surprise, we find similar performance in the in-season climate drivers. One of the possible explanations is the aggregation level of the indicators. Generally, Quantile mapping-based methods outperform when the target variable is at high temporal resolution, specially daily data (Teutschbein and Seibert, 2012). On the other hand, at monthly scale, simpler methods such the linear scaling can already present high robustness (Moemken and Pinto, 2022; Bayar et al., 2023). As additional caution, it has been shown that quantile mapping can also produce significant pitfalls in the climate signal form the original GCM simulation (Chandel et al., 2024). Notwithstanding this, it is also important to mention that applying bias correction is delicated itself, as it adjusts the statistical distribution of the variable rather than addressing the misrepresentation of physical process associated with it (Maraun et al., 2017). Under this consideration, it is in fact recommended to rely on varios bias correction methods rather than a single one (Laux et al., 2021).

The contributions to changes in yield shock are identified using two complementary approaches. On the one hand, changes in variable distributions are analyzed by focusing on the top predictors from the models. This approach relies on information derived from the Gini index impurity during model calibration. However, it provides a limited perspective, as it faces the causality–casualty dilemma. For instance, in the case of $Tmean$ in February in Romania, both the predictor and the probabilities of yield shock increase, which may suggest a direct relationship at first glance. Additionally, this method overlooks potential shifts in variable importance resulting from changes in the nature of the predictors themselves. Nevertheless, similar to the composite analysis presented in Chapters 6 and

Chapter 7, the dual distribution approach offers an initial overview of the potential drivers behind changes in yield shock risk.

For the challenge presented in this chapter, Shapley values are of great advantage to identify causes of losses (Jones et al., 2022). By using the historical period as a reference, the most important contributors (to both positive and negative changes in crop yield shock risk) under warmer climates are disentangled. The results do not only display similar behaviors (like the ones obtained from Gini index and partial dependence plots in Chapter 7) but also point to other potentially relevant predictors. With the information obtained from Shapley values we learn that the identified key sub-seasonal climate drivers of crop yield shock would remain important in each domain in future climate change scenarios. For example, even thought the increase in winter wheat yield shock losses in Germany can be attributed to warmer conditions in December, the risk of frost damage would remain. Another example is the one from Poland, where the higher temperatures throughout the winter months point towards a diminishment in the chance of losses. The main limitation of Shapley values is the statistical model itself. In other words, this approach can not identify potential drivers when these ones were entirely missing during the training process (Abramoff et al., 2023).

Answer to RQ3

By encompassing the discussion and results from this chapter, RQ3 is answered as follows:

RQ3: How would the risk of maize and winter wheat yield losses vary across Europe in a warmer climate from a statistical modeling perspective?
For maize, based on a GCM–RCM model ensemble under the RCP8.5 scenario, there is only a slight increase in the risk of yield shock along the 21st century. Under GWL2 and GWL3 conditions in the studied domain (France, Romania, and Spain), the low agreement in precipitation signal produces high uncertainty in the probabilities. However, hotter, drier, and higher diurnal temperature range conditions during spring and summer months would still contribute to yield shocks. Furthermore, the expected warmer conditions in September would likely contribute to a lower risk of losses in France and Spain under GWL2 and GWL3.
For winter wheat, the changes in yield shock risk across the studied countries (France, Germany, Poland, Romania, Spain, and the UK) are contrasting. The expected increase in temperature would lead to higher probabilities of yield shock in France, Germany and Romania, but would benefit the suitability in Poland. Warmer conditions in December would contribute to higher risk in France and Germany; in contrast, elevated winter temperatures in Poland and Romania would reduce the probabilities of shock. Expected warmer and drier conditions in the spring months would increase the likelihood of yield shocks across the continent but especially in Romania and Spain. In the UK, as precipitation patterns are projected to remain relatively stable under warmer climate scenarios, no substantial trends are expected in the probabilities of winter yield shock.

With the inclusion of climate model uncertainty and future projections, this chapter disentangles the spatial heterogeneity of crop yield shock changes in a warmer climate. Increasing temperatures expected under GWL2 and GWL3 would have a two fold effect. Warmer temperatures durnig winter months would lead to higher risk of losses in France and Germany, but paradoxically lower risk in Poland and Romania. The warming expected in spring and early summer months would contribute towards higher probabilities of wheat yield shock across the continent. The low agreement in precipitation and diurnal temperature range signal provokes higher uncertainty in maize yield shock probabilities, with solely slight increase in yield shock in France. As in the UK, since summer rainfall patterns are likely to stay similar in a warmer climate, the expected chances of winter wheat yield shocks would probably remain unchanged.

9 Conclusions

This is the concluding chapter of the thesis. It first summarizes the main points of the thesis and the overarching conclusions. Lastly, the chapter discusses the whole work in a holistic framework by highlighting the implications, acknowledging the limitations and the considerations for future research.

9.1 Summary and key findings

Ongoing climate change raises concerns about the suitability of agriculture across Europe. Increasing climate variability, observed in higher frequency and intensity of extreme weather events, has led to stronger drops in crop yield and production (Bednar-Friedl et al., 2022). With statistical and machine learning, it is possible to infer the most relevant climate drivers of substantial crop losses (defined as "yield shock" in this thesis), and thereafter guide stakeholders and policy makers towards ensuring food security and financial stability in the sector (Kalkuhl et al., 2016). For this, the predictors should properly represent climate variability and the model should be sufficiently flexible to capture the non-linear interaction, grounded on adequate validation methods (Greener et al., 2022). At the European level, previous research has focused on individual countries by disregarding a standard spatial comparison, or used process-based crop models, which are prone to underestimating crop failure (Webber et al., 2020). By using statistical modeling, this thesis addresses the spatial heterogeneity of the most important in-season climate drivers of major crops across Europe in present and future climate change scenarios.

On the added value of variable complexity using Least Absolute Shrinkage and Selection Operator compared to Random Forest

The first Research Question (RQ1) is framed on the discussion of variable complexity. The way climate drivers are represented in statistical models is scarcely discussed, specially in the context of substantial losses (Beillouin et al., 2020). Therefore, Chapter 6 disentangles the advantages and disadvantages of using complex-defined variables instead of simple-defined ones in a study case of silage maize yield shock in Germany. For this, we compare two different statistical models. The first one, Least Absolute Shrinkage and Selection Operator (LASSO), is a linear regression-like method that builds a model by seeking the best performance while shrinking the parameters' values to zero. The second one, Random Forest is a highly flexible non parametric model, which is based on an ensemble of classification trees.

The results show that hybrid-based groups of variables enhance predictive accuracy when using LASSO. On the other hand, Random Forest displays high-performance skills regardless of the variable's complexity. The non-linear nature of this method captures more adequately the relationships between weather and climate drivers (without the need for complex variable transformations). Taking this into account, a combination of both cold temperatures during April and high and dry conditions during July increases the chances of silage maize yield shock in Germany. The results from Random Forest also reveal a high chance of silage maize yield shock under cold temperatures in July (which is not captured by LASSO). Historical silage maize yield losses feature particularly high-temperature conditions during July and cumulative cold during April. As a summary, RQ1 can be answered as follows:

RQ1: To what extent does increasing the complexity in the definition of climate predictors improve the performance of silage maize yield shocks predictions in Germany?
When addressing the climate drivers of silage maize yield shock in Germany, LASSO performance improves by considering a combination of both simple-defined and complex-defined input variables.
Conversely, Random Forest models perform consistently well regardless of predictor complexity, highlighting their ability to capture non-linear relationships without relying on complex variables.

On the country-to-country heterogeneity of climate-related crop yield losses across Europe

With the acquired knowledge from Chapter 6, we proceed to the second Research Question (RQ2), focused on the country-to-country comparison across Europe. Most of the literature in the region investigates the impact at individual country (Ben-Ari et al., 2018; Webber et al., 2020), without assessing the spatial heterogeneity across the continent. The only attempt to do this was either by using coarse resolution and tackling seasonal drivers (Zhu et al., 2021) or by using process-based crop models (van der Velde et al., 2018). Chapter 7 employs the Global Data of Historical Yields dataset (GDHY, Iizumi and Sakai, 2020), a hybrid reported yield and satellite-based dataset, to disentangle the spatial heterogeneity of the agricultural impacts across Europe. The most relevant in-season climate drivers of three maize producer (France, Romania and Spain) and six winter wheat producers (France, Germany, Poland, Romania, Spain and the UK) are investigated. For this, an ensemble of Random Forest is employed for each country and crop specifically (9 ensembles in total).

The results illustrate the spatial heterogeneity of the impacts. In particular, maize yield shocks are primarily influenced by precipitation shortage. In France and Romania, the risk mainly increases with drier conditions and a high diurnal temperature range during the summer months; additionally, cold temperatures in May also affect the losses in France. In Spain, maize yield shock are more closely linked to low rainfall during the spring months. For winter wheat, cold, wet, warm, and dry conditions are all relevant in explaining significant losses. Specifically, yield shocks are associated with warm Decembers in France and Germany, cold winters in Romania and Poland, and generally drier

or warmer conditions during the spring months in Spain and Romania. The results also indicate a strong impact of wet conditions and a low diurnal temperature range during June in the UK. Therefore, RQ2 is summarized as follows:

RQ2: What are the country-to-country variations in the in-season climate drivers of maize and winter wheat yield shock across European countries?
Maize yield shock is mostly related to drier conditions across Europe, but the month of occurrence is different, i.e. spring months in Spain and summer months in France and Romania.
Winter wheat yield shock can be associated to temperature variability in center and eastern Europe (France, Germany, Poland and Romania), with warm, cold winters and warm early summer months being equivalently crucial; Spain is subjected to dry conditions in the spring months, while in the UK it is mostly driven by high rain in June.

On the future climate change influence on crop yield shock variability from a statistical modeling perspective

The Research Question 3 (RQ3) assesses the future impact of climate change on crop yield shock across Europe. The suitability of agriculture in Europe under warmer climate scenarios is primarily addressed in the context of crop yield variability, often using process-based crop models (Webber et al., 2018; Bednar-Friedl et al., 2022). Using the statistical models developed in Chapter 7, it is possible to evaluate how a warmer climate alters the expected probabilities of yield shocks and their potential drivers. This analysis uses a set of eight Global Climate Model–Regional Climate Model (GCM–RCM) chains developed under CMIP5 and downscaled through EURO-CORDEX. The focus is on examining how long-term crop yield shocks vary under 2 °C and 3 °C warming scenarios (GWL2 and GWL3 respectively), along with identifying the most relevant in-season drivers.

The results, presented in Chapter 8, reveal contrasting responses depending on the crop-country combination. For maize yield shock, low agreement among models regarding precipitation signals results in greater uncertainty and weak trends in the risk of losses. Despite this, drier conditions would remain as main driver of losses under GWL2 and GWL3. For winter wheat, yield shock probabilities increase in France, Germany, Romania, and Spain, while remaining unchanged or showing a decreasing trend in Poland and the UK. As the average monthly temperatures are expected to increase in the future (with high agreement between models), the chances of cold temperature impacts would probably decline, particularly in Germany, Poland, and Romania. However, this would also lead to higher losses in France and Germany due to warmer temperatures in December. Furthermore, higher temperatures during spring and early summer months are projected to increase the probabilities of losses across most of the continent. For the case of Spain and the UK, the low agreement in precipitation signal leads to unchanged average probabilities of loses.Based on these findings, RQ3 is answered as follows:

RQ3: How would the risk of maize and winter wheat yield losses vary across Europe in a warmer climate from a statistical modeling perspective?
For maize, the low agreement in precipitation signal produces high uncertainty in the underlying yield shock probabilities for France, Romania and Spain.
In the case of winter wheat, the expected increase in temperature would lead to higher probabilities of yield shock in France, Germany and Romania, but would benefit the suitability in Poland. In Spain and the UK, the low consistency in precipitation patterns results in little to no change in the average probability of losses.

This thesis addresses the limitations of statistical modeling in agricultural meteorology and establish a fairly robust comparison of in-season climate drivers of major crops yield shock across Europe. **Therefore, the overall conclusions of this thesis are:**

- **Effective statistical modeling of crop yield losses from in-season climate drivers depend on both variable definition and model flexibility. Linear models like LASSO benefit from using complex predictor definitions, while non-linear models such as Random Forest can capture key interactions using simpler variables.**
- **With the GDHY and statistical models, it is possible to assess the impact of in-season climate variability on major crop losses. The information is important for understanding the historical agricultural failures across Europe and to assess potential drivers in future climate change scenarios.**
- **Maize yield shocks across Europe are largely driven by dry conditions, with regional differences in the month of impact. In France and Romania, losses are primarily associated with low summer months precipitation, while in Spain they are linked to dry conditions in spring months. Uncertainty in future precipitation projections under climate warming makes trends in maize yield risk difficult to determine.**
- **Winter wheat yield shocks can result from warm, cold, dry, or wet conditions, underscoring the importance of regional climatology in impact assessments. Future changes in losses are mainly driven by temperature trends. Warming in northern and eastern Europe (Germany, Poland, and Romania) may lower frost risk and improve crop suitability but could also interfere with vernalization, particularly in France and Poland. At the same time, rising temperatures in spring and early summer are expected to increase yield shock risk across the continent.**

9.2 Discussion, implications and outlook

The results have implications for several sectors, which are discussed below. The findings contribute towards better adaptation decisions for buffering short- and long-term

climate change impacts on agriculture. This section additionally addresses the challenges presented throughout the study and proposes feasible pathways for overcoming them.

As agriculture entails socio-economic decisions, addressing only the impacts from climate drivers can be limiting. The way this thesis applies statistical modeling is by partially assuming some physical understanding on the impacts. This is reflected in the use of several climate indicators spamming the crop cycle rather than focusing on the most studied ones like drought or heatwaves. This approach validates the models by considering our physical understanding and allow space for unexplored links between the chosen climate predictors and crop yield shock (Tredennick et al., 2021). However, we are also disregarding potential non-climatic stressors such as vulnerability, agricultural decisions (e.g. fertilization, cover crops) or the economic-political context (Kinnunen et al., 2022; Teixeira et al., 2023). Thereafter, future research pathways would benefit from integrating political decisions and socio-economical factors to the agricultural model (Ziv et al., 2020).

As mentioned above, the key climate drivers of yield losses identified by the statistical models match the most sensitive stages of maize and wheat. For the case of maize, low precipitation conditions during summer months in France, Germany and Romania enhance the risk of losses, which roughly coincide with flowering dates in each country (Olesen et al., 2012). Consequently, maize could benefit in these regions from implementing irrigation systems that would mitigate both the dry and potentially warm temperatures of summer (Huynh et al., 2019; Parent et al., 2018). This would remain true also for future climate change scenarios, even thought the precipitation trends are contrasting between models (Bednar-Friedl et al., 2022). Conversely, in the case of Spain, prolonged drought are expected under warmer climate, questioning the actual water available for irrigation (Rodríguez Díaz et al., 2007). This can also lead to higher costs in irrigation and would compromise the decision from farmers in cultivating. In this sense, water reservoir management for irrigation systems are currently being explored, which would potentially mitigate the impact of drought in agriculture (Ho and Ehret, 2025).

In the case of winter wheat, by tackling each country individually, the results obtained in this thesis suggest considering specific adaptation measurements. Winter wheat has a longer season than maize, and consequently, it is exposed to more stressors. The crop does not benefit from either extreme low or high temperatures during winter as it requires cold exposure for later blooming (vernalization) and is yet affected by frost. The higher temperatures expected in winter in France and Germany, two of the top wheat producers worldwide, would likely disrupts vernalization, which questions the suitability of winter wheat under warmer climate (Martin et al., 2025). This does not hold true to Poland that, conversely, would benefit from lower risk of frost and opens new opportunities to stakeholders. Generally speaking in terms of temperature, northern regions are expected to be higher suitable than southern regions, which opens new opportunities for stakeholders (Trnka et al., 2011). However, other adverse weather extremes like early heatwaves are expected to increase in the north (Trnka et al., 2015). This would require to explore alternative adaptation measurements (as it is discussed below).

One way to adapt towards climate resilient cropping systems are by introducing new crop varieties. For centuries, farmers have chosen the most optimal varieties for the average

environmental conditions of their land (Bradshaw, 2017). This is today obtained by intensive breeding, where shorter growing season length, higher environmental stress tolerance and higher yield varieties are sought (Mao et al., 2023; Atlin et al., 2017; Bradshaw, 2017). Thereby, one option for climate adaptation is the choice of the adequate crop variety for the upcoming new environmental condition (Olesen et al., 2011). For example, maize yield across Europe can substantially increase with shorter cycle varieties, keeping the crop away from summer heatwaves and prolonged drought exposure (Parent et al., 2018). Moreover, farmers would then avoid the use of costly irrigation systems (García-Garizábal et al., 2014). In the case of wheat, we observe strong heterogeneity in the stressors across Europe. In France and Germany, reduced-flowering time varieties (with lower vernalization requirements) could alleviate the impacts of warmer winters (Kamran et al., 2014). In Romania or Spain, the focus should be on higher heat and drought tolerance varieties (Xynias et al., 2020; Bednar-Friedl et al., 2022). Furthermore, breeders should contemplate potential diseases proliferation, which are expected to increase under warmer climate (Miedaner and Juroszek, 2021).

It is important to mention that, when this thesis discusses crop suitability, it does not consider land use and soil properties. On the one hand, as previously mentioned, warmer and wetter conditions in northern Europe opens new opportunities for stakeholders in these areas. Specifically in Chapter 8 we find that wheat yield shock risk would remain stable or diminish in future climate in Poland and the UK. On the other hand, isolating these factors can be challenging since soil properties and land use should also be addressed. In this sense, it has been shown that some crops, like wheat, are mostly cultivated under marginally suitable areas, and expansion is constrained by wooden and grass lands (Dornik et al., 2024). With increasing land protection policies, extensive agricultural practice would rather be limited (Köninger et al., 2022; Boix-Fayos and De Vente, 2023). In this case, exploring sustainable intensification or climate-smart agricultural practices (for instance crop rotation) could enhance land productivity (MacLaren et al., 2022). Another factor to consider is soil erosion. With likely higher precipitation in northern areas, soil erosion (produced by water) would increase, leading to soil loss and reduced land suitability (Panagos et al., 2021). Therefore, future research on land suitability should also encompass soil property changes as well as the policy aspects of land use.

Additionally, the findings of this thesis can benefit the insurance sector. In the first place, farmers could ensure financial stability by purchasing specific weather-index insurance (Bucheli et al., 2023). This type of insurance is tailored to specific weather extremes; it has lower costs than traditional indemnity insurance and helps avoid moral hazard issues. Weather index insurance can increase the economic stability of farmers by obtaining coverage from specific weather extremes. A practical example comes from eastern Germany, where a pilot heat index insurance designed for wheat and oilseed rape farmers reduced financial risk by approximately 20% by using hourly temperature data during key growth phases (Bucheli et al., 2022). Despite a weather-index insurance market in Europe, some weather and climate extremes are underrepresented (Bucheli et al., 2022). However, it is also true that, with higher risk of losses, farmers' willingness to pay would be compromised by potential higher premium values (Zhllima et al., 2025). This could be compensated by new governmental subsidies that would enhance ensure economic stability (Bednar-Friedl et al., 2022).

The developed models in this thesis could enhance agricultural seasonal forecast systems (van der Velde et al., 2018). The Joint Research Center (JRC) of the European Commission (EC) makes in-season forecast of expected crop yield by using Crop simulation Models (CSMs) and parametrtic statistical models (van der Velde et al., 2018). Thus, on the one hand, the obtained results can serve as guidance for improve process-based crop simulation models, which are thereafter used for forecasting (Webber et al., 2020). The other alternative is to consider the statistical models of this thesis as forecast tools themselves. Subsequently, a future step of this thesis is to explore the predictability skill of the Random Forest models by using seasonal forecast meteorological data, for example like the one developed by the European Centre for Medium-Range Weather Forecasts (ECMWF, Hersbach et al., 2020).

Moreover, this thesis presents some methodological limitations that should be mentioned. By using a small set of well-defined predictors, the Random Forest models already capture key weather hazards associated with yield shocks. This highlights the usefulness of flexible models that rely on broadly defined indicators of climate extremes. However, despite the range of definitions explored in Chapter 6, some important stressors remain unaddressed. For example, the current indicators do not explicitly account for evapotranspiration, which is critical for understanding water availability, atmospheric demand, and plant health (Allen et al., 1998; Murphy and Hurtado, 2020). Another overlooked factor is hailstorms, which are among the most damaging localized weather hazards and can cause severe yield losses (Kunz et al., 2018). Although Chapter 6 does not include these stressors directly, some of their effects may be indirectly captured. Variables such as temperature, diurnal temperature range, or cumulative precipitation are often correlated with the omitted ones. However, dealing with such co-linearity is complex. Several statistical methods exist to address this challenge (Shi et al., 2013). To reduce redundancy among input variables, future work could consider the use of combined stress indices. One example is the integrated drought and heat stress metric proposed by Zampieri et al. (2017). This type of approach could improve both model performance and interpretability

On the other hand, the thesis could benefit from a more universal-based input approach, meaning the use of several domains in conjunction (Kratzert et al., 2019). The rationale behind this method is to overcome the limitations of Random Forest in extrapolating data. This constraint explains why the individual models in Chapter 7 do not adequately capture extreme weather events, and why the trends in crop yield risk do not exceed an average of 10% in Chapter 8. In fact, for prediction tasks that require extrapolation, simple models can outperform complex black-box models by approximately 40% (Lakshminarayanan et al., 2017; Muckley et al., 2023). Even when using country-independent models, one way to mitigate this issue is to train the model on diverse datasets and domains (Kratzert et al., 2019). However, this approach should also account for the phenological stages during which crops are exposed to specific climate events, rather than relying on Gregorian-calendar–based aggregated indices. Additionally, the contrasting climatologies that ultimately led to the development of divergent crop varieties could limit the predictability of the models (Zampieri et al., 2017; Lima et al., 2021). These considerations could offer a more accurate assessment and potentially enhance our understanding of the impact of extreme weather events on crop yield.

The results from this thesis would presumably improve by using a wider and new generation of models and datasets. Chapter 6 and Chapter 7 are based on the version 23.0e and 27.0e of the ensemble mean of E-OBS, when the recently released 31.0e includes a higher amount of stations in the interpolation (European Climate Assessment & Dataset, 2024). The results obtained from Chapter 8, based only on eight RCM-GCM model, can be enhances by using a wider model ensemble (Moemken et al., 2018). Furthermore, CMIP6 and CORDEX-based downscaled models are currently in development and expected to become available soon (Katragkou et al., 2024). With updated parametrizations, data input and inclusions of more sources of emission variability like aerosol forcing, CMIP6 showed higher independence between the Shared Socio-economic Pathway and GCMs (Chen et al., 2023). Therefore, this would expand our physical understanding on the impact under warmer climate, but would also likely increase the uncertainty in some regions (Zhang and Chen, 2021).

As a final point, future research should expand its focus to include the impact of climate extremes on non-staple crops (Bednar-Friedl et al., 2022). While maize and winter wheat, along with soybean and rice, are vital for global food security, other crop groups such as fruits and vegetables are equally important for human dietary health (Slavin and Lloyd, 2012). Despite their nutritional and economic significance, the effects of extreme weather events on these high-value crops remain underexplored (Cogato et al., 2019). A major concern regarding this area is the limited availability and quality of crop-specific data (European Commission – Directorate-General for Agriculture and Rural Development – Unit A.3, 2023). As the economic value and dietary relevance of non-staple crops continue to grow, improving our understanding of their vulnerability to climate variability will be critical for developing resilient agricultural systems.

In summary, this thesis shows the sensitivity of predictor and statistical model choice when assessing weather and climate drivers of agricultural losses. The refined models provide insight into the most relevant national weather and climate drivers of yield shock. Ultimately, the information of this thesis contributes towards agricultural adaptation to climate change.

Acknowledgment

(Warning: There are sentences that I wrote in Spanish. I found that to be more personal.)

I met a lot of people during this journey who, in one way or another, have contributed to completing this milestone in my life. Most importantly, it is not possible at all to disentangle the PhD experience from my personal realizations. I will try to recall each of you.

The first person I would like to thank is Olga, my bachelor-master supervisor, who encouraged me to pursue a PhD abroad and to try again after the first attempt. I am grateful to the Prague community, especially Toly and Thilo, who made my wait totally pleasurable.I also want to thank Veronica and Gerardo, who were the first to introduce me to the country.

I have to say that my first months in Karlsruhe were, for lack of a better word, incomprehensible. Still, I fondly remember the time spent with Paul, the late lunches with Antonio, *Dani y nuestras noches de ping-pong*, Katharina and our early complaints, and of course Hannah M., who was extremely important in my first months. *Obviamente destaco el tiempo compartido con Fede W. y Seba.* You were crucial in making me feel comfortable in this new place. Thank you.

Some people within the professional environment have accompanied me throughout these four years. I cannot close this thesis without thanking my EDIPI colleagues: Aleksa, Anastasiya, Anupama, Bianca, Emma, Ferran, Inovasita, Jamie, Mireia, Sohan, Thessa, Valeria, and Vinita. One of the best parts of the PhD was interacting with you in each training. I was inspired by your decisions, personalities, independence, and persistence beyond personal and even political challenges. Looking back, I acknowledge how lucky I was to share time with you. I appreciate it a lot! I also want to express my gratitude to my office colleagues and former colleagues, including Praveen, Ting-Chen, Armenia, Eleonora, Magdalena, Marie, and Andrea, for the many conversations and valuable advice at different stages of my PhD. Lastly, I want to thank Tatiana. I think you had to swallow most of my falls, and you were there in one of the most difficult times of my PhD and personal life. Thanks for listening and for holding space during those moments.

I would also like to thank my secondment hosts in Zurich. First, I thank Reto for providing me with the space to learn about the insurance and reinsurance sector. Just so you know, my first time in Zurich was a sharp turn in my personal path. I also want to thank Luka and Sonia, two people with the most outstanding knowledge I have ever met.

I am extremely grateful to all the people I met within the music and roommates community in Karlsruhe. Jamming with Tarik, Latif, and Max in the park always lifted my mood. It was magical to spend time with you, guys. I also want to express my gratitude to Hannah K., Matteo, Simone, Rene, Tabea and Hannah B., who were always open to share valuable time and helping me feel more at home.

Quiero agradecer a toda la banda argentina, chilena y colombiana de Karlsruhe. Pienso en la música, mates, fasos, charlas y cafés que compartí con Juan, Chine, Rulo, Luca, Sara, Tobi Luisa, Lina, Marisol, Steffan, Cata, Vicente y Jorge; me han dado un gran soporte emocional en todos estos años. Entre los mencionados, hay gente de lo más "manijas", aventureros, humildes e inspiradores, que me mostraron distintas perspectivas de vida, me escucharon y me levantaron el ánimo en muchos momentos. También quiero darle las gracias a Lisandro, que estuvo desde el principio hasta el final del viaje acompañándome y fumándose mis quejas; gracias por los mates y la buena onda.

Agradezco profundamente todo el apoyo que tuve, de forma remota y presencial, desde Argentina. Esto incluye a mi familia: Ariel, Viviana, Gus, Marce, Raquel, Horacio, Bren, Noe, Feli, Marco y, por supuesto, Pierito. Quiero agradecer especialmente a Viviana por todo su apoyo en la etapa más difícil del doctorado, y a Ariel por su incondicional expresión de amor, cariño y escucha. Agradezco de corazón a todo el grupo de agrometeorología y a Vane P. por sus consejos y su perspectiva profesional. También agradezco a Winter, Alexander, Alex, Santi, Jessi, Meli, Mechi, Tomi, Juli, Mati, Eze, Ari Jaki y, por supuesto, a Anahí P. Con algunos tuve largas charlas a lo largo de los años, mientras que otros me ayudaron en momentos muy cruciales del proceso. Quiero agradecer especialmente a Ivo, con quien compartimos largas charlas personales en los lugares más recónditos de la Patagonia. Por último, quiero reconocer profundamente el trabajo de Cecilia, quien me acompañó en un proceso de desarrollo personal que nunca habría imaginado.

Lastly but most importantly, I would like to acknowledge my supervisors and advisors. First, I thank Julia, my informal but main supervisor in my first years. I think that you had the most difficult task and I want to profoundly acknowledge your effort and commitment. I also want to thank you for listening and for your outstanding patience. I would also like to thank Alex. Though it was originally never your task, you accepted being my advisor in the last stage of my PhD. I believe your pragmatism and determination were crucial in helping me finish my thesis. And finally, I thank my main supervisor, Joaquim. I believe I learned a lot from you and your philosophy of working and I could see my development thanks to your advice. I think this PhD was challenging. But we made it.

Appendices

A Appendix to Chapter 4

Figure A1: Series of reported national data extracted from FAO (FAO, 2024a). Total production (top panel), total harvested area (mid panel), and average yield (bottom panel) for the 8 biggest European maize producers (in colours).

Bayesian Information Criterion

The Bayesian information criterion (BIC) is defined as:

$$BIC = 2 \times loglik + log(N) \times k \tag{A.1}$$

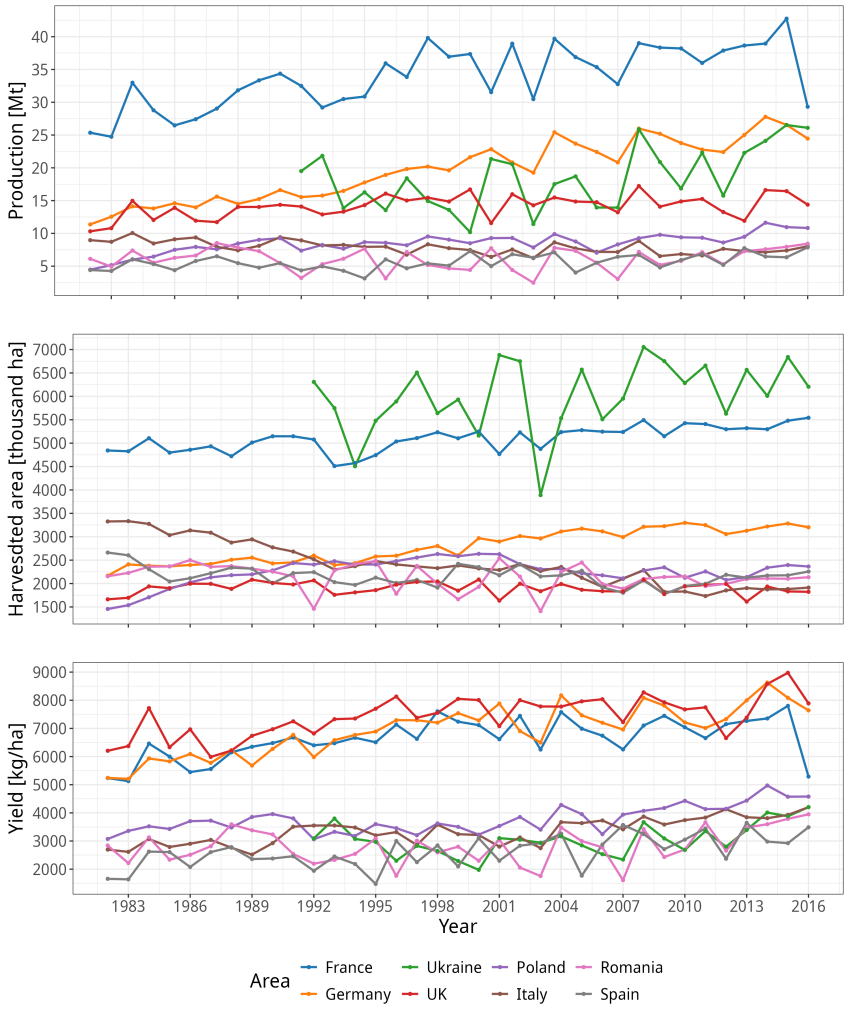

Figure A2: Same as Figure A1, but for winter wheat.

Where *loglik* refers to the log-likelihood (Section 2.4), k is the number of predictors and N is the number of observations.

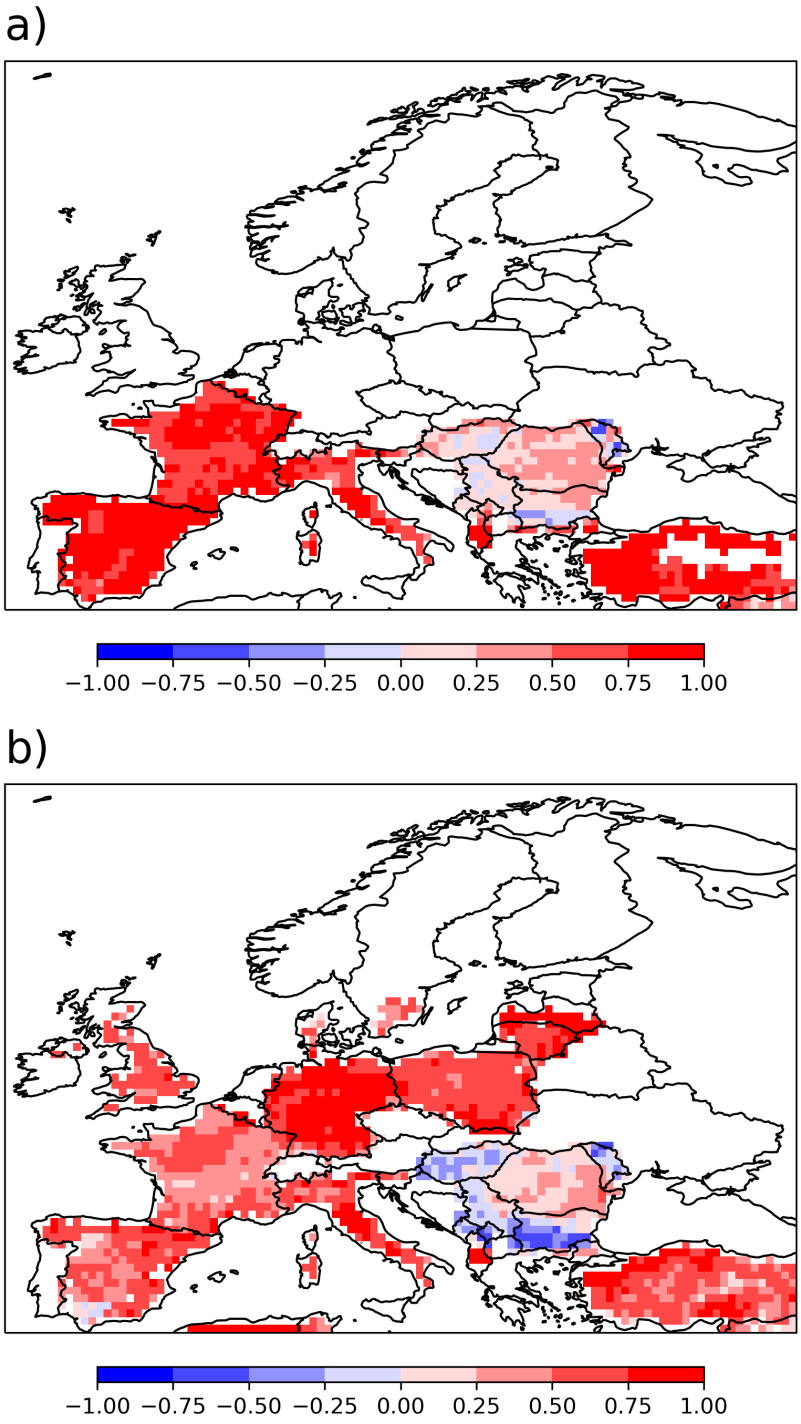

Figure A3: Pearson correlation between time series and yield for maize (a) and winter wheat (b) yield series, using the GDHY for the 1982-2016 period.

B Appendix to Chapter 6

Table B.1: Coefficient values for each predictor per model in LASSO. Variables are sorted by decreasing absolute value. The number on the left side of the underscore corresponds to the month.

Simple		**Frequency**		**Cumulative**		**All**		**Forward**		**Backward**	
07_TX	3.80	07_TX90p	1.82	07_TX90pDD	1.63	07_TX90p	1.62	07_TX90p	1.93	07_TX	2.51
07_PP	-1.95	07_PPlt1	1.74	07_SPltn05	-1.10	07_TX	1.19	07_PPlt1	1.55	07_PP	-1.63
09_TN	-1.05	04_TN10p	0.75	04_TN10pDD	-1.08	07_PPlt1	1.05	07_TX	1.36	04_TN10pDD	-1.21
04_TX	-0.65	06_PPlt1	0.62	08_SPltn05	-0.67	04_TN10pDD	-0.94	04_TN10pDD	-1.19	07_TX90p	1.16
08_PP	-0.51	08_PPlt1	0.61	05_TN10pDD	0.60	06_PPlt1	0.61	08_PPlt1	0.82	05_TN10pDD	0.94
05_TN	0.43	08_TX90p	0.28	06_SPltn05	-0.45	08_PPlt1	0.60	05_TN10pDD	0.72	04_TX90pDD	0.87
04_PP	-0.41	05_TN10p	-0.17	05_SPgt05	0.44	05_TN10pDD	0.52	06_SPltn05	-0.48	05_TX	-0.83
08_TX	0.38			08_TX90pDD	0.34	05_SPltn05	-0.47	08_PP	-0.38	04_SPltn05	0.82
05_TX	-0.34			09_TN10pDD	-0.25	05_SPgt05	0.43	05_SPltn05	-0.36	05_SPltn05	-0.81
09_TX	-0.27			05_SPltn05	-0.16	07_SPltn05	-0.41	09_TX	-0.33	04_PP	-0.72
06_PP	-0.20			04_SPltn05	0.06	08_SPltn05	-0.32	06_TN10pDD	0.30	08_SPltn05	-0.72
						08_TX90pDD	0.29	04_PP	-0.27	06_TN10pDD	0.54
						06_SPltn05	-0.24	07_PP90p	-0.21	04_TX	-0.47
						09_TX	-0.21	05_TX	-0.09	06_SPltn05	-0.44
						06_TN10pDD	0.20			08_TX	0.31
						07_PP	-0.19				
						04_PP	-0.15				
						09_TN10pDD	-0.10				
						04_TN10p	0.08				
						04_TX	-0.07				
						08_PP	-0.01				

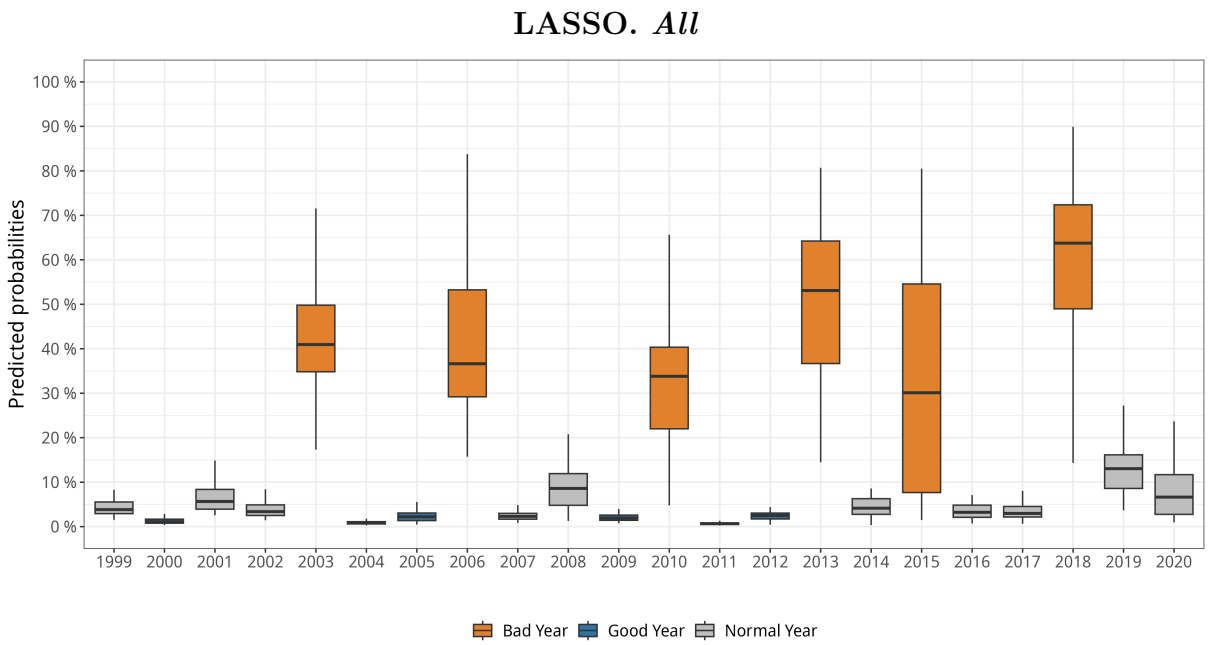

Figure B1: Year-to-year distribution of the predicted probability in group *All* using LASSO. Orange-coloured boxplots correspond to the six bad years and blue-coloured to the six good years.

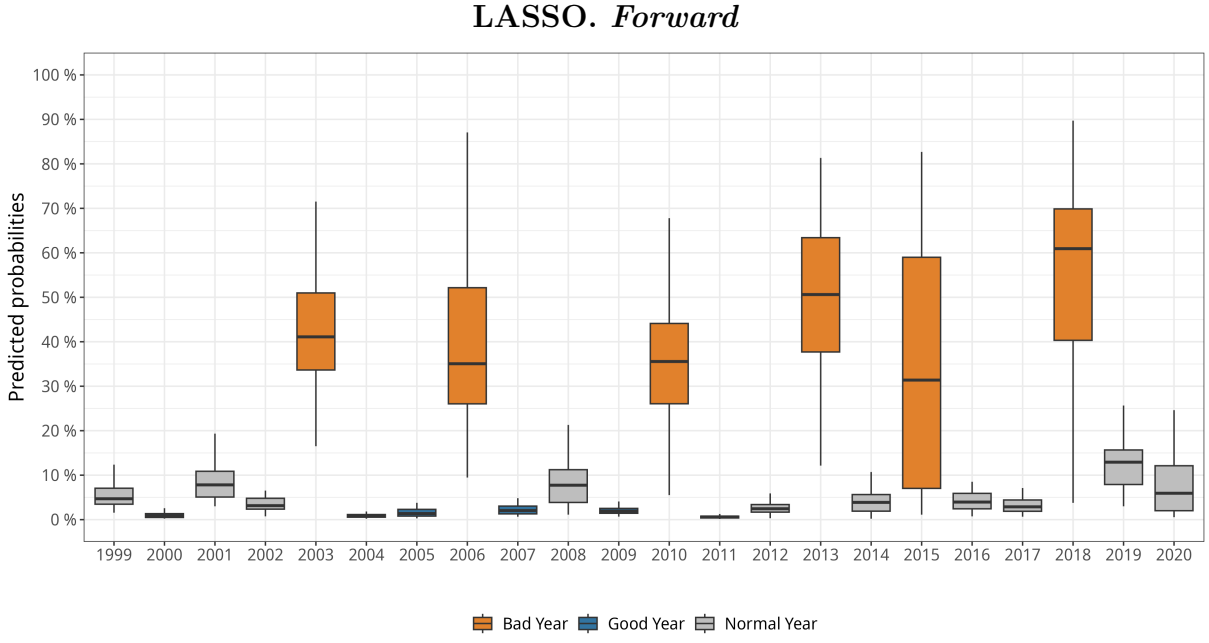

Figure B2: Same as Figure B1, but for group *Forward*.

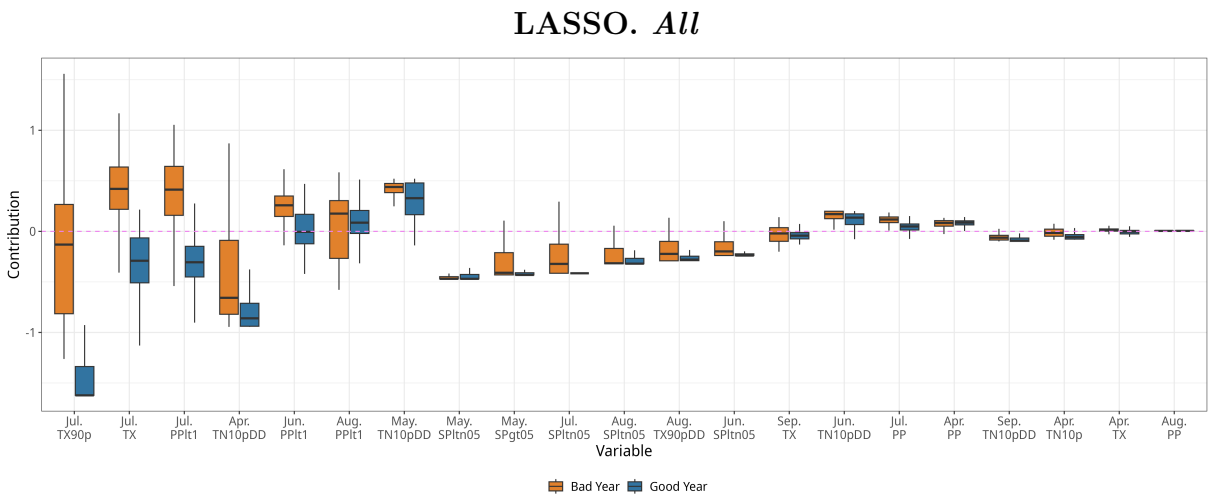

Figure B3: Composite distribution of the variable contribution to the predicted probabilities in *All* group. The variables in x-axis are organized by absolute coefficient values (as in Table S1). The dashed-horizontal violet line indicates a "null contribution". Composites were made using the six bad years (orange-coloured boxplots) and the six good years (blue-coloured boxplots).

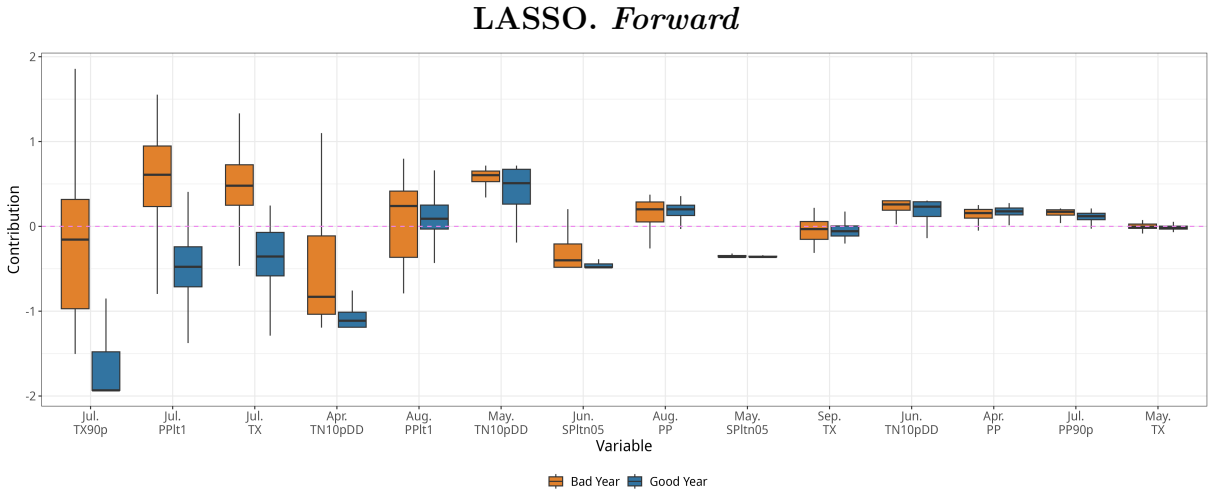

Figure B4: Same as Figure B3, but for group *Forward*.

Table B.2: Worst years predicted (in descendent order) for the six groups obtained by using Random Forest.

Simple	Frequency	Cumulative	All	Forward	Backward
2013	2018	2013	2013	2018	2013
2018	2013	2018	2018	2013	2018
2010	2003	2003	2003	2003	2003
2003	2010	2010	2010	2010	2010
2006	2006	2006	2006	2006	2006
2015	2015	2015	2015	2015	2015

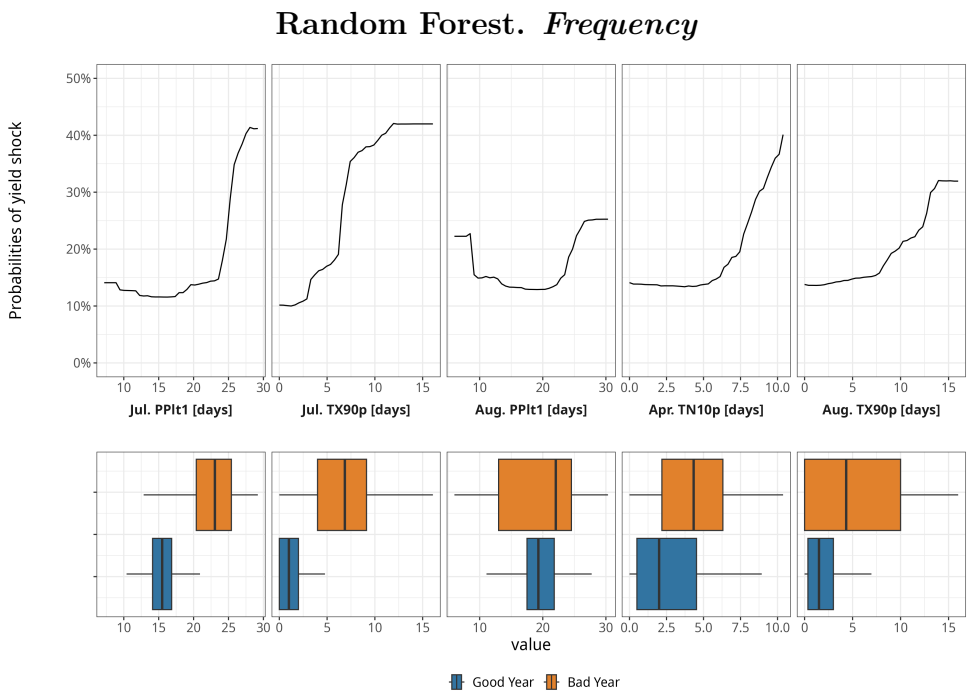

Figure B5: (top row) Partial dependence plots for the top 5 predictors for group *Frequency* and (bottom row) the associated variable distribution during good years (blue) and bad years (orange).

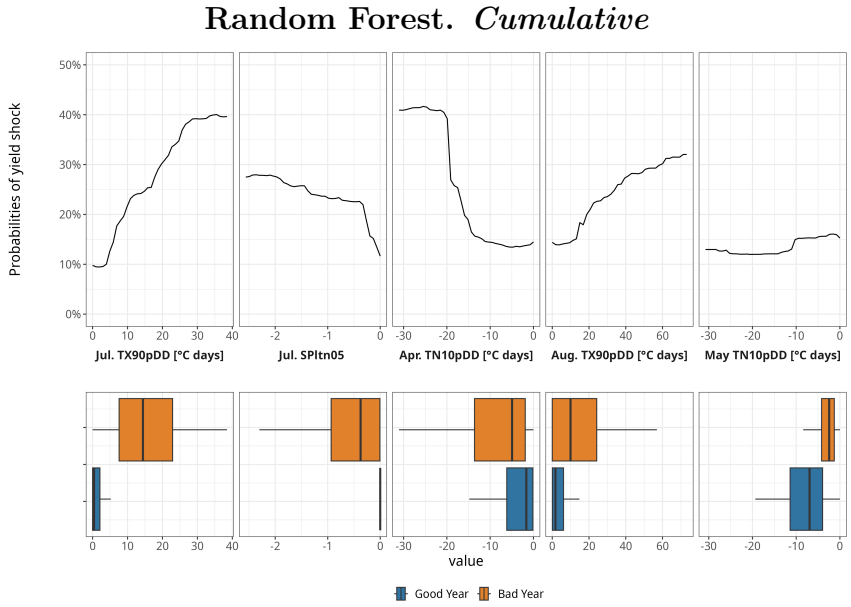

Figure B6: Same as Figure B5, but for group *Cumulative*.

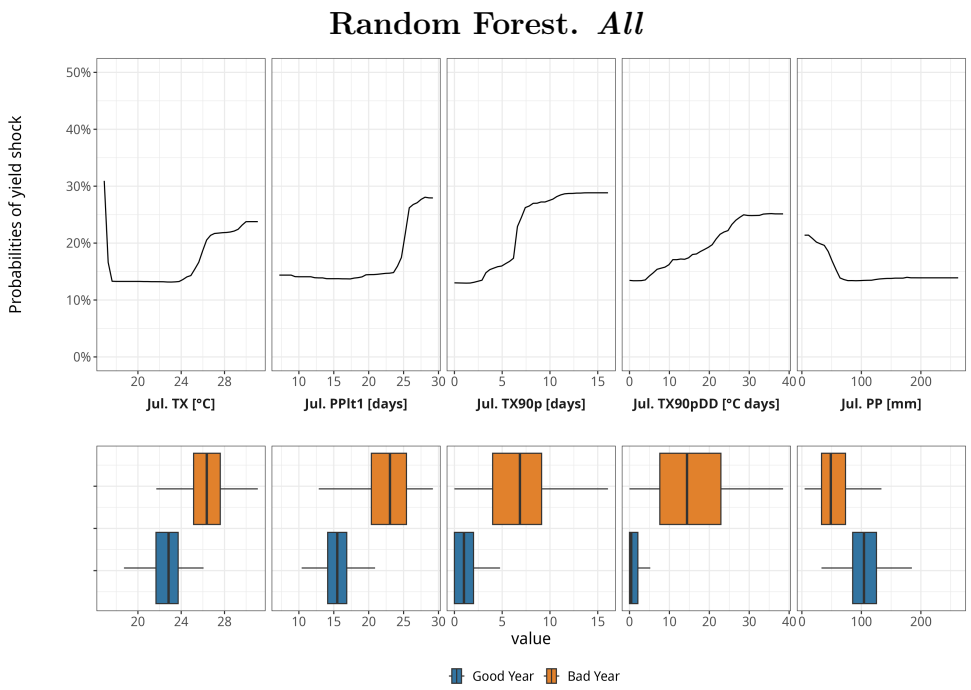

Figure B7: Same as Figure B5, but for group *All*.

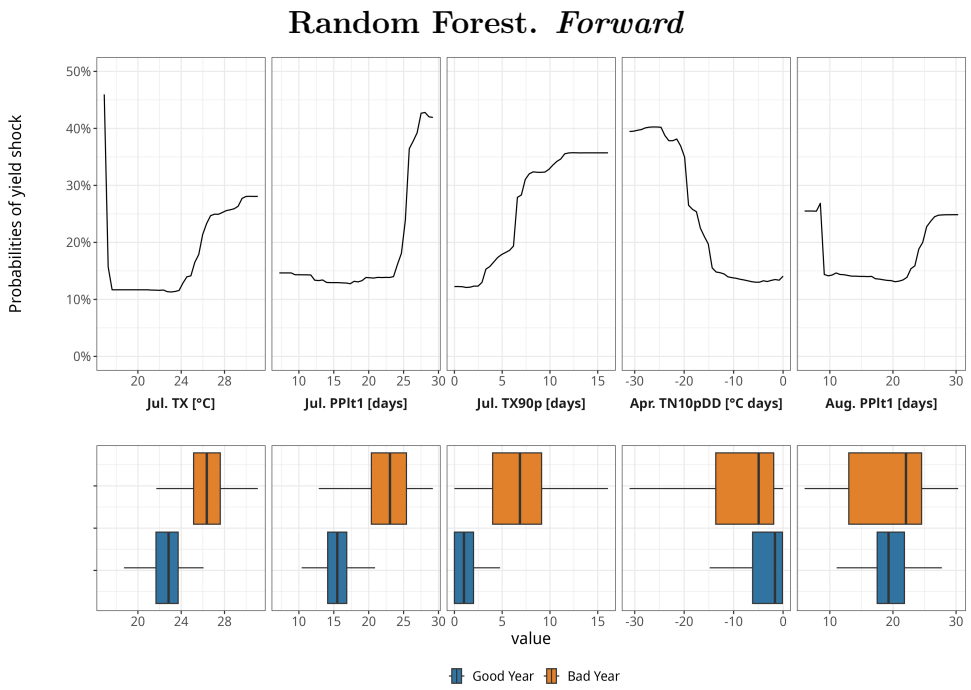

Figure B8: Same as Figure B5, but for group *Forward*.

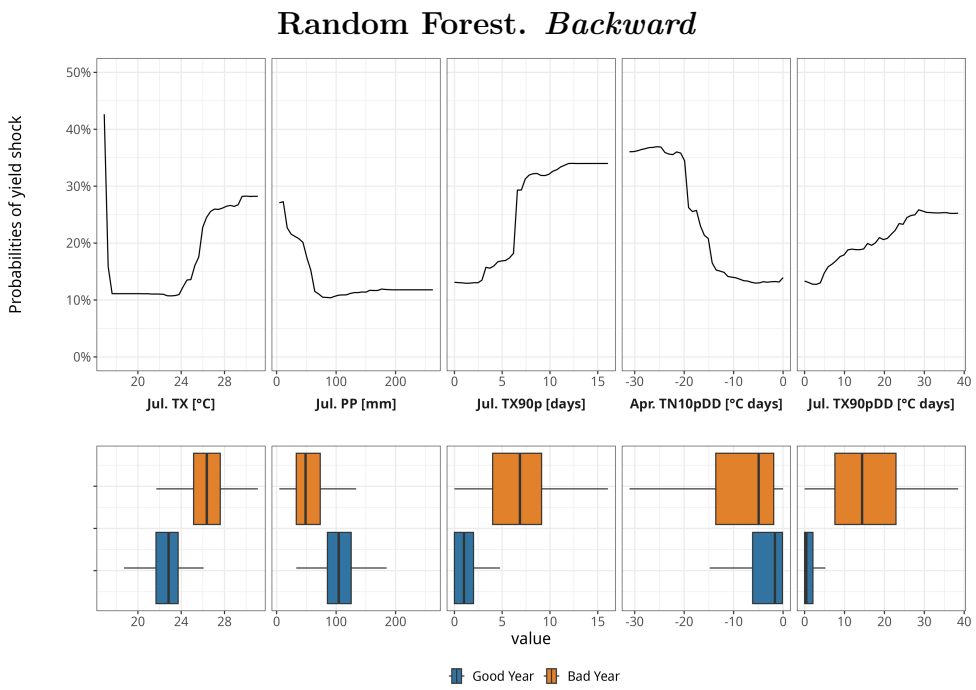

Figure B9: Same as Figure B5, but for group *Backward*.

C Appendix to Chapter 7

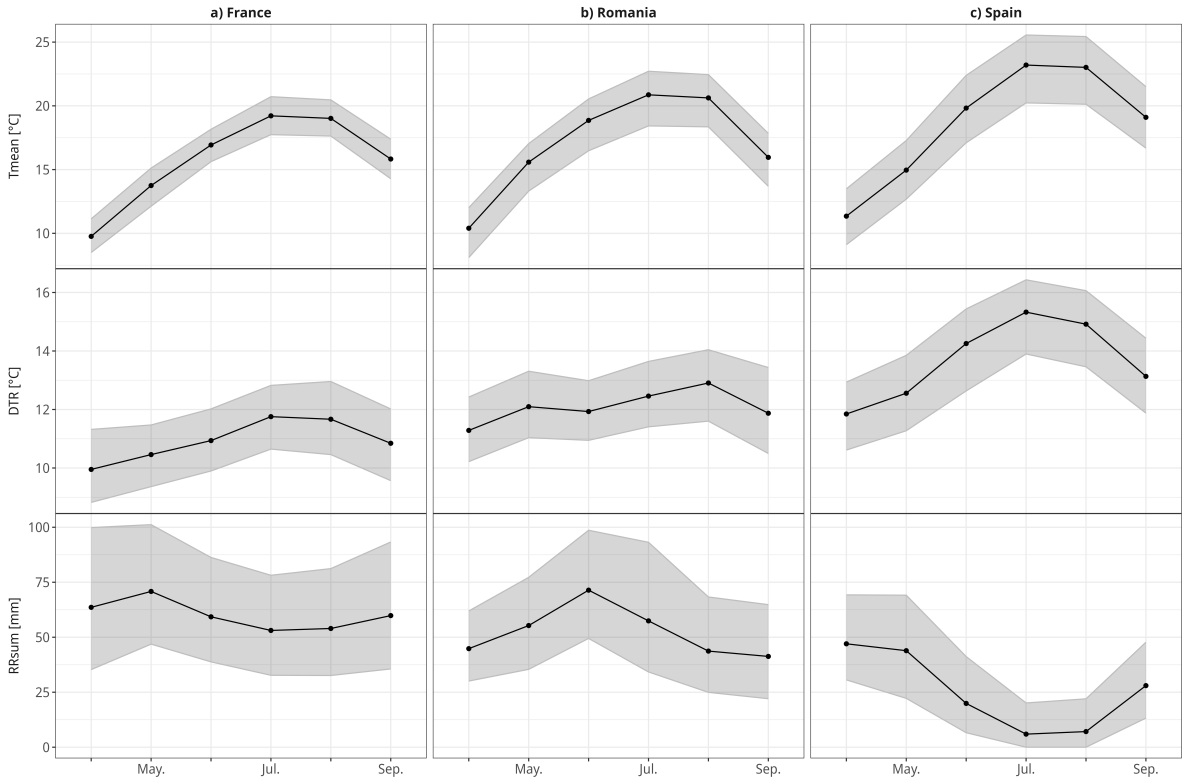

Figure C1: Series of median (opaque lines) and interquartile range (shade) for the three climate indicators (in rows) along the three countries (in panels).

Climatology of selected predictors for studying maize yield shock in France, Romania and Spain

We provide a climatological description of the selected weather and climate indicators only for France, Romania and Spain.

Figure C1 displays the climatology of the selected weather and climate drivers of maize yield shock by month (x-axis), type (in rows) and country (in columns). $Tmean$ follows the seasonal variability, with a progressive increase from April, reaching peak values in July and August and dropping in September. The three countries present values around 10 °C in April. Spain (Figure C1c) has the highest values of $Tmean$ in the summer months (with $Tmean$ over 20 °C), followed by Romania (Figure C1b) and finally by France France

(Figure C1a), where $Tmean$ reach values between 10 °C and 20 °C in the summer months. Additionally, Spain tends to have higher uncertainty (i.e., a higher interquartile range) within the sub-seasonal scale than other countries.

Similar to $Tmean$, in Figure C1, we observe that DTR tends to be higher in the summer months than in the spring months. France and Romania present relatively low variability of DTR throughout the selected months, with values ranging between 4 °C and 7 °C in April and September for both countries and with values around 6 °C for France and 8 °C for Romania in the summer months. Spain presents the highest DTR values throughout the selected months and the highest intermonthly variability. DTR has values of around 7 °C in April and can reaches overall values of 11 °C in July.

The behaviour of $RRsum$ is rather country-specific. However, we observe overall higher values in spring months than in the summer months. France has a stationary pattern, with median values between 50 mm and 75 mm, with the highest values observed during May (between 50 mm and 100 mm). Romania presents slightly higher seasonal variability, with peak values of $RRsum$ in June and the lowest values in August and September. Spain has the lowest overall precipitation, with $RRsum$ values oscillating between 50 mm in April and dropping to almost null values in July and August.

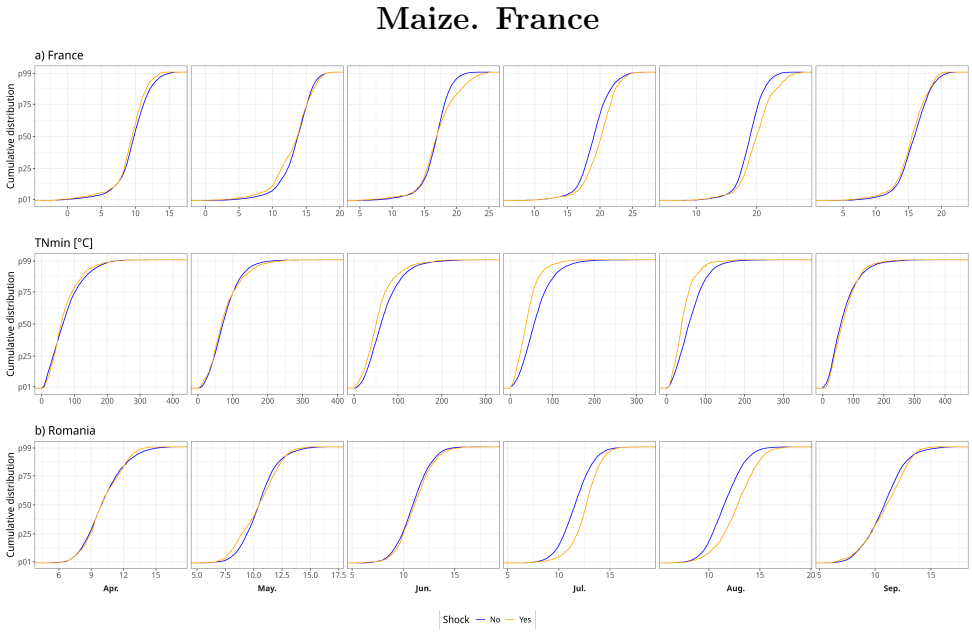

Figure C2: Cumulative distribution for the selected predictors during yield shock (orange) and no yield shock (blue) in France.

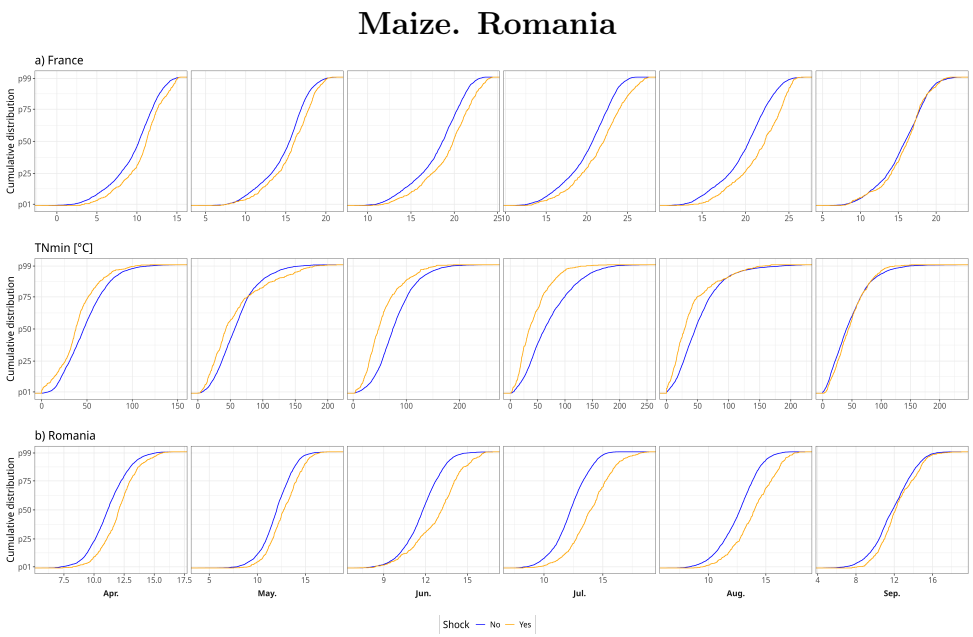

Figure C3: Same as Figure C2, but in Romania.

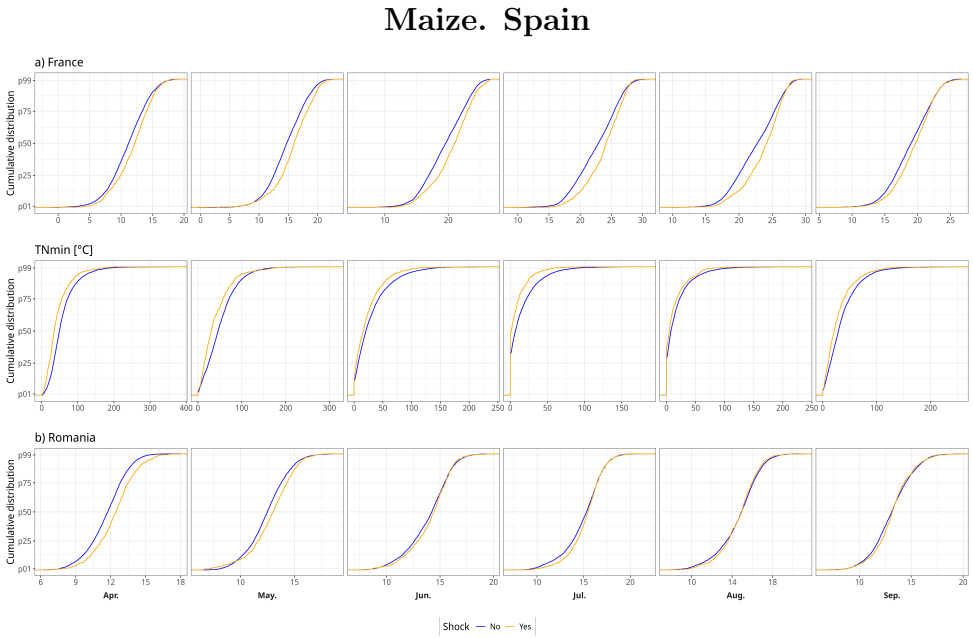

Figure C4: Same as Figure C2, but in Spain.

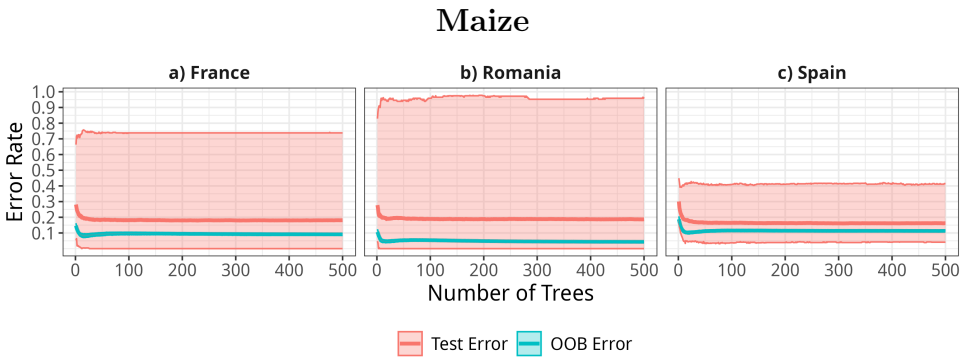

Figure C5: Error rate and test error as a function of number of trees for the ensemble of Random Forest models per country (in panels), using the maize yield shock data. The solid lines denote the average value between the models, and the shades represent the uncertainty range by using the 5^{th} and 95^{th} percentile. The OOB error (turquoise) is built by the Out-Of-Bag (OOB) sampling method (James et al., 2021), and the test error (red) is built by using the leave-one-year-out data.

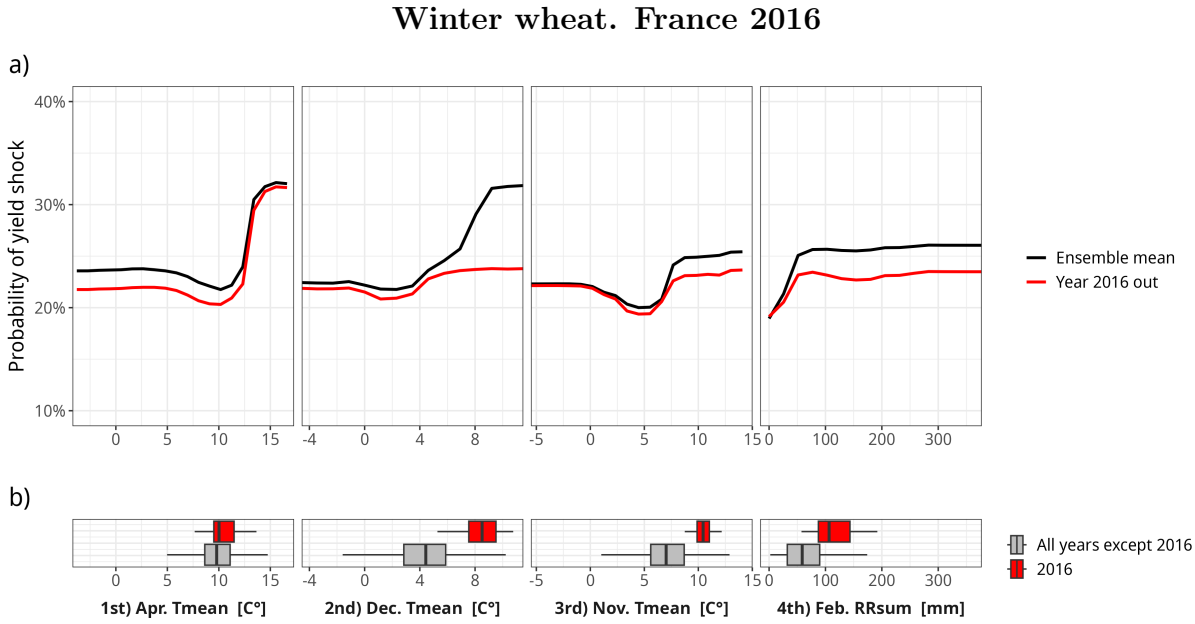

Figure C6: (a) Partial dependence plots for the three most important variables (according to Figure 7.8) for the ensemble model (black line) and the model leaving-2016-out (red line), and (b) data distribution during the studied period without considering 2016 (grey) and only for 2016 (red) in France for winter wheat models.

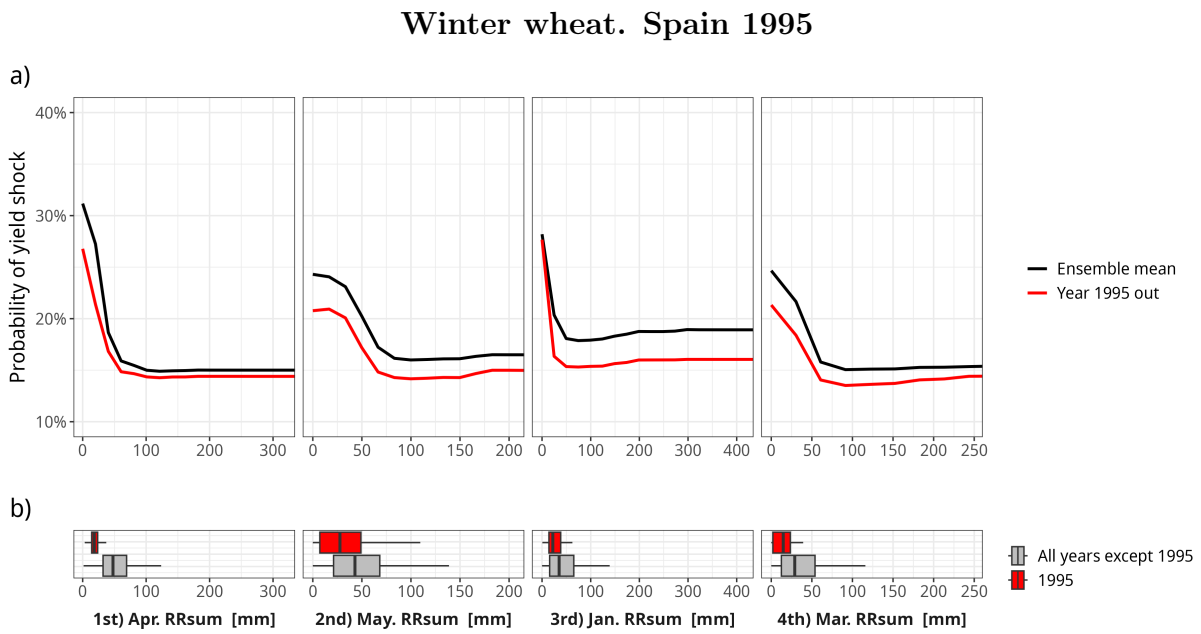

Figure C7: Same as FIgure C6 but for the case of 1995 in Spain.

D Appendix to Chapter 8

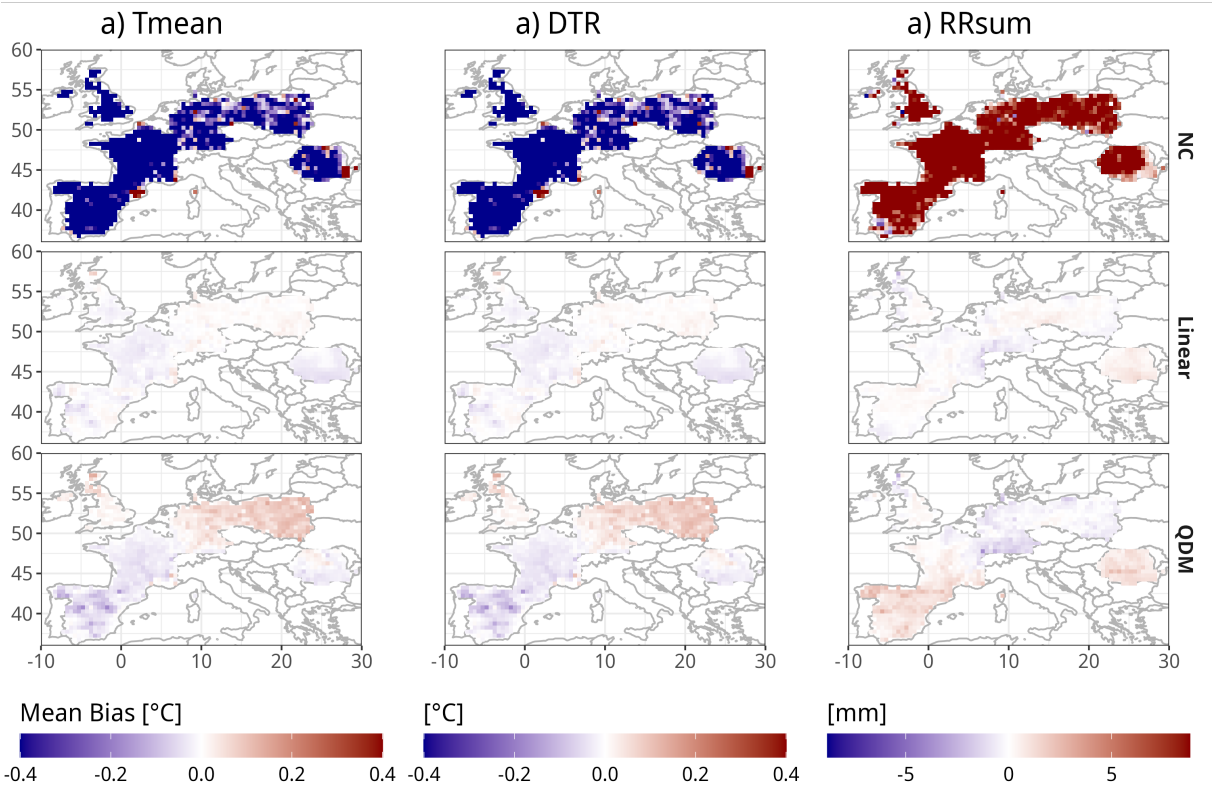

Figure D1: Average bias between the simulations and E-OBS data during the historical period for each variable (columns) for NC, Linear scaling and QDM (rows). The bias is computed as the average bias for each month, variable, and model divided by the mean of the observed data. The average bias is computed by averaging the bias across months for each model and finally averaging across models.

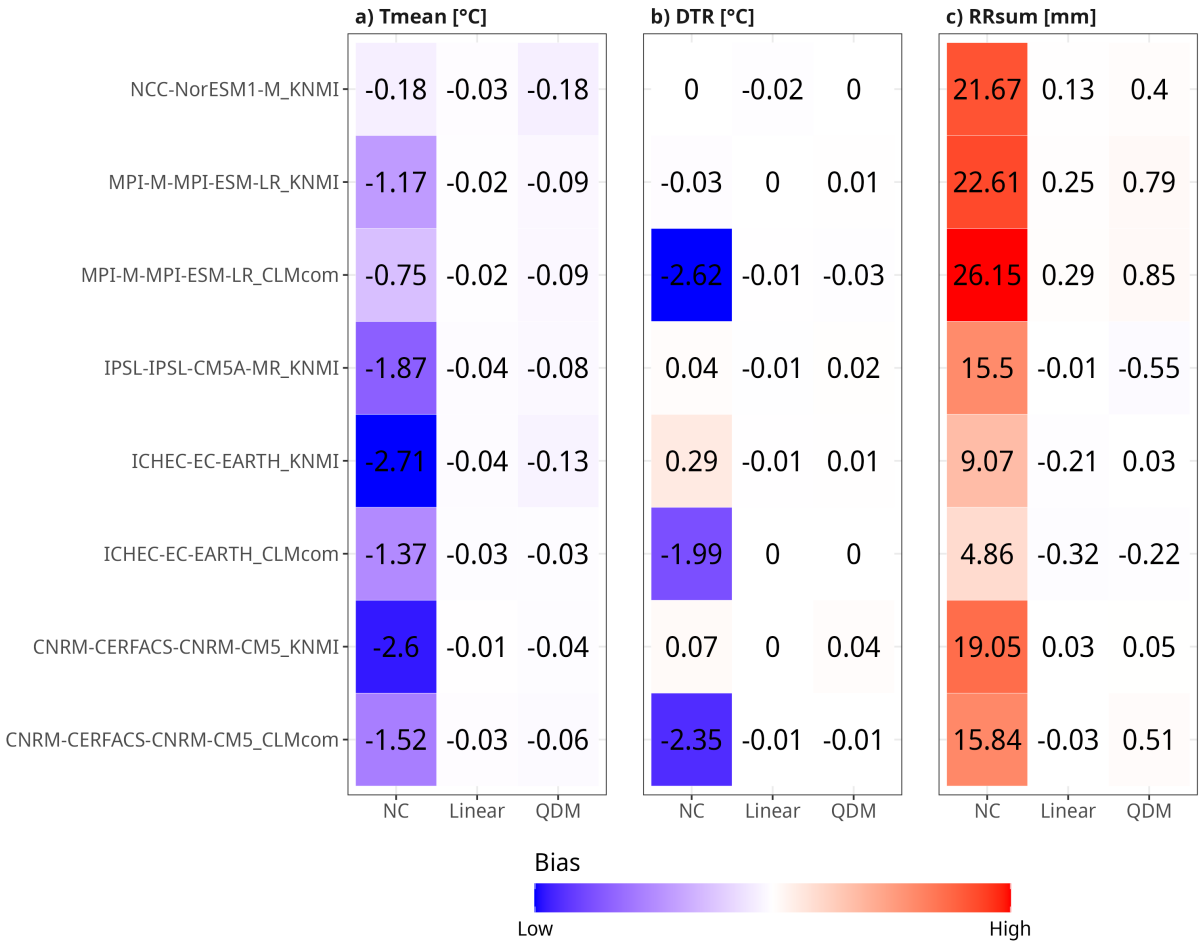

Figure D2: Average bias between the simulations and E-OBS data during the historical period for each variable (panels) for NC, Linear scaling and QDM (columns) and for each model (rows). The displayed values (black text) is calculated by computing bias for each grid point, month and variable, and then averaging across the domain and months. The colorbar (blue-white-red) display the normalize bias per model (0% for white and blue-red towards higher bias).

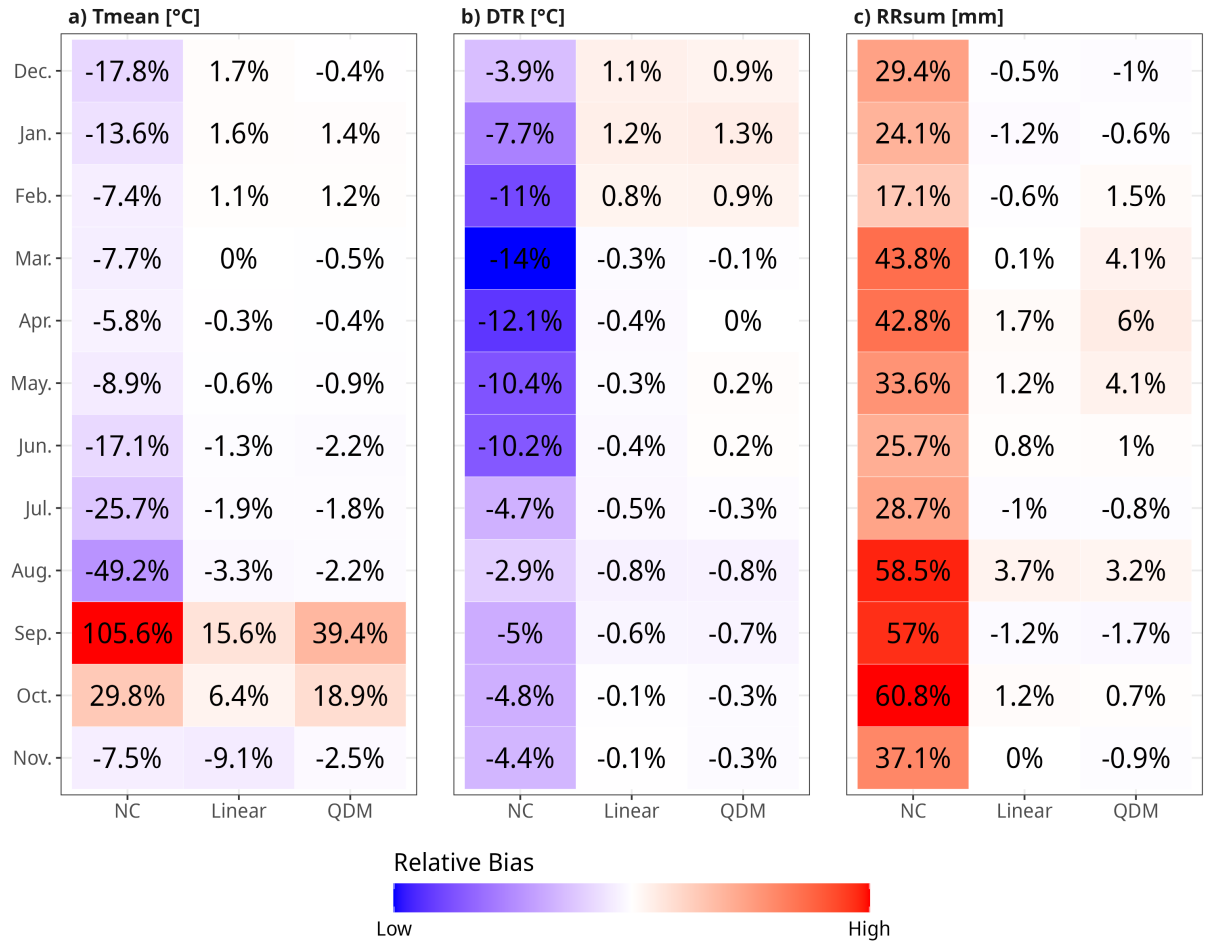

Figure D3: Average relative bias between the simulations and E-OBS data during the historical period for each variable (panels) for NC, Linear scaling and QDM (columns) and for each month (rows). The displayed values (black text) is calculated by computing relative bias for each grid point, model and variable, and then averaging across the domain and model respectively. The colorbar (blue-white-red) display the normalize bias per model (0% for white and blue-red towards higher bias).

Figure D4: Similar to Figure D3, but for the biases (without relativizing).

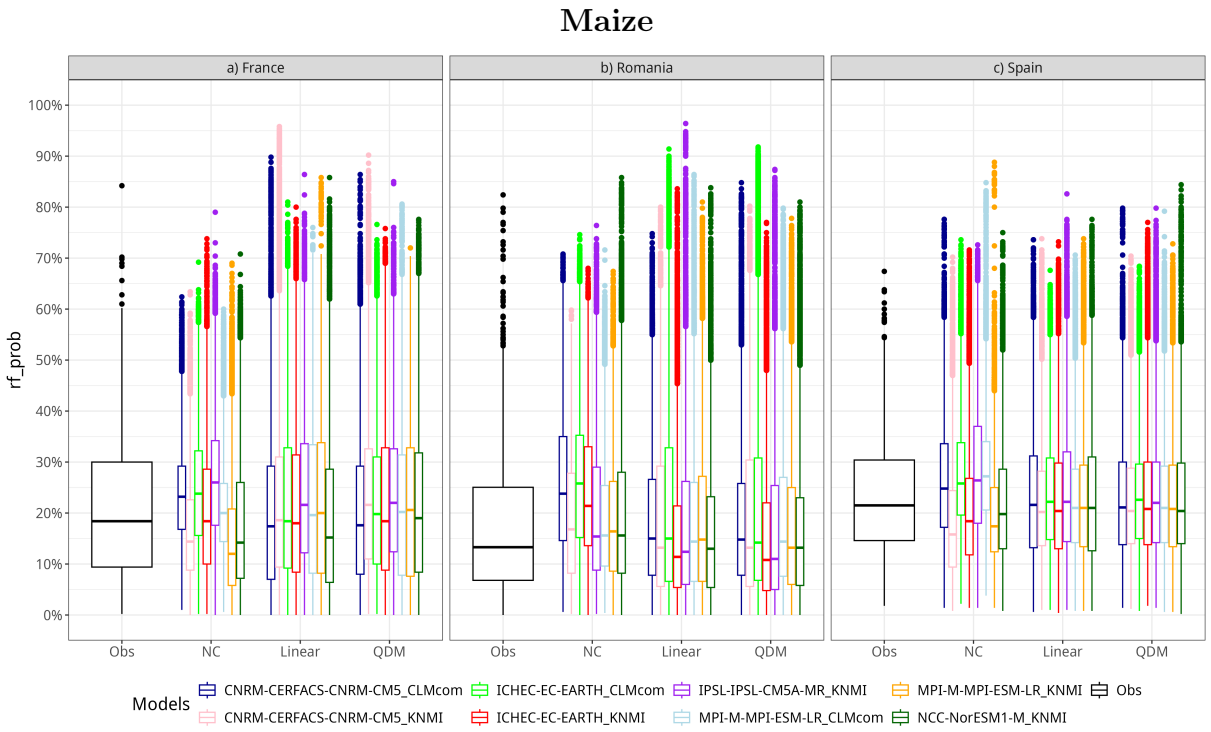

Figure D5: Predicted probabilities of maize yield shocks by GCM–RCM model chains (colored boxes) and observations (black-framed box) for NC under two bias correction methods (x-axis) across the three countries (panels). The horizontal line within each box represents the median, the box borders indicate the interquartile range, and the whiskers show the 10^{th}–90^{th} percentiles. Outliers are displayed as dots. Observed probabilities are estimated using a leave-one-year-out model and year-out data.

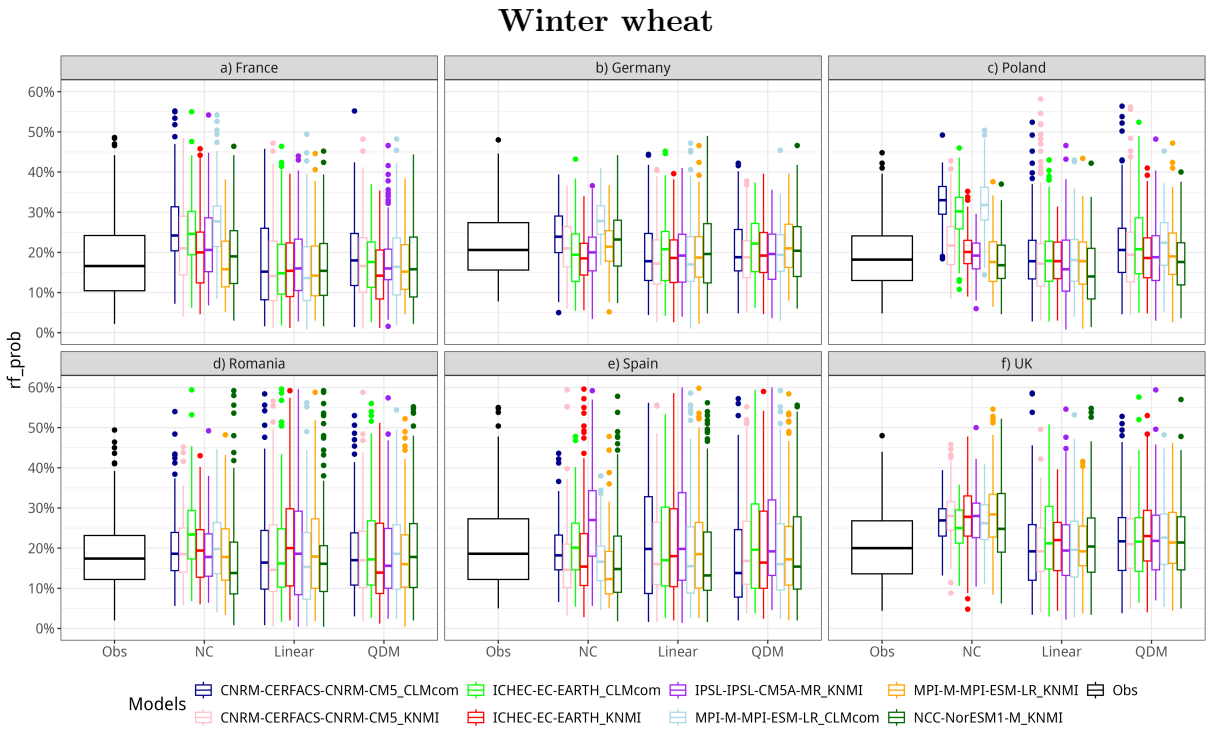

Figure D6: Same as Figure D5 but for winter wheat.

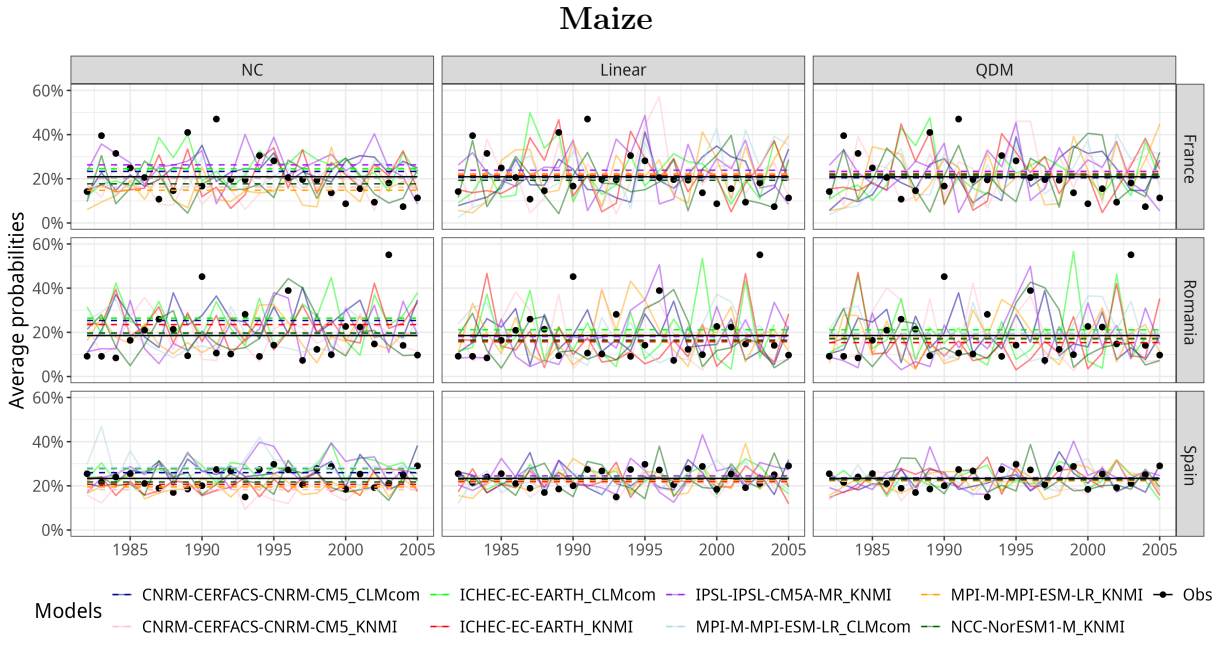

Figure D7: Predicted probabilities of maize yield shock by country (rows), method(columns) and model (colors). The year-to-year variability is displayed in transparent lines.Thick opac lines display the long-term expected trends, estimated by using LOESS method (Wickham et al., 2016).

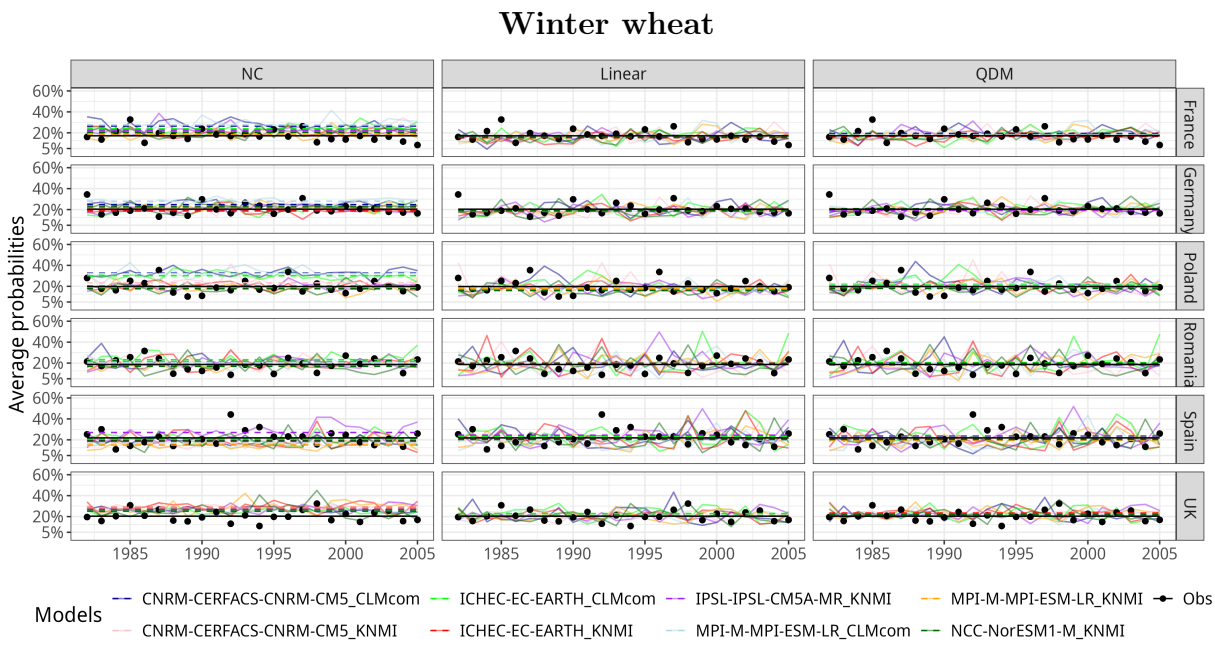

Figure D8: Same as Figure D7 but for winter wheat.

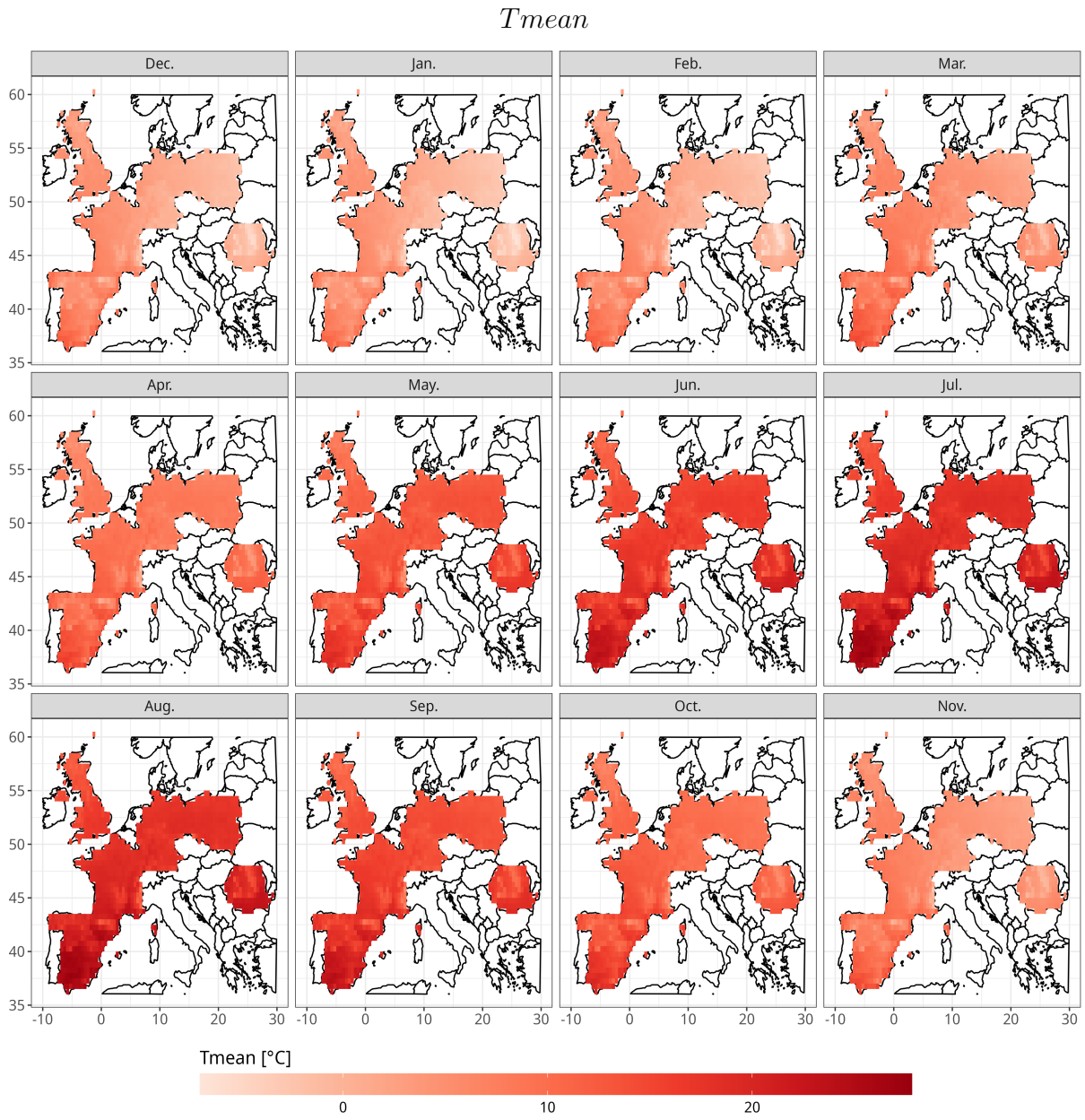

Figure D9: Average monthly *Tmean* across models and bias correction in the historical period (1982-2005).

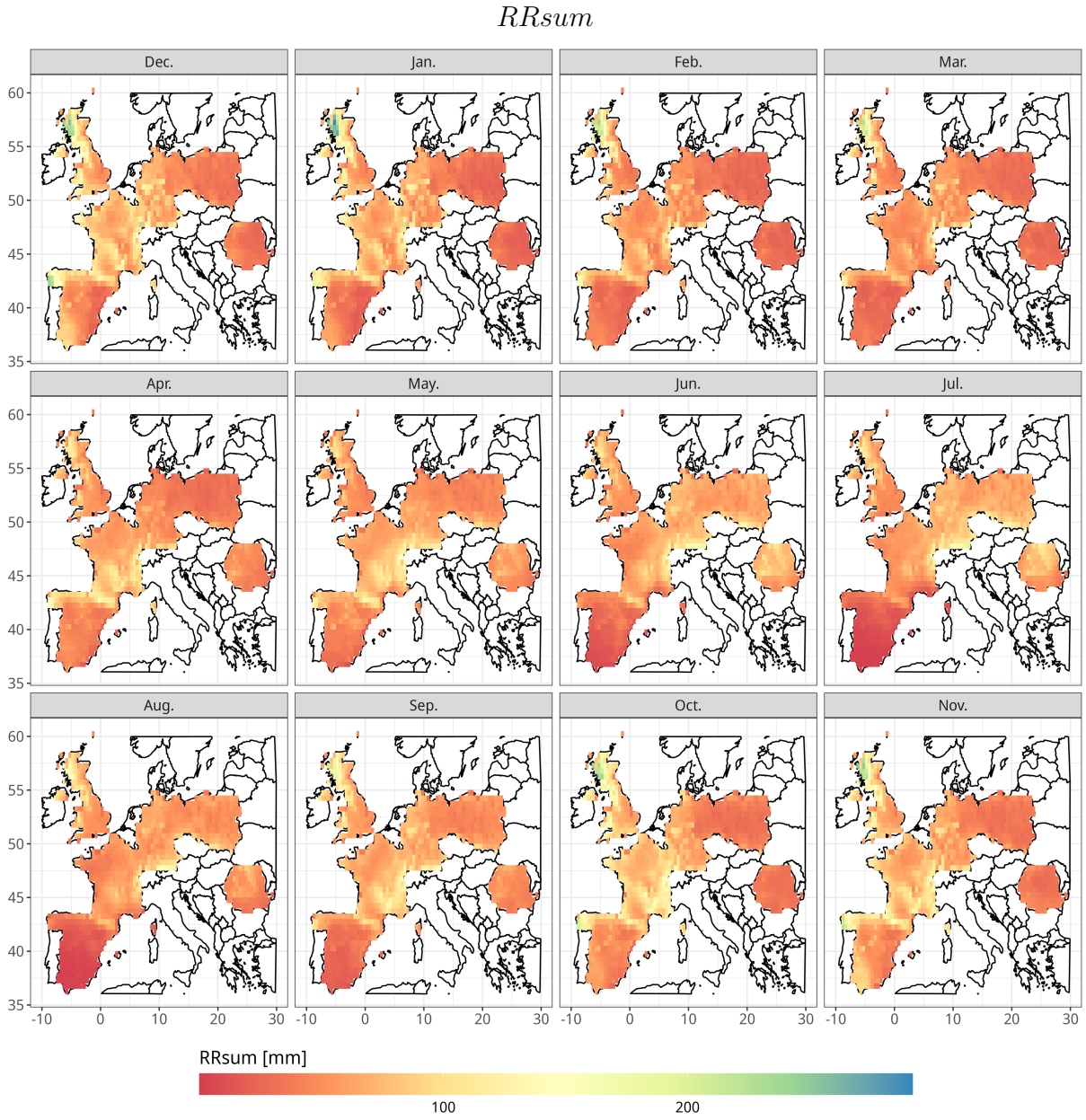

Figure D10: Same as Figure D9 but for *RRsum*

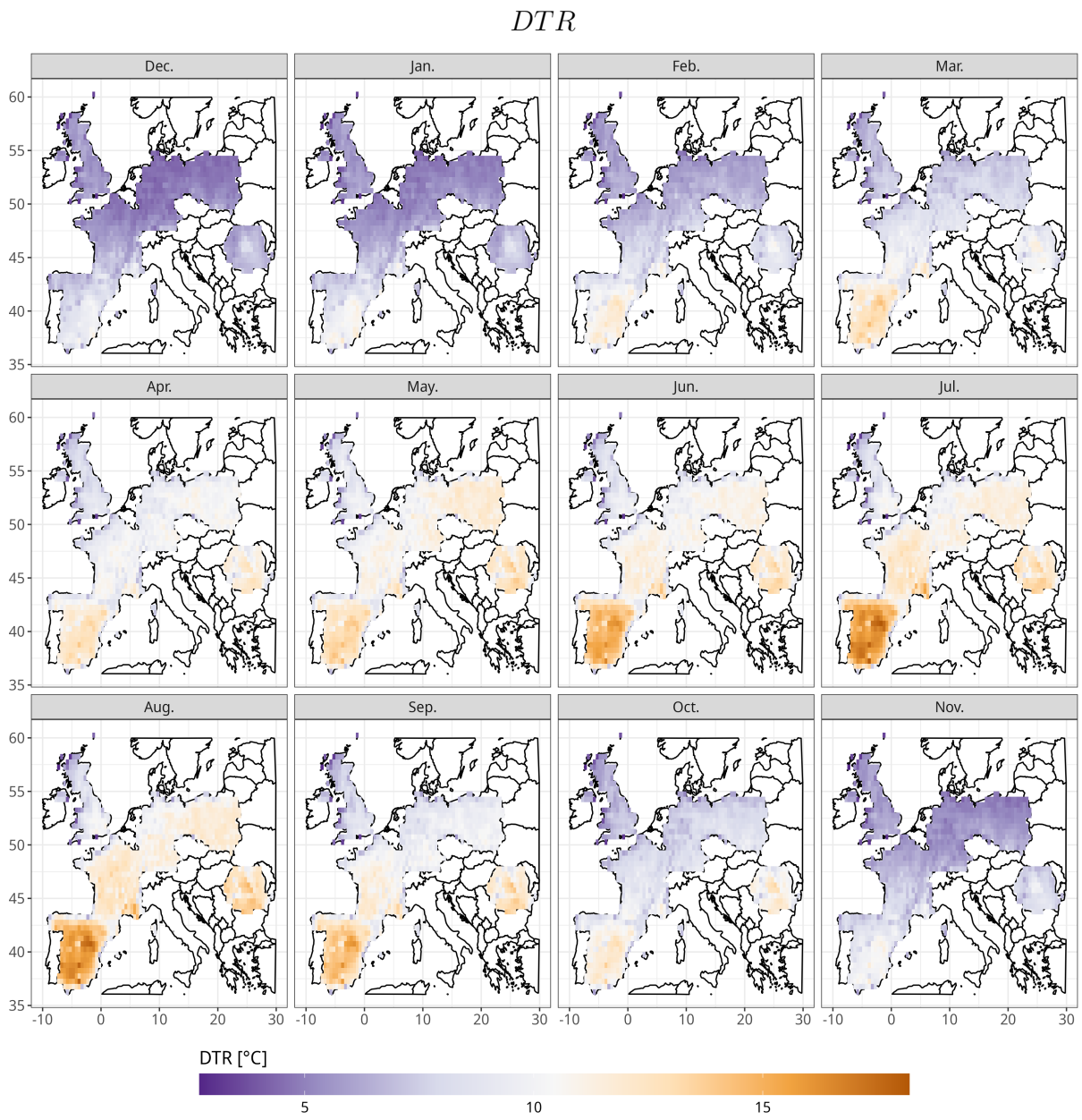

Figure D11: Same as Figure D9 but for DTR

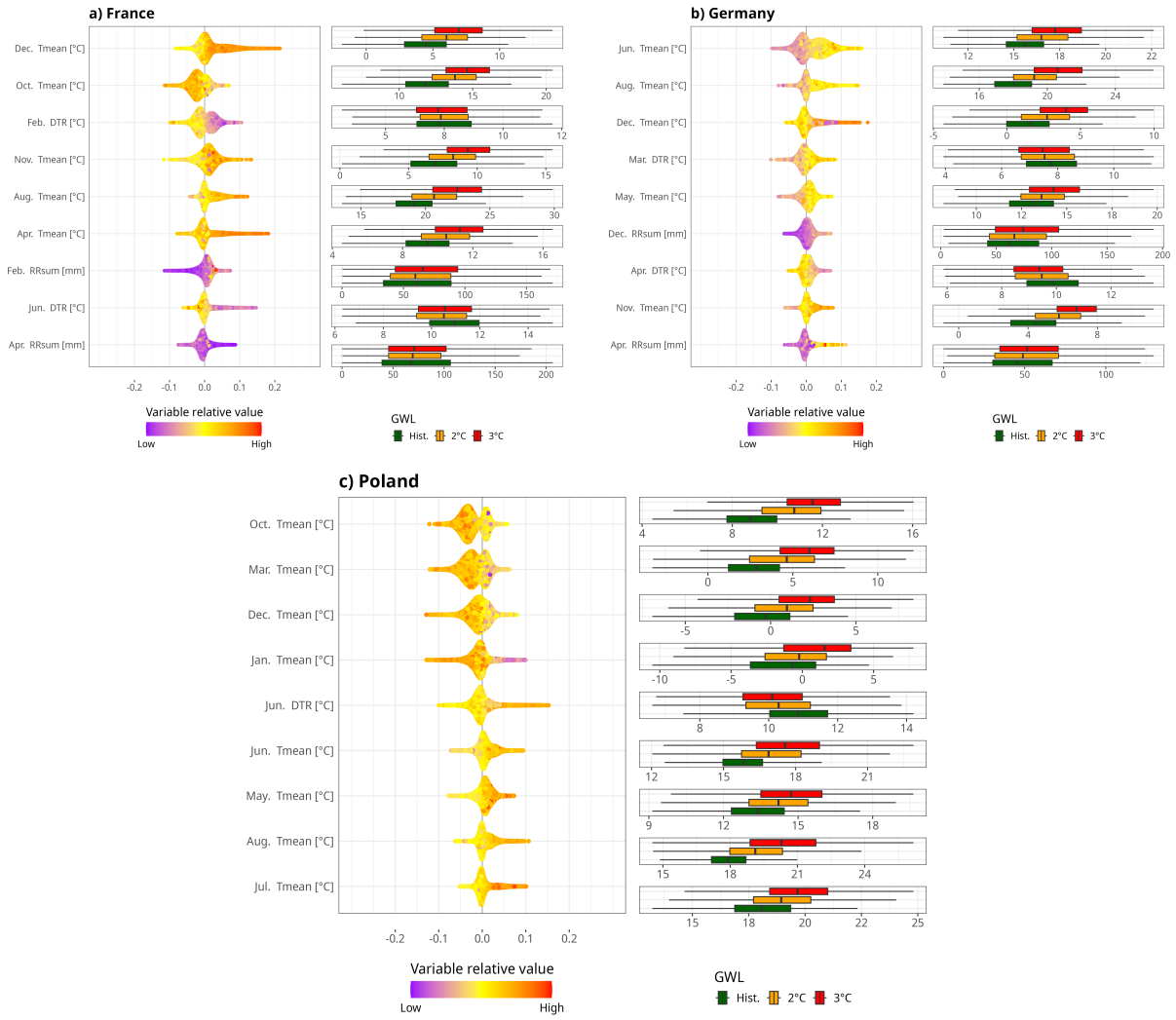

Figure D12: For winter wheat in France (a), Germany (b) and Poland (c). Top nine contributors (left panel) SHAP values and relative feature value (in colors), and (left panel) variable distribution during the historical period, GWL2 and GWL3 (colors). Part 1.

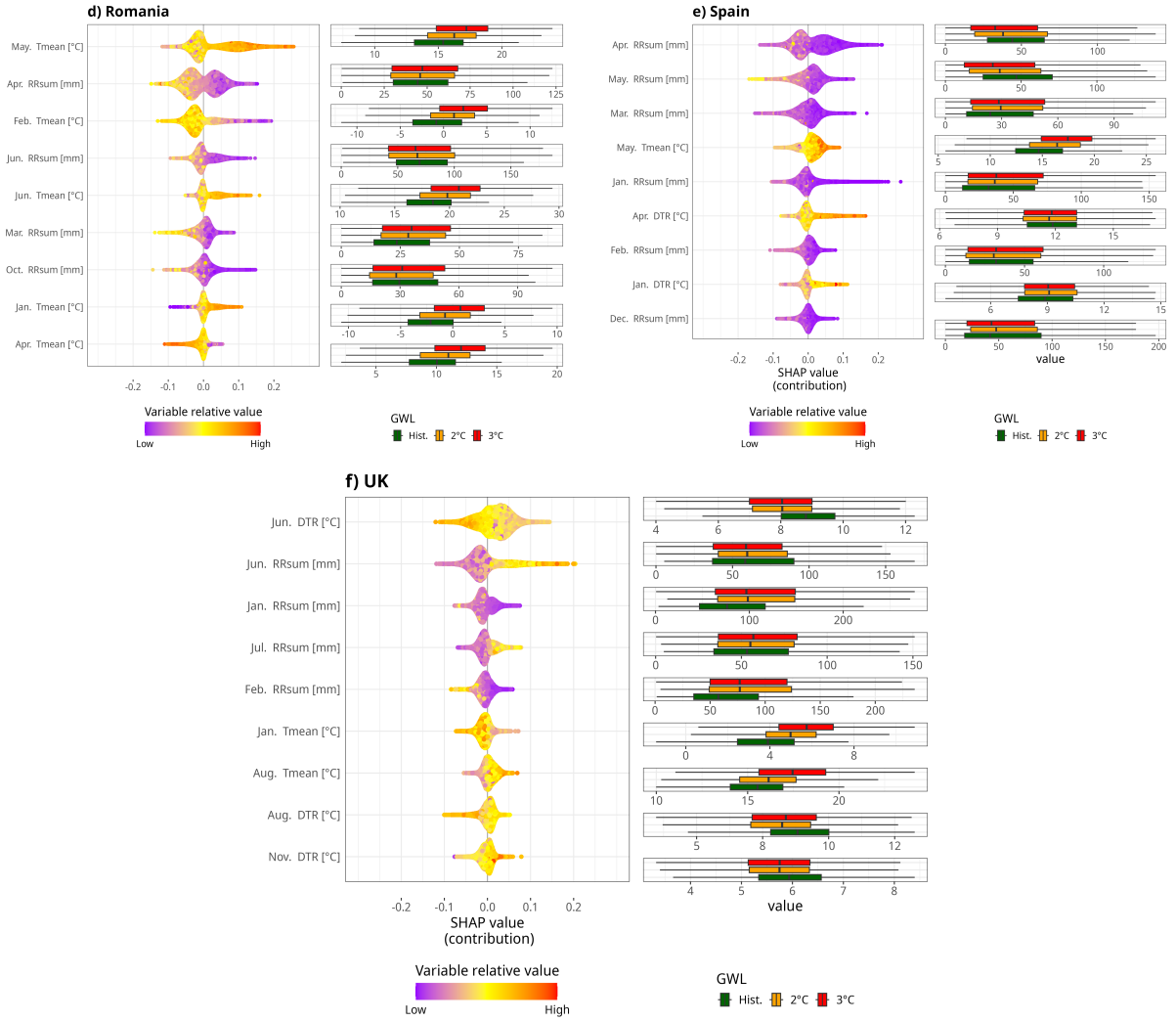

Figure D13: Same as Figure D12 but for Romania (d), Spain (e) and the UK (f).

Bibliography

Abramoff, Rose Z, Philippe Ciais, Peng Zhu, Toshihiro Hasegawa, Hitomi Wakatsuki, and David Makowski (2023). "Adaptation strategies strongly reduce the future impacts of climate change on simulated crop yields". In: *Earth's Future* 11.4, e2022EF003190.

Ahrens, C. Donald (2009). *Meteorology Today: An Introduction to Weather, Climate, and the Environment*. 9th ed. Belmont, CA: Brooks/Cole, CengageLearning. 549 pp. ISBN: 978-0-495-55573-5.

Ali, Peshawa Jamal Muhammad, Rezhna Hassan Faraj, Peshawa J Muhammad Ali, and Rezhna H Faraj (2014). "Data Normalization and Standardization: A Technical Report". In: *Mach Learn Tech Rep* 1.1.

Allen, R.G., L.S. Pereira, D. Raes, and M. Smith (1998). *Crop Evapotranspiration - Guidelines for Computing Crop Water Requirements - FAO Irrigation and Drainage Paper 56*. Rome, Italy: FAO - Food and Agriculture Organization of the United. ISBN: 92-5-104219-5.

American Meteorological Society (2012). *Hail - Glossary of Meteorology*. URL: `https://glossary.ametsoc.org/wiki/Hail` (visited on 02/12/2025).

Andarzian, Bahram, Gerrit Hoogenboom, Mohammad Bannayan, Mahvash Shirali, and Behnam Andarzian (2015). "Determining Optimum Sowing Date of Wheat Using CSM-CERES-Wheat Model". In: *Journal of the Saudi Society of Agricultural Sciences* 14.2, pp. 189–199. ISSN: 1658-077X. DOI: `10.1016/j.jssas.2014.04.004`.

Andrade, Fernando H., María E. Otegui, and Claudia Vega (2000). "Intercepted Radiation at Flowering and Kernel Number in Maize". In: *Agronomy Journal* 92.1, pp. 92–97. ISSN: 1435-0645. DOI: `10.2134/agronj2000.92192x`.

Andrade, Fernando H. and Victor O. Sadras (2002). *BASES PARA EL MANEJO DEL MAIZ, EL GIRASOL Y LA SOJA*. Argentina: E. E.A. INTA Balcarce - F .C. A. U .N .M.P . ISBN: 987 -521-047 - 1.

Assel, Melissa, Daniel D. Sjoberg, and Andrew J. Vickers (2017). "The Brier Score Does Not Evaluate the Clinical Utility of Diagnostic Tests or Prediction Models". In: *Diagnostic and Prognostic Research* 1.1, p. 19. ISSN: 2397-7523. DOI: `10.1186/s41512-017-0020-3`.

Atlin, GN, JE Cairns, and B Das (2017). *Rapid breeding and varietal replacement are critical to adaptation of cropping systems in the developing world to climate change. Glob Food Sec 12: 31–37.*

Attri, Meenakshi, Vijay Bharti, Nesar Ahmad Nesar, Swati Mehta, Ranjeet Singh Bochalya, Kanik Kumar Bansal, and Rubby Sandhu (2022). "Improved Irrigation Practices for Higher Agricultural Productivity: A Review". In: *International Journal of Environ-*

ment and Climate Change, pp. 51–61. ISSN: 2581-8627. DOI: 10.9734/ijecc/2022/v12i930737.

Barlow, K. M., B. P. Christy, G. J. O'Leary, P. A. Riffkin, and J. G. Nuttall (2015). "Simulating the Impact of Extreme Heat and Frost Events on Wheat Crop Production: A Review". In: *Field Crops Research* 171, pp. 109–119. ISSN: 0378-4290. DOI: 10.1016/j.fcr.2014.11.010.

Baum, M. E., S. V. Archontoulis, and M. A. Licht (2019). "Planting Date, Hybrid Maturity, and Weather Effects on Maize Yield and Crop Stage". In: *Agronomy Journal* 111.1, pp. 303–313. ISSN: 1435-0645. DOI: 10.2134/agronj2018.04.0297.

Bayar, Ali Serkan, M Tuğrul Yılmaz, İsmail Yücel, and Paul Dirmeyer (2023). "CMIP6 Earth system models project greater acceleration of climate zone change due to stronger warming rates". In: *Earth's Future* 11.4, e2022EF002972.

Bechoux, N., G. Bernier, and P. Lejeune (2000). "Environmental Effects on the Early Stages of Tassel Morphogenesis in Maize (Zea Mays L.)" In: *Plant, Cell & Environment* 23.1, pp. 91–98. ISSN: 1365-3040. DOI: 10.1046/j.1365-3040.2000.00515.x.

Bednar-Friedl, B., R. Biesbroek, D.N. Schmidt, P. Alexander, K.Y. Børsheim, J. Carnicer, E. Georgopoulou, M. Haasnoot, G. Le Cozannet, P. Lionello, O. Lipka, C. Möllmann, V. Muccione, T. Mustonen, D. Piepenburg, and L. Whitmarsh (2022). "Europe". In: *Climate Change 2022 – Impacts, Adaptation and Vulnerability: Working Group II Contribution to the Sixth Assessment Report of the Intergovernmental Panel on Climate Change*. 1st ed. Climate Change 2022: Impacts, Adaptation and Vulnerability. Contribution of Working Group II to the Sixth Assessment Report of the Intergovernmental Panel on Climate Change. Cambridge University Press, Cambridge, UK and New York, NY, USA: Cambridge University Press, pp. 1817–1927. ISBN: 978-1-009-32584-4. DOI: 10.1017/9781009325844.

Beillouin, Damien, Bernhard Schauberger, Ana Bastos, Phillipe Ciais, and David Makowski (2020). "Impact of Extreme Weather Conditions on European Crop Production in 2018". In: *Philosophical Transactions of the Royal Society B: Biological Sciences* 375.1810, p. 20190510. DOI: 10.1098/rstb.2019.0510.

Ben-Ari, Tamara, Juliette Adrian, Tommy Klein, Pierluigi Calanca, Marijn Van der Velde, and David Makowski (2016). "Identifying Indicators for Extreme Wheat and Maize Yield Losses". In: *Agricultural and Forest Meteorology* 220, pp. 130–140. ISSN: 0168-1923. DOI: 10.1016/j.agrformet.2016.01.009.

Ben-Ari, Tamara, Julien Boé, Philippe Ciais, Remi Lecerf, Marijn Van der Velde, and David Makowski (2018). "Causes and Implications of the Unforeseen 2016 Extreme Yield Loss in the Breadbasket of France". In: *Nature Communications* 9.1, p. 1627. ISSN: 2041-1723. DOI: 10.1038/s41467-018-04087-x.

Beniston, Martin, David B. Stephenson, Ole B. Christensen, Christopher A. T. Ferro, Christoph Frei, Stéphane Goyette, Kirsten Halsnaes, Tom Holt, Kirsti Jylhä, Brigitte Koffi, Jean Palutikof, Regina Schöll, Tido Semmler, and Katja Woth (2007). "Future Extreme Events in European Climate: An Exploration of Regional Climate Model Projections". In: *Climatic Change* 81.1, pp. 71–95. ISSN: 1573-1480. DOI: 10.1007/s10584-006-9226-z.

Bento, Virgílio A., Andreia F. S. Ribeiro, Ana Russo, Célia M. Gouveia, Rita M. Cardoso, and Pedro M. M. Soares (2021). "The Impact of Climate Change in Wheat and Barley

Yields in the Iberian Peninsula". In: *Scientific Reports* 11.1, p. 15484. ISSN: 2045-2322. DOI: 10.1038/s41598-021-95014-6.

Bentsen, M., I. Bethke, J. B. Debernard, T. Iversen, A. Kirkevåg, Ø Seland, H. Drange, C. Roelandt, I. A. Seierstad, C. Hoose, and J. E. Kristjánsson (2013). "The Norwegian Earth System Model, NorESM1-M – Part 1: Description and Basic Evaluation of the Physical Climate". In: *Geoscientific Model Development* 6.3, pp. 687–720. ISSN: 1991-959X. DOI: 10.5194/gmd-6-687-2013.

Bevacqua, Emanuele, Carlo De Michele, Colin Manning, Anaïs Couasnon, Andreia F. S. Ribeiro, Alexandre M. Ramos, Edoardo Vignotto, Ana Bastos, Suzana Blesić, Fabrizio Durante, John Hillier, Sérgio C. Oliveira, Joaquim G. Pinto, Elisa Ragno, Pauline Rivoire, Kate Saunders, Karin van der Wiel, Wenyan Wu, Tianyi Zhang, and Jakob Zscheischler (2021). "Guidelines for Studying Diverse Types of Compound Weather and Climate Events". In: *Earth's Future* 9.11, e2021EF002340. ISSN: 2328-4277. DOI: 10.1029/2021EF002340.

Blunden, Jessica, A Abdallah, Robert Adler, Rob Allan, Dayana Arce, Anthony Argueez, John Augustine, Cesar Azorin-Molina, Julian Baez, Jonathan Barichivich, et al. (2017). "State of the Climate in 2016". In: *Bulletin of the American Meteorological Society* 98.8.

Blunden, Jessica and Derek S Arndt (2016). "State of the climate in 2015". In: *Bulletin of the American Meteorological Society* 97.8, Si–S275.

– (2019). "State of the Climate in 2018". In: *Bulletin of the American Meteorological Society* 100.9, Si–S306.

Blunden, Jessica, Derek S Arndt, and Molly O Baringer (2011). "State of the climate in 2010". In: *Bulletin of the American Meteorological Society* 92.6, S1–S236.

Blunden, Jessica and Derek S. Arndt (2013). "State of the Climate in 2012". In: *Bulletin of the American Meteorological Society* 94.8, S1–S258. DOI: 10.1175/2013BAMSStateoftheClimate.1.

– (2014). "State of the Climate in 2013". In: *American Meteorological Society* 95.7.

Boix-Fayos, Carolina and Joris De Vente (2023). "Challenges and potential pathways towards sustainable agriculture within the European Green Deal". In: *Agricultural Systems* 207, p. 103634.

Bradshaw, John E (2017). "Plant breeding: past, present and future". In: *Euphytica* 213.3, p. 60.

Brás, Teresa Armada, Júlia Seixas, Nuno Carvalhais, and Jonas Jägermeyr (2021). "Severity of Drought and Heatwave Crop Losses Tripled over the Last Five Decades in Europe". In: *Environmental Research Letters* 16.6, p. 065012. ISSN: 1748-9326. DOI: 10.1088/1748-9326/abf004.

Breiman, Leo, ed. (1998). *Classification and Regression Trees*. 1. CRC Press repr. Boca Raton, Fla.: Chapman & Hall/CRC. 358 pp. ISBN: 978-0-412-04841-8.

Breiman, Leo and Adel Cutler (2022). *Package "randomForest"*. University of California, Berkeley: Berkeley.

Bucheli, Janic, Nina Conrad, Stefan Wimmer, Tobias Dalhaus, and Robert Finger (2023). "Weather Insurance in European Crop and Horticulture Production". In: *Climate Risk Management* 41, p. 100525. ISSN: 2212-0963. DOI: 10.1016/j.crm.2023.100525.

Bucheli, Janic, Mélissa Uldry, and Robert Finger (2022). "Heat Risks in Swiss Milk Production". In: *Journal of the Agricultural and Applied Economics Association* 1.3, pp. 304–319. ISSN: 2769-2485. DOI: 10.1002/jaa2.24.

Busuioc, Aristita, Alexandru Dumitrescu, Elena Soare, and Alina Orzan (2007). "Summer anomalies in 2007 in the context of extremely hot and dry summers in Romania". In: *Romanian Journal of Meteorology* 9.1-2, pp. 1–17.

Butzer, Karl W and Georgina H Endfield (2012). *Critical perspectives on historical collapse*.

Călugăr, Roxana Elena, Andrei Varga, Carmen Daniela Vana, Loredana Ancuța Ceclan, Ionuț Racz, Felicia Chețan, Alina Șimon, Călin Popa, Nicolae Tritean, Florin Russu, et al. (2024). "Influence of Changing Weather on Old and New Maize Hybrids: A Case Study in Romania". In: *Plants* 13.23, p. 3322.

Calvin, Katherine et al. (2023). *IPCC, 2023: Climate Change 2023: Synthesis Report. Contribution of Working Groups I, II and III to the Sixth Assessment Report of the Intergovernmental Panel on Climate Change [Core Writing Team, H. Lee and J. Romero (Eds.)]. IPCC, Geneva, Switzerland.* Intergovernmental Panel on Climate Change (IPCC). DOI: 10.59327/IPCC/AR6-9789291691647.

Cannon, Alex J, Stephen R Sobie, and Trevor Q Murdock (2015). "Bias correction of GCM precipitation by quantile mapping: how well do methods preserve changes in quantiles and extremes?" In: *Journal of Climate* 28.17, pp. 6938–6959.

Cardell, Maria F, Arnau Amengual, Romualdo Romero, and Climent Ramis (2020). "Future Extremes of Temperature and Precipitation in Europe Derived from a Combination of Dynamical and Statistical Approaches". In: *International Journal of Climatology* 40.11, pp. 4800–4827. ISSN: 0899-8418. DOI: 10.1002/joc.6490.

Carvalho, D, S Cardoso Pereira, and A Rocha (2021). "Future surface temperatures over Europe according to CMIP6 climate projections: an analysis with original and bias-corrected data". In: *Climatic Change* 167, pp. 1–17.

Casanueva, A., C. Rodríguez-Puebla, M. D. Frías, and N. González-Reviriego (2014). "Variability of Extreme Precipitation over Europe and Its Relationships with Teleconnection Patterns". In: *Hydrology and Earth System Sciences* 18.2, pp. 709–725. ISSN: 1027-5606. DOI: 10.5194/hess-18-709-2014.

Caubel, J., I. Garcia de Cortazar-Atauri, A. C. Vivant, M. Launay, and N. de Noblet-Ducoudré (2018). "Assessing Future Meteorological Stresses for Grain Maize in France". In: *Agricultural Systems* 159, pp. 237–247. ISSN: 0308-521X. DOI: 10.1016/j.agsy.2017.02.010.

Ceglar, A., R. van der Wijngaart, A. de Wit, R. Lecerf, H. Boogaard, L. Seguini, M. van den Berg, A. Toreti, M. Zampieri, D. Fumagalli, and B. Baruth (2019a). "Improving WOFOST Model to Simulate Winter Wheat Phenology in Europe: Evaluation and Effects on Yield". In: *Agricultural Systems* 168, pp. 168–180. ISSN: 0308-521X. DOI: 10.1016/j.agsy.2018.05.002.

Ceglar, A., M. Zampieri, A. Toreti, and F. Dentener (2019b). "Observed Northward Migration of Agro-Climate Zones in Europe Will Further Accelerate Under Climate Change". In: *Earth's Future* 7.9, pp. 1088–1101. ISSN: 2328-4277. DOI: 10.1029/2019EF001178.

Ceglar, Andrej, Andrea Toreti, Rémi Lecerf, Marijn Van der Velde, and Frank Dentener (2016). "Impact of Meteorological Drivers on Regional Inter-Annual Crop Yield Variability in France". In: *Agricultural and Forest Meteorology* 216, pp. 58–67. ISSN: 0168-1923. DOI: 10.1016/j.agrformet.2015.10.004.

Chandel, Vikram Singh, Udit Bhatia, Auroop R Ganguly, and Subimal Ghosh (2024). "State-of-the-Art Bias Correction of Climate Models Misrepresent Climate Science and

Misinform Adaptation". In: *Environmental Research Letters* 19.9, p. 094052. ISSN: 1748-9326. DOI: 10.1088/1748-9326/ad6d82.

Chatzopoulos, Thomas, Ignacio Pérez Domínguez, Matteo Zampieri, and Andrea Toreti (2020). "Climate Extremes and Agricultural Commodity Markets: A Global Economic Analysis of Regionally Simulated Events". In: *Weather and Climate Extremes*. Innovations in Managing Climate Risks and Building Resilience in Agriculture 27, p. 100193. ISSN: 2212-0947. DOI: 10.1016/j.wace.2019.100193.

Chen, D, M Rojas, B.H. Samset, K. Cobb, A. iongue Niang, P. dwards, S. Emori, S.H. Faria, E. Hawkins, P. Hope, P. Huybrechts, M. Meinshausen, S.K. Mustafa, G.-K. Plattner, and A.-M. Tréguier (2023). "Framing, Context, and Methods". In: *Climate Change 2021 – The Physical Science Basis: Working Group I Contribution to the Sixth Assessment Report of the Intergovernmental Panel on Climate Change*. 1st ed. Cambridge University Press. ISBN: 978-1-009-15789-6. DOI: 10.1017/9781009157896.

Chen, D., M. Rojas, B.H. Samset, K. Cobb, A. Diongue Niang, P. Edwards, S. Emori, S.H. Faria, P. Hawkins, P. Hope, M. Huybrechts, M Meinshausen, S.K. Mustafa, G.-K. Plattner, and A.-M. Tréguier (2021). "Framing, Context, and Methods." In: *Climate Change 2021: The Physical Science Basis. Contribution of Working Group I to the Sixth Assessment Report of the Intergovernmental Panel on Climate Change [Masson-Delmotte, V., P. Zhai, A. Pirani, S.L. Connors, C. Péan, S. Berger, N. Caud, Y. Chen, L. Goldfarb, M.I. Gomis, M. Huang, K. Leitzell, E. Lonnoy, J.B.R. Matthews, T.K. Maycock, T. Waterfield, O. Yelekçi, R. Yu, and B. Zhou (Eds.)]*. 1st ed. Cambridge University Press. ISBN: 978-1-009-15789-6. DOI: 10.1017/9781009157896.

Chicco, Davide and Giuseppe Jurman (2020). "The Advantages of the Matthews Correlation Coefficient (MCC) over F1 Score and Accuracy in Binary Classification Evaluation". In: *BMC Genomics* 21.1, p. 6. ISSN: 1471-2164. DOI: 10.1186/s12864-019-6413-7.

Chicco, Davide, Matthijs J. Warrens, and Giuseppe Jurman (2021). "The Matthews Correlation Coefficient (MCC) Is More Informative Than Cohen's Kappa and Brier Score in Binary Classification Assessment". In: *IEEE Access* 9, pp. 78368–78381. ISSN: 2169-3536. DOI: 10.1109/ACCESS.2021.3084050.

Clarke, D, T M Hess, D Haro-Monteagudo, M. A. Semenov, and J W Knox (2021). "Assessing Future Drought Risks and Wheat Yield Losses in England". In: *Agricultural and Forest Meteorology* 297, p. 108248. ISSN: 0168-1923. DOI: 10.1016/j.agrformet.2020.108248.

Cleveland, William S. (1979). "Robust Locally Weighted Regression and Smoothing Scatterplots". In: *Journal of the American Statistical Association* 74.368, pp. 829–836. ISSN: 0162-1459. DOI: 10.1080/01621459.1979.10481038.

Cogato, Alessia, Franco Meggio, Massimiliano De Antoni Migliorati, and Francesco Marinello (2019). "Extreme Weather Events in Agriculture: A Systematic Review". In: *Sustainability* 11.9 (9), p. 2547. ISSN: 2071-1050. DOI: 10.3390/su11092547.

Collins, Matthew, Reto Knutti, Julie Arblaster, Jean-Louis Dufresne, Thierry Fichefet, Xuejie Gao, William J Gutowski Jr, Tim Johns, Gerhard Krinner, Mxolisi Shongwe, Andrew J Weaver, Michael Wehner, Myles R Allen, Tim Andrews, Urs Beyerle, Cecilia M Bitz, Sandrine Bony, Ben B B Booth, Harold E Brooks, Victor Brovkin, Oliver Browne, Claire Brutel-Vuilmet, Mark Cane, Robin Chadwick, Ed Cook, Kerry H Cook, Michael Eby, John Fasullo, Chris E Forest, Piers Forster, Peter Good, Hugues Goosse, Jonathan M Gregory, Gabriele C Hegerl, Paul J Hezel, Kevin I Hodges, Marika M

Holland, Markus Huber, Manoj Joshi, Viatcheslav Kharin, Yochanan Kushnir, David M Lawrence, Robert W Lee, Spencer Liddicoat, Christopher Lucas, Wolfgang Lucht, Jochem Marotzke, François Massonnet, H Damon Matthews, Malte Meinshausen, Colin Morice, Alexander Otto, Christina M Patricola, Gwenaëlle Philippon, Stefan Rahmstorf, William J Riley, Oleg Saenko, Richard Seager, Jan Sedláček, Len C Shaffrey, Drew Shindell, Jana Sillmann, Bjorn Stevens, Peter A Stott, Robert Webb, Giuseppe Zappa, Kirsten Zickfeld, Sylvie Joussaume, Abdalah Mokssit, Karl Taylor, and Simon Tett (2013). "Long-Term Climate Change: Projections, Commitments and Irreversibility". In: *Climate Change 2013: The Physical Science Basis. Contribution of Working Group I to the Fifth Assessment Report of the Intergovernmental Panel on Climate Change [Stocker, T.F., D. Qin, G.-K. Plattner, M. Tignor, S.K. Allen, J. Boschung, A. Nauels, Y. Xia, V. Bex and P.M. Midgley (Eds.)]* Cambridge, United Kingdom and New York, NY, USA.: Cambridge University Pres.

Coppola, Erika, Rita Nogherotto, James M. Ciarlo', Filippo Giorgi, Erik Van Meijgaard, Nikolay Kadygrov, Carley Iles, Lola Corre, Marit Sandstad, Samuel Somot, Pierre Nabat, Robert Vautard, Guillaume Levavasseur, Clemens Schwingshackl, Jana Sillmann, Erik Kjellström, Grigory Nikulin, Emma Aalbers, Geert Lenderink, Ole B. Christensen, Fredrik Boberg, Silje Lund Sørland, Marie-Estelle Demory, Katharina Bülow, Claas Teichmann, Kirsten Warrach-Sagi, and Volker Wulfmeyer (2021). "Assessment of the European Climate Projections as Simulated by the Large EURO-CORDEX Regional and Global Climate Model Ensemble". In: *Journal of Geophysical Research: Atmospheres* 126.4, e2019JD032356. ISSN: 2169-897X, 2169-8996. DOI: 10.1029/2019JD032356.

Cornes, Richard C., Gerard Van Der Schrier, Else J. M. Van Den Besselaar, and Philip D. Jones (2018). "An Ensemble Version of the E-OBS Temperature and Precipitation Data Sets". In: *Journal of Geophysical Research: Atmospheres* 123.17, pp. 9391–9409. ISSN: 2169897X. DOI: 10.1029/2017JD028200.

Cottrell, Richard S., Kirsty L. Nash, Benjamin S. Halpern, Tomas A. Remenyi, Stuart P. Corney, Aysha Fleming, Elizabeth A. Fulton, Sara Hornborg, Alexandra Johne, Reg A. Watson, and Julia L. Blanchard (2019). "Food Production Shocks across Land and Sea". In: *Nature Sustainability* 2.2 (2), pp. 130–137. ISSN: 2398-9629. DOI: 10.1038/s41893-018-0210-1.

Crafts-Brandner, Steven J. and Michael E. Salvucci (2002). "Sensitivity of Photosynthesis in a C4 Plant, Maize, to Heat Stress". In: *Plant Physiology* 129.4, pp. 1773–1780. ISSN: 1532-2548, 0032-0889. DOI: 10.1104/pp.002170.

Croitoru, Adina-Eliza, Iulian-Horia Holobaca, Catalin Lazar, Florin Moldovan, and Alexandru Imbroane (2012). "Air Temperature Trend and the Impact on Winter Wheat Phenology in Romania". In: *Climatic Change* 111.2, pp. 393–410. ISSN: 1573-1480. DOI: 10.1007/s10584-011-0133-6.

Cuculeanu, Vasile, Adriana Marica, and Catalin Simota (1999). "Climate change impact on agricultural crops and adaptation options in Romania". In: *Climate Research* 12.2-3, pp. 153–160.

Curtis, B.C., S. Rajaram, and H. Gómez Macpherson (2002). *BREAD WHEAT. Improvement and Production*. Rome, Italy: FOOD and AGRICULTURE ORGANIZATION OF THE UNITED NATIONS.

Cutler, D. Richard, Thomas C. Edwards Jr., Karen H. Beard, Adele Cutler, Kyle T. Hess, Jacob Gibson, and Joshua J. Lawler (2007). "Random Forests for Classification in Ecology". In: *Ecology* 88.11, pp. 2783–2792. ISSN: 1939-9170. DOI: 10.1890/07-0539.1.

D'Amour, Christopher Bren, Leonie Wenz, Matthias Kalkuhl, Jan Christoph Steckel, and Felix Creutzig (2016). "Teleconnected Food Supply Shocks". In: *Environmental Research Letters* 11.3, p. 035007. ISSN: 1748-9326. DOI: 10.1088/1748-9326/11/3/035007.

De Sousa, Telma, Miguel Ribeiro, Carolina Sabença, and Gilberto Igrejas (2021). "The 10,000-Year Success Story of Wheat!" In: *Foods* 10.9, p. 2124. ISSN: 2304-8158. DOI: 10.3390/foods10092124. PMID: 34574233.

Djanaguiraman, M., S. Narayanan, E. Erdayani, and P. V. V. Prasad (2020). "Effects of High Temperature Stress during Anthesis and Grain Filling Periods on Photosynthesis, Lipids and Grain Yield in Wheat". In: *BMC Plant Biology* 20.1, p. 268. ISSN: 1471-2229. DOI: 10.1186/s12870-020-02479-0.

Dornik, Andrei, Marinela Adriana Cheţan, Tania Elena Crişan, Raul Heciko, Alexandru Gora, Lucian Drăguţ, and Panos Panagos (2024). "Geospatial evaluation of the agricultural suitability and land use compatibility in Europe's temperate continental climate region". In: *International Soil and Water Conservation Research* 12.4, pp. 908–919.

Dos Santos, Tiago Benedito, Alessandra Ferreira Ribas, Silvia Graciele Hülse de Souza, Ilara Gabriela Frasson Budzinski, and Douglas Silva Domingues (2022). "Physiological Responses to Drought, Salinity, and Heat Stress in Plants: A Review". In: *Stresses* 2.1 (1), pp. 113–135. ISSN: 2673-7140. DOI: 10.3390/stresses2010009.

Du, Xiong, Zhen Gao, Xiaonuo Sun, Dahong Bian, Jianhong Ren, Peng Yan, and Yanhong Cui (2022). "Increasing Temperature during Early Spring Increases Winter Wheat Grain Yield by Advancing Phenology and Mitigating Leaf Senescence". In: *Science of The Total Environment* 812, p. 152557. ISSN: 0048-9697. DOI: 10.1016/j.scitotenv.2021.152557.

Dufresne, J-L, M-A Foujols, Sébastien Denvil, Arnaud Caubel, Olivier Marti, Olivier Aumont, Yves Balkanski, Slimane Bekki, Hugo Bellenger, Rachid Benshila, et al. (2013). "Climate change projections using the IPSL-CM5 Earth System Model: from CMIP3 to CMIP5". In: *Climate dynamics* 40, pp. 2123–2165.

Edenhofer, O., R. Pichs-Madruga, Y. Sokona, S. Kadner, J. C. Minx, S. Brunner, S. Agrawala, G. Baiocchi, I. A. Bashmakov, G. Blanco, J. Broome, T. Bruckner, M. Bustamante, L. Clarke, M. Conte Grand, F. Creutzig, X. Cruz-Núñez, S. Dhakal, N. K. Dubash, P. Eickemeier, E. Farahani, M. Fischedick, M. Fleurbaey, R. Gerlagh, L. Gómez-Echeverri, S. Gupta, J. Harnisch, K. Jiang, F. Jotzo, S. Kartha, S. Klasen, C. Kolstad, V. Krey, H. Kunreuther, O. Lucon, O. Masera, Y. Mulugetta, R. B. Norgaard, A. Patt, N. H. Ravindranath, K. Riahi, J. Roy, A. Sagar, R. Schaeffer, S. Schlömer, K. C. Seto, K. Seyboth, R. Sims, P. Smith, E. Somanathan, R. Stavins, C. von Stechow, T. Sterner, T. Sugiyama, S. Suh, D. Ürge-Vorsatz, K. Urama, A. Venables, D. G. Victor, E. Weber, D. Zhou, J. Zou, and T. Zwickel (2014). "Technical Summary". In: *Climate Change 2014: Mitigation of Climate Change. Contribution of Working Group III to the Fifth Assessment Report of the Intergovernmental Panel on Climate Change*. Ed. by O. Edenhofer, R. Pichs-Madruga, Y. Sokona, E. Farahani, S. Kadner, K. Seyboth, A. Adler, I. Baum, S. Brunner, P. Eickemeier, B. Kriemann, J. Savolainen, S. Schlömer, C. von Stechow, T. Zwickel, and J. C. Minx. Cambridge, United Kingdom and New York, NY, USA: Cambridge University Press.

European Climate Assessment & Dataset (2024). *ENSEMBLES Daily Gridded Dataset (E-OBS)*. https://www.ecad.eu/download/ensembles/download.php. Accessed: 2025-05-30.

European Commission (2024). *The Common Agricultural Policy. A Partnership between Europe and Farmer*.

European Commission – Directorate-General for Agriculture and Rural Development – Unit A.3 (2023). *Assessing data gaps to evaluate CAP Strategic Plans: Report of the Good Practice Workshop 8–9 June 2023, Malmö, Sweden*. Technical Report. Brussels, Belgium: European Commission.

European Commission Joint Research Centre (2025). *JRC Global Agriculture*. https://wad.jrc.ec.europa.eu/globalagriculture. Accessed: 2025-06-10.

European Commission. JRC (2020). *Climate Change Impacts and Adaptation in Europe: JRC PESETA IV Final Report*. LU: Publications Office.

Eurostat (2025). *NUTS – Nomenclature of territorial units for statistics: Background*. https://ec.europa.eu/eurostat/web/nuts/background. Accessed: 2025-05-19.

Eyring, Veronika, Sandrine Bony, Gerald A. Meehl, Catherine A. Senior, Bjorn Stevens, Ronald J. Stouffer, and Karl E. Taylor (2016). "Overview of the Coupled Model Intercomparison Project Phase 6 (CMIP6) Experimental Design and Organization". In: *Geoscientific Model Development* 9.5, pp. 1937–1958. ISSN: 1991-959X. DOI: 10.5194/gmd-9-1937-2016.

FAO (1992). *Maize in Human Nutrition*. II. Series. Rome, Italy. ISBN: 92-5-103013-8.

– (2022). *FAO/WHO Global Individual Food Consumption Data Tool (GIFT): Methodological Document FOOD GROUPS AND SUBGROUPS*. FAO.

– (2023a). *Statistical Yearbook 2023*. FAO Statistical Yearbook – World Food and Agriculture 2023. Rome, Italy: FAO. 384 p. ISBN: 978-92-5-138262-2. DOI: 10.4060/cc8166en.

– (2023b). *The Impact of Disasters on Agriculture and Food Security 2023 – Avoiding and Reducing Losses through Investment in Resilience*. Rome, Italy: FAO. 168 p. ISBN: 978-92-5-138194-6. DOI: 10.4060/cc7900en.

– (2024a). *FAOSTAT*. URL: https://www.fao.org/faostat/en/#home (visited on 04/01/2024).

– (2024b). *Maize*. Food and Agricultural Organization of the United Nations. URL: https://www.fao.org/land-water/databases-and-software/crop-information/maize/en/ (visited on 08/06/2024).

– (2024c). *Wheat*. Food and Agricultural Organization of the United Nations. URL: https://www.fao.org/land-water/databases-and-software/crop-information/wheat/en/ (visited on 08/09/2024).

FAO, IFAD, UNICEF, WFP, and WHO (2023). *He State of Food Security and Nutrition in the World 2023. Urbanization, Agrifood Systems Transformation and Healthy Diets across the Rural–Urban Continuum*. The State of Food Security and Nutrition in the World (SOFI). Rome, Italy: FAO; IFAD; UNICEF; WFP; WHO. 316 p. ISBN: 978-92-5-137226-5. DOI: 10.4060/cc3017en.

Feng, Sifang and Zengchao Hao (2020). "Quantifying Likelihoods of Extreme Occurrences Causing Maize Yield Reduction at the Global Scale". In: *Science of The Total Environment* 704, p. 135250. ISSN: 0048-9697. DOI: 10.1016/j.scitotenv.2019.135250.

Fink, Andreas H., Tim Brücher, Andreas Krüger, Gregor C. Leckebusch, Joaquim G. Pinto, and Uwe Ulbrich (2004). "The 2003 European Summer Heatwaves and Drought

–Synoptic Diagnosis and Impacts". In: *Weather* 59.8, pp. 209–216. ISSN: 0043-1656, 1477-8696. DOI: 10.1256/wea.73.04.

Flannery, Kent V. (1973). "The Origins of Agriculture". In: *Annual Review of Anthropology* 2, pp. 271–310. ISSN: 0084-6570. JSTOR: 2949273.

Fontana, G., A. Toreti, A. Ceglar, and G. De Sanctis (2015). "Early Heat Waves over Italy and Their Impacts on Durum Wheat Yields". In: *Natural Hazards and Earth System Sciences* 15.7, pp. 1631–1637. ISSN: 1561-8633. DOI: 10.5194/nhess-15-1631-2015.

Fortems-Cheiney, Audrey, Gilles Foret, Guillaume Siour, Robert Vautard, Sophie Szopa, Gaelle Dufour, Augustin Colette, Gwendoline Lacressonniere, and Matthias Beekmann (2017). "A 3° C global RCP8. 5 emission trajectory cancels benefits of European emission reductions on air quality". In: *Nature Communications* 8.1, p. 89.

Friedman, Jerome H. (2001). "Greedy Function Approximation: A Gradient Boosting Machine". In: *The Annals of Statistics* 29.5, pp. 1189–1232. ISSN: 0090-5364. JSTOR: 2699986.

Friedman, Jerome, Hastie, Trevor, Tibshirani, Robert, Narasimhan, Balasubramanian Narasimhan, Tay, Kenneth, and Simon, Noah (2021). "Package 'Glmnet'". In: *CRAN R Repositary.*

García-Garizábal, I, J Causapé, R Abrahao, and D Merchan (2014). "Impact of climate change on Mediterranean irrigation demand: historical dynamics of climate and future projections". In: *Water resources management* 28.5, pp. 1449–1462.

Gebauer, Anika, Ali Sakhaee, Axel Don, Matteo Poggio, and Mareike Ließ (2022). "Topsoil Texture Regionalization for Agricultural Soils in Germany—An Iterative Approach to Advance Model Interpretation". In: *Frontiers in Soil Science* 1. ISSN: 2673-8619.

Giorgetta, Marco A, Johann Jungclaus, Christian H Reick, Stephanie Legutke, Jürgen Bader, Michael Böttinger, Victor Brovkin, Traute Crueger, Monika Esch, Kerstin Fieg, et al. (2013). "Climate and carbon cycle changes from 1850 to 2100 in MPI-ESM simulations for the Coupled Model Intercomparison Project phase 5". In: *Journal of Advances in Modeling Earth Systems* 5.3, pp. 572–597.

Giorgi, Filippo (2019). "Thirty Years of Regional Climate Modeling: Where Are We and Where Are We Going Next?" In: *Journal of Geophysical Research: Atmospheres* 124.11, pp. 5696–5723. ISSN: 2169-8996. DOI: 10.1029/2018JD030094.

Giorgi, Filippo and William J. Gutowski Jr (2015). "Regional Dynamical Downscaling and the CORDEX Initiative". In: *Annual Review of Environment and Resources* 40 (Volume 40, 2015), pp. 467–490. ISSN: 1543-5938, 1545-2050. DOI: 10.1146/annurev-environ-102014-021217.

Gobin, A. (2010). "Modelling Climate Impacts on Crop Yields in Belgium". In: *Climate Research* 44.1, pp. 55–68. ISSN: 0936-577X, 1616-1572. DOI: 10.3354/cr00925.

Goldstein, Alex, Adam Kapelner, Justin Bleich, and Emil Pitkin (2015). "Peeking Inside the Black Box: Visualizing Statistical Learning With Plots of Individual Conditional Expectation". In: *Journal of Computational and Graphical Statistics* 24.1, pp. 44–65. ISSN: 1061-8600. DOI: 10.1080/10618600.2014.907095.

Gornott, Christoph and Frank Wechsung (2016). "Statistical Regression Models for Assessing Climate Impacts on Crop Yields: A Validation Study for Winter Wheat and Silage Maize in Germany". In: *Agricultural and Forest Meteorology* 217, pp. 89–100. ISSN: 0168-1923. DOI: 10.1016/j.agrformet.2015.10.005.

Greener, Joe G, Shaun M Kandathil, Lewis Moffat, and David T Jones (2022). "A guide to machine learning for biologists". In: *Nature reviews Molecular cell biology* 23.1, pp. 40–55.

Greenwell, Brandon and Maintainer Brandon Greenwell (2020). "Package 'fastshap'". In: *URL: https://CRAN. R-project. org/package= fastshap R package version 0.0* 7.

Guo, Jian, Lingling Qu, Qi Wei, and Dalei Lu (2022). "Effects of post-silking low temperature on the starch and protein metabolism, endogenous hormone contents, and quality of grains in waxy maize". In: *Frontiers in Plant Science* 13, p. 988172.

Gutiérrez, J. M., R. G. Jones, G. T. Narisma, L. M. Alves, M. Amjad, I. V. Gorodetskaya, M. Grose, N. A. B. Klutse, S. Krakovska, J. Li, D. Martínez-Castro, L. O. Mearns, S. H. Mernild, T. Ngo-Duc, B. van den Hurk, and J.-H. Yoon (2021). "Atlas". In: *Climate Change 2021: The Physical Science Basis. Contribution of Working Group I to the Sixth Assessment Report of the Intergovernmental Panel on Climate Change*. Ed. by V. Masson-Delmotte, P. Zhai, A. Pirani, S. L. Connors, C. Péan, S. Berger, N. Caud, Y. Chen, L. Goldfarb, M. I. Gomis, M. Huang, K. Leitzell, E. Lonnoy, J. B. R. Matthews, T. K. Maycock, T. Waterfield, O. Yelekçi, R. Yu, and B. Zhou. Cambridge, United Kingdom and New York, NY, USA: Cambridge University Press, pp. 1927–2058. DOI: 10.1017/9781009157896.02.

Hall, Alex (2014). "Projecting Regional Change. How Accurate Are Regional Projections of Climate Change Derived from Downscaling Global Climate Model Results?" In: *Science* 346.6216, pp. 1461–1462. DOI: 10.1126/science.aaa0629.

Harkness, Caroline, Mikhail A. Semenov, Francisco Areal, Nimai Senapati, Miroslav Trnka, Jan Balek, and Jacob Bishop (2020). "Adverse Weather Conditions for UK Wheat Production under Climate Change". In: *Agricultural and Forest Meteorology* 282–283, p. 107862. ISSN: 0168-1923. DOI: 10.1016/j.agrformet.2019.107862.

Hawkins, Ed, Thomas E Fricker, Andrew J Challinor, Christopher AT Ferro, Chun Kit Ho, and Tom M Osborne (2013a). "Increasing influence of heat stress on French maize yields from the 1960s to the 2030s". In: *Global change biology* 19.3, pp. 937–947.

– (2013b). "Increasing Influence of Heat Stress on French Maize Yields from the 1960s to the 2030s". In: *Global Change Biology* 19.3, pp. 937–947. ISSN: 1365-2486. DOI: 10.1111/gcb.12069.

Hazeleger, Wilco, X Wang, Camiel Severijns, S Ştefănescu, R Bintanja, Andreas Sterl, Klaus Wyser, T Semmler, S Yang, B Van den Hurk, et al. (2012). "EC-Earth V2. 2: description and validation of a new seamless earth system prediction model". In: *Climate dynamics* 39, pp. 2611–2629.

Hersbach, Hans, Bill Bell, Paul Berrisford, Shoji Hirahara, András Horányi, Joaquín Muñoz-Sabater, Julien Nicolas, Carole Peubey, Raluca Radu, Dinand Schepers, et al. (2020). "The ERA5 global reanalysis". In: *Quarterly journal of the royal meteorological society* 146.730, pp. 1999–2049.

Ho, Sarah Qunh-Giang and Uwe Ehret (2025). "Is drought protection possible without compromising flood protection? Estimating the potential dual-use benefit of small flood reservoirs in southern Germany". In: *Hydrology and Earth System Sciences* 29.13, pp. 2785–2810.

Hu, Tongxi, Xuesong Zhang, Sami Khanal, Robyn Wilson, Guoyong Leng, Elizabeth M. Toman, Xuhui Wang, Yang Li, and Kaiguang Zhao (2024). "Climate Change Impacts on Crop Yields: A Review of Empirical Findings, Statistical Crop Models, and Machine

Learning Methods". In: *Environmental Modelling & Software* 179, p. 106119. ISSN: 1364-8152. DOI: 10.1016/j.envsoft.2024.106119.

Hurrell, James W, Yochanan Kushnir, Geir Ottersen, and Martin Visbeck (2003). "An overview of the North Atlantic oscillation". In: *Geophysical monograph-American geophysical union* 134, pp. 1–36.

Huynh, Hien T., J. Hufnagel, Angelika Wurbs, and Sonoko D. Bellingrath-Kimura (2019). "Influences of Soil Tillage, Irrigation and Crop Rotation on Maize Biomass Yield in a 9-Year Field Study in Müncheberg, Germany". In: *Field Crops Research* 241, p. 107565. ISSN: 0378-4290. DOI: 10.1016/j.fcr.2019.107565.

Iglesias, Ana, M Neil Ward, Manuel Menendez, and Cynthia Rosenzweig (2003). "Water availability for agriculture under climate change: understanding adaptation strategies in the Mediterranean". In: *Climate change in the Mediterranean, socio-economic perspectives of impacts, vulnerability and adaptation. Giupponi, C. and M. Shechter (eds). Edward Elgar, United Kingdom*, pp. 75–93.

Iizumi, Toshichika (2019). *Global Dataset of Historical Yields v1.2 and v1.3 Aligned Version*. PANGAEA. DOI: 10.1594/PANGAEA.909132.

Iizumi, Toshichika and Toru Sakai (2020). "The Global Dataset of Historical Yields for Major Crops 1981–2016". In: *Scientific Data* 7.1 (1), p. 97. ISSN: 2052-4463. DOI: 10.1038/s41597-020-0433-7.

Iizumi, Toshichika, Masayuki Yokozawa, Gen Sakurai, Maria Isabel Travasso, Vladimir Romanenkov, Pascal Oettli, Terry Newby, Yasushi Ishigooka, and Jun Furuya (2014). "Historical Changes in Global Yields: Major Cereal and Legume Crops from 1982 to 2006". In: *Global Ecology and Biogeography* 23.3, pp. 346–357. ISSN: 1466-8238. DOI: 10.1111/geb.12120.

IPCC (2023). *Climate Change 2021 – The Physical Science Basis: Working Group I Contribution to the Sixth Assessment Report of the Intergovernmental Panel on Climate Change*. 1st ed. Cambridge, United Kingdom and New York, NY, USA: Cambridge University Press. 2391 pp. DOI: 10.1017/9781009157896.

Jacob, Daniela, Juliane Petersen, Bastian Eggert, Antoinette Alias, Ole Bøssing Christensen, Laurens M. Bouwer, Alain Braun, Augustin Colette, Michel Déqué, Goran Georgievski, Elena Georgopoulou, Andreas Gobiet, Laurent Menut, Grigory Nikulin, Andreas Haensler, Nils Hempelmann, Colin Jones, Klaus Keuler, Sari Kovats, Nico Kröner, Sven Kotlarski, Arne Kriegsmann, Eric Martin, Erik van Meijgaard, Christopher Moseley, Susanne Pfeifer, Swantje Preuschmann, Christine Radermacher, Kai Radtke, Diana Rechid, Mark Rounsevell, Patrick Samuelsson, Samuel Somot, Jean-Francois Soussana, Claas Teichmann, Riccardo Valentini, Robert Vautard, Björn Weber, and Pascal Yiou (2014). "EURO-CORDEX: New High-Resolution Climate Change Projections for European Impact Research". In: *Regional Environmental Change* 14.2, pp. 563–578. ISSN: 1436-378X. DOI: 10.1007/s10113-013-0499-2.

James, Gareth, Daniela Witten, Trevor Hastie, and Robert Tibshirani (2021). *An Introduction to Statistical Learning: With Applications in R*. Springer Texts in Statistics. New York, NY: Springer US. ISBN: 978-1-0716-1417-4. DOI: 10.1007/978-1-0716-1418-1.

Jamieson, PD, MA Semenov, IR Brooking, and GS Francis (1998). "Sirius: a mechanistic model of wheat response to environmental variation". In: *European Journal of Agronomy* 8.3-4, pp. 161–179.

Jones, Edward J, Thomas FA Bishop, Brendan P Malone, Patrick J Hulme, Brett M Whelan, and Patrick Filippi (2022). "Identifying causes of crop yield variability with interpretive machine learning". In: *Computers and electronics in agriculture* 192, p. 106632.

Jones, James W., John M. Antle, Bruno Basso, Kenneth J. Boote, Richard T. Conant, Ian Foster, H. Charles J. Godfray, Mario Herrero, Richard E. Howitt, Sander Janssen, Brian A. Keating, Rafael Munoz-Carpena, Cheryl H. Porter, Cynthia Rosenzweig, and Tim R. Wheeler (2017a). "Brief History of Agricultural Systems Modeling". In: *Agricultural Systems* 155, pp. 240–254. ISSN: 0308-521X. DOI: 10.1016/j.agsy.2016.05.014.

– (2017b). "Toward a New Generation of Agricultural System Data, Models, and Knowledge Products: State of Agricultural Systems Science". In: *Agricultural Systems* 155, pp. 269–288. ISSN: 0308-521X. DOI: 10.1016/j.agsy.2016.09.021.

Kalkuhl, Matthias, Joachim Von Braun, and Maximo Torero, eds. (2016). *Food Price Volatility and Its Implications for Food Security and Policy*. International Food Policy Research Institute (IFPRI). Spring Open. Cambridge, United Kingdom and New York, NY, USA: Cambridge University Press. ISBN: 978-3-319-28199-5. DOI: 10.1007/978-3-319-28201-5.

Kallos, George, Marina Astitha, Petros Katsafados, and Chris Spyrou (2007). "Long-Range Transport of Anthropogenically and Naturally Produced Particulate Matter in the Mediterranean and North Atlantic: Current State of Knowledge". In: *Journal of Applied Meteorology and Climatology* 46.8, pp. 1230–1251. ISSN: 1558-8424, 1558-8432. DOI: 10.1175/JAM2530.1.

Kamran, Atif, Muhammad Iqbal, and Dean Spaner (2014). "Flowering time in wheat (Triticum aestivum L.): a key factor for global adaptability". In: *Euphytica* 197.1, pp. 1–26.

Katragkou, Eleni, SP Sobolowski, Claas Teichmann, Fabien Solmon, Vasileios Pavlidis, Diana Rechid, Peter Hoffmann, Jesús Fernández, Grigory Nikulin, and Daniela Jacob (2024). "Delivering an improved framework for the new generation of CMIP6-driven EURO-CORDEX regional climate simulations". In: *Bulletin of the American Meteorological Society* 105.6, E962–E974.

Katsenios, Nikolaos, Panagiotis Sparangis, Dimitrios Leonidakis, George Katsaros, Ioanna Kakabouki, Dimitrios Vlachakis, and Aspasia Efthimiadou (2021). "Effect of genotype× environment interaction on yield of maize hybrids in Greece using AMMI analysis". In: *Agronomy* 11.3, p. 479.

Kautz, Lisa-Ann, Olivia Martius, Stephan Pfahl, Joaquim G. Pinto, Alexandre M. Ramos, Pedro M. Sousa, and Tim Woollings (2022). "Atmospheric Blocking and Weather Extremes over the Euro-Atlantic Sector – a Review". In: *Weather and Climate Dynamics* 3.1, pp. 305–336. DOI: 10.5194/wcd-3-305-2022.

Kim, Kwang-Hyung, Yasuhiro Doi, Navin Ramankutty, and Toshichika Iizumi (2021). "A Review of Global Gridded Cropping System Data Products". In: *Environmental Research Letters* 16.9, p. 093005. ISSN: 1748-9326. DOI: 10.1088/1748-9326/ac20f4.

Kinnunen, Pekka, Matias Heino, Vilma Sandström, Maija Taka, Deepak K Ray, and Matti Kummu (2022). "Crop yield loss risk is modulated by anthropogenic factors". In: *Earth's future* 10.9, e2021EF002420.

Kluyver, Thomas (2013). "A Global Perspective on the Origins of Agriculture: The Importance of Unconscious Selection". The University of Sheffield.

Knox, Jerry, Andre Daccache, Tim Hess, and David Haro (2016). "Meta-Analysis of Climate Impacts and Uncertainty on Crop Yields in Europe". In: *Environmental Research Letters* 11.11, p. 113004. ISSN: 1748-9326. DOI: 10.1088/1748-9326/11/11/113004.

Köninger, Julia, Panagiotis Panagos, Arwyn Jones, MJI Briones, and Alberto Orgiazzi (2022). "In defence of soil biodiversity: Towards an inclusive protection in the European Union". In: *Biological Conservation* 268, p. 109475.

Kratzert, Frederik, Daniel Klotz, Guy Shalev, Günter Klambauer, Sepp Hochreiter, and Grey Nearing (2019). "Towards learning universal, regional, and local hydrological behaviors via machine learning applied to large-sample datasets". In: *Hydrology and Earth System Sciences* 23.12, pp. 5089–5110.

Krauskopf, Tomáš and Radan Huth (2020). "Temperature Trends in Europe: Comparison of Different Data Sources". In: *Theoretical and Applied Climatology* 139.3–4, pp. 1305–1316. ISSN: 0177-798X, 1434-4483. DOI: 10.1007/s00704-019-03038-w.

Kuhn, Max, Jed Wing, Steve Weston, Andre Williams, Chris Keefer, Allan Engelhardt, Tony Cooper, Zachary Mayer, Brenton Kenkel, and R Core Team (2023). "Package 'Caret'. Classification and Regression Training". In.

Kunz, Michael, Ulrich Blahak, Jan Handwerker, Manuel Schmidberger, Heinz Jürgen Punge, Susanna Mohr, Elody Fluck, and Kris M. Bedka (2018). "The Severe Hailstorm in Southwest Germany on 28 July 2013: Characteristics, Impacts and Meteorological Conditions". In: *Quarterly Journal of the Royal Meteorological Society* 144.710, pp. 231–250. ISSN: 1477-870X. DOI: 10.1002/qj.3197.

Lakshminarayanan, Balaji, Alexander Pritzel, and Charles Blundell (2017). "Simple and scalable predictive uncertainty estimation using deep ensembles". In: *Advances in neural information processing systems* 30.

Laux, Patrick, Reimund P. Rötter, Heidi Webber, Diarra Dieng, Jaber Rahimi, Jianhui Wei, Babacar Faye, Amit K. Srivastava, Jan Bliefernicht, Oluwafemi Adeyeri, Joel Arnault, and Harald Kunstmann (2021). "To Bias Correct or Not to Bias Correct? An Agricultural Impact Modelers' Perspective on Regional Climate Model Data". In: *Agricultural and Forest Meteorology* 304–305, p. 108406. ISSN: 0168-1923. DOI: 10.1016/j.agrformet.2021.108406.

Lazoglou, Georgia, Theo Economou, Christina Anagnostopoulou, George Zittis, Anna Tzyrkalli, Pantelis Georgiades, and Jos Lelieveld (2024). "Multivariate adjustment of drizzle bias using machine learning in European climate projections". In: *Geoscientific Model Development* 17.11, pp. 4689–4703.

Le Roux, Renan, Carina Furusho-Percot, Jean-Charles Deswarte, Marie-Odile Bancal, Karine Chenu, Nathalie de Noblet-Ducoudré, Iñaki García de Cortázar-Atauri, Alexis Durand, Burak Bulut, Olivier Maury, et al. (2024). "Mapping the race between crop phenology and climate risks for wheat in France under climate change". In: *Scientific Reports* 14.1, p. 8184.

Le Treut, H, R Sommerville, U Cubasch, Y Ding, C Mauritzen, A Mokssit, T Peterson, and M Prather (2007). "Historical Overview of Climate Change Science". In: *Climate Change 2007: The Physical Science Basis. Contribution of Working Group I to the Fourth Assessment Report of the Intergovernmental Panel on Climate Change [Solomon, S., D. Qin, M. Manning, Z. Chen, M. Marquis, K.B. Averyt, M. Tignor and H.L. Miller (Eds.)]* Cambridge, United Kingdom and New York, NY, USA.: Cambridge University Pres.

Leff, Billie, Navin Ramankutty, and Jonathan A. Foley (2004). "Geographic Distribution of Major Crops across the World". In: *Global Biogeochemical Cycles* 18.1, 2003GB002108. ISSN: 0886-6236, 1944-9224. DOI: 10.1029/2003GB002108.

Lépy, Élise and Leena Pasanen (2017). "Observed Regional Climate Variability during the Last 50 Years in Reindeer Herding Cooperatives of Finnish Fell Lapland". In: *Climate* 5.4 (4), p. 81. ISSN: 2225-1154. DOI: 10.3390/cli5040081.

Levinson, D.H. and J.H. Lawrimore (2008). *State of the Climate in 2007*. Vol. 89. 7 vols. American Meteorological Society.

Lhotka, Ondřej and Jan Kyselý (2022). "The 2021 European Heat Wave in the Context of Past Major Heat Waves". In: *Earth and Space Science* 9.11, e2022EA002567. ISSN: 2333-5084. DOI: 10.1029/2022EA002567.

Licker, Rachel, Matt Johnston, Jonathan A. Foley, Carol Barford, Christopher J. Kucharik, Chad Monfreda, and Navin Ramankutty (2010). "Mind the Gap: How Do Climate and Agricultural Management Explain the 'Yield Gap' of Croplands around the World?" In: *Global Ecology and Biogeography* 19.6, pp. 769–782. ISSN: 1466-8238. DOI: 10.1111/j.1466-8238.2010.00563.x.

Lima, Valter Jário de, Adrian Gracia-Romero, Fatima Zahra Rezzouk, Maria Carmen Diez-Fraile, Ismael Araus-Gonzalez, Samuel Henrique Kamphorst, Antonio Teixeira do Amaral Júnior, Shawn C Kefauver, Nieves Aparicio, and Jose Luis Araus (2021). "Comparative performance of high-yielding European wheat cultivars under contrasting Mediterranean conditions". In: *Frontiers in Plant Science* 12, p. 687622.

Lischeid, Gunnar, Heidi Webber, Michael Sommer, Claas Nendel, and Frank Ewert (2022). "Machine Learning in Crop Yield Modelling: A Powerful Tool, but No Surrogate for Science". In: *Agricultural and Forest Meteorology* 312, p. 108698. ISSN: 0168-1923. DOI: 10.1016/j.agrformet.2021.108698.

Lobell, David B., Graeme L. Hammer, Greg McLean, Carlos Messina, Michael J. Roberts, and Wolfram Schlenker (2013). "The Critical Role of Extreme Heat for Maize Production in the United States". In: *Nature Climate Change* 3.5 (5), pp. 497–501. ISSN: 1758-6798. DOI: 10.1038/nclimate1832.

Lobell, David B., Wolfram Schlenker, and Justin Costa-Roberts (2011). "Climate Trends and Global Crop Production Since 1980". In: *Science* 333.6042, pp. 616–620. DOI: 10.1126/science.1204531.

Lu, Junyu, Gregory J. Carbone, and Peng Gao (2017). "Detrending Crop Yield Data for Spatial Visualization of Drought Impacts in the United States, 1895–2014". In: *Agricultural and Forest Meteorology* 237–238, pp. 196–208. ISSN: 0168-1923. DOI: 10.1016/j.agrformet.2017.02.001.

Luo, Qunying (2011). "Temperature Thresholds and Crop Production: A Review". In: *Climatic Change* 109.3, pp. 583–598. ISSN: 1573-1480. DOI: 10.1007/s10584-011-0028-6.

Ma, Lawrence and Lin Zou (2024). "A Creative Computing Approach to Forecasting Yield Shock of Winter Wheat". In: *2024 IEEE 24th International Conference on Software Quality, Reliability, and Security Companion (QRS-C)*. 2024 IEEE 24th International Conference on Software Quality, Reliability, and Security Companion (QRS-C), pp. 1203–1212. DOI: 10.1109/QRS-C63300.2024.00158.

MacLaren, Chloe, Andrew Mead, Derk van Balen, Lieven Claessens, Ararso Etana, Janjo de Haan, Wiepie Haagsma, Ortrud Jäck, Thomas Keller, Johan Labuschagne, et al.

(2022). "Long-term evidence for ecological intensification as a pathway to sustainable agriculture". In: *Nature Sustainability* 5.9, pp. 770–779.

Madsen, H., D. Lawrence, M. Lang, M. Martinkova, and T. R. Kjeldsen (2014). "Review of Trend Analysis and Climate Change Projections of Extreme Precipitation and Floods in Europe". In: *Journal of Hydrology* 519, pp. 3634–3650. ISSN: 0022-1694. DOI: 10.1016/j.jhydrol.2014.11.003.

Mahesh, Batta et al. (2020). "Machine learning algorithms-a review". In: *International Journal of Science and Research (IJSR).[Internet]* 9.1, pp. 381–386.

Mäkinen, H., J. Kaseva, M. Trnka, J. Balek, K. C. Kersebaum, C. Nendel, A. Gobin, J. E. Olesen, M. Bindi, R. Ferrise, M. Moriondo, A. Rodríguez, M. Ruiz-Ramos, J. Takáč, P. Bezák, D. Ventrella, F. Ruget, G. Capellades, and H. Kahiluoto (2018). "Sensitivity of European Wheat to Extreme Weather". In: *Field Crops Research* 222, pp. 209–217. ISSN: 0378-4290. DOI: 10.1016/j.fcr.2017.11.008.

Mamassi, Achraf, Riad Balaghi, Krishna Prasad Devkota, Hamza Bouras, Mohamed El-Gharous, and Bernard Tychon (2023). "Modeling Genotype × Environment × Management Interactions for a Sustainable Intensification under Rainfed Wheat Cropping System in Morocco". In: *Agriculture & Food Security* 12.1, p. 22. ISSN: 2048-7010. DOI: 10.1186/s40066-023-00428-2.

Mao, Hude, Cong Jiang, Chunlei Tang, Xiaojun Nie, Linying Du, Yuling Liu, Peng Cheng, Yunfeng Wu, Huiquan Liu, Zhensheng Kang, et al. (2023). "Wheat adaptation to environmental stresses under climate change: Molecular basis and genetic improvement". In: *Molecular Plant* 16.10, pp. 1564–1589.

Maraun, Douglas (2016). "Bias Correcting Climate Change Simulations - a Critical Review". In: *Current Climate Change Reports* 2.4, pp. 211–220. ISSN: 2198-6061. DOI: 10.1007/s40641-016-0050-x.

Maraun, Douglas, Theodore G. Shepherd, Martin Widmann, Giuseppe Zappa, Daniel Walton, José M. Gutiérrez, Stefan Hagemann, Ingo Richter, Pedro M. M. Soares, Alex Hall, and Linda O. Mearns (2017). "Towards Process-Informed Bias Correction of Climate Change Simulations". In: *Nature Climate Change* 7.11, pp. 764–773. ISSN: 1758-6798. DOI: 10.1038/nclimate3418.

Maraun, Douglas and Martin Widmann (2018). *Statistical downscaling and bias correction for climate research*. Cambridge University Press.

Marcu, Viorela and Stelian Alexandru Borz (2013). "Global Warming and Extreme Meteorological Phenomena Recorded in the First 12 Years of the 21 st Century in Romania". In: *Rural Development 2013 The Sixth International Scientific Conference Proceedings*. Vol. 6, pp. 349–354.

Martin, Lioba Lucia, Andrew Smerald, Ralf Kiese, Tatiana Klimiuk, Patrick Ludwig, Antonio Sánchez Benítez, Helge Goessling, and Clemens Scheer (2025). "The vulnerability of European agricultural areas to anthesis heat stress increases with climate change". In: *Environmental Research: Food Systems*.

Maryam, Ammara and Shumaila Nasreen (2012). "A Review: Water Logging Effects on Morphological, Anatomical, Physiological and Biochemical Attributes of Food and Cash Crops". In: *Environ Sci.*.

Maton, Laure, Jacques-Eric Bergez, and Delphine Leenhardt (2007). "Modelling the Days Which Are Agronomically Suitable for Sowing Maize". In: *European Journal of Agronomy* 27.1, pp. 123–129. ISSN: 1161-0301. DOI: 10.1016/j.eja.2007.02.007.

Matthews, B. W. (1975). "Comparison of the Predicted and Observed Secondary Structure of T4 Phage Lysozyme". In: *Biochimica et Biophysica Acta (BBA) - Protein Structure* 405.2, pp. 442–451. ISSN: 0005-2795. DOI: 10.1016/0005-2795(75)90109-9.

Mayer, Michael and Adrian Stando (2025). "Package 'shapviz'". In: *URL: https://cran.r-project.org/web/packages/shapviz/shapviz.pdf* 7.

McKee, Thomas B, Nolan J Doesken, and John Kleist (1993). "The Relationship of Drought Frequency and Duration to Time Scales". In: *In Proceedings of the 8th Conference on Applied Climatology* 17.22, pp. 179–183.

Meijgaard, Erik van, LH Van Ulft, WJ Van de Berg, FC Bosveld, BJJM Van den Hurk, G Lenderink, and AP Siebesma (2008). *The KNMI regional atmospheric climate model RACMO, version 2.1*. KNMI De Bilt, The Netherlands.

Micu, Dana, Elena-Ana Popovici, Loredana-Elena Havriş, and Carmen-Sofia Dragotă (2017). "HEAT STRESS-CROP YIELDS INTERACTIONS UNDER SUMMER WARMING TRENDS: INSIGHTS FOR THE SOUTHERN CROPPING LOWLANDS OF ROMANIA". In: *Romanian Journal of Geography/Revue Roumaine de Géographie* 61.2.

Miedaner, Thomas and Peter Juroszek (2021). "Climate change will influence disease resistance breeding in wheat in Northwestern Europe". In: *Theoretical and Applied Genetics* 134.6, pp. 1771–1785.

Mishra, Ashok K. and Vijay P. Singh (2010). "A Review of Drought Concepts". In: *Journal of Hydrology* 391.1, pp. 202–216. ISSN: 0022-1694. DOI: 10.1016/j.jhydrol.2010.07.012.

Moemken, Julia and Joaquim G. Pinto (2022). "Recurrence of Drought Events Over Iberia. Part I: Methodology and Application for Present Climate Conditions". In: *Tellus A* 74.1 (1), pp. 222–235. ISSN: 1600-0870. DOI: 10.16993/tellusa.50.

Moemken, Julia, Mark Reyers, Hendrik Feldmann, and Joaquim G. Pinto (2018). "Future Changes of Wind Speed and Wind Energy Potentials in EURO-CORDEX Ensemble Simulations". In: *Journal of Geophysical Research: Atmospheres* 123.12, pp. 6373–6389. ISSN: 2169-8996. DOI: 10.1029/2018JD028473.

Molina, M. O., E. Sánchez, and C. Gutiérrez (2020). "Future Heat Waves over the Mediterranean from an Euro-CORDEX Regional Climate Model Ensemble". In: *Scientific Reports* 10.1, p. 8801. ISSN: 2045-2322. DOI: 10.1038/s41598-020-65663-0.

Molnar, Christoph (2020). *Interpretable machine learning*. Lulu. com.

Moss, Richard H., Jae A. Edmonds, Kathy A. Hibbard, Martin R. Manning, Steven K. Rose, Detlef P. van Vuuren, Timothy R. Carter, Seita Emori, Mikiko Kainuma, Tom Kram, Gerald A. Meehl, John F. B. Mitchell, Nebojsa Nakicenovic, Keywan Riahi, Steven J. Smith, Ronald J. Stouffer, Allison M. Thomson, John P. Weyant, and Thomas J. Wilbanks (2010). "The next Generation of Scenarios for Climate Change Research and Assessment". In: *Nature* 463.7282, pp. 747–756. ISSN: 1476-4687. DOI: 10.1038/nature08823.

Muckley, Eric S, James E Saal, Bryce Meredig, Christopher S Roper, and John H Martin (2023). "Interpretable models for extrapolation in scientific machine learning". In: *Digital Discovery* 2.5, pp. 1425–1435.

Murphy, Guillermo M. and Rafael H. Hurtado (2020). *Agrometeorología*. Buenos Aires City, Argentina: Facultad de Agronomia. ISBN: 978-987-3738-26-5.

Neumann, Mathias, Adam Moreno, Christopher Thurnher, Volker Mues, Sanna Härkönen, Matteo Mura, Olivier Bouriaud, Mait Lang, Giuseppe Cardellini, Alain Thivolle-Cazat,

Karol Bronisz, Jan Merganic, Iciar Alberdi, Rasmus Astrup, Frits Mohren, Maosheng Zhao, and Hubert Hasenauer (2016). "Creating a Regional MODIS Satellite-Driven Net Primary Production Dataset for European Forests". In: *Remote Sensing* 8.7, p. 554. ISSN: 2072-4292. DOI: 10.3390/rs8070554.

Ngoune Tandzi, Liliane and Charles Shelton Mutengwa (2020). "Estimation of Maize (Zea Mays L.) Yield Per Harvest Area: Appropriate Methods". In: *Agronomy* 10.1 (1), p. 29. ISSN: 2073-4395. DOI: 10.3390/agronomy10010029.

Nóia Júnior, Rogério de S., Deswarte, Jean-Pierre Cohan, Pierre Martre, Marijn van der Velde, Remi Lecerf, Heidi Webber, Frank Ewert, Alex C. Ruane, Gustavo A. Slafer, and Senthold Asseng (2023). "The Extreme 2016 Wheat Yield Failure in France". In: *Global Change Biology* 29.11, pp. 3130–3146. ISSN: 1365-2486. DOI: 10.1111/gcb.16662.

Olesen, J. E., M. Trnka, K. C. Kersebaum, A. O. Skjelvåg, B. Seguin, P. Peltonen-Sainio, F. Rossi, J. Kozyra, and F. Micale (2011). "Impacts and Adaptation of European Crop Production Systems to Climate Change". In: *European Journal of Agronomy* 34.2, pp. 96–112. ISSN: 1161-0301. DOI: 10.1016/j.eja.2010.11.003.

Olesen, J.E., C.D. Børgesen, L. Elsgaard, T. Palosuo, R.P. Rötter, A.O. Skjelvåg, P. Peltonen-Sainio, T. Börjesson, M. Trnka, F. Ewert, S. Siebert, N. Brisson, J. Eitzinger, E.D. van Asselt, M. Oberforster, and H.J. van der Fels-Klerx (2012). "Changes in Time of Sowing, Flowering and Maturity of Cereals in Europe under Climate Change". In: *Food Additives & Contaminants: Part A* 29.10, pp. 1527–1542. ISSN: 1944-0049. DOI: 10.1080/19440049.2012.712060. PMID: 22934894.

Oteros, Jose, Herminia García-Mozo, Roser Botey, Antonio Mestre, and Carmen Galán (2015). "Variations in Cereal Crop Phenology in Spain over the Last Twenty-Six Years (1986–2012)". In: *Climatic Change* 130.4, pp. 545–558. ISSN: 1573-1480. DOI: 10.1007/s10584-015-1363-9.

Panagos, Panos, Cristiano Ballabio, Mihaly Himics, Simone Scarpa, Francis Matthews, Mariia Bogonos, Jean Poesen, and Pasquale Borrelli (2021). "Projections of soil loss by water erosion in Europe by 2050". In: *Environmental Science & Policy* 124, pp. 380–392.

Parent, Boris, Margot Leclere, Sébastien Lacube, Mikhail A. Semenov, Claude Welcker, Pierre Martre, and François Tardieu (2018). "Maize Yields over Europe May Increase in Spite of Climate Change, with an Appropriate Use of the Genetic Variability of Flowering Time". In: *Proceedings of the National Academy of Sciences* 115.42, pp. 10642–10647. DOI: 10.1073/pnas.1720716115.

Parker, P. S., J. S. Shonkwiler, and J. Aurbacher (2017). "Cause and Consequence in Maize Planting Dates in Germany". In: *Journal of Agronomy and Crop Science* 203.3, pp. 227–240. ISSN: 09312250. DOI: 10.1111/jac.12182.

Páscoa, P., C. M. Gouveia, A. Russo, and R. M. Trigo (2017). "The Role of Drought on Wheat Yield Interannual Variability in the Iberian Peninsula from 1929 to 2012". In: *International Journal of Biometeorology* 61.3, pp. 439–451. ISSN: 1432-1254. DOI: 10.1007/s00484-016-1224-x.

Peichl, Michael, Stephan Thober, Volker Meyer, and Luis Samaniego (2018). "The Effect of Soil Moisture Anomalies on Maize Yield in Germany". In: *Natural Hazards and Earth System Sciences* 18.3, pp. 889–906. ISSN: 1561-8633. DOI: 10.5194/nhess-18-889-2018.

Peichl, Michael, Stephan Thober, Luis Samaniego, Bernd Hansjürgens, and Andreas Marx (2021). "Machine-Learning Methods to Assess the Effects of a Non-Linear Damage Spectrum Taking into Account Soil Moisture on Winter Wheat Yields in Germany". In: *Hydrology and Earth System Sciences* 25.12, pp. 6523–6545. ISSN: 1027-5606. DOI: 10.5194/hess-25-6523-2021.

Peña-Angulo, D., F. Reig-Gracia, F. Domínguez-Castro, J. Revuelto, E. Aguilar, G. van der Schrier, and S. M. Vicente-Serrano (2020). "ECTACI: European Climatology and Trend Atlas of Climate Indices (1979–2017)". In: *Journal of Geophysical Research: Atmospheres* 125.16, e2020JD032798. ISSN: 2169-8996. DOI: 10.1029/2020JD032798.

Piperno, Dolores R., Anthony J. Ranere, Irene Holst, Jose Iriarte, and Ruth Dickau (2009). "Starch Grain and Phytolith Evidence for Early Ninth Millennium B.P. Maize from the Central Balsas River Valley, Mexico". In: *Proceedings of the National Academy of Sciences* 106.13, pp. 5019–5024. DOI: 10.1073/pnas.0812525106.

Pithan, Felix, Gunilla Svensson, Rodrigo Caballero, Dmitry Chechin, Timothy W. Cronin, Annica M. L. Ekman, Roel Neggers, Matthew D. Shupe, Amy Solomon, Michael Tjernström, and Manfred Wendisch (2018). "Role of Air-Mass Transformations in Exchange between the Arctic and Mid-Latitudes". In: *Nature Geoscience* 11.11, pp. 805–812. ISSN: 1752-0908. DOI: 10.1038/s41561-018-0234-1.

Porter, John R and Megan Gawith (1999). "Temperatures and the Growth and Development of Wheat: A Review". In: *European Journal of Agronomy* 10.1, pp. 23–36. ISSN: 1161-0301. DOI: 10.1016/S1161-0301(98)00047-1.

Posthumus, H., J. Morris, T.m. Hess, D. Neville, E. Phillips, and A. Baylis (2009). "Impacts of the Summer 2007 Floods on Agriculture in England". In: *Journal of Flood Risk Management* 2.3, pp. 182–189. ISSN: 1753-318X. DOI: 10.1111/j.1753-318X.2009.01031.x.

Potapov, Peter, Svetlana Turubanova, Matthew C Hansen, Alexandra Tyukavina, Viviana Zalles, Ahmad Khan, Xiao-Peng Song, Amy Pickens, Quan Shen, and Jocelyn Cortez (2022). "Global maps of cropland extent and change show accelerated cropland expansion in the twenty-first century". In: *Nature Food* 3.1, pp. 19–28.

Prăvălie, Remus, Igor Sîrodoev, Cristian Patriche, Bogdan Roșca, Adrian Piticar, Georgeta Bandoc, Lucian Sfică, Adrian Tișcovschi, Monica Dumitrașcu, Carmen Chifiriuc, et al. (2020). "The impact of climate change on agricultural productivity in Romania. A country-scale assessment based on the relationship between climatic water balance and maize yields in recent decades". In: *Agricultural Systems* 179, p. 102767.

Pujol Andreu, Josep (2011). "Wheat Varieties and Technological Change in Europe, 19th and 20th Centuries: New Issues in Economic History." In: *Sociedad Española de Historia Agraria (SEHA)* 54.5.

Putelat, Thibaut, Andrew P. Whitmore, Nimai Senapati, and Mikhail A. Semenov (2021). "Local Impacts of Climate Change on Winter Wheat in Great Britain". In: *Royal Society Open Science* 8.6, p. 201669. DOI: 10.1098/rsos.201669.

Ramankutty, Navin, Jonathan A. Foley, John Norman, and Kevin McSweeney (2002). "The Global Distribution of Cultivable Lands: Current Patterns and Sensitivity to Possible Climate Change". In: *Global Ecology and Biogeography* 11.5, pp. 377–392. ISSN: 1466-8238. DOI: 10.1046/j.1466-822x.2002.00294.x.

Ranum, Peter, Juan Pablo Peña-Rosas, and Maria Nieves Garcia-Casal (2014). "Global Maize Production, Utilization, and Consumption". In: *Annals of the New York Academy of Sciences* 1312.1, pp. 105–112. ISSN: 1749-6632. DOI: 10.1111/nyas.12396.

Ray, Deepak K., James S. Gerber, Graham K. MacDonald, and Paul C. West (2015). "Climate Variation Explains a Third of Global Crop Yield Variability". In: *Nature Communications* 6.1, p. 5989. ISSN: 2041-1723. DOI: 10.1038/ncomms6989.

Rebetez, M., O. Dupont, and M. Giroud (2009). "An Analysis of the July 2006 Heatwave Extent in Europe Compared to the Record Year of 2003". In: *Theoretical and Applied Climatology* 95.1–2, pp. 1–7. ISSN: 0177-798X, 1434-4483. DOI: 10.1007/s00704-007-0370-9.

Reidsma, Pytrik, Frank Ewert, Alfons Oude Lansink, and Rik Leemans (2010). "Adaptation to Climate Change and Climate Variability in European Agriculture: The Importance of Farm Level Responses". In: *European Journal of Agronomy*. Cropping Systems Design: New Methods for New Challenges 32.1, pp. 91–102. ISSN: 1161-0301. DOI: 10.1016/j.eja.2009.06.003.

Rey, D, A Garrido, MI Mínguez, and M Ruiz-Ramos (2011). "Impact of climate change on maize's water needs, yields and profitability under various water prices in Spain". In: *Spanish Journal of Agricultural Research* 9.4, pp. 1047–1058.

Rezaei, Ehsan Eyshi, Stefan Siebert, and Frank Ewert (2015). "Intensity of heat stress in winter wheat—phenology compensates for the adverse effect of global warming". In: *Environmental Research Letters* 10.2, p. 024012.

Ritchie, Steven W. and J.J. Hanway (1986). *How a Corn Plant Develops*. 48. Iowa State University of Science and Technology, Cooperative Extension Service.

Rockel, Burkhard, Andreas Will, and Andreas Hense (2008). "The Regional Climate Model COSMO-CLM (CCLM)". In: *Meteorologische Zeitschrift* 17.4, pp. 347–348. ISSN: 0941-2948. DOI: 10.1127/0941-2948/2008/0309.

Rodríguez Díaz, J.A., E.K. Weatherhead, J.W. Knox, and E. Camacho (2007). "Climate change impacts on irrigation water requirements in the Guadalquivir river basin in Spain". In: *Regional Environmental Change* 7.3, pp. 149–159.

Rousi, Efi, Andreas H. Fink, Lauren S. Andersen, Florian N. Becker, Goratz Beobide-Arsuaga, Marcus Breil, Giacomo Cozzi, Jens Heinke, Lisa Jach, Deborah Niermann, Dragan Petrovic, Andy Richling, Johannes Riebold, Stella Steidl, Laura Suarez-Gutierrez, Jordis S. Tradowsky, Dim Coumou, André Düsterhus, Florian Ellsäßer, Georgios Fragkoulidis, Daniel Gliksman, Dörthe Handorf, Karsten Haustein, Kai Kornhuber, Harald Kunstmann, Joaquim G. Pinto, Kirsten Warrach-Sagi, and Elena Xoplaki (2023). "The Extremely Hot and Dry 2018 Summer in Central and Northern Europe from a Multi-Faceted Weather and Climate Perspective". In: *Natural Hazards and Earth System Sciences* 23.5, pp. 1699–1718. ISSN: 1684-9981. DOI: 10.5194/nhess-23-1699-2023.

Rowlandson, Tracy, Mark Gleason, Paulo Sentelhas, Terry Gillespie, Carla Thomas, and Brian Hornbuckle (2015). "Reconsidering Leaf Wetness Duration Determination for Plant Disease Management". In: *Plant Disease* 99.3, pp. 310–319. ISSN: 0191-2917. DOI: 10.1094/PDIS-05-14-0529-FE.

Ruane, Alex C, Meridel Phillips, Jonas Jägermeyr, and Christoph Müller (2024). "Nonlinear climate change impacts on crop yields may mislead stakeholders". In: *Earth's Future* 12.4, e2023EF003842.

Russo, Simone, Jana Sillmann, and Erich M. Fischer (2015). "Top Ten European Heatwaves since 1950 and Their Occurrence in the Coming Decades". In: *Environmental Research Letters* 10.12, p. 124003. ISSN: 1748-9326. DOI: 10.1088/1748-9326/10/12/124003.

Sacks, William J., Delphine Deryng, Jonathan A. Foley, and Navin Ramankutty (2010). "Crop Planting Dates: An Analysis of Global Patterns". In: *Global Ecology and Biogeography* 19.5, pp. 607–620. ISSN: 1466-8238. DOI: 10.1111/j.1466-8238.2010.00551.x.

Sánchez, Berta, Anton Rasmussen, and John R Porter (2014). "Temperatures and the Growth and Development of Maize and Rice: A Review". In: *Global Change Biology* 20.2, pp. 408–417. ISSN: 1365-2486. DOI: 10.1111/gcb.12389.

Schmitt, Jonas, Frank Offermann, Mareike Söder, Cathleen Frühauf, and Robert Finger (2022). "Extreme Weather Events Cause Significant Crop Yield Losses at the Farm Level in German Agriculture". In: *Food Policy* 112, p. 102359. ISSN: 0306-9192. DOI: 10.1016/j.foodpol.2022.102359.

Schwalm, Christopher R, Spencer Glendon, and Philip B Duffy (2020). "RCP8. 5 tracks cumulative CO2 emissions". In: *Proceedings of the National Academy of Sciences* 117.33, pp. 19656–19657.

Senapati, Nimai, Simon Griffiths, Malcolm Hawkesford, Peter R Shewry, and Mikhail A Semenov (2020). "Substantial increase in yield predicted by wheat ideotypes for Europe under future climate". In: *Climate Research* 80.3, pp. 189–201.

Seneviratne, S.I, X. Zhang, M. Adnan, W. Badi, C. Dereczynski, A. Di Luca, S. Ghosh, I. Iskandar, J. Kossin, S. Lewis, F. Otto, I. Pinto, M. Satoh, S.M. Vicente-Serrano, M. Wehner, and B. Zhou (2021). "Weather and Climate Extreme Events in a Changing Climate". In: *Climate Change 2021 – The Physical Science Basis: Working Group I Contribution to the Sixth Assessment Report of the Intergovernmental Panel on Climate Change*. 1st ed. Climate Change 2021: The Physical Science Basis. Contribution of Working Group I to the Sixth Assessment Report of the Intergovernmental Panel on Climate Change. Cambridge, United Kingdom and New York, NY, USA: Cambridge University Press, pp. 1513–1766. ISBN: 978-1-009-15789-6. DOI: 10.1017/9781009157896.

Shapley, Lloyd S et al. (1953). "A value for n-person games". In.

Shewry, Peter R. and Sandra J. Hey (2015). "The Contribution of Wheat to Human Diet and Health". In: *Food and Energy Security* 4.3, pp. 178–202. ISSN: 2048-3694. DOI: 10.1002/fes3.64.

Shi, Wenjiao, Fulu Tao, and Zhao Zhang (2013). "A Review on Statistical Models for Identifying Climate Contributions to Crop Yields". In: *Journal of Geographical Sciences* 23.3, pp. 567–576. ISSN: 1861-9568. DOI: 10.1007/s11442-013-1029-3.

Siebert, Stefan, Heidi Webber, Gang Zhao, and Frank Ewert (2017). "Heat Stress Is Overestimated in Climate Impact Studies for Irrigated Agriculture". In: *Environmental Research Letters* 12.5, p. 054023. ISSN: 1748-9326. DOI: 10.1088/1748-9326/aa702f.

Slavin, Joanne L. and Beate Lloyd (2012). "Health Benefits of Fruits and Vegetables". In: *Advances in Nutrition* 3.4, pp. 506–516. ISSN: 2161-8313. DOI: 10.3945/an.112.002154.

Smith, Donald L. and Chantal Hamel, eds. (1999). *Crop Yield: Physiology and Processes*. Berlin ; New York: Springer. 504 pp. ISBN: 978-3-540-64477-4.

Smith, Melinda D. (2011). "An Ecological Perspective on Extreme Climatic Events: A Synthetic Definition and Framework to Guide Future Research". In: *Journal of Ecology* 99.3, pp. 656–663. ISSN: 1365-2745. DOI: 10.1111/j.1365-2745.2011.01798.x.

Spinoni, Jonathan, Gustavo Naumann, Jürgen V. Vogt, and Paulo Barbosa (2015). "The Biggest Drought Events in Europe from 1950 to 2012". In: *Journal of Hydrology: Regional Studies* 3, pp. 509–524. ISSN: 2214-5818. DOI: 10.1016/j.ejrh.2015.01.001.

Spiridonov, Vlado and Mladjen Ćurić (2021). *Fundamentals of Meteorology*. Cham: Springer International Publishing. DOI: 10.1007/978-3-030-52655-9.

Stainoh, Federico, Julia Mömken, Celia M. Gouveia, and Joaquim G. Pinto (2024). "A Comparison of Climate Drivers' Impacts on Silage Maize Yield Shock in Germany". In: *Theoretical and Applied Climatology*. DOI: 10.1007/s00704-024-05179-z.

Statistisches Bundesamt (Destatis) (2025). *GENESIS-Online: Tabelle 41241-01-03-4*. https://www.regionalstatistik.de/genesis/online/table/41241-01-03-4. Accessed: 2025-05-19.

Stocker, T. (2011). *Introduction to Climate Modeling*. Springer. 179 pp.

Stone, P. J., I. B. Sorensen, and P. D. Jamieson (1999). "Effect of Soil Temperature on Phenology, Canopy Development, Biomass and Yield of Maize in a Cool-Temperate Climate". In: *Field Crops Research* 63.2, pp. 169–178. ISSN: 0378-4290. DOI: 10.1016/S0378-4290(99)00033-7.

Supit, I., C. A. van Diepen, H. L. Boogaard, F. Ludwig, and B. Baruth (2010). "Trend Analysis of the Water Requirements, Consumption and Deficit of Field Crops in Europe". In: *Agricultural and Forest Meteorology* 150.1, pp. 77–88. ISSN: 0168-1923. DOI: 10.1016/j.agrformet.2009.09.002.

Taiz, Lincoln and Eduardo Zeiger (2002). *Plant Physiology*. 3rd ed. Vol. 91. 690 pp.

Taylor, Karl E., Ronald J. Stouffer, and Gerald A. Meehl (2012). "An Overview of CMIP5 and the Experiment Design". In: *Bulletin of the American Meteorological Society* 93.4, pp. 485–498. DOI: 10.1175/BAMS-D-11-00094.1.

Tayyar, Emun (2010). "Variation in Grain Yield and Quality of Romanian Bread Wheat Varieties Compared to Local Varieties in Northwestern Turkey". In: *Romanian Biotechnological Letters* 15.2.

Teichmann, Claas, Katharina Bülow, Juliane Otto, Susanne Pfeifer, Diana Rechid, Kevin Sieck, and Daniela Jacob (2018). "Avoiding Extremes: Benefits of Staying below +1.5 °C Compared to +2.0 °C and +3.0 °C Global Warming". In: *Atmosphere* 9.4 (4), p. 115. ISSN: 2073-4433. DOI: 10.3390/atmos9040115.

Teixeira, da Silva Jaime A, Inna Koblianska, and Anatolii Kucher (2023). "Agricultural production in Ukraine: An insight into the impact of the Russo-Ukrainian war on local, regional and global food security". In: *Journal of Agricultural Sciences (Belgrade)* 68.2, pp. 121–140.

Tenaillon, Maud Irène and Alain Charcosset (2011). "A European perspective on maize history". In: *Comptes Rendus. Biologies* 334.3, pp. 221–228. ISSN: 1768-3238. DOI: 10.1016/j.crvi.2010.12.015.

Teutschbein, Claudia and Jan Seibert (2012). "Bias Correction of Regional Climate Model Simulations for Hydrological Climate-Change Impact Studies: Review and Evaluation of Different Methods". In: *Journal of Hydrology* 456–457, pp. 12–29. ISSN: 00221694. DOI: 10.1016/j.jhydrol.2012.05.052.

Tho, Kim E., Elizabeth Brisco-McCann, Prissana Wiriyajitsomboon, and Mary K. Hausbeck (2019). "Effects of Temperature, Relative Humidity, and Plant Age on Bacterial Disease of Onion Plants". In: *Plant Health Progress* 20.4, pp. 200–206. ISSN: 1535-1025. DOI: 10.1094/PHP-05-19-0038-RS.

Tibshirani, Robert (1996). "Regression Shrinkage and Selection Via the Lasso". In: *Journal of the Royal Statistical Society: Series B (Methodological)* 58.1, pp. 267–288. ISSN: 0035-9246. DOI: 10.1111/j.2517-6161.1996.tb02080.x.

Tredennick, Andrew T., Giles Hooker, Stephen P. Ellner, and Peter B. Adler (2021). "A Practical Guide to Selecting Models for Exploration, Inference, and Prediction in Ecology". In: *Ecology* 102.6, e03336. ISSN: 1939-9170. DOI: 10.1002/ecy.3336.

"Trends in Air Mass Frequencies across Europe | Theoretical and Applied Climatology" (2022). In: *Theoretical and Applied Climatology* 148, pp. 105–120. DOI: 10.1007/s00704-022-03921-z.

Trevaskis, Ben (2010). "The Central Role of the VERNALIZATION1 Gene in the Vernalization Response of Cereals". In: *Functional Plant Biology* 37.6, pp. 479–487. ISSN: 1445-4416. DOI: 10.1071/FP10056.

Trigo, Ricardo M., Timothy J. Osborn, and João M. Corte-Real (2002). "The North Atlantic Oscillation Influence on Europe: Climate Impacts and Associated Physical Mechanisms". In: *Climate Research* 20.1, pp. 9–17. ISSN: 0936-577X, 1616-1572. DOI: 10.3354/cr020009.

Trnka, M., Jørgen Eivind Olesen, K. C. Kersebaum, A. O. Skjelvåg, J. Eitzinger, B. Seguin, P. Peltonen-Sainio, R. Rötter, Ana Iglesias, S. Orlandini, M. Dubrovský, P. Hlavinka, J. Balek, H. Eckersten, E. Cloppet, P. Calanca, A. Gobin, V. Vučetić, P. Nejedlik, S. Kumar, B. Lalic, A. Mestre, F. Rossi, J. Kozyra, V. Alexandrov, D. Semerádová, and Z. Žalud (2011). "Agroclimatic Conditions in Europe under Climate Change". In: *Global Change Biology* 17.7, pp. 2298–2318. ISSN: 1365-2486. DOI: 10.1111/j.1365-2486.2011.02396.x.

Trnka, Miroslav, Petr Hlavinka, and Mikhail A. Semenov (2015). "Adaptation Options for Wheat in Europe Will Be Limited by Increased Adverse Weather Events under Climate Change". In: *Journal of The Royal Society Interface* 12.112, p. 20150721. DOI: 10.1098/rsif.2015.0721.

Ul Hassan, Mahmood, Tassaduq Rasool, Chandni Iqbal, Adnan Arshad, Muhammad Abrar, Muhammad Mohsin Abrar, Muhammad Habib-ur-Rahman, Mehmood Ali Noor, Alam Sher, and Shah Fahad (2022). "Linking Plants Functioning to Adaptive Responses Under Heat Stress Conditions: A Mechanistic Review". In: *Journal of Plant Growth Regulation* 41.7, pp. 2596–2613. ISSN: 1435-8107. DOI: 10.1007/s00344-021-10493-1.

Van der Velde, M., B. Baruth, A. Bussay, A. Ceglar, S. Garcia Condado, S. Karetsos, R. Lecerf, R. Lopez, A. Maiorano, L. Nisini, L. Seguini, and M. van den Berg (2018). "In-Season Performance of European Union Wheat Forecasts during Extreme Impacts". In: *Scientific Reports* 8.1 (1), p. 15420. ISSN: 2045-2322. DOI: 10.1038/s41598-018-33688-1.

Van der Velde, Marijn, Francesco N. Tubiello, Anton Vrieling, and Fayçal Bouraoui (2012). "Impacts of Extreme Weather on Wheat and Maize in France: Evaluating Regional Crop Simulations against Observed Data". In: *Climatic Change* 113.3, pp. 751–765. ISSN: 1573-1480. DOI: 10.1007/s10584-011-0368-2.

Van Oort, P. A. J., B. G. H. Timmermans, H. Meinke, and M. K. Van Ittersum (2012). "Key Weather Extremes Affecting Potato Production in The Netherlands". In: *European Journal of Agronomy* 37.1, pp. 11–22. ISSN: 1161-0301. DOI: 10.1016/j.eja.2011.09.002.

Van Oort, P. A. J., B. G. H. Timmermans, R. L. M. Schils, and N. van Eekeren (2023). "Recent Weather Extremes and Their Impact on Crop Yields of the Netherlands". In: *European Journal of Agronomy* 142, p. 126662. ISSN: 1161-0301. DOI: 10.1016/j.eja.2022.126662.

Vautard, Robert, Andreas Gobiet, Stefan Sobolowski, Erik Kjellström, Annemiek Stegehuis, Paul Watkiss, Thomas Mendlik, Oskar Landgren, Grigory Nikulin, Claas Teichmann, and Daniela Jacob (2014). "The European Climate under a 2 °C Global Warming". In: *Environmental Research Letters* 9.3, p. 034006. ISSN: 1748-9326. DOI: 10.1088/1748-9326/9/3/034006.

Vogel, Elisabeth, Markus G. Donat, Lisa V. Alexander, Malte Meinshausen, Deepak K. Ray, David Karoly, Nicolai Meinshausen, and Katja Frieler (2019). "The Effects of Climate Extremes on Global Agricultural Yields". In: *Environmental Research Letters* 14.5, p. 054010. ISSN: 1748-9326. DOI: 10.1088/1748-9326/ab154b.

Vogel, Johannes, Pauline Rivoire, Cristina Deidda, Leila Rahimi, Christoph A. Sauter, Elisabeth Tschumi, Karin van der Wiel, Tianyi Zhang, and Jakob Zscheischler (2021). "Identifying Meteorological Drivers of Extreme Impacts: An Application to Simulated Crop Yields". In: *Earth System Dynamics* 12.1, pp. 151–172. ISSN: 2190-4979. DOI: 10.5194/esd-12-151-2021.

Voldoire, Aurore, Emilia Sanchez-Gomez, Dea Salas y Mélia, B Decharme, Christophe Cassou, Stéphane Sénési, Sophie Valcke, Isabelle Beau, A Alias, Matthieu Chevallier, et al. (2013). "The CNRM-CM5. 1 global climate model: description and basic evaluation". In: *Climate dynamics* 40, pp. 2091–2121.

Wan, Wei, Zhong Liu, Jiahui Li, Jianing Xu, Hanqing Wu, and Zhaohui Xu (2022). "Spatiotemporal Patterns of Maize Drought Stress and Their Effects on Biomass in the Northeast and North China Plain from 2000 to 2019". In: *Agricultural and Forest Meteorology* 315, p. 108821. ISSN: 0168-1923. DOI: 10.1016/j.agrformet.2022.108821.

Wang, Xinlei, Jianxi Huang, Quanlong Feng, and Dongqin Yin (2020). "Winter Wheat Yield Prediction at County Level and Uncertainty Analysis in Main Wheat-Producing Regions of China with Deep Learning Approaches". In: *Remote Sensing* 12.11 (11), p. 1744. ISSN: 2072-4292. DOI: 10.3390/rs12111744.

Watson, R.T., M.C. Zinyowera, and R.H. Moss (1997). *The Regional Impacts of Climate Change: An Assessment of Vulnerability*. UK: Cambridge University Press. pp 517.

Webber, Heidi, Frank Ewert, Jørgen E. Olesen, Christoph Müller, Stefan Fronzek, Alex C. Ruane, Maryse Bourgault, Pierre Martre, Behnam Ababaei, Marco Bindi, Roberto Ferrise, Robert Finger, Nándor Fodor, Clara Gabaldón-Leal, Thomas Gaiser, Mohamed Jabloun, Kurt-Christian Kersebaum, Jon I. Lizaso, Ignacio J. Lorite, Loic Manceau, Marco Moriondo, Claas Nendel, Alfredo Rodríguez, Margarita Ruiz-Ramos, Mikhail A. Semenov, Stefan Siebert, Tommaso Stella, Pierre Stratonovitch, Giacomo Trombi, and Daniel Wallach (2018). "Diverging Importance of Drought Stress for Maize and Winter Wheat in Europe". In: *Nature Communications* 9.1, p. 4249. ISSN: 2041-1723. DOI: 10.1038/s41467-018-06525-2.

Webber, Heidi, Gunnar Lischeid, Michael Sommer, Robert Finger, Claas Nendel, Thomas Gaiser, and Frank Ewert (2020). "No Perfect Storm for Crop Yield Failure in Germany". In: *Environmental Research Letters* 15.10, p. 104012. ISSN: 1748-9326. DOI: 10.1088/1748-9326/aba2a4.

Whittingham, Mark J., Philip A. Stephens, Richard B. Bradbury, and Robert P. Freckleton (2006). "Why Do We Still Use Stepwise Modelling in Ecology and Behaviour?" In: *Journal of Animal Ecology* 75.5, pp. 1182–1189. ISSN: 1365-2656. DOI: 10.1111/j.1365-2656.2006.01141.x.

Wickham, Hadley, Winston Chang, and Maintainer Hadley Wickham (2016). "Package 'ggplot2'". In: *Create elegant data visualisations using the grammar of graphics. Version* 2.1, pp. 1–189.

Wilks, Daniel S. (2006). *Statistical Methods in the Atmospheric Sciences*. 2nd ed. International Geophysics Series volume 91. Amsterdam Paris: Elsevier. ISBN: 978-0-12-751966-1.

Wu, Felicia and Hasan Guclu (2013). "Global Maize Trade and Food Security: Implications from a Social Network Model". In: *Risk Analysis* 33.12, pp. 2168–2178. ISSN: 1539-6924. DOI: 10.1111/risa.12064.

Wu, Xiuchen, Hongyan Liu, Xiaoyan Li, Yuhong Tian, and Miguel D Mahecha (2017). "Responses of winter wheat yields to warming-mediated vernalization variations across temperate Europe". In: *Frontiers in Ecology and Evolution* 5, p. 126.

Xu, Chenchen, Xin Wang, Yi Wu, Jia Gao, Ping Zhang, Yating Zhao, Xiaoli Liu, Pu Wang, and Shoubing Huang (2024). "Molecular mechanisms underlying low temperature inhibition of grain filling in maize (Zea mays L.): Coordination of growth and cold responses". In: *The Plant Journal* 119.2, pp. 982–997.

Xu and Ridout (2001). "Effects of Prevailing Wind Direction on Spatial Statistics of Plant Disease Epidemics". In: *Journal of Phytopathology* 149.3–4, pp. 155–166. ISSN: 1439-0434. DOI: 10.1046/j.1439-0434.2001.00591.x.

Xynias, Ioannis N, Ioannis Mylonas, Evangelos G Korpetis, Elissavet Ninou, Aphrodite Tsaballa, Ilias D Avdikos, and Athanasios G Mavromatis (2020). "Durum wheat breeding in the Mediterranean region: Current status and future prospects". In: *Agronomy* 10.3, p. 432.

Yamori, Wataru, Kouki Hikosaka, and Danielle A. Way (2014). "Temperature Response of Photosynthesis in C3, C4, and CAM Plants: Temperature Acclimation and Temperature Adaptation". In: *Photosynthesis Research* 119.1, pp. 101–117. ISSN: 1573-5079. DOI: 10.1007/s11120-013-9874-6.

Zadoks, J.C., T.T. Chang, and C.F. Konzak (1974). "A Decimal Code for the Growth Stages of Cereals". In: *Weed research* 6, pp.415–421.

Zajac, Zuzanna, Oscar Gomez, Emiliano Gelati, Marijn van der Velde, Simona Bassu, Andrej Ceglar, Ordan Chukaliev, Lorenzo Panarello, Renate Koeble, Maurits van den Berg, Stefan Niemeyer, and Davide Fumagalli (2022). "Estimation of Spatial Distribution of Irrigated Crop Areas in Europe for Large-Scale Modelling Applications". In: *Agricultural Water Management* 266, p. 107527. ISSN: 0378-3774. DOI: 10.1016/j.agwat.2022.107527.

Zampieri, M, A Ceglar, F Dentener, and A Toreti (2018). "Understanding and Reproducing Regional Diversity of Climate Impacts on Wheat Yields: Current Approaches,

Challenges and Data Driven Limitations". In: *Environmental Research Letters* 13.2, p. 021001. ISSN: 1748-9326. DOI: 10.1088/1748-9326/aaa00d.

– (2017). "Wheat Yield Loss Attributable to Heat Waves, Drought and Water Excess at the Global, National and Subnational Scales". In: *Environmental Research Letters* 12.6, p. 064008. ISSN: 1748-9326. DOI: 10.1088/1748-9326/aa723b.

Zhang, Shaobo and Jie Chen (2021). "Uncertainty in projection of climate extremes: A comparison of CMIP5 and CMIP6". In: *Journal of Meteorological Research* 35.4, pp. 646–662.

Zhao, Gang, Heidi Webber, Holger Hoffmann, Joost Wolf, Stefan Siebert, and Frank Ewert (2015). "The Implication of Irrigation in Climate Change Impact Assessment: A European-wide Study". In: *Global Change Biology* 21.11, pp. 4031–4048. ISSN: 1365-2486. DOI: 10.1111/gcb.13008.

Zhao, Jianjun, Vani Kulkarni, Liu Nini, Dunia Del Carpio, Johan Bucher, and Guusje Bonnema (2010). "BrFLC2 (FLOWERING LOCUS C) as a Candidate Gene for a Vernalization Response QTL in Brassica Rapa". In: *Journal of experimental botany* 61, pp. 1817–25. DOI: 10.1093/jxb/erq048.

Zhllima, Edvin, Orjon Xhoxhi, Drini Imami, and Engjell Skreli (2025). "Unlocking crop insurance: exploring farmers' demand and willingness to pay in the agriculture sector". In: *Journal of Agribusiness in Developing and Emerging Economies*.

Zhou, Ziming, Zhiming Yu, and Sihan Gao (2022). "Climate Shocks and Farmers' Agricultural Productive Investment: Resisting Risk or Escaping Production?" In: *Frontiers in Ecology and Evolution* 10. ISSN: 2296-701X. DOI: 10.3389/fevo.2022.895265.

Zhu, Peng, Rose Abramoff, David Makowski, and Philippe Ciais (2021). "Uncovering the Past and Future Climate Drivers of Wheat Yield Shocks in Europe With Machine Learning". In: *Earth's Future* 9.5, e2020EF001815. ISSN: 2328-4277. DOI: 10.1029/2020EF001815.

Ziv, Guy, Michael Beckmann, James Bullock, Anna Cord, Ruth Delzeit, Cristina Domingo, Gunnar Dreßler, Nina Hagemann, Joan Masó, Birgit Müller, et al. (2020). "BESTMAP: behavioural, ecological and socio-economic tools for modelling agricultural policy". In: *Research Ideas and Outcomes* 6, e52052.